Gaining insight into the pathology of

4H leukodystrophy

using patient-specific iPSC-based models

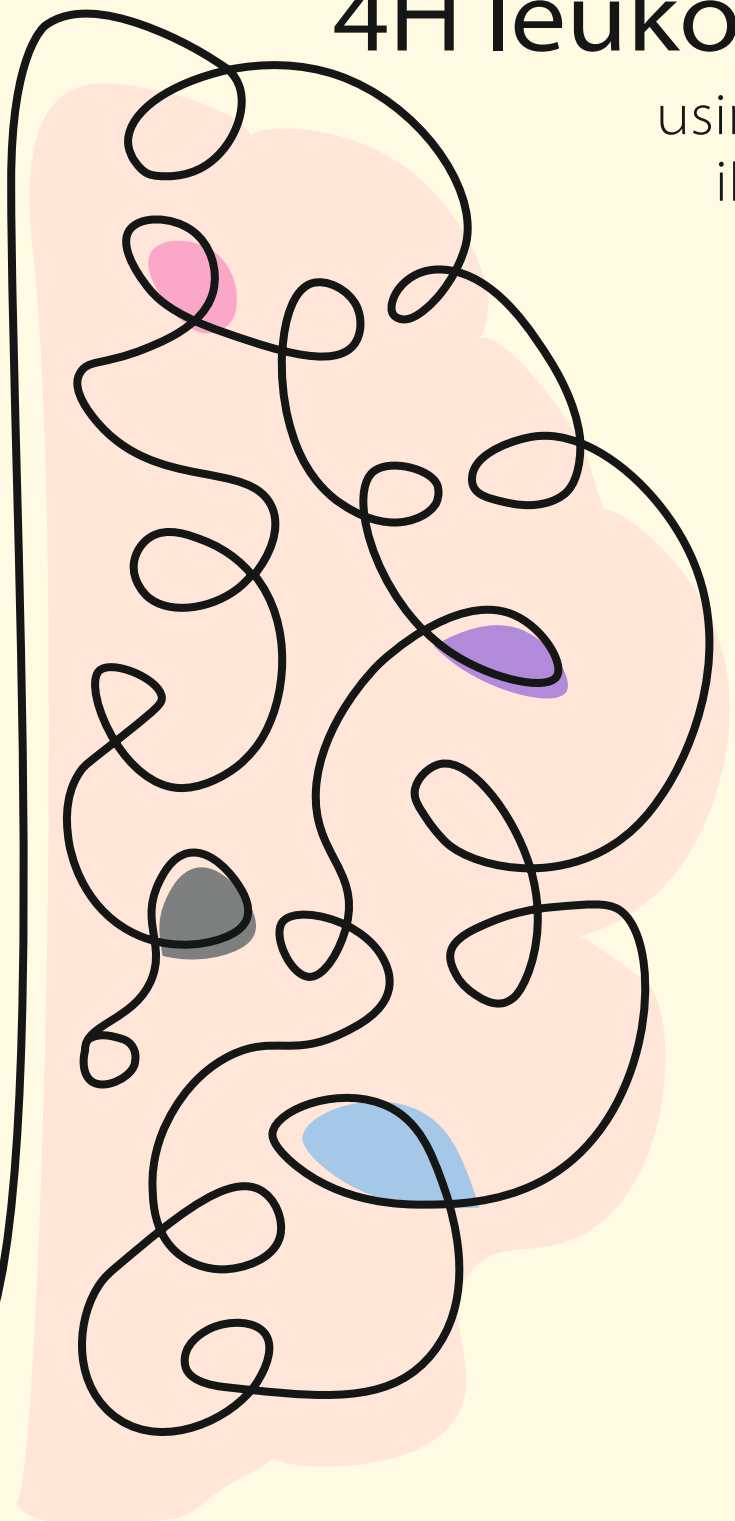

Liza M. L. Kok

GAINING INSIGHT INTO THE PATHOLOGY OF 4H LEUKODYSTROPHY USING PATIENT-SPECIFIC IPSC-BASED MODELS

Liza M. L. Kok

Cover design by Liza M. L Kok “Brain and bee hive side-by-side”

Cover explanation: The brain is a complex organ, composed of many specialized cell types that work together to function harmoniously. To me, this has similarities with a beehive as bees in the hive have specialized jobs and the entire colony depends on each job being fulfilled correctly. One bee, the queen, has a clear function: to lay eggs. Nowadays, this is common knowledge, but for long it was thought that the big bee, is the ruler, and hence it must be the king! They couldn’t have been more wrong.
Similarly, in this thesis, we sought to uncover which cell in the hypomyelinated 4H brain isn’t performing its role correctly. Rather than focusing solely on the most obvious suspect, we broadened our investigation—because, as with the bees, what seems logically is not always true!

Layout: Liza M. L. Kok

Printing: Ridderprint, www.ridderprint.nl

ISBN: 978-94-6522-527-2

Publication of this thesis was financially supported by the Graduate School Neurosciences Amsterdam Rotterdam (ONWAR)

VRIJE UNIVERSITEIT

GAINING INSIGHT INTO THE PATHOLOGY OF 4H LEUKODYSTROPHY USING PATIENT-SPECIFIC IPSC-BASED MODELS

ACADEMISCH PROEFSCHRIFT

ter verkrijging van de graad Doctor of Philosophy aan
de Vrije Universiteit Amsterdam,
op gezag van de rector magnificus
prof.dr. J.J.G. Geurts,
volgens besluit van de decaan
van de Faculteit der Bètawetenschappen
in het openbaar te verdedigen
op vrijdag 19 september 2025 om 9.45 uur
in de universiteit

door

Liza Martha Linda Kok

geboren te Wervershoof

promotoren:	prof.dr. V.M. Heine prof.dr. N.I. Wolf
promotiecommissie:	prof.dr. R.E. van Kesteren dr. S. Dooves prof.dr. N. Nadif Kasri prof.dr. D. Pajkrt dr. N. Hamilton

TABLE OF CONTENTS

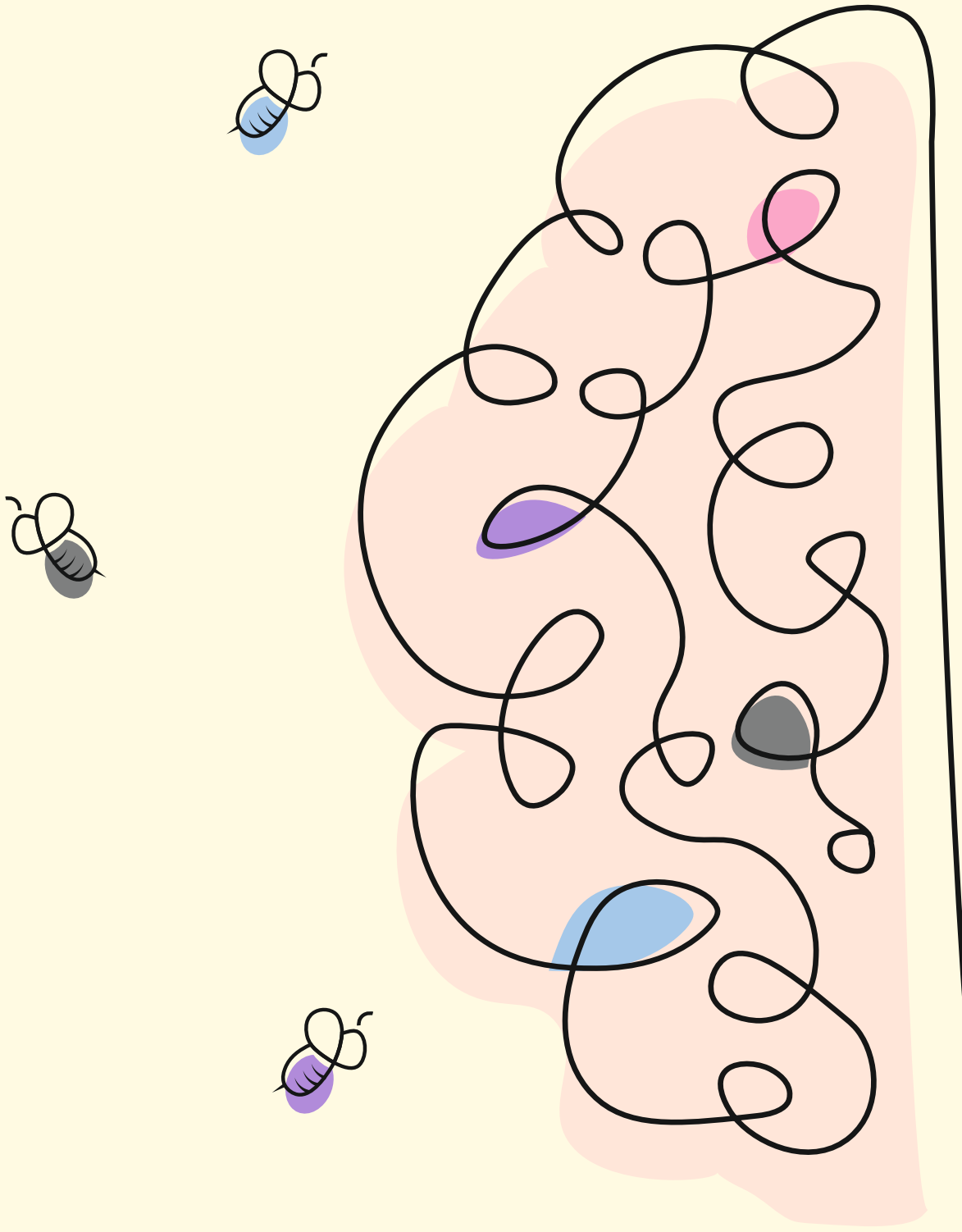

01

General introduction

Liza M. L. Kok

The human brain is an incredibly complex organ, housing billions of interconnected neurons and glial cells that form highly specialized networks. Despite remarkable advancements in neuroscience, many of the brain's functions and developmental processes remain only partially understood. What is clear, however, is that even minor deviations from normal brain development can lead to profound neurological and cognitive impairments. Among the many disorders that disrupt brain function are leukodystrophies—a diverse group of genetic diseases primarily affecting the brain's white matter. One of the white matter components often affected is myelin, the insulating sheath that surrounds neuronal axons and facilitates efficient electrical signal transmission.

One such leukodystrophy is 4H leukodystrophy, a disease that used to be characterized by hypomyelination along with hypodontia and hypogonadotropic hypogonadism. However, when in 2011 mutations in genes encoding for subunits of RNA polymerase III - a ubiquitous protein essential for cellular transcription - were identified as disease-causing variants, more patients with a wider range of clinical presentations were diagnosed. While the identification of the mutations provided an important first step toward understanding the genetic basis of 4H syndrome, it also raised critical questions about the underlying disease mechanisms and, most importantly, which cells should be the target of future treatments. Current treatments remain supportive, focusing on symptom management rather than addressing the root cause. Identifying which cell types are primarily affected and elucidating the processes disrupted by Pol III mutations are crucial steps toward developing targeted therapies.

In this thesis, we aim to bridge this knowledge gap by modelling the cellular phenotypes of 4H leukodystrophy using human induced pluripotent stem cells (hiPSCs) and advanced *in vitro* systems. These models allow us to explore how Pol III defects affect brain cell development, particularly those involved in myelination and neuronal function. Through these studies, we seek to uncover disease mechanisms, identify vulnerable cell types, and evaluate potential therapeutic targets that could pave the way for future treatments.

4H SYNDROME - Clinical spectrum

Leukodystrophies are a large and heterogeneous group of genetic brain white matter disorders. Often they are diagnosed in childhood and have a progressive nature that leads to early death (van der Knaap et al., 2019). One of the more prevalent leukodystrophies is 4H syndrome (OMIM 612440) which is named after its characteristic clinical symptoms: hypomyelination, hypogonadotropic hypogonadism and hypodontia (Schmidt et al., 2020; Wolf, 2014). The first symptom, hypomyelination, is defined as a reduced amount or lack of normal myelin in the central nervous system (CNS), which can be diagnosed using MRI (Wolf et al., 2021). Patients often show cerebellar atrophy as well (Takanashi et al., 2014). Hypogonadotropic hypogonadism means that the hypothalamus or pituitary gland is not stimulating the testes or ovaries to produce sufficient sex hormones, leading to absent or abnormal puberty development (Fraietta et al., 2013). The last of the three typical symptoms is hypodontia, the absence of one or multiple primary or permanent teeth (Al-Ani et al., 2017). Even though these symptoms are characteristic for 4H, they are not always all present. The presentation of 4H ranges from very severe to mild and even asymptomatic young adults are described. The mildest patients present with isolated hypogonadotropic hypogonadism (Richards et al., 2017) while more severe patients seem to have a predominant neurological phenotype sometimes without typical hypomyelination (DeGasperis et al., 2020; Harting et al., 2020; La Piana et al., 2016; Wolf, 2014).

There is not only heterogeneity in the presentation of the characteristic symptoms, there is also a wide spectrum of other symptoms and signs of the disease amongst which are other neurological presentations such as delay in motor development in early life and/or regression of motor development later in life, often resulting in wheelchair dependence. Additionally, many patients show cerebellar features such as ataxia and dysarthria. Later, pyramidal features such as the development of spasticity can be seen but this is more rare. Also non-neurological symptoms such as short stature, caused by endocrine abnormalities, and myopia (shortsightedness) are observed. Furthermore additional dental abnormalities like natal teeth, delayed dentition, and unusual order of tooth eruption are not uncommon. (Pelletier et al., 2021; Wolf, 2014). Craniofacial features may also be seen (Mirchi et al., 2023). A graphical representation of the wide spectrum of clinical symptoms is depicted in Figure 1.

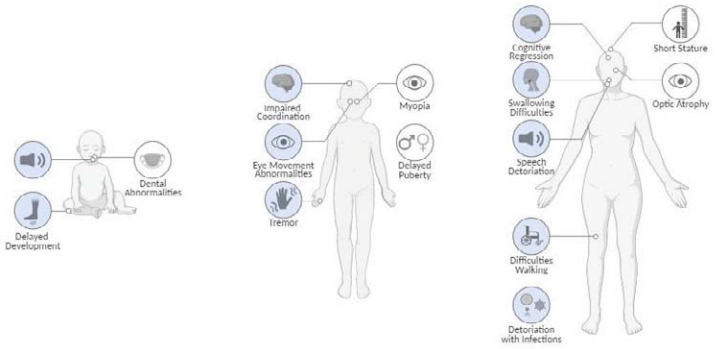

Figure 1: Clinical presentation of 4H syndrome. Neurological (blue) and non-neurological (white) clinical presentations. Created using BioRender.com.

4H SYNDROME – Current Treatments

Due to its multisystem involvement, 4H leukodystrophy requires multidisciplinary care involving several subspecialists, including endocrinologists, neurologists, dentists, and clinical geneticists. Current treatment strategies are symptom-based, focusing on managing the broad range of clinical features associated with the disorder. Management of the three hallmark symptoms involves supportive care such as physical and occupational therapy for motor and neurological issues that might be caused by hypomyelination, hormone replacement therapy (HRT) for hypogonadotropic hypogonadism (Billington et al., 2015; Nwatamole et al., 2024), and specialized dental evaluations to address hypodontia.

While these interventions can improve the quality of life for affected individuals, there is currently no curative therapy for 4H syndrome. Its progressive nature and clinical variability stress the urgent need for novel therapeutic strategies targeting and curing the underlying pathology. Identifying specific therapeutic targets at the molecular and cellular level will be crucial in developing future disease-modifying therapies. Advances in understanding 4H syndrome's genetic and cellular basis hold promise for translating research findings into meaningful clinical interventions.

In summary, 4H syndrome is a relatively prevalent leukodystrophy with a highly variable clinical presentation and progressive disease course. Current treatments remain supportive, focusing on symptom management and improving patients' quality of life, but they lack curative potential (Adang et al., 2017). To provide novel perspectives new curative treatment strategies are urgently needed. To develop these, we need to understand the targets for therapies.

4H SYNDROME - Genetic basis

The identification of the genetic basis of 4H leukodystrophy marked a critical step toward understanding the disease and developing targeted therapies. Prior to 2011, patients were diagnosed solely based on clinical features, with no molecular explanation for the disease (Timmons et al., 2006; Wolf et al., 2005; Wolf et al., 2007). This changed with the discovery of mutations in genes encoding subunits of RNA polymerase III (Pol III), a key enzyme involved in the transcription of small, non-coding RNAs essential for cellular function.

The first identified mutations were identified in the *POLR3A* gene, which encodes one of the 17 subunits of Pol III, followed shortly by the identification of mutations in *POLR3B*, which encodes another subunit of the enzyme's catalytic core (Bernard et al., 2011; Tetreault et al., 2011). These findings established Pol III as the central molecular player in the disease. In subsequent studies, rarer mutations were discovered in additional Pol III subunits, including *POLR3K* and *POLR3D*, as well as *POLR1C*, a shared subunit between Pol III and RNA polymerase I (Dorboz et al., 2018; Macintosh, Perrier, et al., 2023; Thiffault et al., 2015). Since all the identified mutations for 4H syndrome are related to genes that encode for subunits of Pol III (Figure 2) (Gauquelin et al., 2019; Wolf, 2014), the disease is also referred to as *POLR3*-related leukodystrophy.

The pathogenic variants observed in these genes are diverse, both in genomic location and mutation type. They include missense, nonsense, and splice-site mutations, as well as small intragenic deletions, deep intronic variants, insertions, and large multiexon deletions (Bernard et al., 2011; Daoud et al., 2013; Gutierrez et al., 2015; Hiraide et al., 2020; La Piana et al., 2016; Potic et al., 2012; Saitsu et al., 2011; Tetreault et al., 2011; Wolf, 2014). The wide range of mutation types highlights the molecular complexity of the disease and suggests the possible need for patient- or mutation-specific therapeutic approaches.

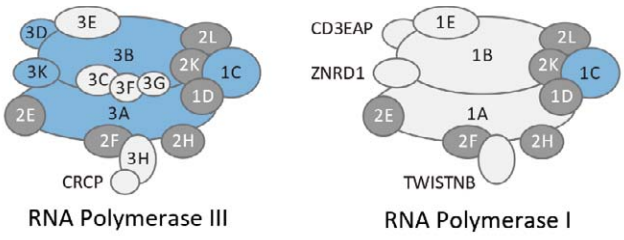

Figure 2: Schematic representation of RNA Polymerase III an I. Subunits in blue are related to 4H syndrome. Figure adapted from Thiffault et al., 2015

RNA POL III - In health

To comprehend the consequences of mutations in RNA polymerase III (Pol III) subunits, it is essential to understand its function under physiological conditions. Pol III is one of three eukaryotic RNA polymerases that transcribe DNA into RNA, each with distinct transcriptional specializations. Pol I transcribes pre-rRNAs, which are processed into the 18S, 5.8S, and 28S ribosomal RNAs (rRNAs), essential components of ribosome assembly. Pol II transcribes protein-coding genes into mRNAs and produces several regulatory RNAs, including most microRNAs (miRNAs) and long non-coding RNAs (lncRNAs). In contrast, Pol III transcribes small, highly abundant non-coding RNAs (ncRNAs), typically less than 350 nucleotides in length, that are essential for various cellular processes.

Among Pol III-transcribed transcripts are nuclear transfer RNAs (tRNAs) and 5S rRNA, which are both integral components of translation (Hoagland et al., 1958; Rosset & Monier, 1963). Ribosome binding and translation regulation are also mediated by Pol III transcripts, specifically, 7SL, BC200, snaR and Alu (Bishop et al., 1970; Houck et al., 1979; Mrazek et al., 2007; Parrott & Mathews, 2007; Watson & Sutcliffe, 1987). Other essential Pol III products are 7SK RNA, U6 and U6atac which are involved in transcription regulation and splicing (Lerner & Steitz, 1979; Zieve & Penman, 1976). Furthermore, transcripts RPPH1 and RMRP are key to tRNA and ribosomal RNA processing, while Y RNA plays a role in RNA stability, replication and translation regulation (Bartkiewicz et al., 1989; Lerner et al., 1981; Reddy et al., 1981). Also vault ribonucleoprotein (RNP) regulation of autophagy is mediated by Pol III transcript, vault RNA (Kedersha & Rome, 1986). Finally, Pol III transcript nc886 is involved in immune signalling (Mrazek et al., 2007; Nandy et al., 2009; Zhou & Van Bortle, 2023).

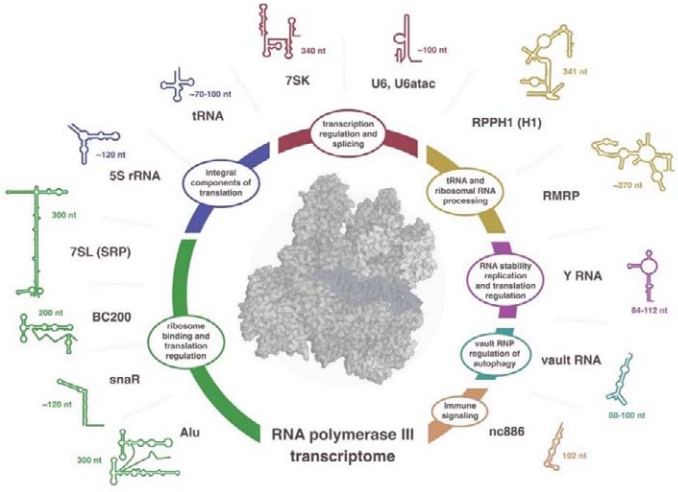

Figure 3: Overview of RNA polymerase III transcriptome. Reused from Zhou & Van Bortle, 2023

These examples illustrate that the Pol III transcriptome is extensive and supports a diverse range of fundamental cellular processes. However, it remains unclear if and how these transcripts and the processes they are involved in are affected by 4H related *POLR3* variants.

RNA POL III - In 4H leukodystrophy

The identification of the causal genes for 4H syndrome significantly improved diagnostic capabilities, yet it raised the question of how mutations in Pol III—a protein that is abundantly expressed and essential for transcription—result in this disease. Despite ongoing research, the precise mechanisms underlying the pathogenesis of 4H leukodystrophy remain unclear.

One proposed mechanism is that certain mutations disrupt the structure, complex formation, or cellular localization of Pol III. For example, mutations in *POLR1C* have been shown to impair the assembly and nuclear import of RNA Pol III (Thiffault et al., 2015). Similarly, mutations in *POLR3B* that map to conserved protein domains have been hypothesized to interfere with DNA binding, modify the catalytic cleft, or disrupt subunit interactions (Tetreault et al., 2011). Experimental studies have shown that a specific *POLR3B* variant affected complex assembly, that could be restored by riluzole administration (Pinard et al., 2022). Another *POLR3B* variant caused aberrant association of individual enzyme subunits rather than affecting overall enzyme assembly (Choquet, Pinard, et al., 2019; Djordjevic et al., 2021).

Another potential pathological mechanism in 4H involves alterations in *POLR3* gene and/or protein expression. In various samples of patients with *POLR3A* variants, amongst which fibroblasts, grey and white matter tissue, decreased Pol IIIA subunit expression has been reported (Bernard et al., 2011; Perrier, Gauquelin, et al., 2020). Similarly, a decrease in *POLR3* gene expression has been described in patients with *POLR3D* variants (Macintosh, Perrier, et al., 2023). Additionally, mutant clones harbouring 4H-related *POLR3A* variants showed reduced Pol IIIA protein and *POLR3A* mRNA levels, however this was not consistent across all clones (Choquet, Forget, et al., 2019). For *POLR3B* variants, decreased gene levels have been described as well (Mattijssen et al., 2024). The afore mentioned findings have only been reported in small cohorts, often linked to variants causing severe phenotypes. This leaves uncertainty about whether these findings are universal.

In line with molecular disruptions of the affected subunits, several studies have documented reduced Pol III transcript levels in various patient-derived samples. Studies have shown that Pol III products such as tRNAs and BC200, which are involved in translation, are dysregulated in patient-derived fibroblasts and cellular models of 4H (Choquet, Forget, et al., 2019). Similar reductions have been observed in fibroblasts from patients with POLR3K variants, where tRNAs, H1 RNA, 5S rRNA, and 7SL RNA were significantly downregulated (Dorboz et al., 2018). Reduced levels of POLR3 transcripts have also been detected in blood RNA samples from patients with *POLR3A* variants (Azmanov et al., 2016). A mouse model with *POLR3A* variants further supports this, showing reduced tRNA levels (Moir et al., 2024). It is also shown in yeast that mutations associated with 4H decrease tRNA transcription (Arimbasseri et al., 2015).

Tissue-specific vulnerability to Pol III mutations may also contribute to 4H syndrome's pathology. For instance, it is hypothesized that oligodendrocytes, which require substantial protein synthesis during myelination, might be particularly affected due to the role of Pol III transcripts in translation (Perrier, Michell-Robinson, et al., 2020). Considering that Pol III products like tRNAs, have tissue specific expression profiles makes this hypothesis even more plausible (Dittmar et al., 2006). Additionally, the introduction of a *POLR3A* variant in MO3.13 cells (human oligodendrocytes) reduced myelin basic protein (MBP) levels in these oligodendrocytes (Choquet, Forget, et al., 2019), further pointing towards oligodendrocyte vulnerability. Additional evidence is found in the fact that OPCs with decreased RNA Pol III subunit expression showed altered oligodendrocyte differentiation, maturation and myelination capacity (Macintosh, Michell-Robinson, et al., 2023). Similarly, a mouse model with *POLR3B* exon 10 deletion exhibited defects in oligodendrocyte proliferation and differentiation, supporting the role of Pol III in myelination (Michell-Robinson et al., 2023).

However, these mechanisms focus mainly on oligodendrocytes, this does not provide an explanation for 4H patients presenting mainly with neurological symptoms. An alternative hypothesis involves cell-type-specific effects mediated by alternative splicing. For instance, the intronic variant c.1771-7C>G in *POLR3A* leads to altered transcripts, including the skipping of exon 14, resulting in a premature stop codon or an in-frame deletion of exons 13 and 14 (Perrier, Gauquelin, et al., 2020) Similarly, *POLR3A* variant c.1771-6C>G is reported to result in exon 14 skip (Azmanov et al., 2016; Yoon Han et al., 2022). And also for POLR3B variants such as c.1625A>G and c.2084-6A>G, mis-splicing has been reported (Daoud et al.,

2013; Mattijssen et al., 2024). Another *POLR3*-related disorder, caused by *POLR3GL* variants, also has splicing alteration (Terhal et al., 2020).

While significant progress has been made in characterizing the molecular and cellular effects of Pol III mutations, and many hypotheses on the disease mechanisms have been formed, no treatment targets have been yet identified. Understanding why certain tissues and cell types are more severely affected in 4H will be critical to develop targeted therapeutic strategies.

CURRENT 4H DISEASE MODELS

To advance knowledge on 4H leukodystrophy, it is essential to develop robust disease models that can capture its complex cellular and molecular phenotypes, enabling the investigation of tissue-specific vulnerability and potential therapeutic targets. The field has made several efforts in this direction. Early attempts using mouse models with known 4H-associated *POLR3A* variants such as c.2015G>A (p.Gly672Glu), did however not have neurological abnormalities or Pol III transcript alterations. Additionally, Polr3a−/−null mice were embryonic lethal (Choquet et al., 2017). Similarly, a mouse model for *POLR3B* variant c.308G>A was embryonic lethal when homozygous. While a double-mutant (Polr3a$^{G672E/null}$ Polr3b$^{+/R103}$) did not show neurological or transcription abnormalities (Choquet, Pinard, et al., 2019). Recent advancements have overcome these problems, and now mouse models harbouring Polr3a and Polr3b variants are available and reflect leukodystrophy phenotypes (Merheb et al., 2021; Michell-Robinson et al., 2023; Moir et al., 2024)

These new disease models are invaluable tools to progress research on 4H leukodystrophy but the absence of phenotypes in the earlier mouse models shows that vulnerability to Pol III mutations likely varies between species, underscoring the need for human-derived models. Considering the many variants causing 4H and the broad clinical spectrum, a patient- and/or mutation-specific approach may be necessary to fully capture the complexity of the disease.

Currently, the availability of human tissue samples from individuals with 4H leukodystrophy is limited. Post-mortem tissue is scarce and typically obtained only at the end stage of the disease, providing limited insight into early disease processes and progression—key aspects for therapy development. While patient-derived fibroblasts have been used, these are not the cells that show defects in 4H. MO3.13 oligodendroglial cell models have been used in

some studies, but do not fully recapitulate the complex neurodevelopmental environment of the human brain. Therefore, more physiologically relevant models that mimic early tissue development are needed to investigate cell-specific vulnerabilities in 4H and identify early potential therapeutic targets.

HUMAN INDUCED PLURIPOTENT STEM CELLS

To overcome these limitations, human pluripotent stem cells have emerged as a powerful alternative. Pluripotent stem cells have the unique ability to self-renew and differentiate into cell types from all three germ layers: endoderm, ectoderm and mesoderm. *In vivo*, pluripotent cells are found in embryos (Thomson et al., 1998). However, by inducing the overexpression of specific transcription factors, somatic cells can be reprogrammed into a pluripotent state, creating human induced pluripotent stem cells (hiPSCs) (Takahashi et al., 2007). These hiPSCs retain the genetic profile of the donor cells and can be differentiated into virtually any cell type, making them particularly suitable for investigating the molecular and cellular mechanisms underlying 4H leukodystrophy.

The versatility of pluripotent stem cells lies in their capacity to generate virtually any cell type through directed differentiation. But now the question emerges, which tissue will be investigated?

KEY PLAYERS IN HYPOMYELINATION AND NEUROLOGICAL DEFICITS IN 4H

Identifying relevant tissues and cell types is essential for understanding the pathophysiology of 4H leukodystrophy and developing targeted therapies. Since 4H usually is characterized primarily by hypomyelination and associated neurological deficits, our focus is on modelling early brain development—the stage when many patients begin to show their first symptoms. This stage of development aligns with essential neurodevelopmental processes such as gliogenesis, myelination and refinement of synapses and circuits (Zhou et al., 2024).

The challenge, however, lies in replicating these highly dynamic processes of human brain development *in vitro*. To gain meaningful insights into 4H pathophysiology, cellular models must reflect aspects of these complex interactions while enabling the study of individual cell-type vulnerabilities. Hence, we focused on a variety of models that centre around key

brain cell types which are known to be involved in different genetic white matter disorders. The following sections provides a brief introduction to the cell lineages we aimed to investigate, and their known involvements in genetic white matter disorders.

Oligodendrocytes

The primary cells responsible for myelination are oligodendrocytes, which originate from NG2-expressing cells known as polydendrocytes or oligodendrocyte precursor cells (OPCs). Mature oligodendrocytes extend multiple protrusions that wrap around axons, forming a lipid-dense myelin sheath. This sheath enhances electrical signal conduction while also providing metabolic support, regulating ion and water homeostasis, and adapting to activity-dependent neuronal signals (Kuhn et al., 2019). Within genetic white matter disorders, some have primary myelin pathology, and hence are classified as myelin disorders (van der Knaap & Bugiani, 2017). Within these myelin disorders, three subcategories can be distinguished based on the type of myelin pathology: hypomyelination, demyelination and myelin vacuolization. An example of a hypomyelinating white matter disorder is Pelizaeus-Merzbachter disease, which is caused by variants in *PLP1*, a gene that is mainly expressed in mature oligodendrocytes (Torii et al., 2014). Metachromatic leukodystrophy (MLD) and Globoid cell leukodystrophy (GLD) also known as Krabbe disease and the cerebral form of X-linked Adrenoleukodystrophy are characterized by demyelination. Those disease are respectively caused by variants in *ASA*, *GALC* and *ABCD1* and cause pathological accumulation of respectively sulfatides and psychosine due to lysosomal storage disorders and very long chain fatty acids due to peroxisomal dysfunction (Abed Rabbo et al., 2021; Berger et al., 2014). The last category is characterized by myelin vacuolization and among this falls the leukodystrophy Canavan disease. Canavan disease is caused by *ASPA* variants a gene that codes for the substrate enzyme aspartoacylase, which hydrolyzes N-acetylaspartic acid (NAA) to acetate and aspartate (Hoshino & Kubota, 2014).

Neurons

Since oligodendrocytes myelinate neuronal axons, neurons are crucial in the mimicking of (hypo)myelination. Neurons transmit information through voltage discharges along their cell membranes. Depending on the neurotransmitters they release at the synapse, neurons are broadly divided into excitatory/glutamatergic or inhibitory/GABAergic subtypes. Certain neuronal subtypes, such as inhibitory parvalbumin-expressing neurons, are particularly likely to be myelinated (Stedehouder et al., 2017). A subclass of genetic white matter

disorders, the leuko-axonopathies, are due to defects in neuron- or axon-specific gene products or they have central disease mechanisms which can be conducted back to axons (van der Knaap & Bugiani, 2017). For example, hypomyelination with atrophy of the basal ganglia and cerebellum (H-ABC) is caused by variants in the *TUBB4A* gene, a gene coding for microtubules highly expressed in the brain (Hamilton et al., 2014). For others such as 4H leukodystrophy the affected gene is generic, but histopathology shows widespread axonal damage, pointing towards important neuroaxonal involvement. However, many end stage brain disorders involve neuronal damage without providing insight in the initial problems (Wolf, 2014).

Astrocytes

While neurons and oligodendrocytes have obvious roles in myelination, other brain cell types, such as astrocytes, also play crucial roles. Astrocytes perform various essential functions, including maintaining brain homeostasis, supporting the blood-brain barrier, and regulating neurotransmitter and lipid metabolism (Hasel et al., 2023). They are morphologically and functionally diverse, exhibiting regional differences in identity and specialization. Some genetic white matter disorders are known to be caused by variants in astrocyte-specific genes or in which astrocytes play crucial roles in the disease mechanisms and are referred to astrocytopathies (van der Knaap & Bugiani, 2017). For example, Alexander disease is a rare genetic astrocytopathy caused by variants in *GFAP*, which codes for glial fibrillary acidic protein (GFAP), an astrocyte-specific cytoskeletal intermediate filament protein (Brenner et al., 2001). For vanishing white matter (VWM) the causative gene is not astrocyte-specific but astrocytes are still central in the pathomechanisms of vanishing white matter. *In vitro* cultures have shown that VWM astrocytes secreted factors affect the oligodendrocyte lineage (Dooves et al., 2016).

Microglia

Microglia may also have an indirect role in 4H-related hypomyelination. Unlike other brain cells, microglia are thought to originate from erythro-myeloid progenitors (EMPs) in the developing yolk sac, making them of mesodermal lineage. Microglia play a dual role in immune defence and brain homeostasis by regulating neurogenesis, promoting neuronal survival, and performing synaptic pruning, thereby enhancing neural network efficiency and maturation (Paolicelli & Ferretti, 2017). Emerging research has begun to explore microglial in 4H leukodystrophy (Moir et al., 2024). Microgliopathies are observed in some white matter disorders, specifically *CSF1R*-related disorders, of which the gene is mainly expressed in

microglia, and Nasu-Hakola disease (Sasaki, 2017). But allogeneic hematopoetic stem cell transplantation (HSCT), thought to replace microglia, has been shown successful in other white matter disorders, specifically in the cerebral from of X-linked adrenoleukodystrophy, metachromatic leukodystrophy and Krabbe disease. This shows the potential involvement of microglia in more leukodystrophies and the potential of microglia as therapeutic strategy (Page et al., 2019).

The human brain comprises highly specialized cell types with diverse functions and complex interactions. Although oligodendrocytes are likely central to 4H-associated hypomyelination, it is essential to consider the broader neural network, including neurons, astrocytes, and microglia as these have proven to be deficient in other genetic white matter disorders. Understanding how these cell types interact in 4H could provide valuable insight into the mechanisms underlying 4H leukodystrophy and guide the development of therapeutic strategies.

IPSC-DERIVED MODELS FOR 4H RESEARCH

Given the limited availability of patient-derived brain tissue, human-induced pluripotent stem cells (hiPSCs) provide a valuable platform for modelling 4H leukodystrophy. Since 4H pathology originates during early brain development, our *in vitro* models focus on recapitulating key developmental stages through directed differentiation protocols. These include generating relevant brain cell types using classical patterning protocols, creating co-cultures, and establishing three-dimensional (3D) brain organoids.

Classical Patterning for Directed Differentiation

Classical patterning protocols aim to recapitulate embryonic development by exposing pluripotent stem cells to specific molecular cues that guide them toward neural fates. This method allows the generation of cell types at sequential developmental stages, reflecting the physiological processes occurring during early brain development. For example, dual SMAD inhibition using dorsomorphin and SB431542 is commonly used to promote neural lineage commitment, inducing a neuroectodermal fate that serves as a starting point for neuronal and glial cell lineages (Nadadhur et al., 2017; Shi et al., 2012). While classical patterning is slow compared to overexpression protocols it preserves the natural progression of cell maturation, making it a valuable tool for studying disorders that manifest during specific developmental stages, such as 4H (Zhang et al., 2013) (Yang et al., 2017).

Combining Cell Types: Towards More Physiological Models

To better reflect the complex, interconnected nature of the human brain, differentiated cell types can be combined into co-culture systems. This approach allows for the study of cell-cell interactions relevant to myelination and neuronal network formation. For instance, neurons and glia can be differentiated separately and later co-cultured at specific maturation stages, enabling the investigation of glial support or impairment to neuron development in 4H (Dooves et al., 2019). This strategy provides an opportunity to model disease-specific cellular interactions while maintaining experimental flexibility.

Alternatively, a more integrated approach involves generating three-dimensional (3D) brain-like structures known as organoids. These self-organizing cultures emerge from pluripotent stem cells when exposed to patterning cues that guide them toward specific brain regions (Lancaster et al., 2013). Organoids offer a more comprehensive representation of brain development, enabling multi-lineage differentiation and spatial organization. Offering a unique platform for studying complex, multi-cellular interactions in 4H leukodystrophy.

Given the importance of replicating early brain development in studying 4H leukodystrophy, this thesis employs a combination of classical patterning-based mono-cultures, co-cultures, and brain organoids. By leveraging these models, we aim to uncover how key brain cell types contribute to the disease's pathophysiology, including hypomyelination and related neurological deficits. This multi-faceted approach provides a platform not only to investigate the molecular and cellular basis but hopefully also helps to pinpoint potential therapeutic targets. Insights gained from these models could inform future treatment strategies, including gene and cell replacement therapies, and the models could be used for high-throughput drug screening for disease-modifying compounds.

BRIDGING RESEARCH TO TREATMENT DEVELOPMENT

While restorative treatments have been developed for some leukodystrophies (Krivit, 2004; Krivit et al., 1999; van den Broek et al., 2018), no such therapies currently exist for 4H. Possibly gene replacement or correction of endogenous mutations could restore Pol III function. Similarly, cell replacement therapy, involving donor cells or *ex vivo* gene-corrected cells, could replenish damaged cell populations. However, developing these therapies requires a deep understanding of which cell types are primarily affected and need to be replaced or corrected.

Less invasive treatment options such as drug therapies that target disrupted pathways could potentially slow or halt disease progression. Identifying such pathways and screening for compounds that alter the pathways requires realistic *in vitro* models that accurately replicate 4H pathology—models that are currently lacking. By establishing such models, this thesis aims to close this gap, facilitating both investigating of therapeutic targets as well as development of models that might be used in future therapeutic screening. This does not only apply to 4H, but might also be used for other leukodystrophies.

THESIS OUTLINE

In this thesis we aim to gain insight into how molecular and cellular mechanisms contribute to the pathology of 4H leukodystrophy using patient-specific iPSC-based models with the goal to facilitate development of new therapeutic strategies. To address this question and also to unravel patient-specific genetics contributing to broad clinical presentations, we used iPSC lines from patients with either *POLR3A* or *POLR3B* variants, that are exonic or intronic and which are relatively common in the 4H patient population (Figure 4).

To investigate if our findings are unique to 4H leukodystrophy or could be translated to other leukodystrophies, some studies also include iPSCs of other leukodsytrophies. Here we provide the research questions, approaches and main results of the following experimental chapters:

Chapter 2: First we explored what genes are dysregulated in brain specific cell types in 4H patient cultures using patient iPSC technology in combination with RNAseq analysis on iPSC-derived cerebellar cells. Downregulation of *ARX*, a gene involved in early brain and interneuron development gave first suggestions to further explore interneuron dysfunction in 4H leukodystrophy. In cortical neuron cultures containing both glutamatergic and GABAergic neuron populations, we confirmed the downregulation of *ARX* in 4H and a reduction in GABAergic synapses. Functional analysis by MEA further pointed towards alterations in the inhibitory neuron population. Initial analysis points to no obvious intrinsic changes in the oligodendrocyte population. Since *ARX* is an important regulator of SHH gradients, we investigated whether targeting the SHH pathway could improve 4H associated GABAergic phenotypes, but no improvements were observed in our assays. In conclusion, we identified cortical interneuron development to be affected in 4H leukodystrophy.

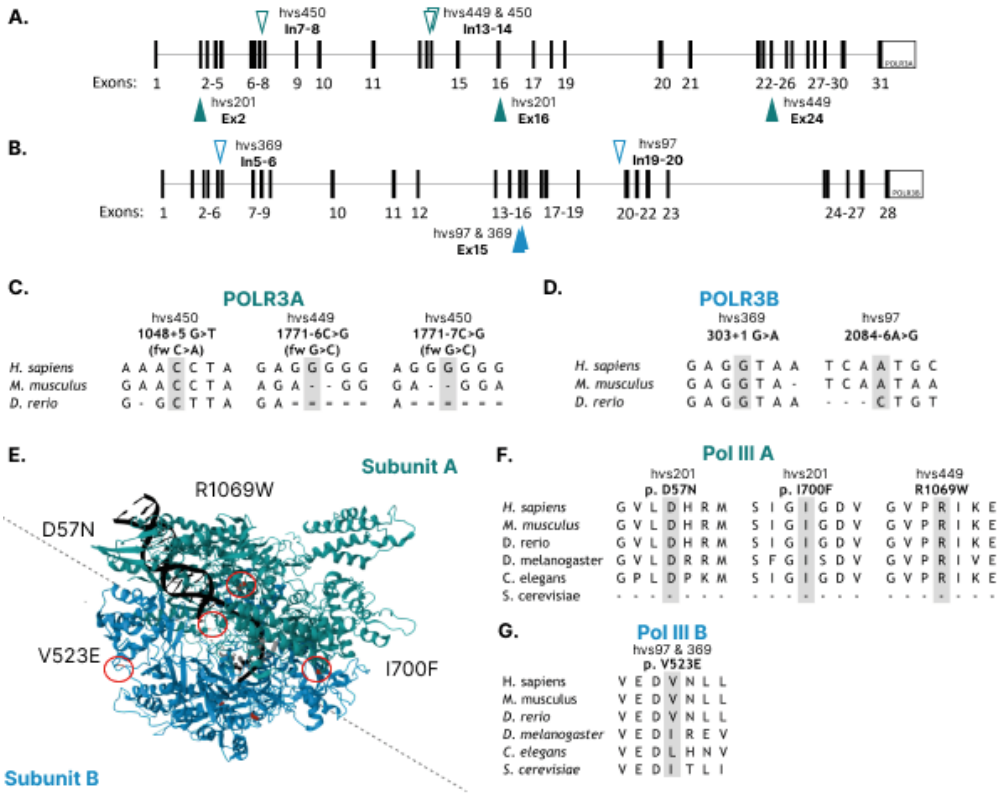

Figure 4: Overview of 4H mutations within this cohort and their evolutionary conservation. Schematic representation of mutations in 4H patient cohort in A) POLR3A gene and B) POLRB gene. Open triangles intron mutations, filled triangles exon mutations. Overview of genetic conservation for C) *POLR3A* and D) *POLR3B* intron variants. E) Reconstruction of protein Pol III A and B subunit with DNA (black) and RNA (gray), and exon mutations (red circles) according to PDB ID: 7DN3 Human RNA Polymerase III elongation complex, images created using Mol* (Li et al., 2021; Sehnal et al., 2021). Conservation of amino acid sequences per mutation in F) Pol III A and G) B subunit. Conservation according to MultiZ alignment of the UCSC Genome Browser on Human GRCh38/hg38 (Nassar et al. 2023). Species: Homo sapiens (human), Mus musculus (mouse), Danio rerio (zebrafish), Drosophila melanogaster (fruit fly), Caenorhabditis elegans (roundworm) and Saccharomyces cerevisiae (yeast). "=" means aligning species has one or more unalignable bases in the gap region, "-" no bases in the aligned species.

Chapter 3: To further explore neuronal phenotypes in 4H leukodystrophy and whether changes are disease-specific or more generally affected in leukodystrophies, we studied key phenotypic and transcriptomic differences between Ctrl, 4H and GLD neurons. By comparing neuronal changes in 4H and GLD, this chapter highlights the heterogeneity of leukodystrophies and the necessity of refining disease models. The findings underscore a

role for neuronal dysfunction in 4H, expanding the focus beyond traditional glial-centric paradigms.

Chapter 4: To study changes in neuron-glia interactions in 4H leukodystrophy and leukodystrophies in general, we developed an EU platform based on myelinating spheroids. As no existing standardized platform to investigate leukodystrophies was in place, we distributed iPSCs for the centralized generation of myelinating spheroids of GLD, CD, 4H and controls. We explored whether these 3D spheroids generate the cellular composition required for the investigation of leukodystrophies, including neurons, oligodendrocytes, and astrocytes. We confirmed relevance for investigating leukodystrophies and report differential expressed genes and significant gene sets that can guide future research directions. In conclusion, this chapter validated the potential of 3D spheroid models for studying leukodystrophies by mimicking disease-relevant cellular interactions. It emphasizes their utility in identifying cell-type-specific vulnerabilities and novel molecular targets, addressing the gap in comprehensive *in vitro* models.

Chapter 5: In the myelinating spheroids, one cell type was not included, the microglia. Hence, we generated a platform for the co-culture of iPSC-derived microglia-like cells and analysed the effect of the microglia on the neuronal cultures using cellomics and multielectrode arrays (MEA). The addition of microglia significantly impacted the cultures. ALD microglia seemed to affect axons different compared to control microglia, while 4H microglia seemed to function fine.

Chapter 6: To explore how patient-specific genetic variants affect *POLR3* gene and protein expression during neuronal lineage differentiation in 4H leukodystrophy, we examined *POLR3* expression levels, protein localization, and developmental dynamics across iPSCs, neural epithelial cells and neurons. We also evaluated whether the genetic background contributes to expression differences. This chapter integrates patient-specific data with iPSC models to elucidate disease mechanisms. By addressing genetic variability, this approach paves the way for precision medicine approaches in 4H leukodystrophy research.

Chapter 7: In this concluding chapter, we evaluate the model systems used throughout the thesis, discussing their advantages, limitations, and suitability for future leukodystrophy research. We provide an overarching synthesis of the knowledge gained from each chapter and how these findings interconnect. Additionally, we present forward-looking perspectives

on how these models could advance toward clinical trials. We explore whether the models and findings generated in this thesis could support the development of targeted therapies and inform future clinical applications.

REFERENCES

Abed Rabbo, M., Khodour, Y., Kaguni, L. S., & Stiban, J. (2021). Sphingolipid lysosomal storage diseases: from bench to bedside. *Lipids Health Dis*, *20*(1), 44. https://doi.org/10.1186/s12944-021-01466-0

Adang, L. A., Sherbini, O., Ball, L., Bloom, M., Darbari, A., Amartino, H., DiVito, D., Eichler, F., Escolar, M., Evans, S. H., Fatemi, A., Fraser, J., Hollowell, L., Jaffe, N., Joseph, C., Karpinski, M., Keller, S., Maddock, R., Mancilla, E.,…Global Leukodystrophy Initiative, C. (2017). Revised consensus statement on the preventive and symptomatic care of patients with leukodystrophies. *Mol Genet Metab*, *122*(1-2), 18-32. https://doi.org/10.1016/j.ymgme.2017.08.006

Al-Ani, A. H., Antoun, J. S., Thomson, W. M., Merriman, T. R., & Farella, M. (2017). Hypodontia: An Update on Its Etiology, Classification, and Clinical Management. *Biomed Res Int*, *2017*, 9378325. https://doi.org/10.1155/2017/9378325

Arimbasseri, A. G., Blewett, N. H., Iben, J. R., Lamichhane, T. N., Cherkasova, V., Hafner, M., & Maraia, R. J. (2015). RNA Polymerase III Output Is Functionally Linked to tRNA Dimethyl-G26 Modification. *PLoS Genet*, *11*(12), e1005671. https://doi.org/10.1371/journal.pgen.1005671

Azmanov, D. N., Siira, S. J., Chamova, T., Kaprelyan, A., Guergueltcheva, V., Shearwood, A. J., Liu, G., Morar, B., Rackham, O., Bynevelt, M., Grudkova, M., Kamenov, Z., Svechtarov, V., Tournev, I., Kalaydjieva, L., & Filipovska, A. (2016). Transcriptome-wide effects of a POLR3A gene mutation in patients with an unusual phenotype of striatal involvement. *Hum Mol Genet*, *25*(19), 4302-4314. https://doi.org/10.1093/hmg/ddw263

Bartkiewicz, M., Gold, H., & Altman, S. (1989). Identification and characterization of an RNA molecule that copurifies with RNase P activity from HeLa cells. *Genes Dev*, *3*(4), 488-499. https://doi.org/10.1101/gad.3.4.488

Berger, J., Forss-Petter, S., & Eichler, F. S. (2014). Pathophysiology of X-linked adrenoleukodystrophy. *Biochimie*, *98*(100), 135-142. https://doi.org/10.1016/j.biochi.2013.11.023

Bernard, G., Chouery, E., Putorti, M. L., Tetreault, M., Takanohashi, A., Carosso, G., Clement, I., Boespflug-Tanguy, O., Rodriguez, D., Delague, V., Abou Ghoch, J., Jalkh, N., Dorboz, I., Fribourg, S., Teichmann, M., Megarbane, A., Schiffmann, R., Vanderver, A., & Brais, B. (2011). Mutations of POLR3A encoding a catalytic subunit of RNA polymerase Pol III cause a recessive hypomyelinating leukodystrophy. *Am J Hum Genet*, *89*(3), 415-423. https://doi.org/10.1016/j.ajhg.2011.07.014

Billington, E., Bernard, G., Gibson, W., & Corenblum, B. (2015). Endocrine Aspects of 4H Leukodystrophy: A Case Report and Review of the Literature. *Case Rep Endocrinol*, *2015*, 314594. https://doi.org/10.1155/2015/314594

Bishop, J. M., Levinson, W. E., Sullivan, D., Fanshier, L., Quintrell, N., & Jackson, J. (1970). The low molecular weight RNAs of Rous sarcoma virus. II. The 7 S RNA. *Virology*, *42*(4), 927-937. https://doi.org/10.1016/0042-6822(70)90341-7

Brenner, M., Johnson, A. B., Boespflug-Tanguy, O., Rodriguez, D., Goldman, J. E., & Messing, A. (2001). Mutations in GFAP, encoding glial fibrillary acidic protein, are associated with Alexander disease. *Nat Genet*, *27*(1), 117-120. https://doi.org/10.1038/83679

Choquet, K., Forget, D., Meloche, E., Dicaire, M. J., Bernard, G., Vanderver, A., Schiffmann, R., Fabian, M. R., Teichmann, M., Coulombe, B., Brais, B., & Kleinman, C. L. (2019). Leukodystrophy-associated POLR3A mutations down-regulate the RNA polymerase III transcript and important regulatory RNA BC200. *J Biol Chem*, *294*(18), 7445-7459. https://doi.org/10.1074/jbc.RA118.006271

Choquet, K., Pinard, M., Yang, S., Moir, R. D., Poitras, C., Dicaire, M. J., Sgarioto, N., Lariviere, R., Kleinman, C. L., Willis, I. M., Gauthier, M. S., Coulombe, B., & Brais, B. (2019). The leukodystrophy mutation Polr3b R103H causes homozygote mouse embryonic lethality and impairs RNA polymerase III biogenesis. *Mol Brain*, *12*(1), 59. https://doi.org/10.1186/s13041-019-0479-7

Choquet, K., Yang, S., Moir, R. D., Forget, D., Lariviere, R., Bouchard, A., Poitras, C., Sgarioto, N., Dicaire, M. J., Noohi, F., Kennedy, T. E., Rochford, J., Bernard, G., Teichmann, M., Coulombe, B., Willis, I. M., Kleinman, C. L., & Brais, B. (2017). Absence of neurological abnormalities in mice homozygous for the Polr3a G672E hypomyelinating leukodystrophy mutation. *Mol Brain*, *10*(1), 13. https://doi.org/10.1186/s13041-017-0294-y

Daoud, H., Tetreault, M., Gibson, W., Guerrero, K., Cohen, A., Gburek-Augustat, J., Synofzik, M., Brais, B., Stevens, C. A., Sanchez-Carpintero, R., Goizet, C., Naidu, S., Vanderver, A., & Bernard, G. (2013). Mutations in POLR3A and POLR3B are a major cause of hypomyelinating leukodystrophies with or without dental abnormalities and/or hypogonadotropic hypogonadism. *J Med Genet*, *50*(3), 194-197. https://doi.org/10.1136/jmedgenet-2012-101357

DeGasperis, S. M., Bernard, G., Wolf, N. I., Miller, E., & Pohl, D. (2020). 4H leukodystrophy: Mild clinical phenotype and comorbidity with multiple sclerosis. *Neurol Genet*, *6*(2), e409. https://doi.org/10.1212/NXG.0000000000000409

Dittmar, K. A., Goodenbour, J. M., & Pan, T. (2006). Tissue-specific differences in human transfer RNA expression. *PLoS Genet*, *2*(12), e221. https://doi.org/10.1371/journal.pgen.0020221

Djordjevic, D., Pinard, M., Gauthier, M. S., Smith-Hicks, C., Hoffman, T. L., Wolf, N. I., Oegema, R., van Binsbergen, E., Baskin, B., Bernard, G., Fribourg, S., Coulombe, B., & Yoon, G. (2021). De novo variants in POLR3B cause ataxia, spasticity, and demyelinating neuropathy. *Am J Hum Genet*, *108*(1), 186-193. https://doi.org/10.1016/j.ajhg.2020.12.002

Dooves, S., Bugiani, M., Postma, N. L., Polder, E., Land, N., Horan, S. T., van Deijk, A. L., van de Kreeke, A., Jacobs, G., Vuong, C., Klooster, J., Kamermans, M., Wortel, J., Loos, M., Wisse, L. E., Scheper, G. C., Abbink, T. E., Heine, V. M., & van der Knaap, M. S. (2016). Astrocytes are central in the pathomechanisms of vanishing white matter. *J Clin Invest*, *126*(4), 1512-1524. https://doi.org/10.1172/JCI83908

Dooves, S., Nadadhur, A., Gasparotto, L., & Heine, V. (2019). Co-culture of Human Stem Cell Derived Neurons and Oligodendrocyte Progenitor Cells. *Bio-Protocol*, *9*(17). https://doi.org/10.21769/BioProtoc.3350

Dorboz, I., Dumay-Odelot, H., Boussaid, K., Bouyacoub, Y., Barreau, P., Samaan, S., Jmel, H., Eymard-Pierre, E., Cances, C., Bar, C., Poulat, A. L., Rousselle, C., Renaldo, F., Elmaleh-Berges, M., Teichmann, M., & Boespflug-Tanguy, O. (2018). Mutation in POLR3K causes hypomyelinating leukodystrophy and abnormal ribosomal RNA regulation. *Neurol Genet*, *4*(6), e289. https://doi.org/10.1212/NXG.0000000000000289

Fraietta, R., Zylberstejn, D. S., & Esteves, S. C. (2013). Hypogonadotropic hypogonadism revisited. *Clinics (Sao Paulo)*, *68 Suppl 1*(Suppl 1), 81-88. https://doi.org/10.6061/clinics/2013(sup01)09

Gauquelin, L., Cayami, F. K., Sztriha, L., Yoon, G., Tran, L. T., Guerrero, K., Hocke, F., van Spaendonk, R. M. L., Fung, E. L., D'Arrigo, S., Vasco, G., Thiffault, I., Niyazov, D. M., Person, R., Lewis, K. S., Wassmer, E., Prescott, T., Fallon, P., McEntagart, M.,…Bernard, G. (2019). Clinical spectrum of POLR3-related leukodystrophy caused by biallelic POLR1C pathogenic variants. *Neurol Genet*, *5*(6), e369. https://doi.org/10.1212/NXG.0000000000000369

Gutierrez, M., Thiffault, I., Guerrero, K., Martos-Moreno, G. A., Tran, L. T., Benko, W., van der Knaap, M. S., van Spaendonk, R. M., Wolf, N. I., & Bernard, G. (2015). Large exonic deletions in POLR3B gene cause

POLR3-related leukodystrophy. *Orphanet J Rare Dis*, *10*, 69. https://doi.org/10.1186/s13023-015-0279-9

Hamilton, E. M., Polder, E., Vanderver, A., Naidu, S., Schiffmann, R., Fisher, K., Raguz, A. B., Blumkin, L., Group, H. A. R., van Berkel, C. G., Waisfisz, Q., Simons, C., Taft, R. J., Abbink, T. E., Wolf, N. I., & van der Knaap, M. S. (2014). Hypomyelination with atrophy of the basal ganglia and cerebellum: further delineation of the phenotype and genotype-phenotype correlation. *Brain*, *137*(Pt 7), 1921-1930. https://doi.org/10.1093/brain/awu110

Harting, I., Al-Saady, M., Krageloh-Mann, I., Bley, A., Hempel, M., Bierhals, T., Karch, S., Moog, U., Bernard, G., Huntsman, R., van Spaendonk, R. M. L., Vreeburg, M., Rodriguez-Palmero, A., Pujol, A., van der Knaap, M. S., Pouwels, P. J. W., & Wolf, N. I. (2020). POLR3A variants with striatal involvement and extrapyramidal movement disorder. *Neurogenetics*, *21*(2), 121-133. https://doi.org/10.1007/s10048-019-00602-4

Hasel, P., Aisenberg, W. H., Bennett, F. C., & Liddelow, S. A. (2023). Molecular and metabolic heterogeneity of astrocytes and microglia. *Cell Metab*, *35*(4), 555-570. https://doi.org/10.1016/j.cmet.2023.03.006

Hiraide, T., Nakashima, M., Ikeda, T., Tanaka, D., Osaka, H., & Saitsu, H. (2020). Identification of a deep intronic POLR3A variant causing inclusion of a pseudoexon derived from an Alu element in Pol III-related leukodystrophy. *J Hum Genet*, *65*(10), 921-925. https://doi.org/10.1038/s10038-020-0786-y

Hoagland, M. B., Stephenson, M. L., Scott, J. F., Hecht, L. I., & Zamecnik, P. C. (1958). A soluble ribonucleic acid intermediate in protein synthesis. *J Biol Chem*, *231*(1), 241-257.

Hoshino, H., & Kubota, M. (2014). Canavan disease: clinical features and recent advances in research. *Pediatr Int*, *56*(4), 477-483. https://doi.org/10.1111/ped.12422

Houck, C. M., Rinehart, F. P., & Schmid, C. W. (1979). A ubiquitous family of repeated DNA sequences in the human genome. *J Mol Biol*, *132*(3), 289-306. https://doi.org/10.1016/0022-2836(79)90261-4

Kedersha, N. L., & Rome, L. H. (1986). Isolation and characterization of a novel ribonucleoprotein particle: large structures contain a single species of small RNA. *J Cell Biol*, *103*(3), 699-709. https://doi.org/10.1083/jcb.103.3.699

Krivit, W. (2004). Allogeneic stem cell transplantation for the treatment of lysosomal and peroxisomal metabolic diseases. *Springer Semin Immunopathol*, *26*(1-2), 119-132. https://doi.org/10.1007/s00281-004-0166-2

Krivit, W., Peters, C., & Shapiro, E. G. (1999). Bone marrow transplantation as effective treatment of central nervous system disease in globoid cell leukodystrophy, metachromatic leukodystrophy, adrenoleukodystrophy, mannosidosis, fucosidosis, aspartylglucosaminuria, Hurler, Maroteaux-Lamy, and Sly syndromes, and Gaucher disease type III. *Curr Opin Neurol*, *12*(2), 167-176. https://doi.org/10.1097/00019052-199904000-00007

Kuhn, S., Gritti, L., Crooks, D., & Dombrowski, Y. (2019). Oligodendrocytes in Development, Myelin Generation and Beyond. *Cells*, *8*(11). https://doi.org/10.3390/cells8111424

La Piana, R., Cayami, F. K., Tran, L. T., Guerrero, K., van Spaendonk, R., Õunap, K., Pajusalu, S., Haack, T., Wassmer, E., Timmann, D., Mierzewska, H., Poll-Thé, B. T., Patel, C., Cox, H., Atik, T., Onay, H., Ozkınay, F., Vanderver, A., van der Knaap, M. S.,…Bernard, G. (2016). Diffuse hypomyelination is not obligate for POLR3-related disorders. *Neurology*, *86*(17), 1622-1626.

Lancaster, M. A., Renner, M., Martin, C. A., Wenzel, D., Bicknell, L. S., Hurles, M. E., Homfray, T., Penninger, J. M., Jackson, A. P., & Knoblich, J. A. (2013). Cerebral organoids model human brain development and microcephaly. *Nature*, *501*(7467), 373-379. https://doi.org/10.1038/nature12517

Lerner, M. R., Boyle, J. A., Hardin, J. A., & Steitz, J. A. (1981). Two novel classes of small ribonucleoproteins detected by antibodies associated with lupus erythematosus. *Science*, *211*(4480), 400-402. https://doi.org/10.1126/science.6164096

Lerner, M. R., & Steitz, J. A. (1979). Antibodies to small nuclear RNAs complexed with proteins are produced by patients with systemic lupus erythematosus. *Proc Natl Acad Sci U S A*, *76*(11), 5495-5499. https://doi.org/10.1073/pnas.76.11.5495

Li, L., Yu, Z., Zhao, D., Ren, Y., Hou, H., & Xu, Y. (2021). Structure of human RNA polymerase III elongation complex. *Cell Res*, *31*(7), 791-800. https://doi.org/10.1038/s41422-021-00472-2

Macintosh, J., Michell-Robinson, M., Chen, X., & Bernard, G. (2023). Decreased RNA polymerase III subunit expression leads to defects in oligodendrocyte development. *Front Neurosci*, *17*, 1167047. https://doi.org/10.3389/fnins.2023.1167047

Macintosh, J., Perrier, S., Pinard, M., Tran, L. T., Guerrero, K., Prasad, C., Prasad, A. N., Pastinen, T., Thiffault, I., Coulombe, B., & Bernard, G. (2023). Biallelic pathogenic variants in POLR3D alter tRNA transcription and cause a hypomyelinating leukodystrophy: A case report. *Front Neurol*, *14*, 1254140. https://doi.org/10.3389/fneur.2023.1254140

Mattijssen, S., Kerkhofs, K., Stephen, J., Yang, A., Han, C. G., Tadafumi, Y., Iben, J. R., Mishra, S., Sakhawala, R. M., Ranjan, A., Gowda, M., Gahl, W. A., Gu, S., Malicdan, M. C., & Maraia, R. J. (2024). A POLR3B-variant reveals a Pol III transcriptome response dependent on La protein/SSB. *bioRxiv*. https://doi.org/10.1101/2024.02.05.577363

Merheb, E., Cui, M. H., DuBois, J. C., Branch, C. A., Gulinello, M., Shafit-Zagardo, B., Moir, R. D., & Willis, I. M. (2021). Defective myelination in an RNA polymerase III mutant leukodystrophic mouse. *Proc Natl Acad Sci U S A*, *118*(40). https://doi.org/10.1073/pnas.2024378118

Michell-Robinson, M. A., Watt, K. E. N., Grouza, V., Macintosh, J., Pinard, M., Tuznik, M., Chen, X., Darbelli, L., Wu, C. L., Perrier, S., Chitsaz, D., Uccelli, N. A., Liu, H., Cox, T. C., Muller, C. W., Kennedy, T. E., Coulombe, B., Rudko, D. A., Trainor, P. A., & Bernard, G. (2023). Hypomyelination, hypodontia and craniofacial abnormalities in a Polr3b mouse model of leukodystrophy. *Brain*, *146*(12), 5070-5085. https://doi.org/10.1093/brain/awad249

Mirchi, A., Guay, S. P., Tran, L. T., Wolf, N. I., Vanderver, A., Brais, B., Sylvain, M., Pohl, D., Rossignol, E., Saito, M., Moutton, S., Gonzalez-Gutierrez-Solana, L., Thiffault, I., Kruer, M. C., Moron, D. G., Kauffman, M., Goizet, C., Sztriha, L., Glamuzina, E.,…Bernard, G. (2023). Craniofacial features of POLR3-related leukodystrophy caused by biallelic variants in POLR3A, POLR3B and POLR1C. *J Med Genet*, *60*(10), 1026-1034. https://doi.org/10.1136/jmg-2023-109223

Moir, R. D., Merheb, E., Chitu, V., Stanley, E. R., & Willis, I. M. (2024). Molecular basis of neurodegeneration in a mouse model of Polr3-related disease. *Elife*, *13*. https://doi.org/10.7554/eLife.95314

Mrazek, J., Kreutmayer, S. B., Grasser, F. A., Polacek, N., & Huttenhofer, A. (2007). Subtractive hybridization identifies novel differentially expressed ncRNA species in EBV-infected human B cells. *Nucleic Acids Res*, *35*(10), e73. https://doi.org/10.1093/nar/gkm244

Nadadhur, A. G., Emperador Melero, J., Meijer, M., Schut, D., Jacobs, G., Li, K. W., Hjorth, J. J. J., Meredith, R. M., Toonen, R. F., Van Kesteren, R. E., Smit, A. B., Verhage, M., & Heine, V. M. (2017). Multi-level characterization of balanced inhibitory-excitatory cortical neuron network derived from human pluripotent stem cells. *PLoS One*, *12*(6), e0178533. https://doi.org/10.1371/journal.pone.0178533

Nandy, C., Mrazek, J., Stoiber, H., Grasser, F. A., Huttenhofer, A., & Polacek, N. (2009). Epstein-barr virus-induced expression of a novel human vault RNA. *J Mol Biol*, *388*(4), 776-784. https://doi.org/10.1016/j.jmb.2009.03.031

Nwatamole, B., Kundu, S., God-dowell O. Odukudu, Prava Basnet, & Mirza, L. (2024). Endocrine Care of a 19-year-old Woman With Isolated Hypogonadotropic Hypogonadism due to 4H Syndrome. In: AACE Clinical Case Reports.

Page, K. M., Stenger, E. O., Connelly, J. A., Shyr, D., West, T., Wood, S., Case, L., Kester, M., Shim, S., Hammond, L., Hammond, M., Webb, C., Biffi, A., Bambach, B., Fatemi, A., & Kurtzberg, J. (2019). Hematopoietic Stem Cell Transplantation to Treat Leukodystrophies: Clinical Practice Guidelines from the Hunter's Hope Leukodystrophy Care Network. *Biol Blood Marrow Transplant*, *25*(12), e363-e374. https://doi.org/10.1016/j.bbmt.2019.09.003

Paolicelli, R. C., & Ferretti, M. T. (2017). Function and Dysfunction of Microglia during Brain Development: Consequences for Synapses and Neural Circuits. *Front Synaptic Neurosci*, *9*, 9. https://doi.org/10.3389/fnsyn.2017.00009

Parrott, A. M., & Mathews, M. B. (2007). Novel rapidly evolving hominid RNAs bind nuclear factor 90 and display tissue-restricted distribution. *Nucleic Acids Res*, *35*(18), 6249-6258. https://doi.org/10.1093/nar/gkm668

Pelletier, F., Perrier, S., Cayami, F. K., Mirchi, A., Saikali, S., Tran, L. T., Ulrick, N., Guerrero, K., Rampakakis, E., van Spaendonk, R. M. L., Naidu, S., Pohl, D., Gibson, W. T., Demos, M., Goizet, C., Tejera-Martin, I., Potic, A., Fogel, B. L., Brais, B.,…Bernard, G. (2021). Endocrine and Growth Abnormalities in 4H Leukodystrophy Caused by Variants in POLR3A, POLR3B, and POLR1C. *J Clin Endocrinol Metab*, *106*(2), e660-e674. https://doi.org/10.1210/clinem/dgaa700

Perrier, S., Gauquelin, L., Fallet-Bianco, C., Dishop, M. K., Michell-Robinson, M. A., Tran, L. T., Guerrero, K., Darbelli, L., Srour, M., Petrecca, K., Renaud, D. L., Saito, M., Cohen, S., Leiz, S., Alhaddad, B., Haack, T. B., Tejera-Martin, I., Monton, F. I., Rodriguez-Espinosa, N.,…Bernard, G. (2020). Expanding the phenotypic and molecular spectrum of RNA polymerase III-related leukodystrophy. *Neurol Genet*, *6*(3), e425. https://doi.org/10.1212/NXG.0000000000000425

Perrier, S., Michell-Robinson, M. A., & Bernard, G. (2020). POLR3-Related Leukodystrophy: Exploring Potential Therapeutic Approaches. *Front Cell Neurosci*, *14*, 631802. https://doi.org/10.3389/fncel.2020.631802

Pinard, M., Dastpeyman, S., Poitras, C., Bernard, G., Gauthier, M. S., & Coulombe, B. (2022). Riluzole partially restores RNA polymerase III complex assembly in cells expressing the leukodystrophy-causative variant POLR3B R103H. *Mol Brain*, *15*(1), 98. https://doi.org/10.1186/s13041-022-00974-z

Potic, A., Brais, B., Choquet, K., Schiffmann, R., & Bernard, G. (2012). 4H syndrome with late-onset growth hormone deficiency caused by POLR3A mutations. *Arch Neurol*, *69*(7), 920-923. https://doi.org/10.1001/archneurol.2011.1963

Reddy, R., Li, W. Y., Henning, D., Choi, Y. C., Nohga, K., & Busch, H. (1981). Characterization and subcellular localization of 7-8 S RNAs of Novikoff hepatoma. *J Biol Chem*, *256*(16), 8452-8457.

Richards, M. R., Plummer, L., Chan, Y. M., Lippincott, M. F., Quinton, R., Kumanov, P., & Seminara, S. B. (2017). Phenotypic spectrum of POLR3B mutations: isolated hypogonadotropic hypogonadism without neurological or dental anomalies. *J Med Genet*, *54*(1), 19-25. https://doi.org/10.1136/jmedgenet-2016-104064

Rosset, R., & Monier, R. (1963). [Apropos of the presence of weak molecular weight RNA in the ribosomes of Escherichia Coli]. *Biochim Biophys Acta*, *68*, 653-656. https://doi.org/10.1016/0006-3002(63)90199-9

Saitsu, H., Osaka, H., Sasaki, M., Takanashi, J., Hamada, K., Yamashita, A., Shibayama, H., Shiina, M., Kondo, Y., Nishiyama, K., Tsurusaki, Y., Miyake, N., Doi, H., Ogata, K., Inoue, K., & Matsumoto, N. (2011). Mutations in POLR3A and POLR3B encoding RNA Polymerase III subunits cause an autosomal-

recessive hypomyelinating leukoencephalopathy. *Am J Hum Genet*, *89*(5), 644-651. https://doi.org/10.1016/j.ajhg.2011.10.003

Sasaki, A. (2017). Microglia and brain macrophages: An update. *Neuropathology*, *37*(5), 452-464. https://doi.org/10.1111/neup.12354

Schmidt, J. L., Pizzino, A., Nicholl, J., Foley, A., Wang, Y., Rosenfeld, J. A., Mighion, L., Bean, L., da Silva, C., Cho, M. T., Truty, R., Garcia, J., Speare, V., Blanco, K., Powis, Z., Hobson, G. M., Kirwin, S., Krock, B., Lee, H.,…Vanderver, A. (2020). Estimating the relative frequency of leukodystrophies and recommendations for carrier screening in the era of next-generation sequencing. *Am J Med Genet A*, *182*(8), 1906-1912. https://doi.org/10.1002/ajmg.a.61641

Sehnal, D., Bittrich, S., Deshpande, M., Svobodova, R., Berka, K., Bazgier, V., Velankar, S., Burley, S. K., Koca, J., & Rose, A. S. (2021). Mol* Viewer: modern web app for 3D visualization and analysis of large biomolecular structures. *Nucleic Acids Res*, *49*(W1), W431-W437. https://doi.org/10.1093/nar/gkab314

Shi, Y., Kirwan, P., & Livesey, F. J. (2012). Directed differentiation of human pluripotent stem cells to cerebral cortex neurons and neural networks. *Nat Protoc*, *7*(10), 1836-1846. https://doi.org/10.1038/nprot.2012.116

Stedehouder, J., Couey, J. J., Brizee, D., Hosseini, B., Slotman, J. A., Dirven, C. M. F., Shpak, G., Houtsmuller, A. B., & Kushner, S. A. (2017). Fast-spiking Parvalbumin Interneurons are Frequently Myelinated in the Cerebral Cortex of Mice and Humans. *Cereb Cortex*, *27*(10), 5001-5013. https://doi.org/10.1093/cercor/bhx203

Takahashi, K., Tanabe, K., Ohnuki, M., Narita, M., Ichisaka, T., Tomoda, K., & Yamanaka, S. (2007). Induction of pluripotent stem cells from adult human fibroblasts by defined factors. *Cell*, *131*(5), 861-872. https://doi.org/10.1016/j.cell.2007.11.019

Takanashi, J., Osaka, H., Saitsu, H., Sasaki, M., Mori, H., Shibayama, H., Tanaka, M., Nomura, Y., Terao, Y., Inoue, K., Matsumoto, N., & Barkovich, A. J. (2014). Different patterns of cerebellar abnormality and hypomyelination between POLR3A and POLR3B mutations. *Brain Dev*, *36*(3), 259-263. https://doi.org/10.1016/j.braindev.2013.03.006

Terhal, P. A., Vlaar, J. M., Middelkamp, S., Nievelstein, R. A. J., Nikkels, P. G. J., Ross, J., Creton, M., Bos, J. W., Voskuil-Kerkhof, E. S. M., Cuppen, E., Knoers, N., & van Gassen, K. L. I. (2020). Biallelic variants in POLR3GL cause endosteal hyperostosis and oligodontia. *Eur J Hum Genet*, *28*(1), 31-39. https://doi.org/10.1038/s41431-019-0427-0

Tetreault, M., Choquet, K., Orcesi, S., Tonduti, D., Balottin, U., Teichmann, M., Fribourg, S., Schiffmann, R., Brais, B., Vanderver, A., & Bernard, G. (2011). Recessive mutations in POLR3B, encoding the second largest subunit of Pol III, cause a rare hypomyelinating leukodystrophy. *Am J Hum Genet*, *89*(5), 652-655. https://doi.org/10.1016/j.ajhg.2011.10.006

Thiffault, I., Wolf, N. I., Forget, D., Guerrero, K., Tran, L. T., Choquet, K., Lavallee-Adam, M., Poitras, C., Brais, B., Yoon, G., Sztriha, L., Webster, R. I., Timmann, D., van de Warrenburg, B. P., Seeger, J., Zimmermann, A., Mate, A., Goizet, C., Fung, E.,…Bernard, G. (2015). Recessive mutations in POLR1C cause a leukodystrophy by impairing biogenesis of RNA polymerase III. *Nat Commun*, *6*, 7623. https://doi.org/10.1038/ncomms8623

Thomson, J. A., Itskovitz-Eldor, J., Shapiro, S. S., Waknitz, M. A., Swiergiel, J. J., Marshall, V. S., & Jones, J. M. (1998). Embryonic Stem Cell Lines Derived from Human Blastocysts. *Science*, *282*(5391), 1145-1147. https://doi.org/10.1126/science.282.5391.1145

Timmons, M., Tsokos, M., Asab, M. A., Seminara, S. B., Zirzow, G. C., Kaneski, C. R., Heiss, J. D., van der Knaap, M. S., Vanier, M. T., Schiffmann, R., & Wong, K. (2006). Peripheral and central hypomyelination with hypogonadotropic hypogonadism and hypodontia. *Neurology*, *67*(11), 2066-2069. https://doi.org/10.1212/01.wnl.0000247666.28904.35

Torii, T., Miyamoto, Y., Yamauchi, J., & Tanoue, A. (2014). Pelizaeus-Merzbacher disease: cellular pathogenesis and pharmacologic therapy. *Pediatr Int*, *56*(5), 659-666. https://doi.org/10.1111/ped.12450

van den Broek, B. T. A., Page, K., Paviglianiti, A., Hol, J., Allewelt, H., Volt, F., Michel, G., Diaz, M. A., Bordon, V., O'Brien, T., Shaw, P. J., Kenzey, C., Al-Seraihy, A., van Hasselt, P. M., Gennery, A. R., Gluckman, E., Rocha, V., Ruggeri, A., Kurtzberg, J., & Boelens, J. J. (2018). Early and late outcomes after cord blood transplantation for pediatric patients with inherited leukodystrophies. *Blood Adv*, *2*(1), 49-60. https://doi.org/10.1182/bloodadvances.2017010645

van der Knaap, M. S., & Bugiani, M. (2017). Leukodystrophies: a proposed classification system based on pathological changes and pathogenetic mechanisms. *Acta Neuropathol*, *134*(3), 351-382. https://doi.org/10.1007/s00401-017-1739-1

van der Knaap, M. S., Schiffmann, R., Mochel, F., & Wolf, N. I. (2019). Diagnosis, prognosis, and treatment of leukodystrophies. *The Lancet Neurology*, *18*(10), 962-972. https://doi.org/10.1016/s1474-4422(19)30143-7

Watson, J. B., & Sutcliffe, J. G. (1987). Primate brain-specific cytoplasmic transcript of the Alu repeat family. *Mol Cell Biol*, *7*(9), 3324-3327. https://doi.org/10.1128/mcb.7.9.3324-3327.1987

Wolf, N. I. (2014). Clinical spectrum of 4H leukodystrophy caused by POLR3A and POLR3B mutations. *Neurology*, *83*, 1898-1905. https://doi.org/10.1212/WNL.0000000000001002

Wolf, N. I., Ffrench-Constant, C., & van der Knaap, M. S. (2021). Hypomyelinating leukodystrophies - unravelling myelin biology. *Nat Rev Neurol*, *17*(2), 88-103. https://doi.org/10.1038/s41582-020-00432-1

Wolf, N. I., Harting, I., Boltshauser, E., Wiegand, G., Koch, M. J., Schmitt-Mechelke, T., Martin, E., Zschocke, J., Uhlenberg, B., Hoffmann, G. F., Weber, L., Ebinger, F., & Rating, D. (2005). Leukoencephalopathy with ataxia, hypodontia, and hypomyelination. *Neurology*, *64*(8), 1461-1464. https://doi.org/10.1212/01.WNL.0000158615.56071.E3

Wolf, N. I., Harting, I., Innes, A. M., Patzer, S., Zeitler, P., Schneider, A., Wolff, A., Baier, K., Zschocke, J., Ebinger, F., Boltshauser, E., & Rating, D. (2007). Ataxia, delayed dentition and hypomyelination: a novel leukoencephalopathy. *Neuropediatrics*, *38*(2), 64-70. https://doi.org/10.1055/s-2007-985137

Yang, N., Chanda, S., Marro, S., Ng, Y. H., Janas, J. A., Haag, D., Ang, C. E., Tang, Y., Flores, Q., Mall, M., Wapinski, O., Li, M., Ahlenius, H., Rubenstein, J. L., Chang, H. Y., Buylla, A. A., Sudhof, T. C., & Wernig, M. (2017). Generation of pure GABAergic neurons by transcription factor programming. *Nat Methods*, *14*(6), 621-628. https://doi.org/10.1038/nmeth.4291

Yoon Han, J., Gon Cho, Y., Park, J., & Jang, W. (2022). A novel variant of the POLR3A gene in a patient with hypomyelinating POLR3-related leukodystrophy. *Clin Chim Acta*, *533*, 15-21. https://doi.org/10.1016/j.cca.2022.06.007

Zhang, Y., Pak, C., Han, Y., Ahlenius, H., Zhang, Z., Chanda, S., Marro, S., Patzke, C., Acuna, C., Covy, J., Xu, W., Yang, N., Danko, T., Chen, L., Wernig, M., & Sudhof, T. C. (2013). Rapid single-step induction of functional neurons from human pluripotent stem cells. *Neuron*, *78*(5), 785-798. https://doi.org/10.1016/j.neuron.2013.05.029

Zhou, S., & Van Bortle, K. (2023). The Pol III transcriptome: Basic features, recurrent patterns, and emerging roles in cancer. *Wiley Interdiscip Rev RNA*, *14*(5), e1782. https://doi.org/10.1002/wrna.1782

Zhou, Y., Song, H., & Ming, G. L. (2024). Genetics of human brain development. *Nat Rev Genet*, *25*(1), 26-45. https://doi.org/10.1038/s41576-023-00626-5

Zieve, G., & Penman, S. (1976). Small RNA species of the HeLa cell: metabolism and subcellular localization. *Cell*, *8*(1), 19-31. https://doi.org/10.1016/0092-8674(76)90181-1

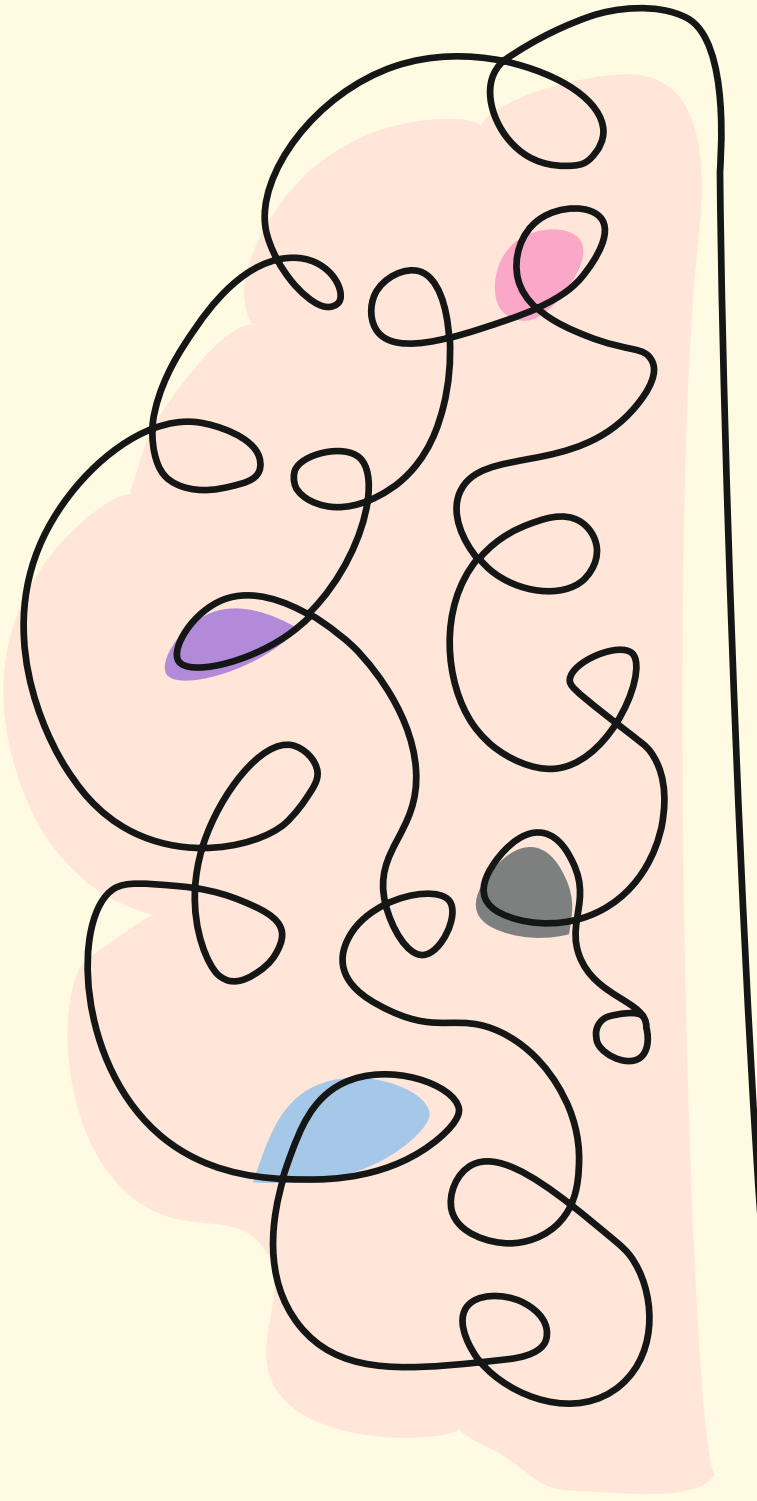

02

Cortical interneuron development is affected in 4H leukodystrophy

Stephanie Dooves, Liza M L Kok, Dwayne B Holmes, Nicole Breeuwsma, Marjolein Breur, Marianna Bugiani, Nicole I Wolf, Vivi M Heine

Brain, 2023

Corrections to this published article are being made because of unconfirmed mutations in one 4H line. However, removal of this line did not change conclusions.

ABSTRACT

4H leukodystrophy is a rare genetic disorder classically characterized by hypomyelination, hypodontia and hypogonadotropic hypogonadism. With the discovery that 4H is caused by mutations that affect RNA polymerase III, mainly involved in the transcription of small non-coding RNAs, also patients with atypical presentations with mainly a neuronal phenotype were identified. Pathomechanisms of 4H brain abnormalities are still unknown and research is hampered by a lack of preclinical models. We aimed to identify cells and pathways that are affected by 4H mutations using induced pluripotent stem cell models.

RNA sequencing analysis on induced pluripotent stem cell-derived cerebellar cells revealed several differentially expressed genes between 4H patients and control samples, including reduced *ARX* expression. As *ARX* is involved in early brain and interneuron development, we studied and confirmed interneuron changes in primary tissue of 4H patients. Subsequently, we studied interneuron changes in more depth and analyzed induced pluripotent stem cell-derived cortical neuron cultures for changes in neuronal morphology, synaptic balance, network activity and myelination. We showed a decreased percentage of GABAergic synapses in 4H, which correlated to increased neuronal network activity. Treatment of cultures with GABA antagonists led to a significant increase in neuronal network activity in control cells but not in 4H cells, also pointing to lack of inhibitory activity in 4H. Myelination and oligodendrocyte maturation in cultures with 4H neurons was normal, and treatment with sonic hedgehog agonist SAG did not improve 4H related neuronal phenotypes. qPCR analysis revealed increased expression of parvalbumin interneuron marker *ERBB4*, suggesting that the development rather than generation of interneurons may be affected in 4H.

Together, these results indicate that interneurons are involved, possibly parvalbumin interneurons, in disease mechanisms of 4H leukodystrophy.

INTRODUCTION

Leukodystrophies are genetic disorders characterized by primary brain white matter involvement. In children, leukodystrophies are often progressive and can lead to early death (van der Knaap et al., 2019). Until several years ago, up to half of patients with leukodystrophies did not receive a genetic diagnosis. Since, developments in next generation sequencing techniques have led to the rapid identification of gene mutations underlying different childhood leukodystrophies, such as *de novo* mutations in structural genes, e.g. TUBB4A, in hypomyelination with atrophy of the basal ganglia and cerebellum (OMIM 612438) or mutations in genes encoding proteins essential for translation, e.g. DARS (OMIM 615281) or RARS (OMIM 616140) in hypomyelinating leukodystrophies (Simons et al., 2013; Taft et al., 2013; Wolf et al., 2021; Wolf, Salomons, et al., 2014). Insights into genetic causes allowed incredible progress in diagnostics, but our understanding of the mechanisms responsible for disease pathology is still lacking (Helman et al., 2015; van der Knaap et al., 2016).

One of the more prevalent leukodystrophies is 4H syndrome (OMIM 612440), originally characterized by hypomyelination, hypogonadotropic hypogonadism, and hypodontia (Schmidt et al., 2020; Vanderver et al., 2013; Wolf, Vanderver, et al., 2014). Other characteristics are cerebellar atrophy and myopia. Epilepsy has been described in some patients. Whole exome sequencing has revealed that 4H leukodystrophy is caused by abnormal RNA polymerase III (POLR3), and so far variants in genes encoding different POLR3 subunits, *POLR3A*, *POLR3B*, *POLR1C* and *POLR3K*, have been identified (Bernard et al., 2011; Dorboz et al., 2018; Tetreault et al., 2011; Thiffault et al., 2015). POLR3 is responsible for the transcription of many different classes of non-protein coding (nc) RNAs, with diverse biological functions, such as transfer (t), ribosomal (r), small nuclear (sn), small nucleolar (sno) and micro (mi) RNAs (Dieci et al., 2007). Given the variety of 4H presentations and the diverse regulatory functions of POLR3 genes, there are many potential pathways and tissue-types to research. Interestingly, some POLR3 mutations do not lead to classic brain white matter defects associated with 4H, but rather show a predominant neuronal phenotype with involvement of the basal ganglia (Harting et al., 2020; La Piana et al., 2016; Wolf, Vanderver, et al., 2014). So, while 4H was originally described as a typical hypomyelinating disorder, it suggests that POLR3 variants could also primarily affect neuronal populations.

The generation of induced pluripotent stem cells (iPSCs) from patient tissue allows for patient-specific disease models starting from early embryonic stage (Takahashi et al., 2007),

and therefore provide a promising tool to study rare diseases like 4H leukodystrophy. To get insight into disease mechanisms and identify genes that are dysregulated by 4H mutations, we generated patient iPSC-derived cerebellar and cortical cell populations, including neuron-oligodendrocyte co-cultures and studied them by transcriptome, cellomics and multi-electrode array (MEA) analysis. In patient iPSC-derived cerebellar neurons we found a significantly lower expression of *ARX*, which is involved in early brain development and severe infantile-onset encephalopathies (Shoubridge et al., 2010). As *ARX* is associated with cortical interneuron development, we performed immunohistochemistry for GAD65/67 on patient material and confirmed alterations in inhibitory neurons in 4H. So, we decided to study the development of cortical neurons in more depth. Indeed, the number of GABAergic synapses was significantly decreased in 4H neuronal cultures, which correlated to an increased neuronal network activity. To further identify the specific subtypes that are affected in 4H, qPCR analysis for the major cortical interneuron populations was performed. Interestingly, the expression of *ERBB4*, important for the development of parvalbumin (PV) interneurons, was significantly increased in 4H neurons. Together, our results show that cortical interneuron development is affected in 4H patients, possibly due to pathway changes involving *ARX* that may affect development of parvalbumin interneurons.

MATERIAL AND METHODS

Patient consent

The Institutional Research Board of the VU University Medical Center approved the study, and written consent was obtained from all participants in accordance with the Declaration of Helsinki.

iPSC culture

Fibroblasts from anonymous donors and 4H patients were reprogrammed into iPSC lines as described previously (Holmes & Heine, 2017a). Briefly, iPSCs were generated using an overexpression of *OCT4*, *SOX2*, *KLF4*, and *C-MYC*. iPSC lines were confirmed for pluripotency by ICC, PCR, alkaline phosphatase, embryoid body formation assay, karyotyping and/or a pluritest. Human embryonic stem cell line H01 was obtained from WiCELL and used as a control line for RNA sequencing experiments. See Supplementary Table 1 for an overview of the iPSC lines. Control and 4H iPSCs were maintained on a vitronectin coating in TeSR E8 medium. Medium was refreshed daily, and cells were passaged once a week using Gentle Cell Dissociation reagent (StemCell Technologies) according to manufacturer's protocol. Cells were split 1:10-1:50 to a new well for further maintenance.

Differentiation in neural cells

Differentiation into cerebellar granule cell neurons was done using a previously reported protocol, involving minimal factors in an N2+B27 neural maintenance medium (NMM), modified for a two-dimensional monolayer culture (Holmes & Heine, 2017a, 2017b).

Cortical neuron differentiation was performed as previously described (Nadadhur et al., 2017) using dual SMAD inhibition and consequent maturation of cells into glutamatergic and GABAergic neurons. For myelinating cultures, human iPSCs were differentiated into glial progenitor cells as previously described (Dooves et al., 2019). To start a co-culture, day 18 cortical neurons were plated on a monolayer of rat astrocytes and matured for ~2 weeks, after which iPSC-derived glial progenitor cells were added to the culture.

See supplementary method section for more details.

RNA sequencing

Total RNA was isolated from cells using TRIzol and chloroform-isopropanol extraction. After quality control samples were run on an Illumina HiSeq2500 according to manufacturer's protocol. Sequencing reads were aligned to Humane Genome hg38. Similarity between fibroblast, iPSC and cerebellar cells was analysed, and the data of iPSC and cerebellar cells were compared to previously published gene expression profiles of 2 iPS cells and 2 granule cells. Differentially expressed genes (DEG) between 4H and control were determined with DESeq2 package in R. See supplementary methods for more details.

qPCR

For quantitative PCR (qPCR) analysis RNA was isolated from neurons using TRIzol-chloroform isolation. After production of cDNA, a qPCR was performed using SYBR green according to manufacturer's protocol. For DEG analysis, data was normalized for housekeeping gene *EIF4G2*. For interneuron subtype analysis, data was normalized for housekeeping gene *EIF4G2* and general neuronal marker *NEUN*. See Supplementary Table 2 for an overview of the primers used. From the results the fold change $2^{-\Delta\Delta CT}$ values were calculated, and the log fold change was used for statistical analysis. Data is shown as relative expression compared to day 30 control neurons.

Immunostaining

Cells were fixed for immunostaining using either 4% PFA or methanol:acetone fixation. Primary antibodies (Supplementary Table 3) were incubated overnight, followed by 2-hour incubation with secondary antibody and embedding with Fluoromount G.

Cortical tissue was obtained from a control (F, 7mo, cause of death: hypoxic ischemic encephalopathy) and two 4H patients (Patient 1: F, 16y, homozygous for a POLR3A variant with comparable signs as donor for iPSC line P4; Patient 2: M, 0y, homozygous POLR3A variant with a severe prenatal presentation) with informed consent of the family. The tissue of Patient 1 was obtained at autopsy at the Erasmus Medical Center Rotterdam, The Netherlands. The tissue was formalin-fixed paraffin-embedded and staining was done on 5 µm-thick sections. Staining was developed with 3,3′-diaminobenzidine (DAB, 1:50, DAKO) and counterstained with haematoxylin.

See supplementary methods for more details about immunostainings.

SAG treatment

Smoothened agonist (SAG; Cayman Chemical) was dissolved in DMSO to a stock concentration of 100 µM. In a pilot experiment 1 line of control and 1 line of 4H neurons were treated with 3 nM, 50 nM, 100 nM or 250 nM SAG either starting from day 18 or day 30 on. Based on the pilot experiment a concentration of 100 nM SAG was chosen, with treatment starting from day 18 until the endpoint of the experiment. SAG or vehicle (1:1000 DMSO) was added twice a week with the medium refreshment.

Multi electrode array

Neuronal activity was measured on 24 well multi-electrode array (MEA) plates (Multi Channel Systems 24W300/30G-288). Cultures were measured weekly for 30 minutes, after which data was analysed with Multiwell-Analyzer software (Multichannel Systems) to determine spike count, burst count and network burst counts from raw data. See supplementary methods for more details.

Statistical analysis

All experiments were repeated on at least 2-3 independent cell batches per patient, and the results of those experiments were averaged to obtain one value per iPSC line. MEA data was

collected on 1 batch of neurons per cell line. All analyses were either done automated or blinded. Neuronal morphology, myelination and the number of GAD65/67$^+$, CTIP2$^+$, OLIG2$^+$ and MBP$^+$ cells were analysed using Columbus software (Perkin Elmer). Synaptic analyses and the percentage of myelinated axons were determined in ImageJ (imagej.nih.gov/ij) using the NeuronJ and SynaptoCount plugins (Supplementary Methods). Statistical analyses were done in IBM SPSS statistics software version 26 (IBM). Data was tested for normality with a Shapiro-Wilk test. Significance was tested with independent samples t-tests (for parametric data) or a Mann-Whitney U test (for non-parametric data). To compare the effect of compounds on MEA data or the effect of SAG treatment paired samples t-test or Wilcoxon signed rank tests were used. All statistical tests were two-tailed and tested against alpha-level $P < 0.05$.

Data availability

The authors confirm that the data supporting the findings of this study are available within the article and its supplementary material.

RESULTS

In vitro products present with iPSC and cerebellar cell identity

As 4H patients with *POLR3B* variants often have cerebellar atrophy, we differentiated iPSCs into cerebellar neurons as described previously (Holmes & Heine, 2017b). We first wanted to establish that reprogramming and differentiation products derived from patient and control fibroblasts were unique cell populations, with relatively little variation due to source material. Further, we tested the validity of the reprogramming protocols by estimating how close each derived cell type resembled published expression profiles. To investigate sample similarity, t-Distributed Stochastic Neighbor Embedding (t-SNE) was performed with perplexity at 5. Cluster analysis showed that samples group together based on cell types (fibroblast, iPSC, product) regardless of cell source (patient or control) (Fig. 1A). The relatively high similarity of samples from the same cell type, regardless of their source, suggests that reprogramming methods were effective at generating a consistent cell type.

To estimate the accuracy of cell reprogramming, pair-wise Spearman's rank correlations were computed for 23 samples from this study and two expression profiles obtained from ENCODE. One was an ENCODE iPSC expression profile (ENCSR722POQ) and the other an ENCODE granule cell expression profile (ENCSR313IUO), both containing two biological

replicates (Fig. 1B). Hierarchical clustering showed that samples in both analyses group by cell type. Colour coding indicates that iPSCs and cerebellar cells are more closely related to the relevant ENCODE profiles, than the other cell types (iPSCs = $P < 0.001$; cerebellar cells = $P < 0.001$). Taken together, fibroblast-derived iPSCs and PSC-derived cerebellar cells can be treated as relevant representatives of those developmental stages/lineages for further analyses.

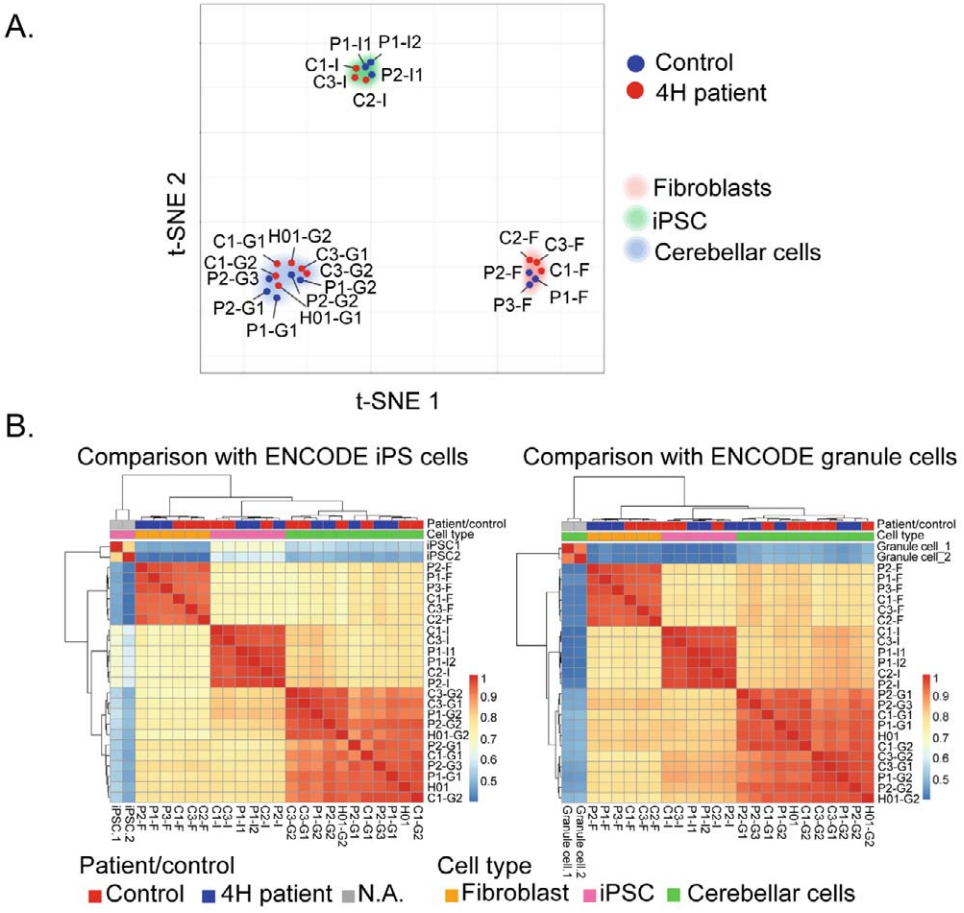

Figure 1. Reprogramming and differentiation leads to distinct cell types. (**A**) shows the projection of 23 samples in 2-dimensional space. Each dot represents a sample that is labelled according to patient/control status. Samples are positioned based on relative similarity, showing that fibroblasts, iPSCs and cerebellar cells cluster together. (**B**) Heat maps of the comparison of expression profiles with ENCODE iPSC and granule cell samples. The heat map represents Spearman's rank correlation coefficient. Patient/control status and cell types are indicated at the *top* of the heat map. C = control; F = fibroblast; G = cerebellar granule cell; I = iPSC; P = patient.

Transcriptome analysis revealed 4H-associated changes in gene expression

RNA sequencing analysis showed several DEGs between 4H patients and controls. In fibroblasts, 29 genes showed a significantly altered expression (Supplementary Table 4), while in iPSCs 20 genes were differentially regulated (Fig. 2A, Supplementary Table 5). Notable DEGs that were downregulated in 4H iPSCs include several genes involved in neural development (*OTX2*, *NPTX1*, *SLITRK6*, *SEMA6A*) and a downregulation of *TMEM64* that plays a role in osteoclast differentiation (Boles et al., 2014; Kim et al., 2013; Mitsogiannis et al., 2017; Mortensen et al., 2015; Sandberg et al., 2014).

In 4H cerebellar cells, 16 genes showed a significant differential expression (Fig. 2B, Supplementary Table 6). 4H cerebellar cells showed an increased expression of *PDPR*, which is associated with intellectual disability (Bruno et al., 2021) and an increased expression of *CBLN1*, a cerebellum-specific precursor protein (Hirai et al., 2005). The downregulation of *ARX* appears to be a potentially significant discovery. *ARX* mutations are associated with several brain disorders, and *ARX* loss of function is associated with abnormal cortical interneuron development and migration (Gecz et al., 2006; Kitamura et al., 2002; Marsh et al., 2016; Sherr, 2003).

Cortical interneuron changes in 4H

We studied whether the decreased *ARX* expression point to cortical interneuron involvement in 4H. iPSCs were differentiated into cortical neurons, i.e. a mixture of GABAergic interneurons and glutamatergic cortical projection neurons, according to previously established protocols (Nadadhur et al., 2017). At this stage, we were able to include 3 additional iPSC lines of *POLR3A* patients (P4-P6, Supplementary Table 1). At a neuronal precursor cell state, cells were harvested for RNA analysis. A selected number of DEGs from the cerebellar cells were tested on immature (day 18) neurons of 4H and controls. No differences in expression levels of *PDPR*, *ITGA11* or *MACIR* (not shown) were observed (Fig. 3A-B). Consistent with the cerebellar cells, *ARX* expression was decreased in neurons of 4H patients (control 1.08 ± 0.31, 4H 0.26 ± 0.10, $t(6) = 12.073$, $P < 0.001$, Fig. 3C), confirming that *ARX* dysregulation may be a common feature in 4H.

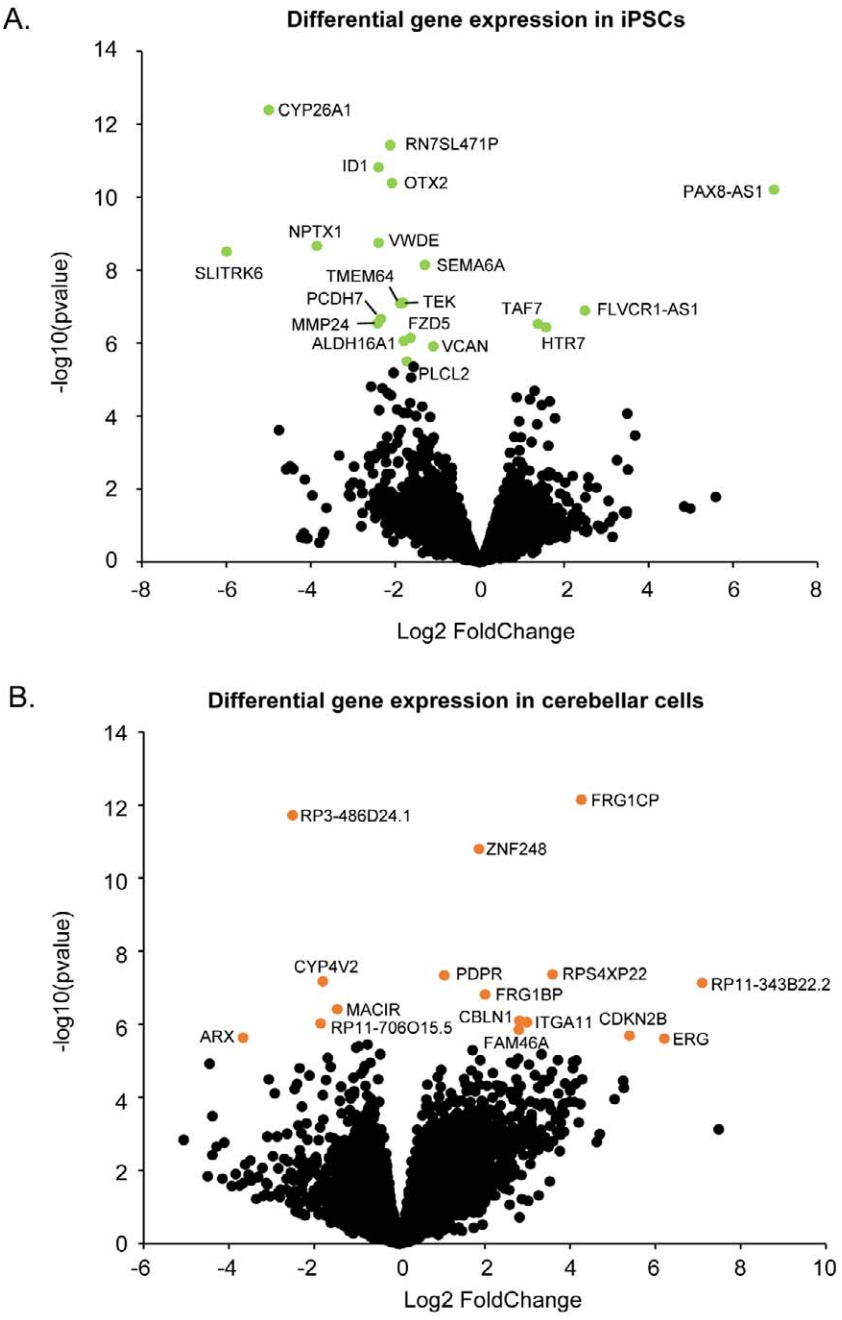

Figure 2. Differential gene expression reveals genes involved in neurodevelopment (**A**) shows a volcano plot of the RNA sequencing data on patient and control iPSCs. DEGs are visualized by a lighter (green) dot and gene label. (**B**) Volcano plot showing DEGs in 4H cerebellar cells. The significant DEGs are indicated with a lighter (orange) dot and gene label.

To confirm that cortical interneurons are affected in primary brain tissue of 4H patients, we studied patient tissue for expression of GAD65/67, a pan GABAergic marker widely used to visualize all inhibitory neurons. Patient tissue showed elevated immunoreactivity for GAD65/67 compared to control, strengthening the hypothesis that cortical interneuron populations are affected in 4H (control 6% of 1315 cells; 4H patient 1 42% of 787 cells; 4H patient 2 36% of 1656 cells; Fig. 3D-E). As patient tissue is extremely scarce and iPSC-based model systems present differential gene expression in 4H cells, we continued functional analysis in iPSC-derived cortical cultures.

The amounts of GABAergic and glutamatergic cells were analysed with staining for GAD65/67 at 5, 10 and 14 weeks post plating of day 18 cortical neurons. No changes in the percentages of GABAergic or glutamatergic cells were observed in 4H cultures (Fig. 3F). To test whether there are differences in neuronal maturity, the neurons were stained for CTIP2, which is expressed in interneurons and projection neurons during fetal development (Chen et al., 2008; Saito et al., 2011). There was an increase in $CTIP2^{+}$ cells in 4H neurons at 14 weeks post plating, which was significant for the interneuron portion (i.e. $CTIP2^{+}GAD65/67^{+}$ cells; control 13.3 ± 2.32, 4H 26.2 ± 13.59, Z = -2.13, P = .033, Fig. 3G), but not for the glutamatergic portion (i.e. $CTIP2^{+}GAD65/67^{-}$ cells; control 6.2 ± 2.71, 4H 9.35 ± 4.19). The decrease in *ARX* expression, increased GAD65/67 immunoreactivity in 4H patient tissue and sustained CTIP2 positivity in iPSC-derived GABAergic cells together suggests altered interneuron development in 4H.

4H neurons show a decreased generation of GABAergic synapses

To investigate how cortical neuron development is affected in 4H, cortical neuronal cultures were matured and analysed for morphology changes (Fig. 4). Morphology of 4H and control neurons was analysed on dendritic (MAP2) and axonal (NF-200) staining with automated morphology analysis using Columbus software (Perkin Elmer). The measured parameters included axonal and dendritic length, branching level, and number of extremities and roots. No significant change in any parameter for neuronal morphology was observed between 4H and control neurons (Fig. 4A-C).

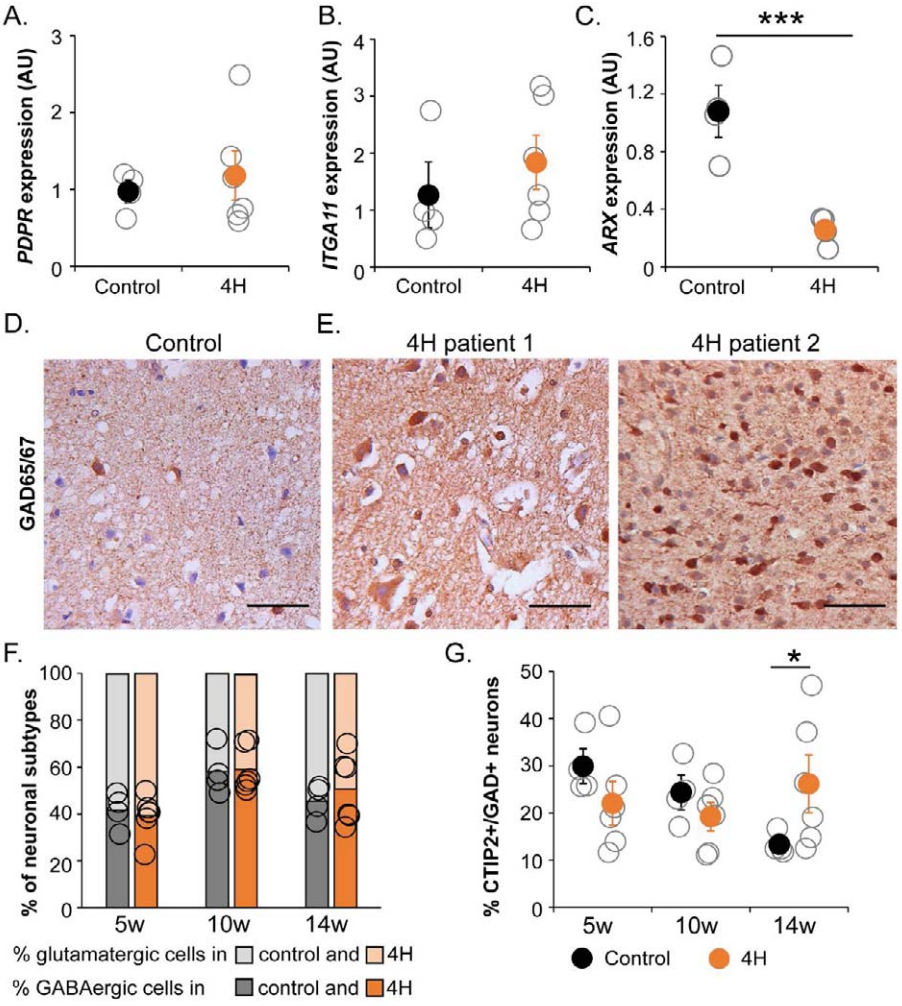

Figure 3. Cortical interneuron changes in 4H. (**A-C**) QPCR analysis shows *PDPR*, *ITGA11* and *ARX* expression in 4H and control neurons. RNA was isolated from cortical neurons at day 18 of the differentiation protocol, which represents an immature state. In 4H neurons, *ARX* expression is significantly downregulated (**C**), while there is no change in *PDPR* or *ITGA11* expression (**A-B**). Immunohistochemical analysis for GAD65/67 on primary cortical tissue of a control individual and two 4H patients showed that the pan interneuron marker is increased in 4H brain tissue (**D-E**). In iPSC-derived cortical neurons the proportion of glutamatergic and GABAergic cells (based on GAD65/67 and MAP2 staining) was not changed between control and 4H cells (**F**). A significant increase in the number of CTIP2 and GAD65/67 double positive cells was observed at 14 weeks post plating (**G**). *** = $P < 0.001$, * = $P < 0.05$, AU = arbitrary units. Open circles represent average per individual patient/control, filled circles represent the mean per genotype. Error bars represent standard error of the mean (SEM). Bars in **F** represent average proportion of GABAergic (dark colours) and glutamatergic (light colours) neurons, with circles representing values of individual lines. Scale bar = 100 µm.

To investigate whether 4H cultures present changes in the synapses, we analysed synaptic marker expression by immunocytochemistry (Fig. 4A). In our cortical neuronal cultures cells differentiate into GABAergic and glutamatergic neurons (Nadadhur et al., 2017), allowing us to study differentiation efficiency into these neuronal subtypes. At day 56 of differentiation, we studied the total number of synapses by quantifying the number of synaptophysin1 puncta per MAP2 dendritic length. We observed no significant change between the 4H and control cultures (control 0.078 ± 0.017, 4H 0.061 ± 0.018, Fig. 4D). To study whether the fraction of inhibitory synapses changed in 4H cultures, we measured the number of GABAergic presynaptic terminals by co-localization of pre-synaptic protein synaptophysin1 puncta with vesicular GABA transporter (VGAT) puncta. While 4H neurons showed a normal amount of synapses, the percentage of GABAergic synapses was significantly decreased from 46.4% in control to 26.1% in 4H neurons ($t(6) = 2.503$, $P = 0.046$, Fig. 4E). The decreased generation of GABAergic synapses confirms that interneuron development is affected in 4H.

4H neurons show altered network activity

To assess whether the decreased percentage of GABAergic synapses had consequences for network activity, we recorded spontaneous activity of developing neuronal networks from three controls and four 4H patients plated on multi-electrode arrays (MEAs) (Fig. 5A). The activity was captured in three parameters namely single spike events, local bursts (spike trains) and network wide bursting events (Fig. 5B). Spontaneous action potential firing in the first weeks mainly consisted of single spike events, while local and network wide bursts occurred as the cultures matured (Fig. 5C-F). Tetrodotoxin administration (TTX, 1 uM) confirmed that baseline activity was depending on sodium ion channels (Supplemental Fig. 1A, D). At 14 weeks post plating, three of four 4H patients showed high levels of local and network bursts, which was mostly absent in control cultures (Fig. 5C, F). This is an indication of hyperactivity in 4H networks, although the network activity was not significantly different from control (spikes control 1.19 ± 0.40, 4H 2.41 ± 1.88; bursts control 1.65 ± 0.13, 4H 5.61 ± 5.21; network bursts control 0.33 ± 0.60, 4H 5.17 ± 5.16). Interestingly, the single 4H line (P3) that did not show an increased number of bursts and network bursts was also the 4H line with the highest percentage of GABAergic synapses. A correlation analysis indeed confirmed significant correlations between the percentage of $VGAT^+$ synapses and the number of bursts ($r = -0.774$, $P = 0.041$) and network bursts ($r = -0.786$, $P = 0.036$), showing a relation between the amount of GABAergic pre-synapses and network activity.

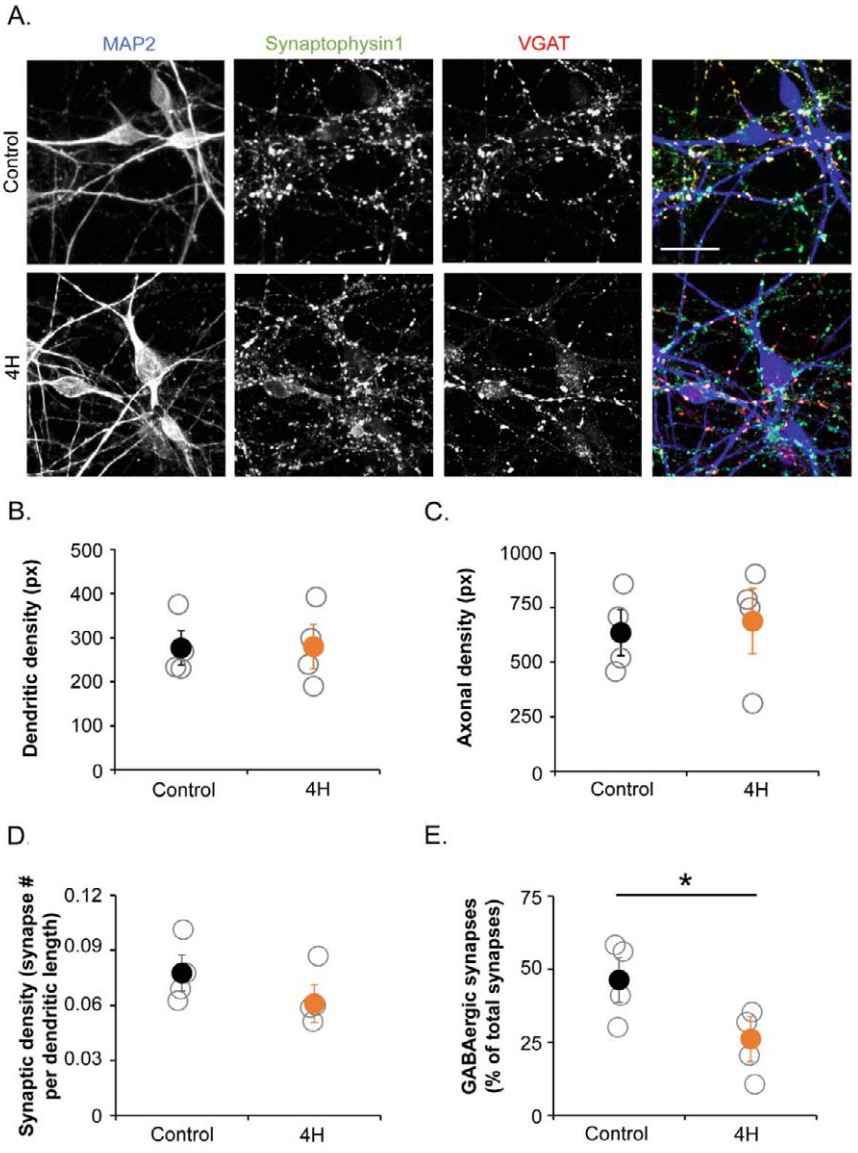

Figure 4. Cortical neurons of 4H patients show a decreased generation of GABAergic synapses. (**A**) Representative images of immunostainings on control and 4H neurons. Neurons are stained for dendrites (MAP2, *left*, blue), all synapses (Synaptophysin1, *middle left*, green) and GABAergic synapses (VGAT, *middle right*, red). Dendritic (**B**) and axonal (**C**) density were not changed in 4H neurons compared to controls. The number of synapses per dendritic length was normal in 4H (**D**), while the percentage of GABAergic synapses was significantly decreased in 4H neurons (**E**). Scalebar = 25 µm , px = pixel, * = $P < 0.05$. (**B-E**) Open circles represent average per individual patient/control, filled circles represent the mean per genotype. Error bars represent SEM.

To establish whether increased network activity in 4H neuronal networks is due to altered synaptic signalling, modulators for glutamate or GABA signalling were added to the cultures at 14 weeks post plating. Network activity was measured for 10 min before and after addition of modulators. Ionotropic AMPA receptor antagonist DNQX (10 uM) or NMDA antagonist APV (50 µM) were used to measure glutamatergic signalling. The inhibition of either one of these glutamate receptors resulted in a significant decrease of spike count for both 4H and control networks (Supplementary Fig. 1B-C, E-F). In line with the spike counts, burst and network bursts mostly disappeared (data not shown), showing that coordinated network activity depended on glutamatergic signalling and showed no obvious differences between 4H and control lines.

To study GABAergic signalling, $GABA_A$ receptor antagonists Bicuculline (30 µM) combined with Gabazine (20 µM) or the neurotransmitter GABA (10 µM) were administered. After addition, GABA antagonists evoked network bursts in controls that were mostly absent before (burst before 2.85 ± 2.00, after 13.5 ± 5.00, Z = -2.201, P = 0.028; network burst before 0 ± 0, after 10.5 ± 6.99, Z = -2.023, P = 0.043, Fig. 5G-J). In contrast, the number of bursts and network bursts did not significantly change in 4H patients (burst before 14.13 ± 12.57, after 18.06 ± 11.60, Z = -1.886, P = 0.059; network burst before 11.7 ± 10.91, after 15.00 ± 12.45, Z = -1.527, P = 0.127, Fig. 5G-J). Administration of GABA decreased neuronal activity in both control and 4H cells (control before 215.13 ± 83.50, after 1.68 ± 0.25, $t(5)$ = 5.005, P = 0.004; 4H before 374.73 ± 212.51, after 32.18 ± 50.59, Z = -2.803, P = 0.005, Fig. 5K,L), showing normal post-synaptic GABAergic response.

This data shows that the decreased generation of GABAergic synapses correlates to an increase in network activity, and there is a decreased response of 4H neurons to treatment with GABA antagonists.

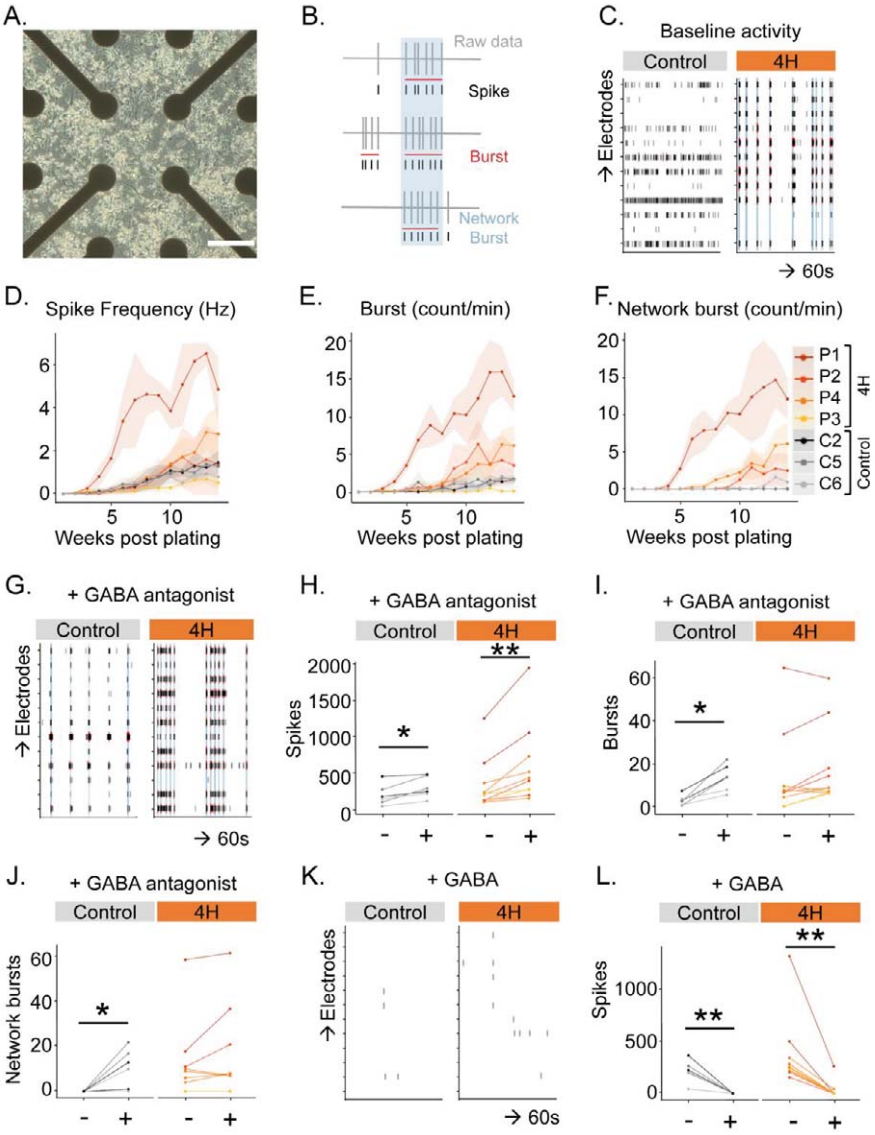

Figure 5. 4H neurons show high network activity and a reduced response to GABA antagonists. (**A**) Brightfield image of neurons plated on MEA. (**B**) Schematic example of spike and burst detection from MEA recording. (**C**) Representative example of baseline activity at 14 weeks post plating over 60 seconds on different electrodes in control and 4H neuronal cultures. Of the 4H neurons 3 out of 4 show an increased spike frequency (**D**), burst count (**E**) and network burst count (**F**) than control lines, although the differences are not statistically significant. (**G**-**J**) After addition of GABA antagonists bicuculline and gabazine, control neurons show a significantly increase in spikes (**H**), burst (**I**) and network bursts (**J**), while 4H neurons only show an increase in spikes (**I**). (**K**-**L**) Addition of GABA decreased the number of spikes in both control and 4H neurons. Scale bar = 200 µm. * = $P < 0.05$, ** = $P < 0.01$ (**D**-**F**) Data-points and lines represent averaged data per patient, with the light areas representing SD per patient. (**H, I, J, L**) data points and lines represent data per well, with lines with the same colour representing wells from the same individual.

4H neurons show robust myelination *in vitro*

A subset of human interneurons, mainly the parvalbumin neurons, is myelinated (Stedehouder et al., 2017) and one of the major characteristics of 4H is hypomyelination. Therefore, we decided to analyse oligodendrocyte maturation and myelination on human neuron-oligodendrocyte co-cultures. We altered a previously published protocol for neuron-OPC culture (Dooves et al., 2019) to generate a myelinating co-culture. Indeed, after 40 days of co-culture we observed robust generation of mature oligodendrocytes (defined as MBP^+ cells) and myelination, shown by overlap between MBP and NF200 staining (Fig. 6A-B). The presence of myelin was confirmed by electron microscopy, which showed compacted myelin sheets around neurites (Fig. 6C).

Next, the myelinating cultures were applied to 4H cell lines. Cortical neurons of 4H or control patients were co-cultured with control glial cells. After 40 days of co-culture cells were fixed and stained for neuron (NF200) and oligodendrocyte markers (OLIG2, MBP). In both 4H and control cultures oligodendrocytes matured into MBP^+ cells and showed myelination of neurites (Fig. 6D). On average there was no statistically significant change in the generation of oligodendrocyte lineage cells in 4H cultures, although three of six patient lines showed a decrease in the percentage of $OLIG2^+$ cells compared to controls (control 52.2 ± 2.74; 4H 37.9 ± 19.29, Fig. 6E). In 4H cultures, the percentage of mature oligodendrocytes ($MBP^+/OLIG2^+$ cells) was about 35% for cultures with control and 4H lines, but the variation between 4H lines was high (36.8 ± 15.97), while maturation was quite stable between control lines (34.5 ± 5.50, Fig. 6F). Myelination was analysed on immunostainings by measuring the percentage of $NF200^+$ neurites that show co-localization with MBP. No changes in the percentage of myelinated neurites were observed between cultures with 4H and control neurons (control 34.7 ± 4.85; 4H 45.1 ± 8.05, Fig. 6G). While this neuron-glia culture set-up provides a novel tool to study myelination defects in brain diseases, we could not identify changes in 4H.

Targeting the SHH pathway does not improve 4H interneuron phenotypes

ARX is an important regulator of SHH gradients during development (Cho et al., 2014), suggesting that the decreased expression of *ARX* in 4H might affect interneuron development through the SHH pathway. We tested the prospects for targeting the SHH pathway in 4H in the cortical neuronal cultures. In a pilot study it was established that twice a week treatment with SHH pathway agonist SAG at 100 nM from day 18 onwards increased the percentage of GABAergic synapses on a 4H line, without any (negative) effects on a control line (Supplementary Fig. 2A).

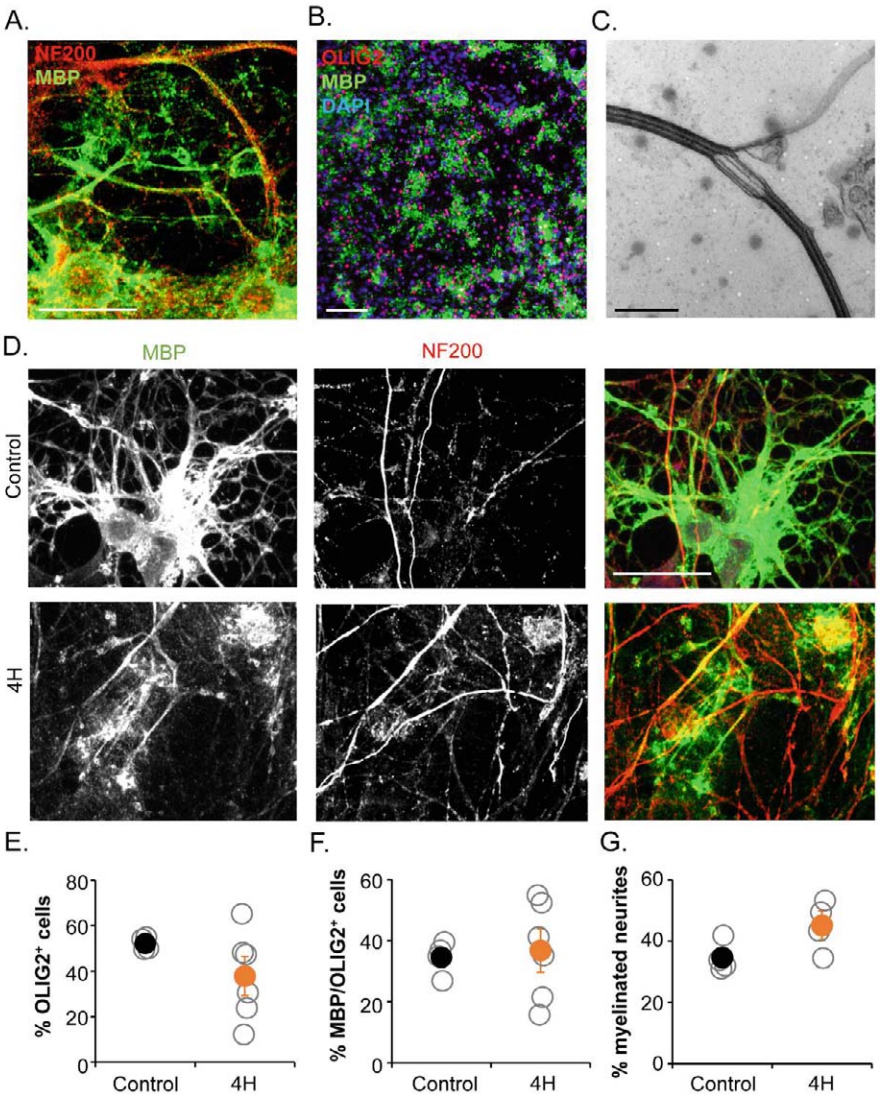

Figure 6. Oligodendrocyte maturation and myelination in co-culture with 4H neurons is normal. A and **B** indicate that neuron-oligodendrocyte co-cultures show robust generation of oligodendrocytes and myelination. (**A**) Staining for myelin protein MBP and axonal marker NF200 shows wrapping of oligodendrocyte processes around axons. (**B**) Staining for MBP and early oligodendrocyte marker OLIG2 shows a robust generation and maturation of oligodendrocytes. (**C**) Electron microscopy confirms the presence of compact myelin sheets around neuronal processes. (**D**) Cultures with 4H or control neurons and control oligodendrocytes both show oligodendrocyte maturation and myelination. Quantification showed no changes in oligodendrocyte generation, defined as the percentage of $DAPI^+$ cells that were $OLIG2^+$ (**E**). Similarly, oligodendrocyte maturation (**F**; percentage of $OLIG2^+$ cells that developed in MBP^+ cells) or the percentage of neurites that is myelinated (**G**) was not changed in cultures with 4H neurons. (**A** and **D**) Scalebar = 25 µm, (**B**) scalebar = 100 µm, (**C**) scalebar = 500 nm. (**E**-**G**) Open circles represent average per individual patient/control, filled circles represent the mean per genotype. Error bars represent SEM.

PCR analysis confirmed upregulation of SHH target *GLI1* in 4H cells after treatment with 100 nM SAG for 2 weeks (Supplementary Fig. 2B-C). As such, all 4H and iPSC lines were treated with 100 nM SAG from day 18 until the end point of the experiment at day 56. Morphology analysis of neurons showed that SAG treatment affected the dendritic complexity by decreasing the number of dendritic segments, extremities and dendritic length per cell in control cells (segments vehicle 6.34 ± 1.07, SAG 4.29 ± 1.12 $t(6) = 2.481$, $P = 0.024$; extremities vehicle 3.34 ± 0.39, SAG 2.36 ± 0.46, $t(6) = 3.176$, $P = 0.010$; length vehicle 283 ± 25, SAG 193 ± 17, $t(6) = 3.194$, $P = 0.019$; Fig. 7A-B). In 4H cells, no significant effect of SAG treatment on neuronal morphology was observed. A paired samples test comparing vehicle and SAG treatment showed that SAG treatment significantly increased the percentage of $VGAT^+$ synapses compared to vehicle treatment (vehicle 31.3 ± 10.19, SAG 34.6 ± 9.93, $t(20) = -2.125$, $P = 0.046$). However, the increase was small and no significant improvement in the 4H lines specifically was observed (Fig. 7C-D). Although SAG treatment was able to increase expression of SHH target *GLI1*, it was not able to improve 4H interneuron development *in vitro*.

4H mutations affect parvalbumin interneuron lineage

Next, we aimed to identify whether specific cortical interneuron subtypes are affected in 4H. Primers targeted the five major human interneuron subtypes: somatostatin (SST), PV, VIP, ID2 and NDNF neurons (Yu et al., 2021). The expression of *NEUN* was decreased in 4H cultures at day 30, although the difference was not significant (control 1.27 ± 0.82, 4H 0.41 ± 0.25, $t(8) = 2.171$, $P = 0.062$, Fig. 8A). However, since a difference in the number of neurons may affect the relative expression of GABAergic markers when only corrected for a housekeeping gene, all other markers were corrected for expression of both *EIF4G2* and *NEUN*. *DLX2* is important for development of cortical interneurons and downregulated upon maturation of neurons (Achim et al., 2014). Indeed, in control cells the *DLX2* expression decreased between day 30 and day 56, which was less pronounced in 4H cells (control day 30 1.98 ± 1.90, day 56 0.31 ± 0.12; 4H day 30 2.06 ± 1.01, day 56 1.61 ± 1.70; Fig. 8B). Despite the decreased number of GABAergic synapses in 4H cultures, markers for specific interneuron subtypes were not significantly decreased in 4H cultures (Fig. 8C-H). In contrast, the expression of *ERBB4*, a marker for PV neurons, was significantly increased in 4H neurons compared to controls (day 30 control 2.28 ± 3.47, 4H 21.45 ± 19.51, $Z = -2.132$, $P = 0.038$; day 56 control 0.42 ± 0.09, 4H 2.50 ± 2.76, $t(6) = -2.710$, $P = 0.035$, Fig. 8H). This suggests that the generation of specific interneuron subtypes is not impaired in 4H, but rather the development or maturation of interneurons may be affected.

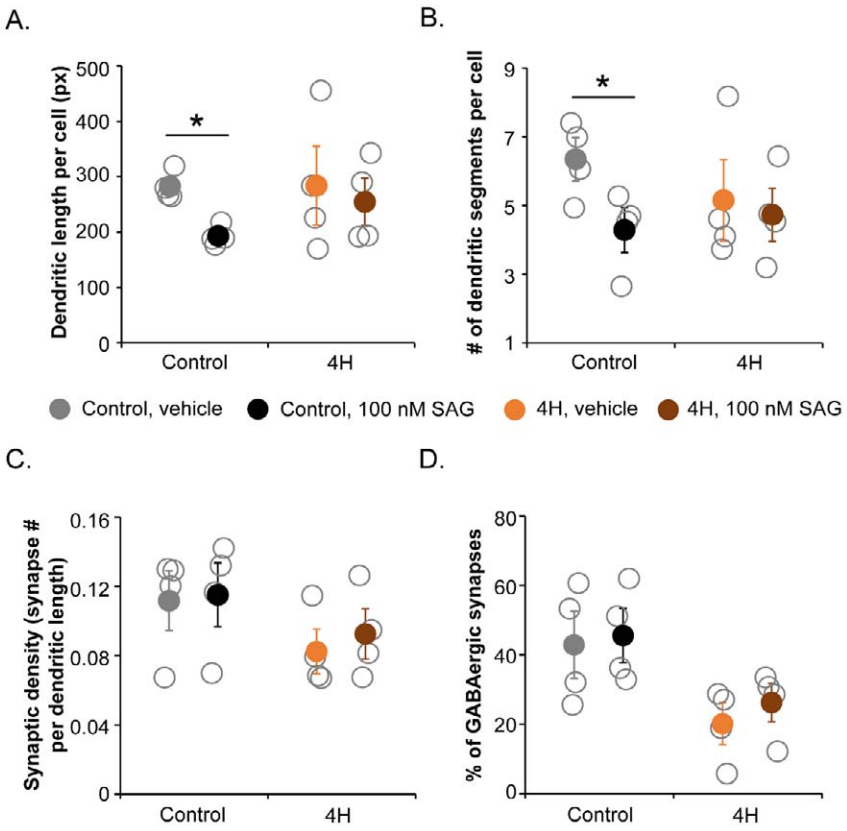

Figure 7. Targeting the SHH pathway in cortical neurons did not improve 4H associated GABAergic phenotypes. Control and 4H neurons were treated with vehicle (DMSO) or 100 nM SAG from day 18 to day 56. After SAG treatment, the dendritic length per cell (**A**) and number of dendritic segments per cell (**B**), both based on MAP2 staining, were significantly decreased in control but not in 4H neurons. No significant changes in the number of synapses per dendritic length (**C**) or the percentage of GABAergic synapses (**D**) were observed. Px = pixels. * $P < 0.05$. Open circles represent average per individual patient/control, filled circles represent the mean per genotype. Error bars represent SEM.

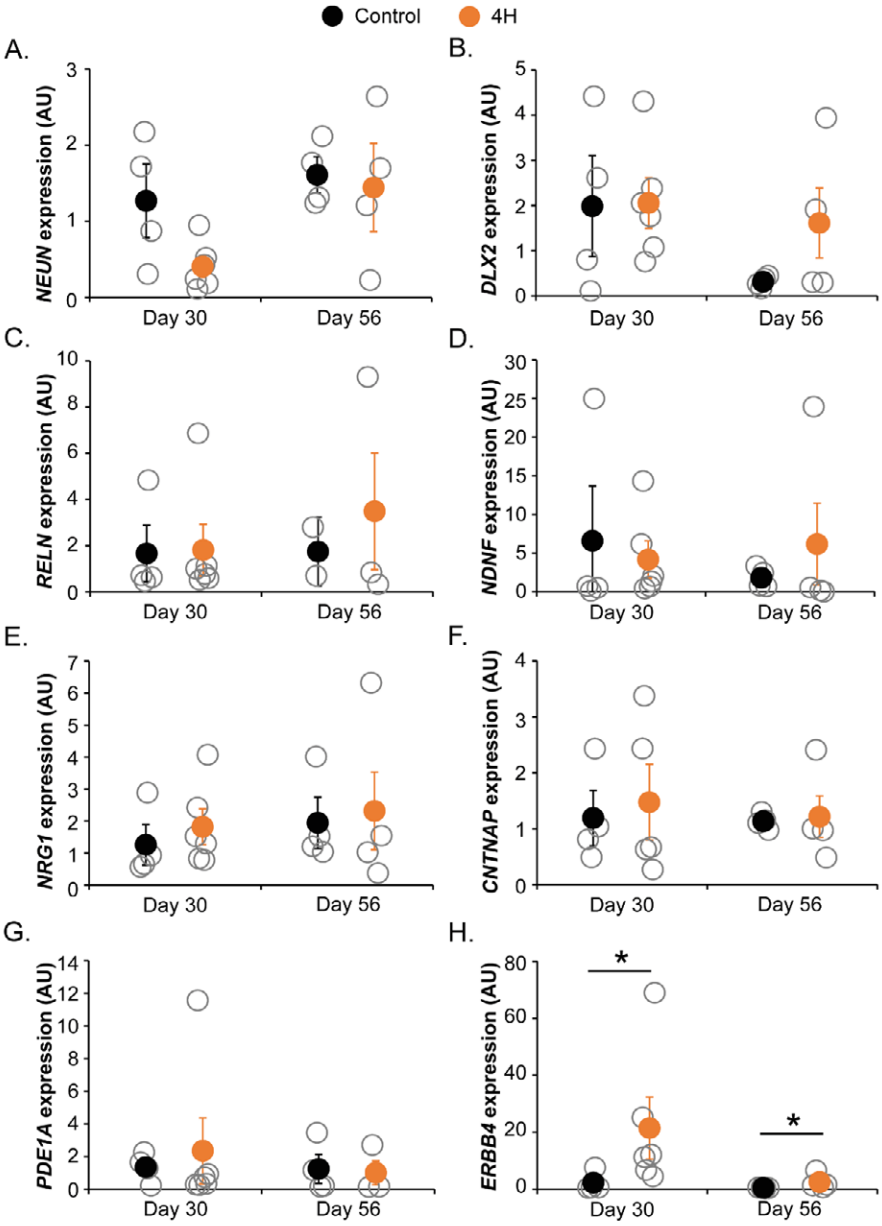

Figure 8. 4H neurons show increased expression of parvalbumin interneuron marker *ERBB4*. QPCR analysis for neuronal and GABAergic markers on day 30 and day 56 control and 4H neurons. (**A**) *NEUN* expression, which is decreased in day 30 4H neurons; therefore **B**-**H** are corrected for both *NEUN* and *EIF4G2* expression. (**B**) Expression of *DLX2* decreased over time in control neurons, which is less pronounced in 4H cells. (**C**-**H**) qPCR analysis of specific interneuron subtypes: (**C**) *RELN*, an early marker for NDNF interneurons, (**D**) *NDNF*, (**E**) *NRG1*, an early marker for ID2 interneurons, (**F**) *CNTNAP*, an early marker for VIP interneurons, (**G**) *PDE1A*, an early marker for SST interneurons and (**H**) *ERBB4*, an early marker for PV interneurons. *ERBB4* expression was significantly increased in 4H neurons at day 30 and day 56 (**H**). AU = arbitrary units, * $P < 0.05$

DISCUSSION

Although the genetic defects causing 4H leukodystrophy have been identified, our knowledge of underlying molecular mechanisms and the affected cellular subtypes is lacking. This study aimed to get more insight into the affected brain cell types and pathways. We started with an unbiased RNA sequencing screen on 4H and control fibroblasts, iPSCs and cerebellar cells. Although only a small number of genes were differentially regulated in all cell types, an interesting finding was the decreased expression of *ARX* in cerebellar cells of 4H patients. Considering the important role of ARX in cortical neuronal development and migration (Joseph et al., 2021; Kitamura et al., 2002; Marsh et al., 2016), we studied GAD65/67 expression in patient tissue and showed an increase in GAD65/67 immunoreactivity confirming interneuron changes in the cortex of 4H patients. In iPSC-derived cortical neuron cultures, 4H neurons also showed decreased expression of *ARX* and affected interneuron development as measured by a decreased percentage of GABAergic synapses. No changes in the proportion of GABAergic cells were observed, suggesting the change in the number of synapses may be due to affected maturation or synapse formation in 4H neurons. The altered synaptic ratio has functional consequences, as it was correlated to an increased network activity. A decreased GABAergic signalling in 4H also became apparent after treatment with GABA antagonists. 4H neurons did not show changes in activity upon treatment with the GABA antagonists, while control cells showed a significantly increased activity after treatment. As ARX was reported to have important roles in the PV interneurons (Joseph et al., 2021), we tested whether specific interneuron lineages were affected in 4H. Indeed, QPCR analysis identified an increase in *ERBB4*, a marker for PV neurons, confirming other results that interneuron regulation may be affected in 4H. Together, interneurons are affected in 4H and we show decreased *ARX* expression in different neuronal subtypes using iPSC models. Cortical neuron cultures identified a decreased number of inhibitory synapses, increased network activity, and the results are specifically pointing to defects in PV neurons.

We focused on the involvement of ARX in 4H leukodystrophy because of its role in cortical development and its association with other disorders. Loss of function mutations in ARX lead to pleiotropic disorders such as X-linked Lissencephaly with Ambiguous Genitalia (XLAG, OMIM 300215), Agenesis of the Corpus Callosum with Abnormal Genitalia (OMIM 30004), and Lissencephaly with cerebellar hypoplasia (Shoubridge et al., 2010). *ARX* impacts interneuron generation, development and migration (Lee et al., 2017) and loss of *ARX* expression in interneurons alters their excitability and causes epilepsy in mice (Joseph et

al., 2021; Marsh et al., 2016). In animal models it was shown that Arx acts with FoxA2 to regulate expression of Shh (Cho et al., 2014). SHH plays important roles in the development of granule cells (and thereby cerebellar volume); oligodendrocytes (and thereby myelination); jaw and teeth; and the eyes (Dahmane & Ruiz i Altaba, 1999; Francis-West et al., 1998; Hardcastle et al., 1998; Kahn et al., 2017; Nery et al., 2001; Ortega et al., 2013; Prykhozhij, 2010). It is possible that POLR3 disorders, and 4H in particular, involve *ARX*-related pathway defects, where altered *ARX* expression drives the clinical phenotype through an ARX to SHH pathway.

Although downregulation of *ARX* may have significant impact on neuronal development, we could not confirm the SHH pathway as a therapeutic target for 4H in our disease model. Neurons were treated with SAG starting from day 18 to day 56 of differentiation. At day 18, the neuronal batches undergo quality control and are frozen for later use. It is possible that treatment starting from day 18 is too late and some of the developmental alterations following a decreased expression of *ARX* and a dysregulated SHH pathway have already taken place. However, this would mean that targeting the SHH pathway is not a viable option for patients, who are generally diagnosed postnatally. Another explanation may be that the SAG concentration was not high enough to activate the SHH pathway, although the expression of SHH target *GLI1* was increased after SAG treatment. It is possible that the affected development of cortical interneurons is caused by mechanisms that do not involve ARX. In this study we were able to show a correlation between *ARX* levels and interneuron generation, but additional studies are needed to show a causal effect between ARX and 4H interneuron development. Additionally, ARX works on SHH-independent pathways. For example ARX may affect histone demethylation through KDM5C (Poeta et al., 2013; Poeta et al., 2021) which has been implicated in neurodevelopmental disorders (Vallianatos et al., 2020). In conclusion, SAG treatment did not revert the neuronal phenotype in our cortical 4H cultures and following studies should reveal whether a changed treatment protocol or different target would have more beneficial effects.

The percentage of GABAergic synapses was significantly decreased in 4H cultures, suggesting an alteration in the synaptic balance. Indeed, network activity measurements showed a higher activity in most 4H cultures, although results did not reach statistical significance. Interestingly, there was a significant correlation between the percentage of GABAergic synapses and the amount of bursts and network burst, showing that synaptic balance changes also have consequences for functional network behaviour. This was also confirmed by the measurement of network activity after treatment with GABA antagonists.

In control cultures, the network activity significantly increased after blocking GABA-A receptors. However, in 4H cultures treatment with GABA antagonists did not significantly change network activity, suggesting that there was less GABAergic signalling that could respond to antagonistic inhibition. Interestingly, the activity in 4H cultures did decrease after addition of GABA, which suggests a normal post-synaptic GABAergic response in 4H cells. The decreased number of inhibitory synapses could be caused by several mechanisms, e.g. reduced network maturation, a reduction in a specific subset of interneurons, less (active) inhibitory synapses per neuron, or an increase in the number excitatory synapses. Follow-up studies should give more insight into this. Also, as patient lines present differential changes, in line with the broad clinical presentation, an increased panel of patient lines would be advised.

In light of our *in vitro* findings, it seems contradictory that GAD65/67 immunoreactivity is higher in 4H postmortem tissue. It could possibly be explained if only a subpopulation of interneurons is affected in 4H, as it is reported that interneuron subtypes have different levels of GAD65 (Kajita & Mushiake, 2021) or it can be indicative of axonal reorganization of remaining interneurons (Peng et al., 2013). Alternatively, the increased GAD65/67 expression does not reflect changes in the interneuron populations but is rather the consequence of hyperexcitability. Epilepsy is a feature in 4H and human post mortem studies on temporal lobe epilepsy have identified increased levels of GAD67 (Neder et al., 2002). In models of epilepsy, upon neuronal excitotoxicity and increased glutamate release, GAD65/67 is upregulated as compensatory mechanism to convert excess of glutamate into GABA (Esclapez & Houser, 1999). If the increase in GAD65/67 immunoreactivity is indeed a secondary effect in 4H this would explain why there is no change in the number of GABAergic cells in the iPSC-derived cultures. However, while postmortem analysis confirmed network changes in 4H, follow-up studies are warranted.

Alterations in GABAergic activity may underlie 4H associated neurological signs like epilepsy, but also hypomyelination. It is currently unknown how POLR3 mutations cause hypomyelination. Coulombe et al. (Coulombe et al., 2021) hypothesized that hypomyelination in 4H is either caused by an unknown POLR3 target that plays a key role in myelin biogenesis, or that POLR3 mutations lead to a globally reduced transcription at a crucial milestone in oligodendrocyte development. We investigated an alternative hypothesis, where the altered myelination is secondary to neuronal dysfunction. Cortical (parvalbumin) interneurons in the human brain are myelinated (Micheva et al., 2016;

Stedehouder et al., 2017), and myelination can be regulated by GABA receptor activity on oligodendrocytes (Pudasaini et al., 2022). To study whether the decreased interneuron generation in 4H cortical cultures also affected myelination a new co-culture protocol was developed. This co-culture of human neurons and glial cells show robust maturation of oligodendrocytes and myelination of human axons, a challenging phenomenon to study *in vitro*. No differences in oligodendrocyte maturation or myelination were observed between cultures with control or 4H neurons. This could suggest that the hypomyelination observed in 4H patients is caused by an oligodendrocyte intrinsic effect, rather than mediated through affected neurons. However, it is also possible that our culture set-up was not sensitive enough to pick up changes in myelination for 4H. The neurons used for the co-culture consist of a mix of GABAergic and glutamatergic neurons, so a myelination defect on interneurons may be masked by normal myelination of glutamatergic neurons. Additionally, PV neurons mature during late development and not all neurons in the presented co-culture system showed myelinated processes. Although the novel neuron-glia co-culture can measure myelination *in vitro*, further improvement of these model systems may be necessary to identify mechanisms underlying hypomyelination in 4H leukodystrophy.

We aimed to identify the interneuron subtype that was most affected in 4H cultures. We were not able to identify a significant decrease in any of the five major cortical interneurons populations (Yu et al., 2021). Instead, we found a significantly increased expression of *ERBB4*, an early marker for PV interneurons. There are a few possible explanations for the discrepancy between the decrease in GABAergic synapses and the increase in *ERBB4* expression. It is possible that interneuron generation in 4H is normal, but that interneurons are affected during later development or maturation stages. This is consistent with the finding that there were no changes in the number of GAD65/67^{+} cells in 4H cultures. As *ERBB4* is an early marker for PV interneurons, it is also possible that the increase reflects a lack of maturation, rather than an actual increase in PV neurons. A defect in maturation would be consistent with the sustained *DLX2* expression, which decreased in control cells between day 30 and day 56, but not in 4H cells. Unfortunately, PV interneurons mature late in cortical development (late gestation/postnatal (Cao et al., 1996; Fung et al., 2010; Ulfig, 2002)), and we were not able to measure *PVALB* expression in our neuronal cultures. PV interneurons are the largest group of GABAergic neurons in the cortex. They are fast spiking interneurons with a high metabolic demand, which makes them vulnerable for injury (Ruden et al., 2021). Interestingly, the development of SST and PV interneurons is depending on SHH levels

(Flandin et al., 2011; Tyson et al., 2015), and deletion of *Arx* in PV neurons led to increased neuronal activity and altered synaptic properties in a mouse model (Joseph et al., 2021). PV interneurons play a crucial role in spike timing of glutamatergic neurons, and abnormalities in PV signalling have been implicated in epilepsy, occasionally seen in 4H patients. For example, optogenetic stimulation of PV neurons can induce ictal events in mice (de Curtis & Avoli, 2016) probably due to a depolarization block (Calin et al., 2021). Overall, our data suggests that PV interneurons may be specifically affected in 4H and should be further studied.

To conclude, transcriptome analysis of cerebellar cells differentiated from patient iPSCs revealed ARX as a potentially important regulator of 4H brain pathomechanisms. Indeed, a decreased expression of *ARX* was confirmed in cortical neuron cultures, which showed affected generation of GABAergic synapses consistent with known effects of ARX on interneuron development. The decrease in GABAergic synapses correlated to increased neuronal network activity. QPCR analysis revealed alterations in *ERBB4* expression, suggesting the PV interneurons might be of particular interest for 4H. Although more research is needed, this study provides a first insight into specific brain cell types and pathomechanisms affected in 4H leukodystrophy.

ACKNOWLEDGEMENTS

The authors would like to thank Kyoko Watanabe and Danielle Posthuma for analysing RNA sequencing data; Jan van Weering, Joke Wortel and Rien Dekker for assistance with electron microscopy; Brendan Lodder for assistance with RNA isolation; and the INF department for the MEA inhibitor compounds NIW is member of the European Reference Network for Rare Neurological Disorders (ERN-RND), project ID 739510.

FUNDING

This study was funded by the European Leukodystrophy Association (ELA 2018-011C3A).

COMPETING INTERESTS

The authors report no competing interests.

AUTHOR CONTRIBUTIONS

SD designed and executed experiments with cortical neurons. LMLK executed MEA experiments and qPCR analysis together with SD and NB. DBH designed and executed RNA sequencing experiments. MB and MB processed and analysed human postmortem tissue. NIW and VMH supervised the project. SD, LMLK, NIW and VMH wrote the manuscript with valuable contributions of all authors.

REFERENCES

Achim, K., Salminen, M., & Partanen, J. (2014). Mechanisms regulating GABAergic neuron development. *Cell Mol Life Sci*, *71*(8), 1395-1415. https://doi.org/10.1007/s00018-013-1501-3

Bernard, G., Chouery, E., Putorti, M. L., Tetreault, M., Takanohashi, A., Carosso, G., Clement, I., Boespflug-Tanguy, O., Rodriguez, D., Delague, V., Abou Ghoch, J., Jalkh, N., Dorboz, I., Fribourg, S., Teichmann, M., Megarbane, A., Schiffmann, R., Vanderver, A., & Brais, B. (2011). Mutations of POLR3A encoding a catalytic subunit of RNA polymerase Pol III cause a recessive hypomyelinating leukodystrophy. *Am J Hum Genet*, *89*(3), 415-423. https://doi.org/10.1016/j.ajhg.2011.07.014

Boles, N. C., Hirsch, S. E., Le, S., Corneo, B., Najm, F., Minotti, A. P., Wang, Q., Lotz, S., Tesar, P. J., & Fasano, C. A. (2014). NPTX1 regulates neural lineage specification from human pluripotent stem cells. *Cell Rep*, *6*(4), 724-736. https://doi.org/10.1016/j.celrep.2014.01.026

Bruno, L. P., Doddato, G., Valentino, F., Baldassarri, M., Tita, R., Fallerini, C., Bruttini, M., Lo Rizzo, C., Mencarelli, M. A., Mari, F., Pinto, A. M., Fava, F., Fabbiani, A., Lamacchia, V., Carrer, A., Caputo, V., Granata, S., Benetti, E., Zguro, K., . . . Ariani, F. (2021). New Candidates for Autism/Intellectual Disability Identified by Whole-Exome Sequencing. *Int J Mol Sci*, *22*(24). https://doi.org/10.3390/ijms222413439

Calin, A., Ilie, A. S., & Akerman, C. J. (2021). Disrupting Epileptiform Activity by Preventing Parvalbumin Interneuron Depolarization Block. *J Neurosci*, *41*(45), 9452-9465. https://doi.org/10.1523/JNEUROSCI.1002-20.2021

Cao, Q. L., Yan, X. X., Luo, X. G., & Garey, L. J. (1996). Prenatal development of parvalbumin immunoreactivity in the human striate cortex. *Cereb Cortex*, *6*(4), 620-630. https://doi.org/10.1093/cercor/6.4.620

Chen, B., Wang, S. S., Hattox, A. M., Rayburn, H., Nelson, S. B., & McConnell, S. K. (2008). The Fezf2-Ctip2 genetic pathway regulates the fate choice of subcortical projection neurons in the developing cerebral cortex. *Proc Natl Acad Sci U S A*, *105*(32), 11382-11387. https://doi.org/10.1073/pnas.0804918105

Cho, G., Lim, Y., Cho, I. T., Simonet, J. C., & Golden, J. A. (2014). Arx together with FoxA2, regulates Shh floor plate expression. *Dev Biol*, *393*(1), 137-148. https://doi.org/10.1016/j.ydbio.2014.06.012

Consortium, E. P. (2012). An integrated encyclopedia of DNA elements in the human genome. *Nature*, *489*(7414), 57-74. https://doi.org/10.1038/nature11247

Coulombe, B., Derksen, A., La Piana, R., Brais, B., Gauthier, M. S., & Bernard, G. (2021). POLR3-related leukodystrophy: How do mutations affecting RNA polymerase III subunits cause hypomyelination? *Fac Rev*, *10*, 12. https://doi.org/10.12703/r/10-12

Dahmane, N., & Ruiz i Altaba, A. (1999). Sonic hedgehog regulates the growth and patterning of the cerebellum. *Development*, *126*(14), 3089-3100. https://doi.org/10.1242/dev.126.14.3089

de Curtis, M., & Avoli, M. (2016). GABAergic networks jump-start focal seizures. *Epilepsia*, *57*(5), 679-687. https://doi.org/10.1111/epi.13370

Dieci, G., Fiorino, G., Castelnuovo, M., Teichmann, M., & Pagano, A. (2007). The expanding RNA polymerase III transcriptome. *Trends Genet*, *23*(12), 614-622. https://doi.org/10.1016/j.tig.2007.09.001

Dooves, S., Nadadhur, A. G., Gasparotto, L., & Heine, V. M. (2019). Co-culture of Human Stem Cell Derived Neurons and Oligodendrocyte Progenitor Cells. *Bio Protoc*, *9*(17), e3350. https://doi.org/10.21769/BioProtoc.3350

Dorboz, I., Dumay-Odelot, H., Boussaid, K., Bouyacoub, Y., Barreau, P., Samaan, S., Jmel, H., Eymard-Pierre, E., Cances, C., Bar, C., Poulat, A. L., Rousselle, C., Renaldo, F., Elmaleh-Berges, M., Teichmann, M., & Boespflug-Tanguy, O. (2018). Mutation in POLR3K causes hypomyelinating leukodystrophy and abnormal ribosomal RNA regulation. *Neurol Genet*, *4*(6), e289. https://doi.org/10.1212/NXG.0000000000000289

Esclapez, M., & Houser, C. R. (1999). Up-regulation of GAD65 and GAD67 in remaining hippocampal GABA neurons in a model of temporal lobe epilepsy. *Journal of Comparative Neurology*, *412*(3), 488-505. https://doi.org/https://doi.org/10.1002/(SICI)1096-9861(19990927)412:3<488::AID-CNE8>3.0.CO;2-6

Flandin, P., Zhao, Y., Vogt, D., Jeong, J., Long, J., Potter, G., Westphal, H., & Rubenstein, J. L. (2011). Lhx6 and Lhx8 coordinately induce neuronal expression of Shh that controls the generation of interneuron progenitors. *Neuron*, *70*(5), 939-950. https://doi.org/10.1016/j.neuron.2011.04.020

Francis-West, P., Ladher, R., Barlow, A., & Graveson, A. (1998). Signalling interactions during facial development. *Mech Dev*, *75*(1-2), 3-28. https://doi.org/10.1016/s0925-4773(98)00082-3

Fung, S. J., Webster, M. J., Sivagnanasundaram, S., Duncan, C., Elashoff, M., & Weickert, C. S. (2010). Expression of interneuron markers in the dorsolateral prefrontal cortex of the developing human and in schizophrenia. *Am J Psychiatry*, *167*(12), 1479-1488. https://doi.org/10.1176/appi.ajp.2010.09060784

Gecz, J., Cloosterman, D., & Partington, M. (2006). ARX: a gene for all seasons. *Curr Opin Genet Dev*, *16*(3), 308-316. https://doi.org/10.1016/j.gde.2006.04.003

Hardcastle, Z., Mo, R., Hui, C. C., & Sharpe, P. T. (1998). The Shh signalling pathway in tooth development: defects in Gli2 and Gli3 mutants. *Development*, *125*(15), 2803-2811. https://doi.org/10.1242/dev.125.15.2803

Harting, I., Al-Saady, M., Krageloh-Mann, I., Bley, A., Hempel, M., Bierhals, T., Karch, S., Moog, U., Bernard, G., Huntsman, R., van Spaendonk, R. M. L., Vreeburg, M., Rodriguez-Palmero, A., Pujol, A., van der Knaap, M. S., Pouwels, P. J. W., & Wolf, N. I. (2020). POLR3A variants with striatal involvement and extrapyramidal movement disorder. *Neurogenetics*, *21*(2), 121-133. https://doi.org/10.1007/s10048-019-00602-4

Helman, G., Van Haren, K., Bonkowsky, J. L., Bernard, G., Pizzino, A., Braverman, N., Suhr, D., Patterson, M. C., Ali Fatemi, S., Leonard, J., van der Knaap, M. S., Back, S. A., Damiani, S., Goldman, S. A., Takanohashi, A., Petryniak, M., Rowitch, D., Messing, A., Wrabetz, L., . . . Consortium, G. (2015). Disease specific therapies in leukodystrophies and leukoencephalopathies. *Mol Genet Metab*, *114*(4), 527-536. https://doi.org/10.1016/j.ymgme.2015.01.014

Hirai, H., Pang, Z., Bao, D., Miyazaki, T., Li, L., Miura, E., Parris, J., Rong, Y., Watanabe, M., Yuzaki, M., & Morgan, J. I. (2005). Cbln1 is essential for synaptic integrity and plasticity in the cerebellum. *Nat Neurosci*, *8*(11), 1534-1541. https://doi.org/10.1038/nn1576

Holmes, D. B., & Heine, V. M. (2017a). Simplified 3D protocol capable of generating early cortical neuroepithelium. *Biol Open*, *6*(3), 402-406. https://doi.org/10.1242/bio.021725

Holmes, D. B., & Heine, V. M. (2017b). Streamlined 3D Cerebellar Differentiation Protocol with Optional 2D Modification. *Jove-Journal of Visualized Experiments*(130). https://doi.org/ARTN e56888 10.3791/56888

Joseph, D. J., Von Deimling, M., Hasegawa, Y., Cristancho, A. G., Ahrens-Nicklas, R. C., Rogers, S. L., Risbud, R., McCoy, A. J., & Marsh, E. D. (2021). Postnatal Arx transcriptional activity regulates functional properties of PV interneurons. *iScience*, *24*(1), 101999. https://doi.org/10.1016/j.isci.2020.101999

Kahn, B. M., Corman, T. S., Lovelace, K., Hong, M., Krauss, R. S., & Epstein, D. J. (2017). Prenatal ethanol exposure in mice phenocopies Cdon mutation by impeding Shh function in the etiology of optic nerve hypoplasia. *Dis Model Mech*, *10*(1), 29-37. https://doi.org/10.1242/dmm.026195

Kajita, Y., & Mushiake, H. (2021). Heterogeneous GAD65 Expression in Subtypes of GABAergic Neurons Across Layers of the Cerebral Cortex and Hippocampus [Original Research]. *Frontiers in Behavioral Neuroscience*, *15*. https://doi.org/10.3389/fnbeh.2021.750869

Kim, H., Kim, T., Jeong, B. C., Cho, I. T., Han, D., Takegahara, N., Negishi-Koga, T., Takayanagi, H., Lee, J. H., Sul, J. Y., Prasad, V., Lee, S. H., & Choi, Y. (2013). Tmem64 modulates calcium signaling during RANKL-mediated osteoclast differentiation. *Cell Metab*, *17*(2), 249-260. https://doi.org/10.1016/j.cmet.2013.01.002

Kitamura, K., Yanazawa, M., Sugiyama, N., Miura, H., Iizuka-Kogo, A., Kusaka, M., Omichi, K., Suzuki, R., Kato-Fukui, Y., Kamiirisa, K., Matsuo, M., Kamijo, S., Kasahara, M., Yoshioka, H., Ogata, T., Fukuda, T., Kondo, I., Kato, M., Dobyns, W. B., . . . Morohashi, K. (2002). Mutation of ARX causes abnormal development of forebrain and testes in mice and X-linked lissencephaly with abnormal genitalia in humans. *Nat Genet*, *32*(3), 359-369. https://doi.org/10.1038/ng1009

La Piana, R., Cayami, F. K., Tran, L. T., Guerrero, K., van Spaendonk, R., Ounap, K., Pajusalu, S., Haack, T., Wassmer, E., Timmann, D., Mierzewska, H., Poll-The, B. T., Patel, C., Cox, H., Atik, T., Onay, H., Ozkinay, F., Vanderver, A., van der Knaap, M. S., . . . Bernard, G. (2016). Diffuse hypomyelination is not obligate for POLR3-related disorders. *Neurology*, *86*(17), 1622-1626. https://doi.org/10.1212/WNL.0000000000002612

Langmead, B., & Salzberg, S. L. (2012). Fast gapped-read alignment with Bowtie 2. *Nat Methods*, *9*(4), 357-359. https://doi.org/10.1038/nmeth.1923

Lee, K., Ireland, K., Bleeze, M., & Shoubridge, C. (2017). ARX polyalanine expansion mutations lead to migration impediment in the rostral cortex coupled with a developmental deficit of calbindin-positive cortical GABAergic interneurons. *Neuroscience*, *357*, 220-231. https://doi.org/10.1016/j.neuroscience.2017.06.010

Liao, Y., Smyth, G. K., & Shi, W. (2013). The Subread aligner: fast, accurate and scalable read mapping by seed-and-vote. *Nucleic Acids Res*, *41*(10), e108. https://doi.org/10.1093/nar/gkt214

Love, M. I., Huber, W., & Anders, S. (2014). Moderated estimation of fold change and dispersion for RNA-seq data with DESeq2. *Genome Biol*, *15*(12), 550. https://doi.org/10.1186/s13059-014-0550-8

Marsh, E. D., Nasrallah, M. P., Walsh, C., Murray, K. A., Nicole Sunnen, C., McCoy, A., & Golden, J. A. (2016). Developmental interneuron subtype deficits after targeted loss of Arx. *BMC Neurosci*, *17*(1), 35. https://doi.org/10.1186/s12868-016-0265-8

Micheva, K. D., Wolman, D., Mensh, B. D., Pax, E., Buchanan, J., Smith, S. J., & Bock, D. D. (2016). A large fraction of neocortical myelin ensheathes axons of local inhibitory neurons. *Elife*, *5*. https://doi.org/10.7554/eLife.15784

Mitsogiannis, M. D., Little, G. E., & Mitchell, K. J. (2017). Semaphorin-Plexin signaling influences early ventral telencephalic development and thalamocortical axon guidance. *Neural Dev*, *12*(1), 6. https://doi.org/10.1186/s13064-017-0083-4

Mortensen, A. H., Schade, V., Lamonerie, T., & Camper, S. A. (2015). Deletion of OTX2 in neural ectoderm delays anterior pituitary development. *Hum Mol Genet*, *24*(4), 939-953. https://doi.org/10.1093/hmg/ddu506

Nadadhur, A. G., Emperador Melero, J., Meijer, M., Schut, D., Jacobs, G., Li, K. W., Hjorth, J. J. J., Meredith, R. M., Toonen, R. F., Van Kesteren, R. E., Smit, A. B., Verhage, M., & Heine, V. M. (2017). Multi-level characterization of balanced inhibitory-excitatory cortical neuron network derived from human pluripotent stem cells. *PLoS One*, *12*(6), e0178533. https://doi.org/10.1371/journal.pone.0178533

Neder, L., Valente, V., Carlotti, C. G., Leite, J. P., Assirati, J. A., Paçó-Larson, M. L., & Moreira, J. E. (2002). Glutamate NMDA Receptor Subunit R1 and GAD mRNA Expression in Human Temporal Lobe Epilepsy. *Cellular and Molecular Neurobiology*, *22*(5), 689-698. https://doi.org/10.1023/A:1021852907068

Nery, S., Wichterle, H., & Fishell, G. (2001). Sonic hedgehog contributes to oligodendrocyte specification in the mammalian forebrain. *Development*, *128*(4), 527-540. https://doi.org/10.1242/dev.128.4.527

Ortega, J. A., Radonjic, N. V., & Zecevic, N. (2013). Sonic hedgehog promotes generation and maintenance of human forebrain Olig2 progenitors. *Front Cell Neurosci*, *7*, 254. https://doi.org/10.3389/fncel.2013.00254

Peng, Z., Zhang, N., Wei, W., Huang, C. S., Cetina, Y., Otis, T. S., & Houser, C. R. (2013). A Reorganized GABAergic Circuit in a Model of Epilepsy: Evidence from Optogenetic Labeling and Stimulation of Somatostatin Interneurons. *The Journal of Neuroscience*, *33*(36), 14392-14405. https://doi.org/10.1523/jneurosci.2045-13.2013

Poeta, L., Fusco, F., Drongitis, D., Shoubridge, C., Manganelli, G., Filosa, S., Paciolla, M., Courtney, M., Collombat, P., Lioi, M. B., Gecz, J., Ursini, M. V., & Miano, M. G. (2013). A regulatory path associated with X-linked intellectual disability and epilepsy links KDM5C to the polyalanine expansions in ARX. *Am J Hum Genet*, *92*(1), 114-125. https://doi.org/10.1016/j.ajhg.2012.11.008

Poeta, L., Padula, A., Lioi, M. B., van Bokhoven, H., & Miano, M. G. (2021). Analysis of a Set of KDM5C Regulatory Genes Mutated in Neurodevelopmental Disorders Identifies Temporal Coexpression Brain Signatures. *Genes (Basel)*, *12*(7). https://doi.org/10.3390/genes12071088

Prykhozhij, S. V. (2010). In the absence of Sonic hedgehog, p53 induces apoptosis and inhibits retinal cell proliferation, cell-cycle exit and differentiation in zebrafish. *PLoS One*, *5*(10), e13549. https://doi.org/10.1371/journal.pone.0013549

Pudasaini, S., Friedrich, V., Buhrer, C., Endesfelder, S., Scheuer, T., & Schmitz, T. (2022). Postnatal myelination of the immature rat cingulum is regulated by GABAB receptor activity. *Dev Neurobiol*, *82*(1), 16-28. https://doi.org/10.1002/dneu.22853

Robinson, M. D., McCarthy, D. J., & Smyth, G. K. (2010). edgeR: a Bioconductor package for differential expression analysis of digital gene expression data. *Bioinformatics*, *26*(1), 139-140. https://doi.org/10.1093/bioinformatics/btp616

Ruden, J. B., Dugan, L. L., & Konradi, C. (2021). Parvalbumin interneuron vulnerability and brain disorders. *Neuropsychopharmacology*, *46*(2), 279-287. https://doi.org/10.1038/s41386-020-0778-9

Saito, T., Hanai, S., Takashima, S., Nakagawa, E., Okazaki, S., Inoue, T., Miyata, R., Hoshino, K., Akashi, T., Sasaki, M., Goto, Y., Hayashi, M., & Itoh, M. (2011). Neocortical layer formation of human developing brains and lissencephalies: consideration of layer-specific marker expression. *Cereb Cortex*, *21*(3), 588-596. https://doi.org/10.1093/cercor/bhq125

Sandberg, C. J., Vik-Mo, E. O., Behnan, J., Helseth, E., & Langmoen, I. A. (2014). Transcriptional profiling of adult neural stem-like cells from the human brain. *PLoS One*, *9*(12), e114739. https://doi.org/10.1371/journal.pone.0114739

Schmidt, J. L., Pizzino, A., Nicholl, J., Foley, A., Wang, Y., Rosenfeld, J. A., Mighion, L., Bean, L., da Silva, C., Cho, M. T., Truty, R., Garcia, J., Speare, V., Blanco, K., Powis, Z., Hobson, G. M., Kirwin, S., Krock, B., Lee, H., . . . Vanderver, A. (2020). Estimating the relative frequency of leukodystrophies and recommendations for carrier screening in the era of next-generation sequencing. *Am J Med Genet A*, *182*(8), 1906-1912. https://doi.org/10.1002/ajmg.a.61641

Sherr, E. H. (2003). The ARX story (epilepsy, mental retardation, autism, and cerebral malformations): one gene leads to many phenotypes. *Curr Opin Pediatr*, *15*(6), 567-571. https://doi.org/10.1097/00008480-200312000-00004

Shoubridge, C., Fullston, T., & Gecz, J. (2010). ARX spectrum disorders: making inroads into the molecular pathology. *Hum Mutat*, *31*(8), 889-900. https://doi.org/10.1002/humu.21288

Simons, C., Wolf, N. I., McNeil, N., Caldovic, L., Devaney, J. M., Takanohashi, A., Crawford, J., Ru, K., Grimmond, S. M., Miller, D., Tonduti, D., Schmidt, J. L., Chudnow, R. S., van Coster, R., Lagae, L., Kisler, J., Sperner, J., van der Knaap, M. S., Schiffmann, R., . . . Vanderver, A. (2013). A de novo mutation in the beta-tubulin gene TUBB4A results in the leukoencephalopathy hypomyelination with atrophy of the basal ganglia and cerebellum. *Am J Hum Genet*, *92*(5), 767-773. https://doi.org/10.1016/j.ajhg.2013.03.018

Stedehouder, J., Couey, J. J., Brizee, D., Hosseini, B., Slotman, J. A., Dirven, C. M. F., Shpak, G., Houtsmuller, A. B., & Kushner, S. A. (2017). Fast-spiking Parvalbumin Interneurons are Frequently Myelinated in the Cerebral Cortex of Mice and Humans. *Cereb Cortex*, *27*(10), 5001-5013. https://doi.org/10.1093/cercor/bhx203

Taft, R. J., Vanderver, A., Leventer, R. J., Damiani, S. A., Simons, C., Grimmond, S. M., Miller, D., Schmidt, J., Lockhart, P. J., Pope, K., Ru, K., Crawford, J., Rosser, T., de Coo, I. F., Juneja, M., Verma, I. C., Prabhakar, P., Blaser, S., Raiman, J., . . . Wolf, N. I. (2013). Mutations in DARS cause hypomyelination with brain stem and spinal cord involvement and leg spasticity. *Am J Hum Genet*, *92*(5), 774-780. https://doi.org/10.1016/j.ajhg.2013.04.006

Takahashi, K., Tanabe, K., Ohnuki, M., Narita, M., Ichisaka, T., Tomoda, K., & Yamanaka, S. (2007). Induction of pluripotent stem cells from adult human fibroblasts by defined factors. *Cell*, *131*(5), 861-872. https://doi.org/10.1016/j.cell.2007.11.019

Tetreault, M., Choquet, K., Orcesi, S., Tonduti, D., Balottin, U., Teichmann, M., Fribourg, S., Schiffmann, R., Brais, B., Vanderver, A., & Bernard, G. (2011). Recessive mutations in POLR3B, encoding the second largest subunit of Pol III, cause a rare hypomyelinating leukodystrophy. *Am J Hum Genet*, *89*(5), 652-655. https://doi.org/10.1016/j.ajhg.2011.10.006

Thiffault, I., Wolf, N. I., Forget, D., Guerrero, K., Tran, L. T., Choquet, K., Lavallee-Adam, M., Poitras, C., Brais, B., Yoon, G., Sztriha, L., Webster, R. I., Timmann, D., van de Warrenburg, B. P., Seeger, J., Zimmermann, A., Mate, A., Goizet, C., Fung, E., . . . Bernard, G. (2015). Recessive mutations in POLR1C cause a leukodystrophy by impairing biogenesis of RNA polymerase III. *Nat Commun*, *6*, 7623. https://doi.org/10.1038/ncomms8623

Tyson, J. A., Goldberg, E. M., Maroof, A. M., Xu, Q., Petros, T. J., & Anderson, S. A. (2015). Duration of culture and sonic hedgehog signaling differentially specify PV versus SST cortical interneuron fates from embryonic stem cells. *Development*, *142*(7), 1267-1278. https://doi.org/10.1242/dev.111526

Ulfig, N. (2002). Calcium-binding proteins in the human developing brain. *Adv Anat Embryol Cell Biol*, *165*, III-IX, 1-92. https://www.ncbi.nlm.nih.gov/pubmed/12236093

Vallianatos, C. N., Raines, B., Porter, R. S., Bonefas, K. M., Wu, M. C., Garay, P. M., Collette, K. M., Seo, Y. A., Dou, Y., Keegan, C. E., Tronson, N. C., & Iwase, S. (2020). Mutually suppressive roles of KMT2A and

KDM5C in behaviour, neuronal structure, and histone H3K4 methylation. *Commun Biol*, *3*(1), 278. https://doi.org/10.1038/s42003-020-1001-6

van der Knaap, M. S., Schiffmann, R., Mochel, F., & Wolf, N. I. (2019). Diagnosis, prognosis, and treatment of leukodystrophies. *Lancet Neurol*, *18*(10), 962-972. https://doi.org/10.1016/S1474-4422(19)30143-7

van der Knaap, M. S., Wolf, N. I., & Heine, V. M. (2016). Leukodystrophies: Five new things. *Neurol Clin Pract*, *6*(6), 506-514. https://doi.org/10.1212/CPJ.0000000000000289

Vanderver, A., Tonduti, D., Bernard, G., Lai, J., Rossi, C., Carosso, G., Quezado, M., Wong, K., & Schiffmann, R. (2013). More than hypomyelination in Pol-III disorder. *J Neuropathol Exp Neurol*, *72*(1), 67-75. https://doi.org/10.1097/NEN.0b013e31827c99d2

Wolf, N. I., Ffrench-Constant, C., & van der Knaap, M. S. (2021). Hypomyelinating leukodystrophies - unravelling myelin biology. *Nat Rev Neurol*, *17*(2), 88-103. https://doi.org/10.1038/s41582-020-00432-1

Wolf, N. I., Salomons, G. S., Rodenburg, R. J., Pouwels, P. J., Schieving, J. H., Derks, T. G., Fock, J. M., Rump, P., van Beek, D. M., van der Knaap, M. S., & Waisfisz, Q. (2014). Mutations in RARS cause hypomyelination. *Ann Neurol*, *76*(1), 134-139. https://doi.org/10.1002/ana.24167

Wolf, N. I., Vanderver, A., van Spaendonk, R. M., Schiffmann, R., Brais, B., Bugiani, M., Sistermans, E., Catsman-Berrevoets, C., Kros, J. M., Pinto, P. S., Pohl, D., Tirupathi, S., Stromme, P., de Grauw, T., Fribourg, S., Demos, M., Pizzino, A., Naidu, S., Guerrero, K., . . . Group, H. R. (2014). Clinical spectrum of 4H leukodystrophy caused by POLR3A and POLR3B mutations. *Neurology*, *83*(21), 1898-1905. https://doi.org/10.1212/WNL.0000000000001002

Yu, Y., Zeng, Z., Xie, D., Chen, R., Sha, Y., Huang, S., Cai, W., Chen, W., Li, W., Ke, R., & Sun, T. (2021). Interneuron origin and molecular diversity in the human fetal brain. *Nat Neurosci*, *24*(12), 1745-1756. https://doi.org/10.1038/s41593-021-00940-3

SUPPLEMENTARY METHODS

Supplementary Table 1. iPSC lines

Line	Genotype	Age	Sex	Repr. method	Used for experiments
C1	Control	3d	M	Lentiviral	RNA sequencing
C2	Control	74d	M	Lentiviral	All
C3	Control	70y	M	Lentiviral	RNA sequencing
C4	Control	19y	F	Lentiviral	Neuronal analysis, Neuron-glia co-culture, qPCR
C5	Control	21y	M	Lentiviral	All except RNA sequencing
C6	Control	19y	M	Lentiviral	All except RNA sequencing
P1	4H (POLR3B)	10y	F	Lentiviral	All
P2	4H (POLR3B)	2y	M	Lentiviral	All
P3	4H (POLR3B)	4.5y	F	Lentiviral	All
P4	4H (POLR3A)	12y	F	Lentiviral	All except RNA sequencing
P5	4H (POLR3A)	24y	M	Sendai	Neuron-glia co-culture, qPCR
P6	4H (POLR3A)	2y	F	Sendai	Neuron-glia co-culture, qPCR

Repr. method: reprogramming method

RNA isolation

Total RNA was isolated from samples in Trizol using a chloroform-isopropanol extraction procedure. Briefly, cells were washed 3x with PBS (Braun Medical) and then incubated in 750uL Trizol for < 2 min at room temperature (RT). Samples in Trizol were transferred to 1.5mL Eppendorf tubes (VWR), dissolving any clumps with gentle titration, and stored at -80 C until needed for RNA isolation. After thawing sample tubes at RT, 150uL of chloroform was added to samples in Trizol, solutions mixed by shaking, and tube allowed to stand for 10min at RT. Tubes were then centrifuged (>13K g, 10min, 4C) and the top, clear liquid layer containing RNA transferred to new tubes. RNA was then precipitated by addition of 350uL isopropanol (Sigma-Aldrich) for every 750uL Trizol in the original sample. The tubes were inverted gently to mix, and the solution was allowed to stand for 10min at RT. The samples were centrifuged again (>13K g, 10min, 4C) and the supernatant was removed from the pellet. The pellet was then washed 2x with EtOH (VWR), with centrifugation after each wash step (7500g, 5min, 4C). The pellet was allowed to air-dry before dissolving in appropriate quantity of DMPC water and stored at -80C until needed. RNA concentration and quality were initially measured on a Nanodrop 3000.

RNA sequencing

Prior to RNAseq, concentration and quality were confirmed using RNA Analysis ScreenTape (Agilent Technologies, USA) on a 2200 TapeStation System (Agilent) to establish RIN scores. RNA samples of sufficient quality were processed according to manufacturer's instructions using the TruSeq Stranded Total RNA Library Prep Kit with Ribo-Zero Human (Illumina Inc., USA), generating tagged cDNA libraries capable for high-throughput RNA sequencing. Library concentration and quality were confirmed using D1000 ScreenTape (Agilent Technologies, USA) on the 2200 TapeStation System (Agilent). Samples were run on a Illumina HiSeq2500 at SR50. Quality control was performed using FastQC, and sequencing reads were aligned to Human Genome hg38 using Bowtie2(Langmead & Salzberg, 2012) with default parameters. Aligned reads were converted into count per gene using featureCount function from Rsubread package(Liao et al., 2013) with gene annotations obtained from GENCODE v26 (https://www.gencodegenes.org/) which contains unique 63,199 genes. Reads Per Kilobase per Million (RPKM) were further computed by using rpkm function from edgeR package(Robinson et al., 2010). Genes were filtered on such with count per million (CPM) > 1 in ≥ 50% of samples per cell type which resulted in 21,542 unique genes including non-coding RNAs.

Sample t-SNE map

To evaluate similarity between samples, we applied the t-Distributed Stochastic Neighbor Embedding (t-SNE) to the RNA-seq expression profiles. The t-SNE non-linearly projects local similarities between samples at the cost of retaining the similarities between dissimilar samples. We first normalized RPKM; zero-mean normalization followed by log2 transformation with pseudo count 1. Then t-SNE was performed 100 times and we selected the solution with the lowest Kullback-Leibler divergence.

Cell type validation with ENCODE samples

Gene expression profiles of 2 iPSC samples and 2 granule cell samples were obtained from ENCODE (ENCSR722POQ for iPSCs and ENCSR313IUO for granule cells). (Consortium, 2012) For expression profiles of ENCSR722PQO, obtained read counts were converted into RPKM as described above. For ENCSR313IUO, Fragments Per Kilobase Per Milling (FPKM) was available. Genes with expression value zero in all samples were filtered out. Since the expression data is not directly comparable between data sets, we performed Spearman's rank correlations across these 4 samples from ENCODE and samples from this study by taking intersect genes (18,719 genes in total).

Differentially expressed gene analysis

Raw count data was used for differentially expressed gene (DEG) analysis with DESeq2 package.(Love et al., 2014) For cell type comparison, we performed DESeq2 for a specific cell type against all other samples and tested all 21,542 genes. Control vs patient DEG was performed per cell type, and genes were further filtered on such with CPM > 1 in ≥ 50% of samples with the testing cell type. The number of tested genes for fibroblast, iPSC and product are 16,890, 18,855 and 19,032 genes, respectively. Genes with absolute log2 fold change (logFC) > 1 and Bonferroni corrected P-value < 0.05 were defined as DEG.

Cortical neuron differentiation

Neurons were generated from iPSCs according to previously published protocol (Nadadhur et al., 2017). Shortly, iPSCs were differentiated into neural epithelial stem cells (NES) using N2/B27 medium supplemented with Dorsomorphin and SB431. Within 1-2 weeks after plating neural rosettes appeared in the culture, which were selected by manual cutting. NES cells were maintained in N2/B27 medium supplemented with FGF2 and EGF for up to 4 passages. To differentiate NES cells into neurons, medium was changed to N2 medium supplemented with SHH for 4 days, followed by 3 days in Neurobasal/B27 medium with Valproic Acid. The day of the medium change to N2 medium with SHH was considered day 1 of neuronal differentiation. At day 8 of differentiation, cells were split into a new PLO/Laminin coated plate in Neurobasal/B27 medium supplemented with BDNF, GDNF, IGF1 and cAMP. At day 18, Neurons were passaged a final time and either frozen for later use or plated on rat astrocytes for further neuronal maturation. From now on, half of the medium was refreshed twice a week. At day 25, neurons were treated with AraC to remove proliferating progenitors. Neurons were kept in culture until day 56 (~5 weeks), at which point they resembled mature neurons in morphology and synaptic marker expression. For MEA and neuronal subtype proportion analysis, cultures were kept until 10 and 14 weeks post plating.

Oligodendrocyte differentiation

Oligodendrocyte progenitor cells (OPCs) were generated from iPSCs according to a previously published protocol (Dooves et al., 2019). Shortly, iPSCs were plated on an anti-adherent plate in N2/B27 medium with EGF, FGF2 and T3 to induce embryoid body formation. From day 2 onwards, RA was additionally added to the medium. At day 10, cells were plated on geltrex coated plates in N2/B27 medium with EGF and T3. At day 18, medium was switched to N2/B27 medium without vitamin A. Throughout the differentiation, cells

were passaged 1:2/1:3 into a new well when they reached confluency, using accutase dissociation. Half of the medium was refreshed every other day. At day 37 medium supplements were changed to EGF, FGF2, mouse Laminin, Vitamin C and T3. At day 39, Dorsomorphin was additionally added to the medium. At day 42, medium supplements were changed to mouse laminin, vitamin C, Dorsomorphin and T3. Cells were kept in these medium until day 67 when they were frozen or replated for neuron-OPC co-cultures.

Neuron-glia co-culture

For myelinating neuron-glia cultures, neurons and glia cells were differentiated from iPSCs as described in the supplementary methods. To promote neuronal maturation, neurons were plated on a monolayer of rat astrocytes. Rat astrocytes were isolated from postnatal day 1 rat cortex using papaïn dissociation. At 1 day and 4 days after dissociation, flasks with rat astrocytes were tapped to detach contaminating cells like oligodendrocytes or microglia as much as possible. Astrocytes were frozen at passage 1 until further use. To start a co-culture, day 18 cortical neurons were plated in Neurobasal/B27 medium supplemented with BDNF, GDNF, cAMP and IGF1. At day 30 of neuronal differentiation, day 67 human glial progenitor cells were added to the culture, and medium was switched to Neurobasal/N1 medium supplemented with T3, NT3, mouse Laminin, BDNF and cAMP. The co-cultures were kept in culture for an additional 40 days and subsequently fixed for immunostaining.

Supplementary Table 2. Primer sequences

Target	Forward primer	Reverse primer
ARX	AAACGCAAACAGAGGCGCTA	CAGTTCCTCCCTGGTGAAGAC
NEUN	TGGCATGACCCTGTACACAC	GCTGCTGCTTCTCTGTAGGG
EIF4G2 (housekeeping)	AGGACCGCATGTTGGAGATT	TGAGGGGATGGATCCAACTTT
NRG1	CGTGGAATCAAACGCTACATCT	TTCACCATGAAGCACTCCCC
PDE1A	CAGCAGTGGACCTGAAGAGTT	TGTGAACTGGTTCTTGCTTCTTG
ERBB4	GTTCAGGATGTGGACGTTGC	ACACACCGTCCTTGTCAAAGT
NDNF	GTGCTTAGCATCTTGGCAGG	TGGAGCAGCACCATCCTTAAA
RELN1	CGTCCTAGTAAGCACTCGCA	TCGCCTAAGTGACCTTCGTC
NEUN	GTCCCTTACTCCGCCAAGAG	CAAGGTCCTCCTTCTCAGGC
DLX2	ATCCAGAAATGTGCCTGCGG	AGCATCCTTCCTCCATTGCTT
CNTNAP2	CGTGGAATCAAACGCTACATCT	TTCACCATGAAGCACTCCCC
PDPR	TGTTGTGGCTGCCGCATTG	GCGGGAAAACAGTTCCATCTCAC
MACIR	GGGCCATCGTACCTGGA	AAGCACCAGTCTGCACAATC
ITGA11	TCGTGCTCCACAGCTGAATC	GACCTCAACCACAGGTTCCC

Immunocytochemistry

Cells were fixed for immunostaining using either 10 min fixation in 4% PFA (GAD65/67, CTIP2, MBP and OLIG2 staining) or by 10 minute fixation in ice cold 1:1 Acetone:Methanol. After fixation, cells were washed 6x 5 min with PBS and incubated in blocking buffer (PBS + 5% NGS + 0.3% Triton X-100 + 0.1% BSA) for 1 hour at RT. Primary antibodies were diluted in blocking buffer and incubated for 1 hour at RT followed by overnight incubation at 4˚C (see Table 2 for primary antibodies). The next day, cells were washed 6x 5min with PBS and incubated in secondary antibodies (Goat-anti-chicken/mouse/guinea pig/rabbit/rat Alexa Fluor 488/568/647) diluted 1:1000 in blocking buffer for 2 hours at RT. Cells were washed 6x 5 min with PBS, incubated in DAPI (1:1000 in PBS) for 1-2 min and embedded on microscope slides using Fluoromount G. Cells were imaged on a Leica DM6000B Fluorescent microscope, or on a Nikon Eclipse Ti confocal microscope for stainings of synapses and myelin. For GAD65/67 and CTIP2 stainings cells were scanned with a CellInsight CX7 HCA (ThermoFisher Scientific) and afterwards analyzed with Columbus software (Perkin Elmer). The proportion of GABAergic cells was determined by the percentage of $MAP2^+$ neurons that were also $GAD65/67^+$. As the neuronal differentiation gives rise to GABAergic and glutamatergic neurons(Nadadhur et al., 2017) we determined the proportion of glutamatergic neurons as the percentage of $MAP2^+$ neurons that were not positive for GAD65/67.

Immunohistochemistry

Formalin-fixed paraffin-embedded tissue was sliced into 5 µm-thick sections. Immunostaining was started by rehydrating sections in xylene and alcohol. Endogenous peroxidase was quenched in 0.3% (w/v) H_20_2 in PBS for 30 minutes, followed by heat induced antigen retrieval in citrate buffer (pH=6). Primary antibody GAD65/67 (1:1000, G-5163, Sigma) was incubated overnight at room temperature. The following day slides were rinsed and incubated with horseradish peroxidase labelled secondary antibodies for 1 hour and developed using 3,3′-diaminobenzidine (DAB, 1:50, DAKO) for 5 minutes. Sections were counterstained with haematoxylin, dehydrated with alcohol and xylene and mounted with Quick-D (Klinipath, 7280). Light microscopy pictures were taken with a Leica DM6000B microscope (Leica microsystems). Quantification of the number of GAD65/67 cells was done by manually counting the number of nuclei and the number of $GAD65/67^+$ nuclei on 4 pictures (10x magnification) of the cortex.

Supplementary Table 3. Primary antibodies for immunostaining

Target	Host	Dilution	Company	Number
CTIP2	Rat	1:250	Abcam	AB18465
GAD65/67	Rabbit	1:1000	Sigma	G5163
MAP2	Chicken	1:5000	Millipore	AB5543
MBP	Rat	1:500	Abcam	AB7349
NF-200	Rabbit	1:1000	Sigma	N4142
NF-H	Mouse	1:100	Hybridomabank	RT-97-s
OLIG2	Rabbit	1:500	Millipore	AB9610
SMI312	Mouse	1:1000	Eurogentech	SMI-312P-050
Synaptophysin1	Guinea Pig	1:1000	Sysy	101-004
VGAT	Rabbit	1:500	Sysy	131-002

Multi electrode array analysis

Day 18 cortical neurons, generated as described above, were plated on PLO/Laminin coated MEA plates (Multi Channel Systems 24W300/30G-288) together with rat astrocytes (1:6 ratio) and cultured as described above. MultiChannel Headstage hardware (Multi Channel Systems) and Mulitwell-Screen software (Multi Channel Systems) were used to record baseline electrophysiological activity. Measurements were performed for 30 minutes (after 10 minutes incubation) while controlling the environment at 37°C and humidified 5% CO_2. Raw data was sampled at 10 kHz and filtered using a high-pass 2nd order Butterworth filter with 100 Hz cut-off and low-pass 4th order Butterworth with 3500 Hz cut-off. The data was analyzed using Multiwell-Analyzer software (Multichannel Systems). Faulty electrodes were manually excluded from the analysis upon visual inspection. Spike detection threshold was set at -5.0 standard deviations from baseline. To start a burst at least 4 consecutive spikes had each to be less than 50 ms apart. Burst events needed a minimal duration of at least 50 ms. If the spikes within a burst are more than 50 ms apart a burst ends, new burst can only start 100 ms after the last burst. Network burst detection was set on 6 (=50%) or more participating channels of which at least 3 (25%) simultaneous. Results were exported and visualized using RStudio, SPSS was used for statistical testing.

To measure the effect of different compounds on neuronal activity in 4H and control cells, cells were treated with either APV (50 µM), DNQX (10 µM), TTX (1 µM), GABA (10 µM) or Bicuculin/Gabazine (30 µM/20 µM), at 14 weeks post plating. In addition, to one well of each line the corresponding solvent (DMSO or H_2O) was added in the same volume as the

compounds. Compounds were mixed in and electrical activity was recorded for 5 minutes at 37°C and 5% CO_2 flow after a 5 minute incubation period under the same conditions. Plain Neurobasal medium was used to wash out the compounds. After washing, 50% of old and 50% of new Neurobasal/B27 medium with fresh supplements (BDNF, GDNF, IGF, cAMP) were added. Cultures were let to recover for 24h before addition of the next compound.

ImageJ analysis

For synaptic analysis the NeuronJ plugin was used to trace MAP2+ dendrites. In SynaptoCount, the dendritic tracing was loaded and used to determine the total number of synapses by counting the number of Synaptophysin1+ puncta present on the dendrites. The amount of VGAT+ synapses was determined by the number of VGAT+/Synaptophysin1+ puncta present on dendrites. The synaptic density was calculated by dividing the total number of synapses by the pixel length of the dendrites. The percentage of VGAT+ synapses was determined by dividing the number of VGAT+ synapses by the total number of synapses. For myelin analysis the NeuronJ plugin was used to trace NF-200$^+$ axons, and the pixel length of axons was measured. Neurite tracings were then loaded on MBP staining, and the pixel length of neurites that showed co-localization of MBP and NF-200 staining was determined. The percentage of myelinated axons was determined by dividing the length of MBP$^+$/NF200$^+$ neurites by the total length of NF200 neurites.

References

Langmead B, Salzberg SL. Fast gapped-read alignment with Bowtie 2. Nat Methods. 2012;9(4):357-359.

Liao Y, Smyth GK, Shi W. The Subread aligner: fast, accurate and scalable read mapping by seed-and-vote. Nucleic Acids Res. 2013;41(10):e108.

Robinson MD, McCarthy DJ, Smyth GK. edgeR: a Bioconductor package for differential expression analysis of digital gene expression data. Bioinformatics. 2010;26(1):139-140.

Consortium EP. An integrated encyclopedia of DNA elements in the human genome. Nature. 2012;489(7414):57-74.

Love MI, Huber W, Anders S. Moderated estimation of fold change and dispersion for RNA-seq data with DESeq2. Genome Biol. 2014;15(12):550.

Nadadhur AG, Emperador Melero J, Meijer M, et al. Multi-level characterization of balanced inhibitory-excitatory cortical neuron network derived from human pluripotent stem cells. PLoS One. 2017;12(6):e0178533.

Dooves S, Nadadhur AG, Gasparotto L, Heine VM. Co-culture of Human Stem Cell Derived Neurons and Oligodendrocyte Progenitor Cells. Bio Protoc. 2019;9(17):e3350.

SUPPLEMENTARY FIGURES

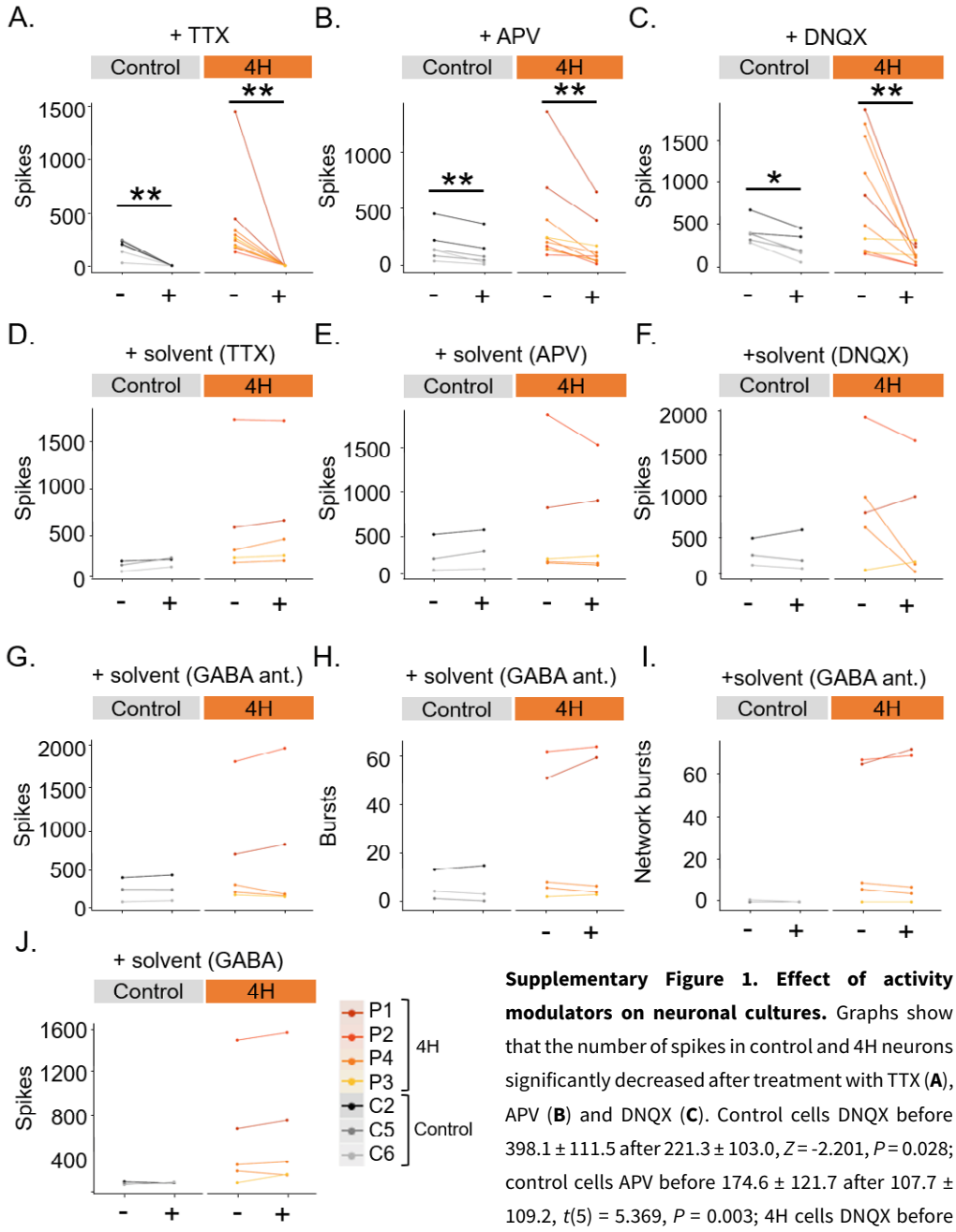

Supplementary Figure 1. Effect of activity modulators on neuronal cultures. Graphs show that the number of spikes in control and 4H neurons significantly decreased after treatment with TTX (**A**), APV (**B**) and DNQX (**C**). Control cells DNQX before 398.1 ± 111.5 after 221.3 ± 103.0, Z = -2.201, P = 0.028; control cells APV before 174.6 ± 121.7 after 107.7 ± 109.2, $t(5)$ = 5.369, P = 0.003; 4H cells DNQX before 834.3 ± 424.1, after 126.6 ± 65.1, $t(9)$ = 3.412, P = 0.008, 4H cells APV before 174.6 ± 121.7, after 107.7 ± 109.2, Z = -2.803, P = 0.005. Addition of solvents to cultures did not influence network activity in any of the conditions (**D**-**J**). (**G**-**I**) GABA ant. = GABA antagonists bicuculline and gabazine. * = $P < 0.05$, ** = $P < 0.01$. Data points and lines represent data per well, with lines with the same color representing wells from the same individual.

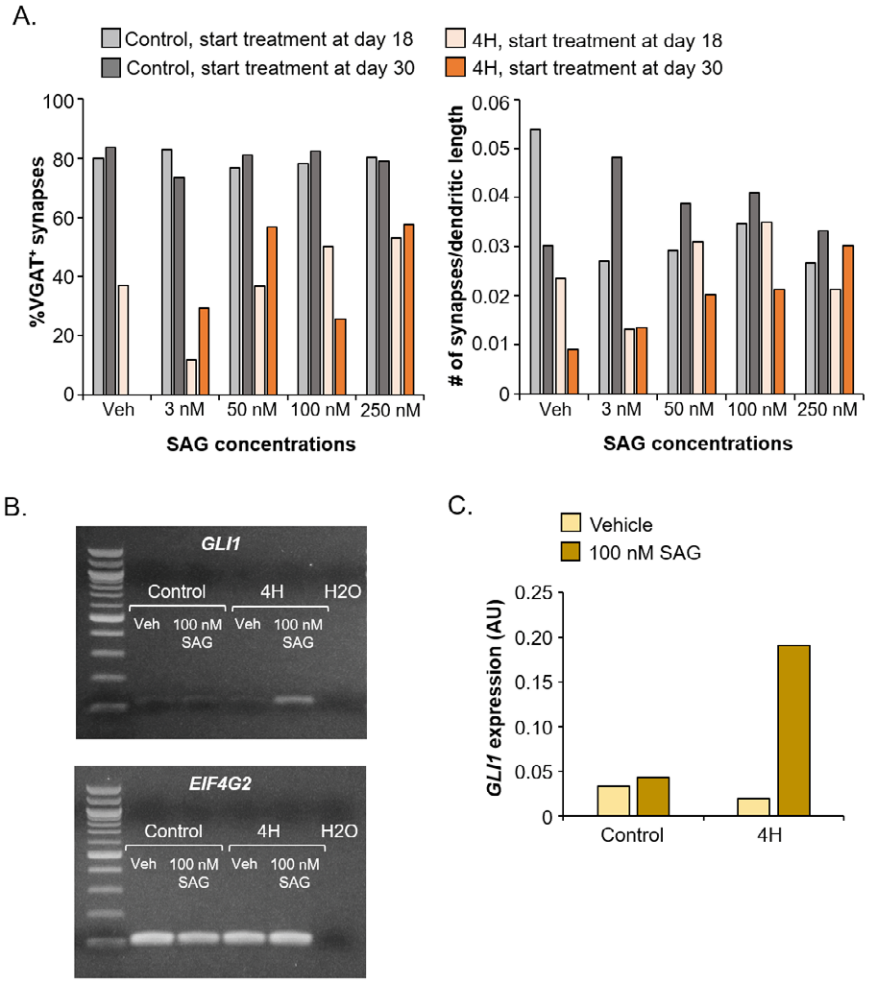

Supplementary Figure 2. Pilot study to test efficacy of SAG concentrations. A control and a 4H line were treated with vehicle, 3 nM, 50 nM, 100 nM or 250 nM SAG, either started from day 18 or day 30 of the neuronal differentiation. (**A**) The left graph shows the percentage of VGAT$^+$ synapses, which did not change in the control line in any treatment condition. However, for the 4H line the percentage of VGAT$^+$ synapses was increased after treatment with 100 or 250 nM SAG. The right graph shows the number of synapses per dendritic length. SAG treatment decreased the number of synapses per dendritic length slightly in the control line, although it was slightly increased in the 4H line with 50 or 100 nM SAG when treatment was started at day 18. (**B**) shows the expression of SHH downstream target *GLI1* and housekeeping gene *EIF4G2* after vehicle or 100 nM SAG treatment in control and 4H cells. Quantification of *GLI1* band intensity shows that, after correction for *EIF4G2* band intensity, the *GLI1* expression is increased in 4H neurons (**C**). Veh = vehicle, AU = arbitrary units.

Supplementary Table 4-6 are available at *Brain* online.

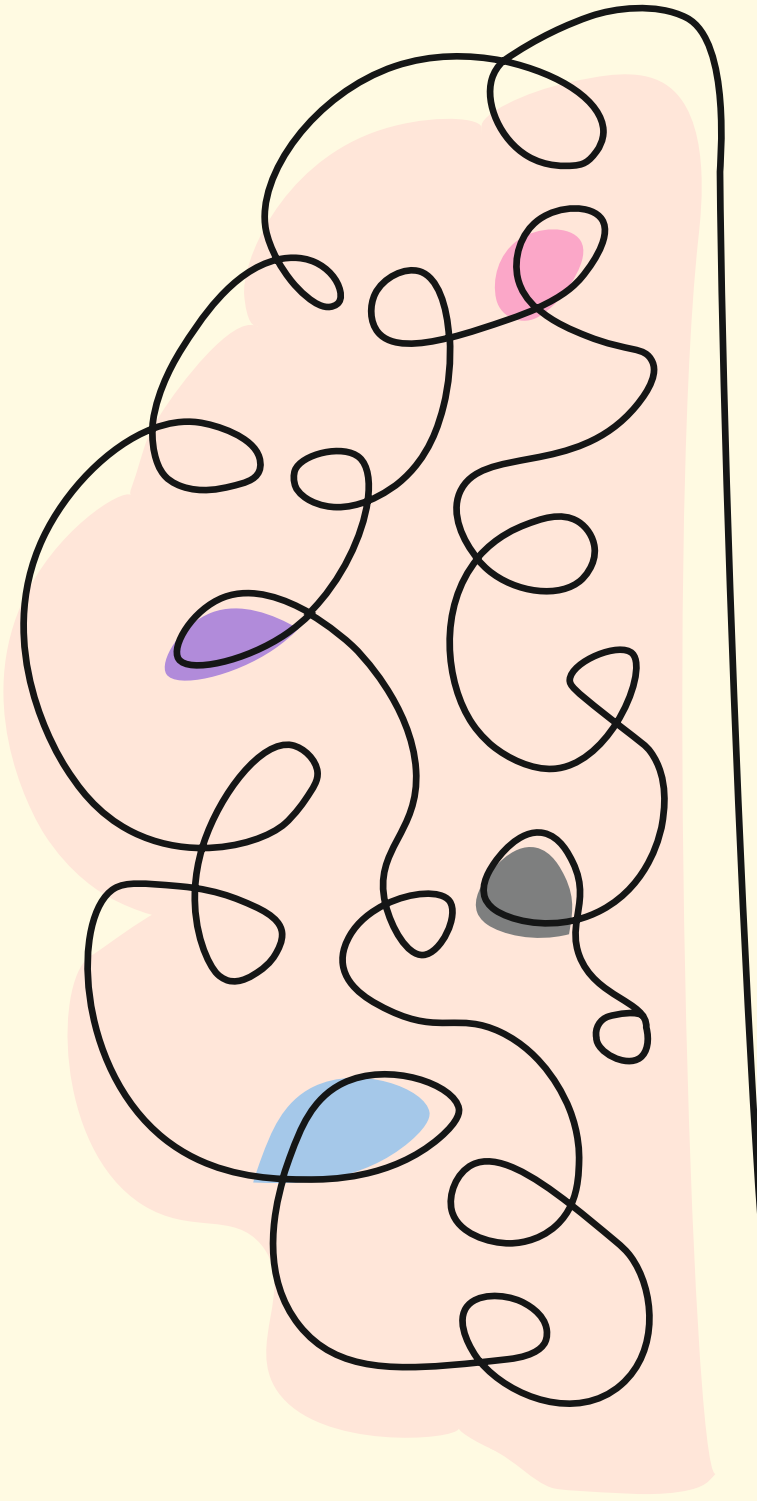

03

Investigating neuron intrinsic defects in 4H and Globoid Leukodystrophy

Liza M. L. Kok, Sandra Braz, Elisabeth Mangiameli, Eduardo Veríssimo, Bruno Cavadas, Joana Rodrigues, Clarissa Rosato, Angela Gritti, Monica Sousa, Vivi M. Heine

ABSTRACT

Leukodystrophies, once considered solely glial disorders, are increasingly associated with neuronal dysfunction. This study examines neuronal involvement in 4H leukodystrophy and globoid cell leukodystrophy (GLD) using human iPSC-derived neuron–astrocyte co-cultures and neuron mono-cultures. In 4H neuron mono-cultures, neurons had shorter neurites and a progressive decline in mitochondrial transport, opposed time increased mitochondrial transport in control neuron cultures. Additionally, transcriptomic analysis of 4H neurons revealed downregulation of genes related to synaptic signalling and cerebral cortex regionalization and development, and upregulation of genes related to morphogenesis and ribosomal pathways, suggesting potential mechanisms underlying 4H neuron abnormalities. In contrast, GLD neurons lacked distinguishing transcriptomic signatures. Also, in GLD neuron-astrocyte co-cultures no significant differences in neurite outgrowth, microtubule dynamics, or mitochondrial transport were observed, and psychosine accumulation, a hallmark of GLD, was absent. In GLD neuron mono-cultures only moderate psychosine accumulation was detected. This study highlights potential molecular pathways in 4H pathology and emphasizes the limitations of current *in vitro* models for studying leukodystrophies, providing a foundation for future research.

INTRODUCTION

Leukodystrophies, a group of inherited disorders characterized by brain white matter abnormalities, were for long viewed as disorders caused by glial dysfunctions. However, findings in recent years also point towards a role for neuronal defects in white matter pathology (Mar & Noetzel, 2010; van der Knaap & Bugiani, 2017). Whether the underlying mechanistic changes are disease-specific or more common among leukodystrophies is unclear. As insight into the mechanisms underlying neuronal dysfunction would facilitate the identification and development of new targeted therapies for leukodystrophies, we set out to study this.

We investigated globoid cell leukodystrophy (GLD) and 4H leukodystrophy, two leukodystrophies with known neuronal involvement. GLD is characterized by neurodegenerative features such as axonal swellings, disrupted microtubule dynamics, and impaired axonal transport, as demonstrated in animal models like the twitcher mouse (Cantuti Castelvetri et al., 2013; Teixeira et al., 2014). These features are thought to result from the accumulation of psychosine, a hallmark of the disease. In 4H leukodystrophy, neuronal defects are less studied. Though initial evidence suggests changes in the inhibitory neuron population (Dooves et al., 2023).

To investigate neurons in these leukodystrophies, we utilized an established human iPSC-derived cortical model (Nadadhur et al., 2017) to assess intrinsic neuron properties such as neurite outgrowth, microtubule dynamics, and mitochondrial transport. In this co-culture system, we did not identify changes in the afore mentioned neuron properties. We hypothesized that healthy astrocytes potentially influence disease phenotypes, hence we assessed neuronal parameters in a neuron-mono culture model as well. Our analysis showed that 4H neuron mono-cultures show decreased neurite length, but only compared to GLD. Additionally, 4H neurons showed a decrease in motility of mitochondria over time, while for GLD and control neurons mitochondria motility increases. Besides this, GLD and 4H neurons did not display significant differences in neurite outgrowth, microtubule dynamics and axonal transport. Additionally, psychosine build-up was lacking in GLD neurons. On the other hand, mRNA sequencing analysis revealed that 4H neurons have a downregulation of genes involved in synaptic signalling and cortical development, alongside upregulation of genes related to developmental and ribosomal pathways. Pathway analysis further indicated potential dysregulation in Notch signalling and protein synthesis pathways in 4H neurons. Together, transcriptional alterations showed

abnormalities in 4H neuron population and provided insights into underlying molecular pathways, emphasizing the need for further studies to elucidate neuron-specific vulnerabilities in leukodystrophies. Importantly, this report highlights the need for careful selection of *in vitro* models to investigate the neuronal aspects of leukodystrophies, as demonstrated by the lack of psychosine build-up in GLD cultures.

RESULTS

Neurite outgrowth, microtubule dynamics and mitochondrial transport unaffected by 4H and GLD in co-culture

To investigate neuronal features in leukodystrophies we used an established human iPSC-derived cortical neuron culture containing both glutamatergic and GABAergic neurons that were matured in presence of rat astrocytes and transduced with EB3-GFP LV at DIV20 (Fig. 1A). At day 21, bright-field imaging showed dense neurite growth in all samples, including controls and leukodystrophy models (Fig. 1B). The neurite length of EB3-GFP transduced neurons was analysed after fixation at DIV21 (Fig. 1B-C) and showed that the cumulative neurite length ranged from 150 to 1019 µm per neuron. Although there was some variation in mean neurite length for cell lines, there were no significant differences in mean neurite length among control, 4H and GLD (Fig. $1D_{1\text{-}2}$). Similarly, axon length was measured, the shortest axon was 46 µm and the longest 438 µm. No significant differences in mean axon length were observed among the phenotypes (Fig. 1E).

To study microtubule dynamics, we investigated EB3 comet density and velocity in growth-cones of iPSC-derived neurons. The 4H lines, in particular hvs201, showed high mean comet density compared to the others (Fig. $1F_1$); however the difference between control, 4H and GLD were not significant ($H(2) = 5.088$, $p = 0.0571$, Fig. $1F_2$). In the EB3 comet speed we also did not identify a difference between controls and any of the leukodystrophies (Fig. 1G).

To study mitochondrial motility, we quantified the percentage of stationary and motile mitochondria by live-cell imaging (Fig. $1H_1$). This revealed no significant differences observed between control, 4H, and GLD groups (Fig. $1H_2$). Mitochondrial transport direction was further analysed, and again no significant differences in the proportions of mitochondria moving anterograde, retrograde, or in both directions were identified (Fig. $1I_1$-I_4). Noteworthy for GLD, the GALC KO line had particularly low percentage of mitochondria moving towards both directions (Fig. $1I_2$).

Lastly, we investigated mitochondria transport length and velocity. Although, for GLD lines the distance and velocity of mitochondria movement was lower than controls for the KO line and higher compared to controls for the KI line, we did not observe a disease specific phenotype (Fig. 1J-K).

In conclusion, besides some subtle trends, we did not identify any significant disease specific phenotypes in 4H or GLD neurons in this co-culture set-up.

No Psychosine Accumulation in GLD Co-Cultures

Based on earlier findings, we expected altered neurite outgrowth, disrupted microtubule dynamics and impaired axonal transport in GLD neurons (Cantuti Castelvetri et al., 2013; Teixeira et al., 2014). As enzyme deficiencies in GLD result in psychosine accumulations, a key disease feature of GLD, we analysed psychosine levels in our cultures at day 21. Surprisingly, psychosine levels were elevated in iPSCs, and in neuron differentiation products but not in co-cultures i.e., levels in GLD co-cultures were similar to those observed in control samples (Fig. 1L). Additionally, no indication of other disturbances in glycosphingolipid metabolism were found (Supplementary Fig. 1A-C).

In summary, no distinct neuronal phenotypes were identified in 4H and GLD neurons based on neurite outgrowth, microtubule dynamics, or mitochondrial transport at 21 days of co-culture. Additionally, psychosine accumulation was not observed in GLD neurons under these conditions.

Distinct mitochondrial dynamics and minimal psychosine accumulation in neuron-mono cultures of leukodystrophies

We hypothesized that presence of healthy rat astrocytes in the iPSC-derived neuron cultures might prevent psychosine accumulation in GLD neurons, potentially masking GLD-specific neuronal features. Therefore, we implemented a neuron-mono culture. To allow for a direct comparison of unique GLD and 4H neuronal phenotypes, we used this setting to model 4H as well. By examining two timepoints, we aimed to capture any dynamic changes in neuronal functioning that might emerge over time (Fig. 2A). We assessed the same neuronal parameters as we did for the co-cultures.

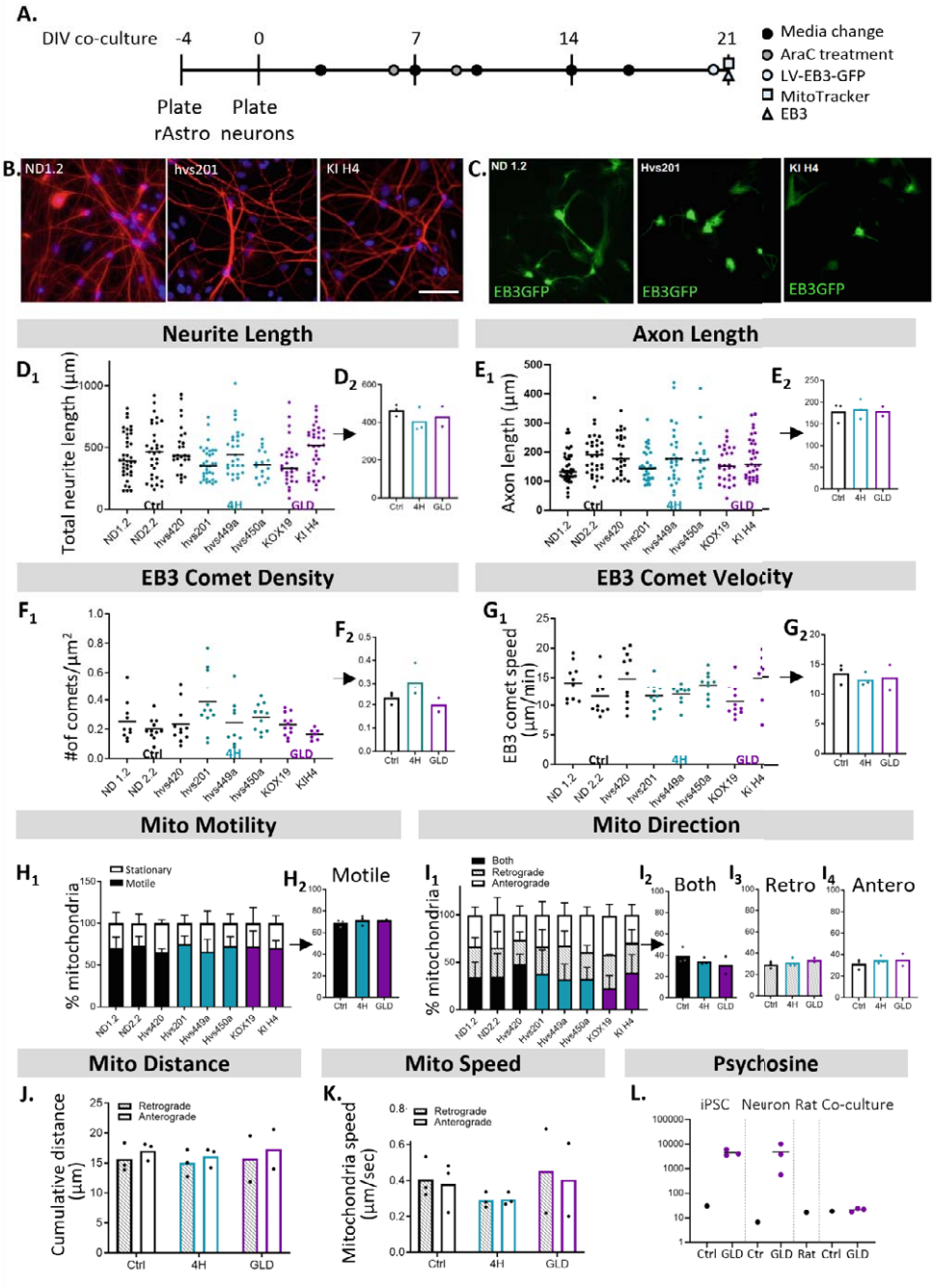
A.
DIV co-culture
-4
0
7
14
21
Plate rAstro
Plate neurons
Media change
AraC treatment
LV-EB3-GFP
MitoTracker
EB3
B.
ND1.2
hvs201
KI H4
C.
ND 1.2
Hvs201
KI H4
EB3GFP
Neurite Length
Axon Length
EB3 Comet Density
EB3 Comet Velocity
Mito Motility
Mito Direction
Mito Distance
Mito Speed
Psychosine
Total neurite length (µm)
Axon length (µm)
#of comets/µm²
EB3 comet speed (µm/min)
% mitochondria
Stationary
Motile
Both
Retrograde
Anterograde
Cumulative distance (µm)
Mitochondria speed (µm/sec)
iPSC Neuron Rat Co-culture
Ctrl
4H
GLD

◀ **Figure 1: Lack of leukodystrophy-specific neuronal defects in co-cultures. A**) Schematic representation of co-culture set-up with rat astrocytes. **B**) Immunofluorescent images of βIII-tubulin staining in control (ND1.2), 4H (hvs201) and GLD (KI H4) neurons showing dense neurite networks. Scale bar = 100 µm. **C**) Representative images of EB3-GFP transduced neurons (control, 4H and GLD) used for quantification of neurite and axonal lengths. Graphs displaying **D**) Neurite length, **E**) Axon length, **F**) EB3 comet density and **G**) EB3 Comet Velocity. Scatter plots represent individual observations, with horizontal lines showing the mean for each cell line. Bar graphs summarize the group mean for either Control (ctrl), 4H or Globoid (GLD) Leukodystrophy with individual dots for cell line means. Mitochondrial (Mito.) **H**) Motility and **I**) Direction are depicted by bar graphs for each line with error bars displaying the standard deviation, as well as bar graphs summarizing the mean for controls, 4H or GLD with dots for cell line means. **J**) Distance and **K**) Speed of mitochondria are depicted by open bars for retrograde travelling mitochondria and open for anterograde travelling mitochondria. Each dot represents a mean for a cell line. **L**) Psychosine concentrations (pmol/gram) measured in iPSCs, DIV0 neurons, rat astrocytes, and co-cultures at DIV21 for control and GLD samples. DIV = days in vitro.

Over time, between 3 and 8 days in vitro (DIV), neurite length increased in all but one GLD line. While on the contrary another GLD line, KI H4, presents a very steep increase in neurite length over time (Fig. $2B_1$). ANOVA showed a significant difference between neurite length of control, 4H and GLD combined ($F(2)=5.657$, $p = 0.0416$, Supplementary Table III). Post-hoc multiple comparisons showed that the difference occurred between 4H and GLD (Mean difference -73.57, $P = 0.0355$; Fig. $2B_2$ and Supplementary Fig. 2A). Similarly, the longest neurite, axon length increased over time, with no observable differences between controls and any of the leukodystrophies (Fig. 2C, Supplementary Fig. 2B). Of note, the GLD 5.2 line was the only line that displayed a decreased mean neurite length and axon length at DIV3 compared to DIV8.

The microtubule dynamics, specifically EB3 comet density, seemed to be slightly lower in both leukodystrophies compared to control, but this difference was not statistically significant (Fig. 2D, Supplementary Fig. 2C). Also, no differences were observed in EB3 comet velocity across control and leukodystrophy groups (Fig. 2E, Supplementary Fig. 2D). To note, ANOVA on EB3 comet velocity was near the significance threshold ($p = 0.07$, Supplementary Table III), post-hoc multiple comparisons showed that this was driven by a difference between 4H and GLD cultures.

Mitochondrial transport analysis in the neuron-mono cultures revealed an increase in the percentage of motile mitochondria over time, between DIV2 and DIV7, in both control and GLD lines, while 4H lines showed a reduction in motile mitochondria over time (Fig. 2F, Supplementary Fig. 2E). In 4H, overall mitochondrial motility was reduced (Fig. 2G,

Supplementary Fig. 2H). The variation between the individual GLD lines was large, potentially pointing to line-specific changes. For example, the GLD KO line exhibited a consistent high percentage of anterograde transport. And the 4H hvs450 line initially displayed high rates of mitochondria moving in both directions, while at DIV7 there was more unidirectional movement. The distance and velocity of mitochondria transport was not significant different between control and leukodystrophies, though both parameters were lowest in the GLD KO line across both timepoints (Fig. 2I–J, Supplementary Fig. 2I), but these trends did not reach statistical significance.

To determine if psychosine accumulation was more pronounced in the absence of astrocytes, we measured psychosine levels in the neuron mono-culture model. Contrary to our expectations, psychosine levels were not significantly elevated in the GLD lines under mono-culture conditions (Fig. 2J). Again, there are also no indication of other disturbances in glycosphingolipid metabolism (Supplementary Fig. 1D-F).

In summary, these results display potential differences in mitochondrial motility, specifically the direction of movement, as a distinguishing feature between 4H and control neurons in mono-culture settings. While these models show potential for investigating neuron intrinsic defects and detection of leukodystrophy-related phenotypes, minimal psychosine accumulation in GLD cultures and variability across individual lines warrant refinement of experimental designs to draw solid conclusions.

► **Figure 2: hiPSC-derived neuron mono-cultures as a more suitable model for leukodystrophy related neuronal defects. A**) Schematic representation of mono-culture set-up. Quantification of **B**) Neurite length, **C**) Axon length, **D**) EB3 comet density and **E**) EB3 Comet Velocity and **F**) Mitochondrial (Mito.) motility. Line graphs connect the mean values for each cell line across timepoints while bar graphs summarize the mean for control, 4H and GLD with dots representing individual cell line means. Mitochondrial **G**) Direction, **H**) Distance, and **I**) Speed are displayed individually for mitochondria travelling retrograde, anterograde or both directions. Related bar graphs can be found in the supplement. **J**) Psychosine concentrations (pmol/gram) in iPSC and neuron mono-cultures at DIV7 from control (ctrl) or GLD cells. DIV = Days in vitro.

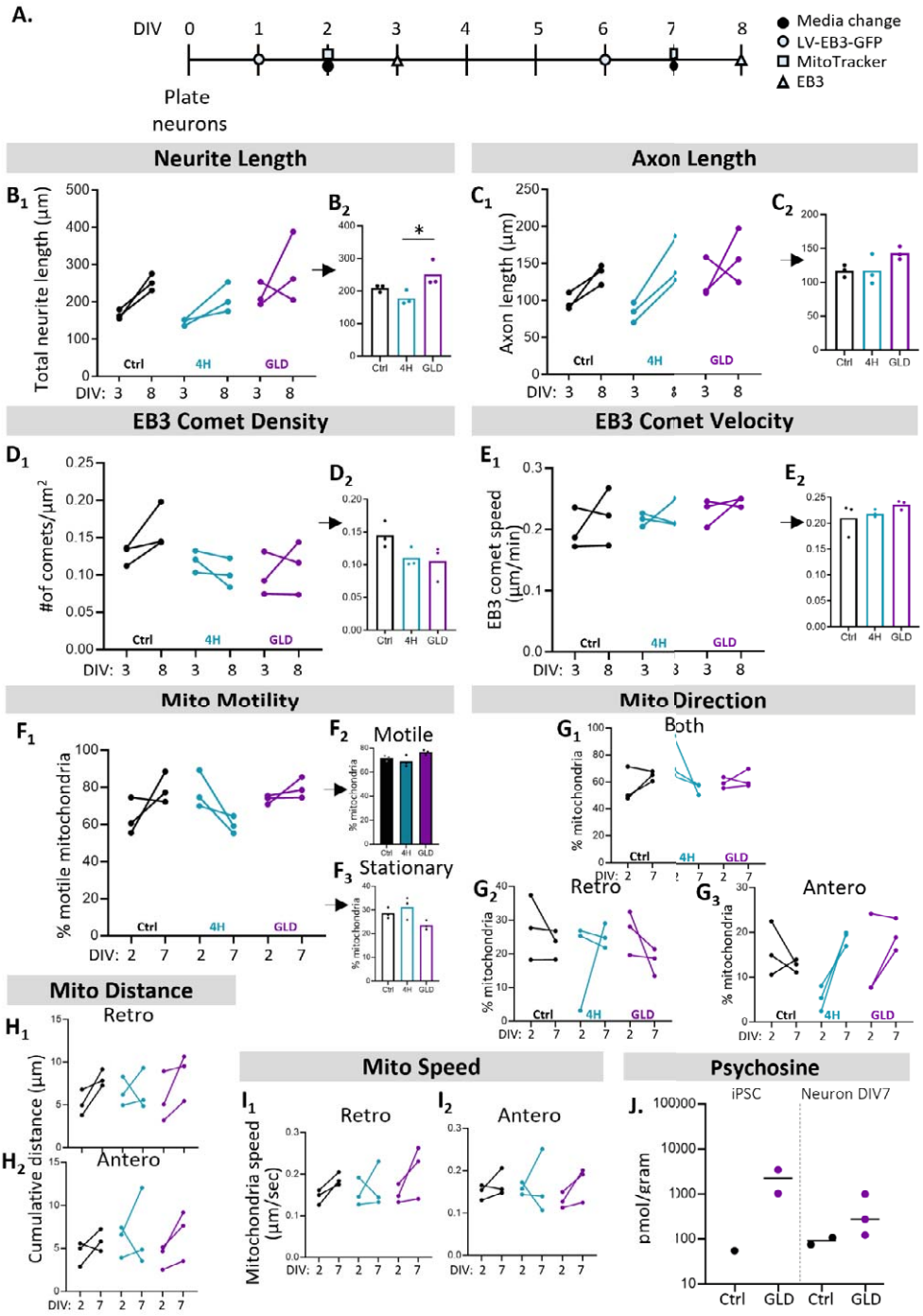
A.
DIV 0 1 2 3 4 5 6 7 8
Media change
LV-EB3-GFP
MitoTracker
EB3
Plate neurons
Neurite Length
Axon Length
Total neurite length (µm)
Axon length (µm)
Ctrl
4H
GLD
DIV: 3 8 3 8 3 8
EB3 Comet Density
EB3 Comet Velocity
#of comets/µm²
EB3 comet speed (µm/min)
Mito Motility
Mito Direction
% motile mitochondria
Motile
Stationary
Both
Retro
Antero
% mitochondria
Mito Distance
Cumulative distance (µm)
Mito Speed
Mitochondria speed (µm/sec)
Psychosine
iPSC
Neuron DIV7
pmol/gram

Exploring Transcriptional Changes Using PCA

To further explore neuronal changes at the molecular levels, we performed bulk RNA sequencing on neuron-mono cultures at day 25. Principal component analysis (PCA) revealed clear separation between control and 4H neurons (Supplementary Fig. 3A-C), while GLD samples did not clearly distinguish from controls and scattered throughout the plots (Supplementary Fig. 3A-B). The limited separation of GLD samples from other controls, made the differential gene expression analysis and gene set enrichment analysis unreliable. We tried to improve contrast by removing KO X19 from the analysis, as this seemed to be the outlier. However, this did not resolve the issue (Supplementary Fig. 3B). Hence, we proceed to discuss only the analysis for 4H compared to control (Supplementary Fig. 3C).

In 4H neurons, we identified 575 differentially expressed genes (DEGs) compared to controls (Fig. 3A). Among these, 304 genes were downregulated, including 136 with log2 fold change less than -1, and 271 genes were upregulated, with 246 showing log2 fold change greater than 1. Notably, the gene *TRIM4*, a gene related to neural tube defects and associated with GO-terms for axons, was most significant downregulated (Zhang et al., 2019). Other interesting downregulated genes are *SLC17A7* (Vglut1) which is synapse related, *RELN* which is linked to interneurons and GO-terms for neuronal migration (Yu et al., 2021) and *LHX2* which is important for neural development (Chou & Tole, 2019). Conversely, *EFCC1*, which is related to GO-terms for calcium binding, is most significant upregulated. Also *IRX1*, *IRX2*, *IRX3*, *NKX1*-2, and *NKX2-2* were significantly upregulated indicating potential dysregulation in pathways associated with neuronal tube patterning and neurogenesis (Bosse et al., 1997).

Pathway analysis reveal 4H neuronal phenotypes

To get a completer and more unbiased overview we performed Gene Set Enrichment Analysis (GSEA). Significant discoveries have an adjusted P-value of < 0.05. However, as this dataset was intended to be exploratory and to assist the formation of new hypothesis and directions for future research, we investigated all findings with an adjusted P < 0.25. Gene ontology (GO) analysis of DEGs revealed downregulation in several neuron-related biological processes, including synaptic signalling, regulation of transsynaptic signalling, pallium and cerebral cortex development and regionalization (Fig. 3B). Specifically, 5 out of 7 genes associated with cerebral cortex regionalization contribute to the finding, strongly suggesting impaired cortical development. Surprisingly, upregulated pathways were often kidney related, which is not meaningful considering our investigation of neuron-mono cultures. However, some genes associated with kidney development such as IRX1, 2 and 3,

are also associated with embryonic morphogenesis and regionalization in general. In the biological process pathways there are also many non-significant but possible relevant mechanisms. Here we see the same division of downregulated neuron-related biological processes and upregulated morphogenesis and embryo development pathways (Supplementary Fig. 4).

GO analysis cellular components identified significant downregulation in genes related to neuronal compartments such as the dendritic tree, somatodendritic compartment, glutamatergic synapse and neuron-to-neuron synapse. Also the non-significant but possibly interesting findings ($P < 0.025$) mainly involve neuron compartments (Fig. 3C). We did not find any significant upregulated pathways, however for the ribosomal subunits a large proportion of genes in this gene set (58% of 171) contribute to the findings, which suggests there might still be an increase in protein synthesis machinery. For molecular functions, only upregulation of DNA binding transcription repressor activity reached adjusted significance, and only GPCR activity was within our <0.25 cutoff (Fig. 3D). Hallmark analysis identified trends in pathways related to Notch signalling, Hedgehog signalling and E2F targets, though none reached statistical significance after adjustment (Fig. 3E). KEGG analysis highlighted ribosomal pathways with high gene set enrichment (72% of 86 genes), though again not significant after adjusting for multiple testing. Notch signalling reappeared in this analysis, potentially indicating disrupted developmental signalling relevant to 4H pathology.

Summarized, bulk RNA sequencing of 4H and GLD neurons in neuron-mono culture conditions identified clear transcriptional differences in 4H. In 4H, we observed downregulation of neuronal processes related to synaptic signalling and cortical development, alongside upregulation of developmental pathways and ribosomal components. Pathway analysis in 4H further indicated potential dysregulation in Notch signalling and protein synthesis, underscoring molecular distinctions specific to 4H.

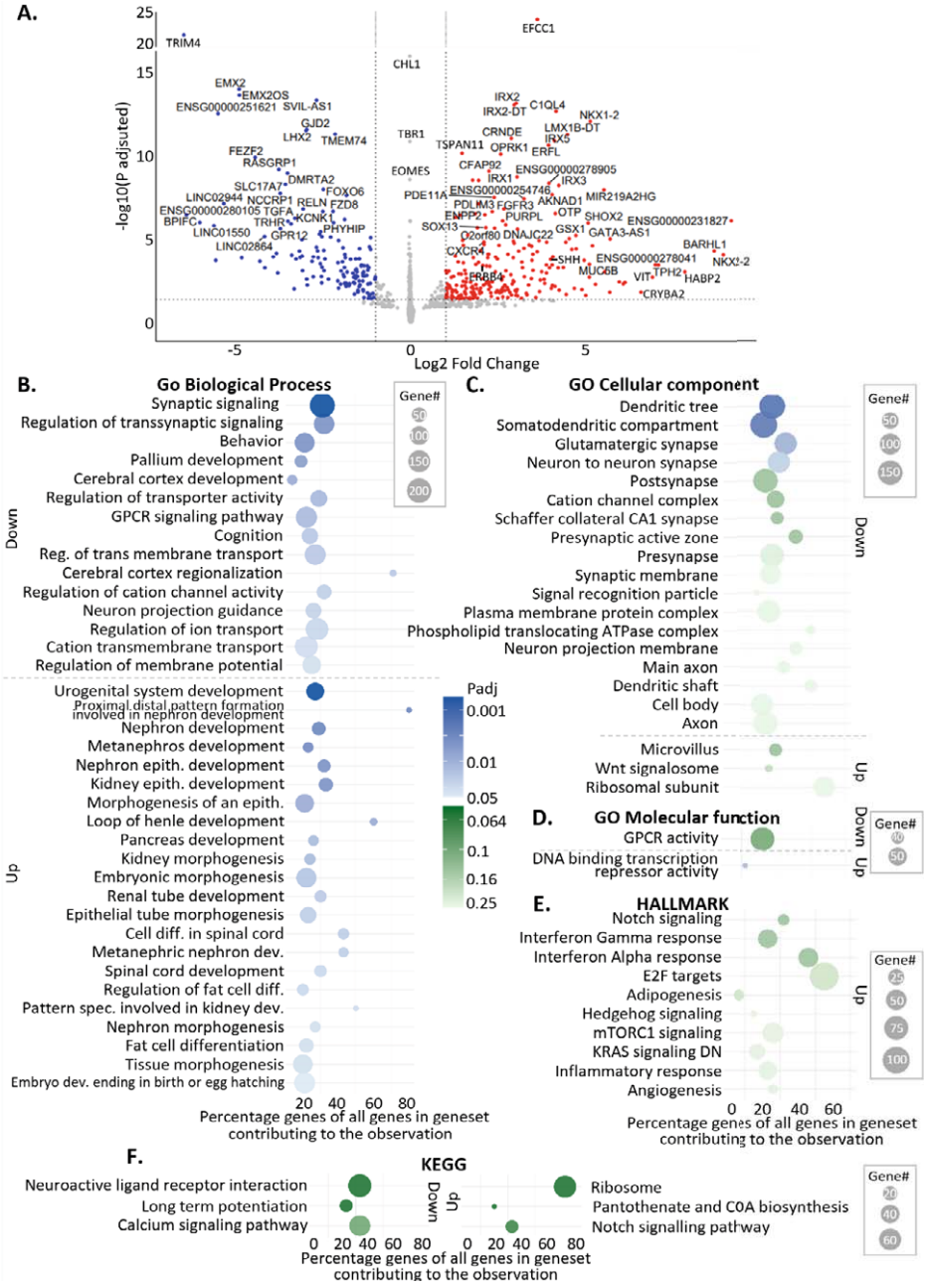

Figure 3: Bulk mRNA sequencing of DIV7 neurons in maturation medium. A) Differential gene expression between control and 4H neurons. Bubble plots representing results from **B**) GO analysis for biological process, **C**) Cellular component, **D**) and Molecular function, **E**) Hallmark analysis, **F**) KEGG analysis. Bubble colour intensity shows significance P adjusted, Blue = significant, Green = non-significant. Bubble size shows the number of genes that contributed to the evidence. The position of the bubble along the x-axis shows the percentage of genes from the entire gene set that contributed to the evidence. GPCR: G protein coupled receptor, Epith. Epithelium, Dev. = development, Diff. = differentiation, Spec. = specification, Reg.=regulation.

DISCUSSION

To investigate neuronal properties in leukodystrophies, this study explored 4H and GLD neuronal phenotypes using patient iPSC-based cortical neuron cultures in presence and absence of rat astrocytes. In mono-culture, 4H neurons had shorter neurites compared to GLD and control neurons, though only reached statistical significance in comparison to GLD. Additionally, 4H neurons showed a decrease in mitochondrial transport between DIV2 and 7 in cultures, while control (and GLD) neuron cultures presented an increase in mitochondrial transport. In addition, transcriptomic analysis in 4H neurons revealed downregulation of synaptic and cortical development genes and upregulation of developmental and ribosomal pathways, suggesting potential mechanisms underlying 4H pathology and underscoring the potential of this model to study 4H specific mechanisms. In GLD cultures, psychosine accumulation, a hallmark of GLD, was not detected in co-culture and only moderately present in the neuron-mono cultures. When rat astrocytes were present in the GLD neuron culture, no significant differences in neurite outgrowth, microtubule dynamics, or mitochondrial transport were observed between groups. Transcriptomic results for GLD were also inconclusive, reinforcing the limitations of these models for studying GLD disease mechanisms.

Missing psychosine accumulation in GLD cultures

We did not observe psychosine accumulation in GLD patient neurons when co-cultured with rodent astrocytes. This suggests that astrocytes may influence metabolic processes in ways that limit the manifestation of leukodystrophy-related neuronal defects. This is in line with the observation that GLD iPSCs grown on healthy donor feeder layers also lacked psychosine build-up. Additionally, it is well-established that astrocytes can present neuroprotective functions (Belanger & Magistretti, 2009). Interestingly, the absence of phenotypic changes in the co-cultures suggests that effective targeting of astrocytes might be a therapeutic strategy for mitigating neuronal defects in GLD. In contrast, co-culture conditions with healthy rat astrocytes in models of 4H have revealed abnormalities in the GABAergic population (Dooves et al., 2023), implying that the lack of phenotypes in GLD co-cultures may be specific to the pathology of the leukodystrophy subtype. This emphasized that we need to optimize *in vitro* models to adequately captures disease-specific changes.

Surprisingly, psychosine did not robustly accumulate in neuron-mono cultures either, except for line KOX19, which showed slightly elevated levels (999 pmol/gram). Considering that accumulation was detected at the neuronal progenitor stage, there is likely some kind

of clearance mechanism of psychosine becoming active at later stages. Possibly, psychosine might be secreted via extracellular vesicles or diluted through passive diffusion during regular media changes (Reiter et al., 2022). In accordance with this hypothesis, the line with the highest psychosine levels (KOX19) in mono-cultures is also the line with the highest level of psychosine at day 18 (10267 pmol/gram) so it could be that this line needs more time to go back to physiological psychosine levels. Interestingly, the KOX19 line also separated from all other samples in the PCA plots derived from mRNA bulk sequencing data, suggesting distinct transcriptomic profiles. However, this divergence did not translate into detectable differences in axon morphology and transport measurements.

These findings highlight the significant influence of experimental conditions on psychosine dynamics, and related neuronal defects. Further investigation is needed to elucidate these mechanisms. It would be interesting to investigate psychosine levels in the media, pharmacologically block extracellular vesicle release, and track psychosine levels across multiple timepoints. Additionally, lipidomic profiling might be useful to better understand psychosine metabolism in models of GLD.

Mitochondrial transport changes in 4H neurons

Previously, we demonstrated that 4H neurons in co-culture with astrocytes exhibit neuronal abnormalities, including increased activity (Dooves et al., 2023). The absence of clear defects in the current study may be due to differences in the parameters assessed or a delayed onset of abnormalities, as prior findings were observed in cultures maintained for up to 14 weeks (Dooves et al., 2023). Nevertheless, a trend towards decreased mitochondrial transport over time in 4H mono-cultures was identified. Mitochondrial transport serves as proxy for axonal transport, a critical process for maintaining neuronal health. Axonal transport is important for delivery of newly synthesized macromolecules and organelles from the cell body to the synapse (anterograde transport) and the return of signalling endosomes and autophagosomes to the cell body for degradation (retrograde). Specifically, mitochondrial transport is dynamically regulated in response to changes in neuronal activity and various physiological and pathological states (MacAskill & Kittler, 2010; Sheng & Cai, 2012). Disrupted axonal transport, including mitochondrial trafficking, are implicated in several neurodegenerative diseases (Berth & Lloyd, 2023). These findings highlight the potential role of mitochondrial transport abnormalities in the pathology of 4H. Future investigations should focus on confirming whether mitochondrial dysfunction contributes to disease progression and on understanding the underlying molecular mechanisms.

Significance of Transcriptomic Findings in 4H Neurons

Transcriptomic analysis of 4H neurons revealed many significant differentially expressed genes between 4H and control neurons. Among the most significant upregulated genes was EFCC1, associated with calcium ion binding and osteogenesis imperfecta. So far, no apparent links with Pol III translation or leukodystrophies can be made. On the contrary, genes related to neural tube defects such as *TRIM4*, *IRX1*, *2* and *3* were differentially expressed and could be more easily linked to neurodevelopmental defects (Zhang et al., 2019). The gene *RELN*, an early marker for NDNF interneurons was differentially expressed, which is inline with previously established interneuron abnormalities in 4H (Dooves et al., 2023).

GSEA analysis showed significant differences in many biological processes related to neuron signalling and development, reinforcing the presence of a neuronal phenotype in 4H neurons. From the cellular component gene sets many were significantly different between 4H and control. While these differences did not point to singular specific defect, it is interesting to note that they are mainly downregulated, potentially indicating an overall decline in neuronal functioning. This is however not captured by our morphological or axonal transport assessments, leading to the hypothesis that the transcriptional changes might precede measurable phenotypes in these parameters. Hence, this emphasizes the need for further research on more mature neurons to capture later-emerging defects.

Although not adjusted for significance, hallmark gene set analysis revealed possible relevance of the upregulation of Notch and MTORC1 signalling. Those pathways are known to stimulate Pol III transcription and ribosome synthesis (Lee et al., 2012; Orellana et al., 2022; Wei et al., 2009). Similarly, upregulation of E2F target gene set was observed. E2F is thought to regulate the production of Pol III-dependent products through interaction with RB (Sizer et al., 2024). Together with the KEGG gene set analysis which shows upregulation of ribosome-related genes, these results suggest potential alterations in translation and Pol III transcription pathways.

Lastly, hallmark gene set analysis shows the possible relevance of hedgehog signalling, previously linked to 4H pathology via *ARX*. Although, the targeting of the Shh pathway could not be confirmed as therapeutic target (Dooves et al., 2023), its recurrence in this analysis is intriguing. However, it is important to interpret this finding with caution, as this gene set consists of a small number of genes and a small percentage contributes to the observation.

Taken together, the detected transcriptomic changes indicate that this model does capture certain aspects of 4H neuronal phenotypes. However, the changes are subtle, and more work needs to be done to confirm the involvement of signalling pathways and/or biological processes in 4H neuronal pathology. To validate the relevance of these findings, future research could focus on the relation of these pathways and Pol III using possible conditional Pol III knock-outs or knock-downs using techniques such as siRNAs. Such investigations should also consider extended culture periods, as models that have shown neuronal phenotypes in 4H involved more mature stages (Dooves et al., 2023).

Conclusion and Future Recommendations

This study revealed limited morphological abnormalities in 4H and GLD neuronal models, with only moderate psychosine accumulation observed in GLD monocultures. While transcriptomic analysis identified molecular changes in 4H neurons, that direct future research opportunities, no conclusive phenotypes were found in GLD models. More appropriate *in vitro* models to address neuronal defects in leukodystrophies are required, especially for GLD. The optimization and identification of such models could start by exploring extended timepoints, psychosine levels over time and lipidomic profiling.

MATERIALS & METHODS

iPSC culture

iPSCs were generated and maintained according to the protocols of the origin institutes (Dooves et al., 2023; Mangiameli et al., 2021). Written consent was obtained from all participants in accordance with the declaration of Helsinki.

Neural Differentiation

Cortical neurons were generated using the previously published protocol using dual SMAD inhibition and consequent maturation of cells into glutamatergic and GABAergic neurons (Nadadhur et al., 2017). Neurons were frozen at day 18 of differentiation in 10% DMSO in KSR.

Neural Maturation Co-Culture

Rat astrocytes were obtained by papaïn dissociation of cortex of postnatal day 1 pups. To minimize contamination of other cells rat astrocytes were vigorously tapped before each medium change. Medium consisted of DMEM/F12 medium + Glutamax + 10% FBS + 1x NEAA

+ 1x Pen/Strep. Astrocytes of passage 3 were frozen (medium with 10% DMSO) and used for experiments. Frozen rat astrocytes were quickly thawed in a water bath and plated at a density of 4k per cm^2 on geltrex coated 4 well-IBIDIs (ibiTreat, 80426). When confluent, 25k neurons per chamber (which equals to 10k neurons per cm^2) were plated on top of the rat astrocytes in NB medium with 20 ng/ml BDNF + 10 ng/ml GDNF + 10 ng/ml IGF1 + 1 µM cAMP. Twice a week half medium changes were performed, with supplements for the entire volume. On DIV6 and DIV10, 1 day before the refreshments, 2 µm of AraC was added, to inhibit proliferation. The next day, half media refreshments were performed until DIV20.

Neural Maturation Mono-Culture

Frozen day 18 neurons were quickly thawed in the water bath and plated at a density of 10k neurons per cm^2 on PLO/Laminin coated 4 well-IBIDIs (ibiTreat) in STEMdiff™ forebrain neuron maturation medium. Full media refreshments were performed twice a week.

Analysis of Sphingolipid Metabolism

In order to analyse cultures on GLD associated deficiencies in sphingolipid metabolism, 1 million neurons were plated at a density of 10k neurons/cm^2 according to previously described co-culture or mono-culture protocols. They were maintained for either 21 days (co-culture) or 7 days (mono-culture). Cells were collected using a cell scraper and pelleted by centrifugation. Supernatant was removed and cell pellets were stored and shipped at -80°C for analysis of glucosylceramide (GlcCer), galactosylceramide (GalCer), glucosylsphingosine (LysoGlcCer) and galactosylsphingosine (LysoGalCer, psychosine) at the Core Facility Metabolomics of the Amsterdam UMC, location AMC, the Netherlands. For iPSC, neuron and rat samples frozen cells (approximately 1 million) were quickly thawed in a water bath and frozen pellets were shipped for analysis.

Live-cell Imaging for Microtubule Dynamics

For the analysis of MT dynamics in the growth cone, we applied a previously described protocol (Sousa et al., 2024). Briefly, neurons were transduced (at DIV20 for co-cultures, or DIV1 and 6 for mono-cultures) with lentivirus expressing CMV-EB3-GFP (27000 transducing unit (TU)/well, plasmid from F. Polleux, Columbia University, USA). 24 hours after, time-lapse recordings were performed in phenol-free media or forebrain maturation media supplemented as mentioned above, at 37°C and 5% CO_2, on a Leica SP8 microscope (Leica Microsystems) and Leica Application Suite X (LAS X) software (version 3.5.7.23225, RRID:SCR_013673) with a HC FLUOTAR L 25x/0.95 W objective. For quantification of EB3

comet growth speed, kymographs were performed using the Fiji Kymotoolbox plugin (distance, *x* axis; time, *y* axis).

Live-cell Imaging for Axonal Transport

Mitochondrial axonal transport was investigated using previously published protocol (Sousa et al., 2024). Briefly, live imaging of iPSC-derived neurons was performed at DIV39 for co-cultures or DIV2 and 7 for mono-cultures. To analyse mitochondria transport, cultures were incubated at 37°C with medium containing, 25 nM MitoTracker™ Orange CMTMRos (Invitrogen, M7510) for 1 h before live imaging. All moving particles were imaged in a confocal Leica SP8 microscope (Leica Microsystems) with LAS X software (version 3.5.7.23225, RRID:SCR_013673) with HC FLUOTAR L 25x/0.95 W objective. Excitation was carried out using 488 or 561 nm laser lines. Image acquisition was performed for 2 min with 2-2.5 sec frame intervals with a pixel size of 0.116 µm. To analyse axonal transport of moving particles, Kymotoolbox plugin from Fiji/ImageJ was used. The percentage of motile mitochondria was obtained by tracking both motile and stationary mitochondria for 2 min.

Neurite Outgrowth and Growth Cone Morphology

Neurite outgrowth was addressed in transduced EB3-GFP neurons only, according to previously described protocol (Pinto-Costa et al., 2020). Neuron cultures were fixed with 4% paraformaldehyde (PFA) followed by incubation with mouse anti–βIII-tubulin (1:1,000; Promega, G7121) overnight at 4°C and secondary antibody incubation (donkey anti-mouse–Alexa Fluor 594, 1:1,000; Jackson ImmunoResearch Labs, 715-585-150). Images were acquired by epifluorescence in a Leica DMI6000 B (Leica) equipped with a Hamamatsu FLASH4.0 digital camera and Leica Application Suite Advanced Fluorescence (LAS AF) software (RRID:SCR_013673). Neurite tracing and branching analyses were manually traced using the FIJI NeuronJ plugin. The longest neurite was considered to be the axon.

RNA Isolation

For RNA isolation from neuron mono-cultures, 1.6M neurons were grown in a density of 40K/cm^2. After one week in STEMdiff™ forebrain neuron maturation medium , and feedings on DIV2 and 5, total RNA was isolated using Trizol Reagent (Thermo Fisher Scientific) according to manufacturer's protocol. Samples were sent for bulk mRNA sequencing (NovaSeqXPlus, Illumina technique) to the Core Facility Genomics (Amsterdam UMC, Amsterdam, The Netherlands) and sequenced at a depth of 40M reads per sample.

mRNA Sequencing Analysis

A pre-established pipeline was used to process the samples[1]. This pipeline performed the quality control of reads, carried the trimming of adapters, aligned the reads and performed the quality control of the resulting alignment. The data was sequenced using a paired-end stranded library (reverse strand) and sequenced using the Illumina technology. Specifically, sequence alignment was carried in STAR v2.7.10a with the human GRCh38 reference (GENCODE v44). Counts per gene were generated by STAR. Prior to alignment, reads were pre-processed in TrimGalore to remove adapters sequences. If after adapter trimming the resulting read had a length below 35 bp, it was removed from the analysis. Count data processed above was evaluated in DESeq2 to detect differentially expressed genes. A principal component analysis was performed to check for outliers and how samples were being separated by cluster. Differential expression (DE) analysis was carried out in R v4.1.2 using DESeq2 (v1.34). For each comparison, the log2FC was shrunken using the apeglm algorithm. Gene-set enrichment analysis, using the pre-ranked list of genes (signed log2FC x -log10(padj)) was done in fgsea using five different molecular ontology databases: Hallmarks (biological states or processes), GO_BP (Biological Process), GO_CC (Cellular Component), GO_MF (Molecular Function) and KEGG (pathways). Only findings with and FDR below 0.25 were considered as a FDR value of 0.25 indicates that the result is likely to be valid 3 out of 4 times, which is reasonable in the setting of exploratory discovery where one is interested in finding candidate hypothesis to be further validated as a results of future research.

Statistics

Data analysis was started by addressing potential outliers, we applied the Robust Regression and Outlier Removal (ROUT) method (Q=1%) (Motulsky & Brown, 2006). For co-cultures, the data exhibited unbalanced sampling and frequent violations of variance homogeneity and normality, hence, group differences were evaluated using the Kruskal-Wallis test, a nonparametric method relatively robust to unequal sample sizes compared to ANOVA. Post-hoc testing with Dunn's multiple comparisons test was performed for near-significant result of comet density. All results are detailed in Supplementary Table II.

[1] https://i3s-bioinformaticsservice.github.io/analysis/transcriptomics/rnaseq_star_default/

Mono-culture analysis is performed by first averaging the observations for each timepoint (per line), followed by an overall average for DIV21 and DIV26. Differences in mean levels were analysed using one-way ANOVA, which was deemed appropriate after confirming normal residuals (Shapiro-Wilk test) and homogeneity of variances (Brown-Forsythe test). To ensure transparency, individual observations for each cell line are plotted in Supplementary Fig. 2, allowing visual assessment of data distribution and variability across groups. All test results for mono-culture are detailed in Supplementary Table III.
All statistical testing was conducted in GraphPad Prism (v.10.2.0).

FUNDING

This work was supported by the European Joint Programme on Rare Diseases (EJPRD19-201, NG4LEUKO).

COMPETING INTERESTS

The authors report no competing interests.

AUTHOR CONTRIBUTIONS

LMLK, EM and CR generated cortical neurons. LMLK performed neuronal maturation and sample collection for sequencing. SB, EV and JR performed neuronal maturation and subsequent neurite outgrowth and microtubule dynamics analysis. BC analysed RNA sequencing experiments. VMH, AG and MS supervised the project. LMLK visualized the data and wrote the chapter in consultation with other authors.

REFERENCES

Belanger, M., & Magistretti, P. J. (2009). The role of astroglia in neuroprotection. *Dialogues Clin Neurosci*, *11*(3), 281-295. https://doi.org/10.31887/DCNS.2009.11.3/mbelanger

Berth, S. H., & Lloyd, T. E. (2023). Disruption of axonal transport in neurodegeneration. *J Clin Invest*, *133*(11). https://doi.org/10.1172/JCI168554

Bosse, A., Zulch, A., Becker, M. B., Torres, M., Gomez-Skarmeta, J. L., Modolell, J., & Gruss, P. (1997). Identification of the vertebrate Iroquois homeobox gene family with overlapping expression during early development of the nervous system. *Mech Dev*, *69*(1-2), 169-181. https://doi.org/10.1016/s0925-4773(97)00165-2

Cantuti Castelvetri, L., Givogri, M. I., Hebert, A., Smith, B., Song, Y., Kaminska, A., Lopez-Rosas, A., Morfini, G., Pigino, G., Sands, M., Brady, S. T., & Bongarzone, E. R. (2013). The sphingolipid psychosine inhibits fast axonal transport in Krabbe disease by activation of GSK3beta and deregulation of molecular motors. *J Neurosci*, *33*(24), 10048-10056. https://doi.org/10.1523/JNEUROSCI.0217-13.2013

Chou, S. J., & Tole, S. (2019). Lhx2, an evolutionarily conserved, multifunctional regulator of forebrain development. *Brain Res*, *1705*, 1-14. https://doi.org/10.1016/j.brainres.2018.02.046

Dooves, S., Kok, L. M. L., Holmes, D. B., Breeuwsma, N., Breur, M., Bugiani, M., Wolf, N. I., & Heine, V. M. (2023). Cortical interneuron development is affected in 4H leukodystrophy. *Brain*, *146*(7), 2846-2860. https://doi.org/10.1093/brain/awad017

Lee, J., Moir, R. D., McIntosh, K. B., & Willis, I. M. (2012). TOR signaling regulates ribosome and tRNA synthesis via LAMMER/Clk and GSK-3 family kinases. *Mol Cell*, *45*(6), 836-843. https://doi.org/10.1016/j.molcel.2012.01.018

MacAskill, A. F., & Kittler, J. T. (2010). Control of mitochondrial transport and localization in neurons. *Trends Cell Biol*, *20*(2), 102-112. https://doi.org/10.1016/j.tcb.2009.11.002

Mangiameli, E., Cecchele, A., Morena, F., Sanvito, F., Matafora, V., Cattaneo, A., Della Volpe, L., Gnani, D., Paulis, M., Susani, L., Martino, S., Di Micco, R., Bachi, A., & Gritti, A. (2021). Human iPSC-based neurodevelopmental models of globoid cell leukodystrophy uncover patient- and cell type-specific disease phenotypes. *Stem Cell Reports*, *16*(6), 1478-1495. https://doi.org/10.1016/j.stemcr.2021.04.011

Mar, S., & Noetzel, M. (2010). Axonal damage in leukodystrophies. *Pediatr Neurol*, *42*(4), 239-242. https://doi.org/10.1016/j.pediatrneurol.2009.08.011

Motulsky, H. J., & Brown, R. E. (2006). Detecting outliers when fitting data with nonlinear regression - a new method based on robust nonlinear regression and the false discovery rate. *BMC Bioinformatics*, *7*, 123. https://doi.org/10.1186/1471-2105-7-123

Nadadhur, A. G., Emperador Melero, J., Meijer, M., Schut, D., Jacobs, G., Li, K. W., Hjorth, J. J. J., Meredith, R. M., Toonen, R. F., Van Kesteren, R. E., Smit, A. B., Verhage, M., & Heine, V. M. (2017). Multi-level characterization of balanced inhibitory-excitatory cortical neuron network derived from human pluripotent stem cells. *PLoS One*, *12*(6), e0178533. https://doi.org/10.1371/journal.pone.0178533

Orellana, E. A., Siegal, E., & Gregory, R. I. (2022). tRNA dysregulation and disease. *Nat Rev Genet*, *23*(11), 651-664. https://doi.org/10.1038/s41576-022-00501-9

Pinto-Costa, R., Sousa, S. C., Leite, S. C., Nogueira-Rodrigues, J., Ferreira da Silva, T., Machado, D., Marques, J., Costa, A. C., Liz, M. A., Bartolini, F., Brites, P., Costell, M., Fassler, R., & Sousa, M. M. (2020). Profilin

1 delivery tunes cytoskeletal dynamics toward CNS axon regeneration. *J Clin Invest*, *130*(4), 2024-2040. https://doi.org/10.1172/JCI125771

Reiter, C. R., Rebiai, R., Kwak, A., Marshall, J., Wozniak, D., Scesa, G., Nguyen, D., Rue, E., Pathmasiri, C., Pijewski, R., van Breemen, R., Cologna, S., Crocker, S. J., Givogri, M. I., & Bongarzone, E. R. (2022). The Pathogenic Sphingolipid Psychosine is Secreted in Extracellular Vesicles in the Brain of a Mouse Model of Krabbe Disease. *ASN Neuro*, *14*, 17590914221087817. https://doi.org/10.1177/17590914221087817

Sheng, Z. H., & Cai, Q. (2012). Mitochondrial transport in neurons: impact on synaptic homeostasis and neurodegeneration. *Nat Rev Neurosci*, *13*(2), 77-93. https://doi.org/10.1038/nrn3156

Sizer, R. E., Butterfield, S. P., Hancocks, L. A., Gato De Sousa, L., & White, R. J. (2024). Selective Occupation by E2F and RB of Loci Expressed by RNA Polymerase III. *Cancers (Basel)*, *16*(3). https://doi.org/10.3390/cancers16030481

Sousa, S. C., Aroso, M., Bessa, R., Verissimo, E., Ferreira da Silva, T., Lopes, C. D. F., Brites, P., Vieira, J., Vieira, C. P., Aguiar, P. C., & Sousa, M. M. (2024). Stretch triggers microtubule stabilization and MARCKS-dependent membrane incorporation in the shaft of embryonic axons. *Curr Biol*, *34*(19), 4577-4588 e4578. https://doi.org/10.1016/j.cub.2024.08.018

Teixeira, C. A., Miranda, C. O., Sousa, V. F., Santos, T. E., Malheiro, A. R., Solomon, M., Maegawa, G. H., Brites, P., & Sousa, M. M. (2014). Early axonal loss accompanied by impaired endocytosis, abnormal axonal transport, and decreased microtubule stability occur in the model of Krabbe's disease. *Neurobiol Dis*, *66*, 92-103. https://doi.org/10.1016/j.nbd.2014.02.012

van der Knaap, M. S., & Bugiani, M. (2017). Leukodystrophies: a proposed classification system based on pathological changes and pathogenetic mechanisms. *Acta Neuropathol*, *134*(3), 351-382. https://doi.org/10.1007/s00401-017-1739-1

Wei, Y., Tsang, C. K., & Zheng, X. F. (2009). Mechanisms of regulation of RNA polymerase III-dependent transcription by TORC1. *EMBO J*, *28*(15), 2220-2230. https://doi.org/10.1038/emboj.2009.179

Yu, Y., Zeng, Z., Xie, D., Chen, R., Sha, Y., Huang, S., Cai, W., Chen, W., Li, W., Ke, R., & Sun, T. (2021). Interneuron origin and molecular diversity in the human fetal brain. *Nat Neurosci*, *24*(12), 1745-1756. https://doi.org/10.1038/s41593-021-00940-3

Zhang, H., Guo, Y., Gu, H., Wei, X., Ma, W., Liu, D., Yu, K., Luo, W., Ma, L., Liu, Y., Xue, J., Huang, J., Wang, Y., Jia, S., Dong, N., Wang, H., & Yuan, Z. (2019). TRIM4 is associated with neural tube defects based on genome-wide DNA methylation analysis. *Clin Epigenetics*, *11*(1), 17. https://doi.org/10.1186/s13148-018-0603-z

SUPPLEMENTARY FIGURES

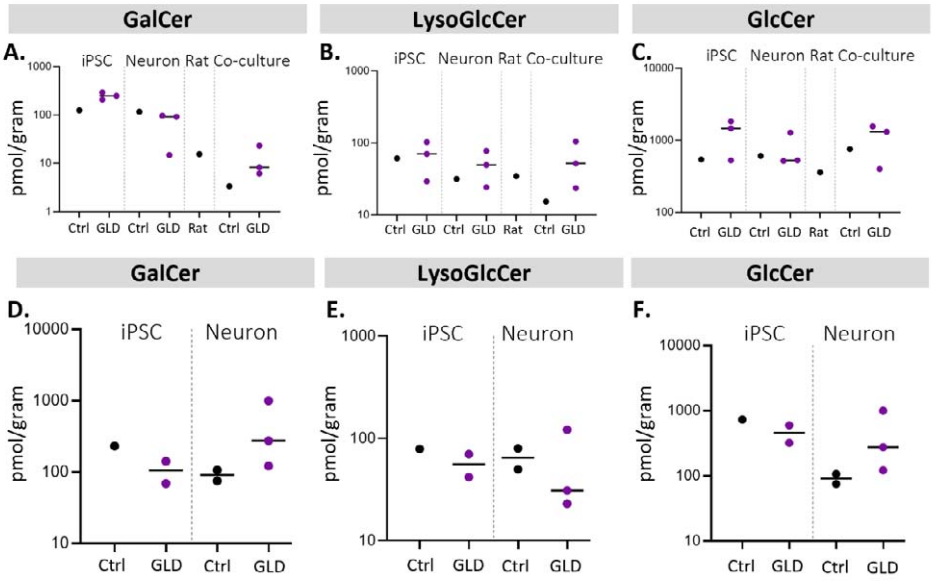

Supplementary Figure 1: Quantification of GalCer, LysoGlcCer, and GlcCer levels in control (Ctrl) and GLD cells. Levels of GalCer (**A**), LysoGlcCer (**B**), and GlcCer (**C**) in iPSCs, DIV0 neurons, rat astrocytes and in DIV21 co-cultures. Each dot represents an individual sample, with control (black) and GLD (purple) groups shown. Rat astrocyte samples are included as additional reference for co-cultures. And comparison of GalCer (**D**), LysoGlcCer (**E**), and GlcCer (**F**) levels in iPSCs and DIV7 neurons in mono-culture from control (black) and GLD (purple) groups. Horizontal lines indicate group means. Lipid quantifications are presented in pmol/gram. Note the log scale for all panels, reflecting the wide range of detected concentrations.

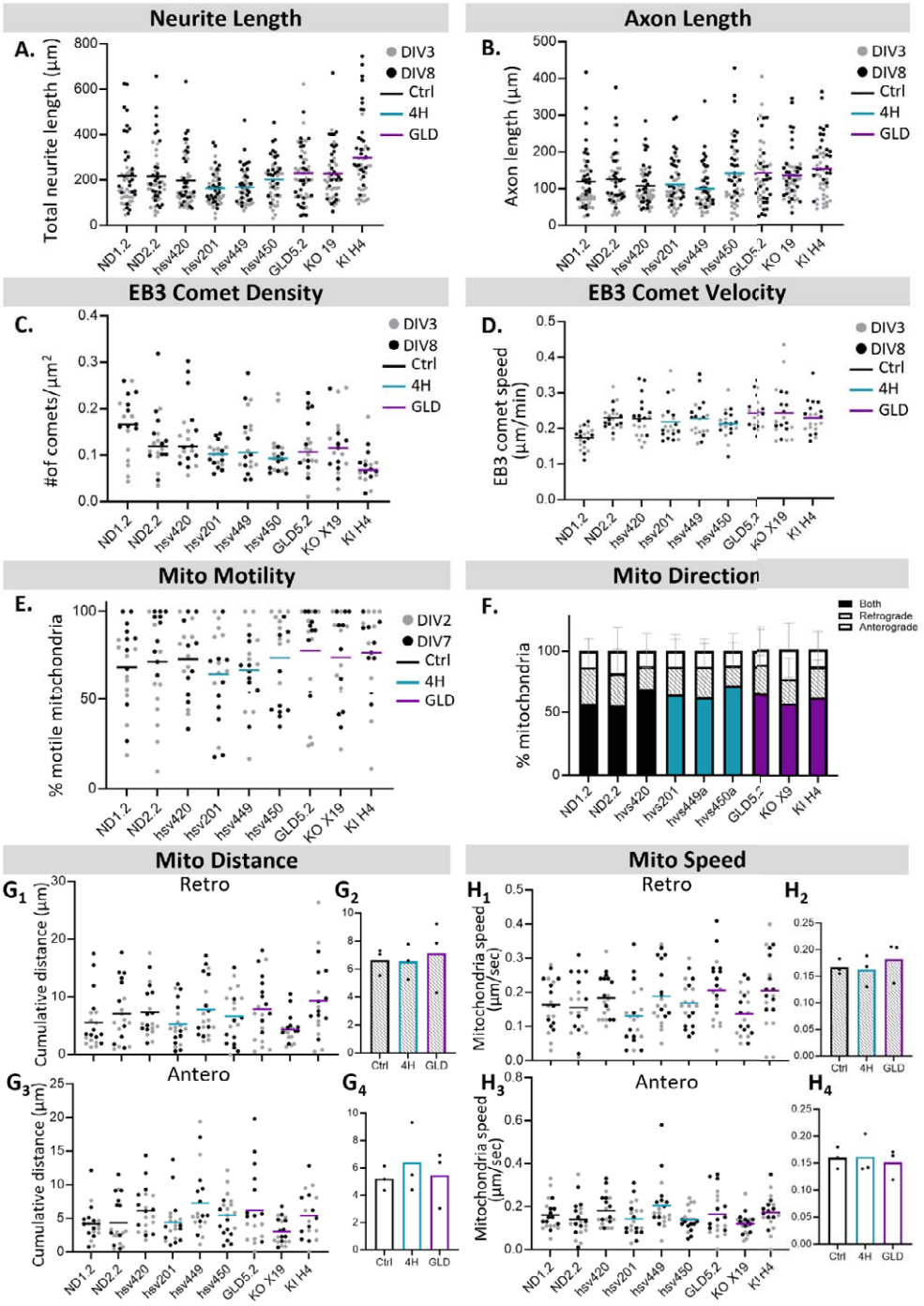
Neurite Length
A.
Total neurite length (µm)
DIV3
DIV8
Ctrl
4H
GLD
ND1.2
ND2.2
hsv420
hsv201
hsv449
hsv450
GLD5.2
KO 19
KI H4
Axon Length
B.
Axon length (µm)
EB3 Comet Density
C.
#of comets/µm²
EB3 Comet Velocity
D.
EB3 comet speed (µm/min)
KO X19
Mito Motility
E.
% motile mitochondria
DIV2
DIV7
Mito Direction
F.
% mitochondria
Both
Retrograde
Anterograde
hvs201
hvs449a
hvs450a
KO X9
Mito Distance
G1
Retro
Cumulative distance (µm)
G2
Ctrl
4H
GLD
G3
Antero
G4
Mito Speed
H1
Mitochondria speed (µm/sec)
H2
H3
H4

◀ **Supplementary Figure 2: Neuronal Features in Mono-cultures by line.** Quantification of **A**) Neurite length, **B**) Axon length, **C**) EB3 comet density, **D**) EB3 Comet Velocity, **E**) Mitochondrial motility, **F**) Mitochondrial motility, **G**) Distance travelled by mitochondria, **H**) Speed of moving mitochondria. Scatter plots represent individual observations, with horizontal lines showing the mean for each cell line. Gray dots for observations on DIV 2 or 3 and black dots for DIV 7 or 8. Bar graphs in G and H figures summarize the group mean for either Control, 4H or Globoid Leukodystrophy with individual dots for cell line means. **F**) Direction of mitochondrial movement are depicted by percentage of mitochondria moving in both (filled bars), retrograde (diagonal striped bars) or anterograde (clear bars) direction. Error bars represent the standard deviation.

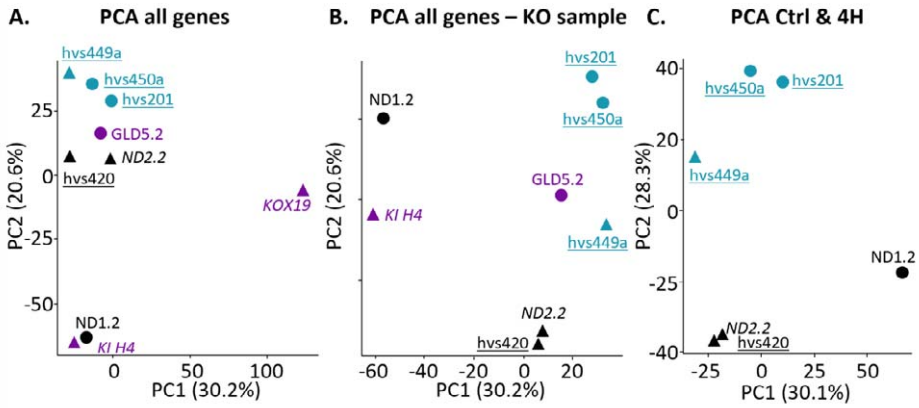

Supplementary Figure 3: Principal Component Analysis (PCA) on bulk mRNA-sequencing of mono-culture neurons. A) PCA of all samples generated from all genes, **B**) PCA from all genes without KO X19 sample and **C**) PCA of control and 4H samples only. GLD samples in purple, 4H in blue and control in black. Triangles represent male donors and circles female donors. Italicized labels indicate isogenic lines. Underlined line names are used to distinguish which lines originate from the Amsterdam institute.

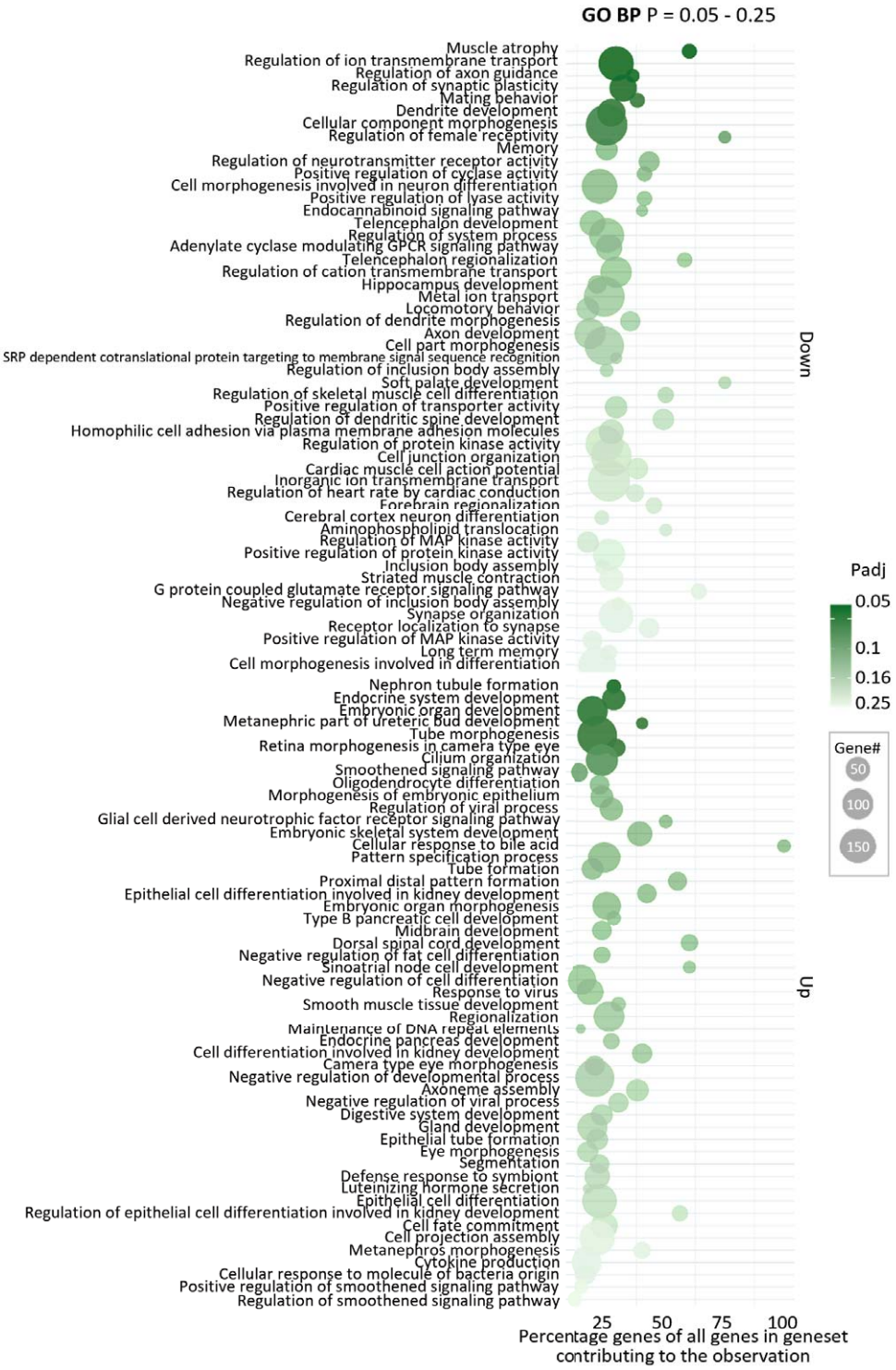
GO BP P = 0.05 - 0.25
Muscle atrophy
Regulation of ion transmembrane transport
Regulation of axon guidance
Regulation of synaptic plasticity
Mating behavior
Dendrite development
Cellular component morphogenesis
Regulation of female receptivity
Memory
Regulation of neurotransmitter receptor activity
Positive regulation of cyclase activity
Cell morphogenesis involved in neuron differentiation
Positive regulation of lyase activity
Endocannabinoid signaling pathway
Telencephalon development
Regulation of system process
Adenylate cyclase modulating GPCR signaling pathway
Telencephalon regionalization
Regulation of cation transmembrane transport
Hippocampus development
Metal ion transport
Locomotory behavior
Regulation of dendrite morphogenesis
Axon development
Cell part morphogenesis
SRP dependent cotranslational protein targeting to membrane signal sequence recognition
Regulation of inclusion body assembly
Soft palate development
Regulation of skeletal muscle cell differentiation
Positive regulation of transporter activity
Regulation of dendritic spine development
Homophilic cell adhesion via plasma membrane adhesion molecules
Regulation of protein kinase activity
Cell junction organization
Cardiac muscle cell action potential
Inorganic ion transmembrane transport
Regulation of heart rate by cardiac conduction
Forebrain regionalization
Cerebral cortex neuron differentiation
Aminophospholipid translocation
Regulation of MAP kinase activity
Positive regulation of protein kinase activity
Inclusion body assembly
Striated muscle contraction
G protein coupled glutamate receptor signaling pathway
Negative regulation of inclusion body assembly
Synapse organization
Receptor localization to synapse
Positive regulation of MAP kinase activity
Long term memory
Cell morphogenesis involved in differentiation
Nephron tubule formation
Endocrine system development
Embryonic organ development
Metanephric part of ureteric bud development
Tube morphogenesis
Retina morphogenesis in camera type eye
Cilium organization
Smoothened signaling pathway
Oligodendrocyte differentiation
Morphogenesis of embryonic epithelium
Regulation of viral process
Glial cell derived neurotrophic factor receptor signaling pathway
Embryonic skeletal system development
Cellular response to bile acid
Pattern specification process
Tube formation
Proximal distal pattern formation
Epithelial cell differentiation involved in kidney development
Embryonic organ morphogenesis
Type B pancreatic cell development
Midbrain development
Dorsal spinal cord development
Negative regulation of fat cell differentiation
Sinoatrial node cell development
Negative regulation of cell differentiation
Response to virus
Smooth muscle tissue development
Regionalization
Maintenance of DNA repeat elements
Endocrine pancreas development
Cell differentiation involved in kidney development
Camera type eye morphogenesis
Negative regulation of developmental process
Axoneme assembly
Negative regulation of viral process
Digestive system development
Gland development
Epithelial tube formation
Eye morphogenesis
Segmentation
Defense response to symbiont
Luteinizing hormone secretion
Epithelial cell differentiation
Regulation of epithelial cell differentiation involved in kidney development
Cell fate commitment
Cell projection assembly
Metanephros morphogenesis
Cytokine production
Cellular response to molecule of bacteria origin
Positive regulation of smoothened signaling pathway
Regulation of smoothened signaling pathway
Down
Up
Padj
0.05
0.1
0.16
0.25
Gene#
50
100
150
25
50
75
100
Percentage genes of all genes in geneset
contributing to the observation

◀ **Supplementary Figure 4: Gene Set Enrichment Analysis Results.** Summary of non-significant but potentially relevant results from GO analysis for biological process on control versus 4H neurons (Adjusted P Value between 0.05 and 0.25). Bubble colour intensity shows P adjusted significance. Bubble size shows the number of genes that contributed to the evidence. The position of the bubble along the x-axis shows the percentage of genes from the entire gene set that contributed to the evidence.

SUPPLEMENTARY TABLES

Supplementary Table I: iPSC lines

Line ID	hPSCreg ID	Origin	Repr. method	Donor sex, age	Status	Disease Gene	Genotype	Isogenic
ND1.2	Life tech., HDF C0135C TIGETi001-A	MLN	mRNA	F, adult	Healthy	n.a.		
ND2.2	Life technologies, HDF C0045C	MLN	mRNA	M, neonatal	Healthy	n.a.		A
hVS420		AMS	Lenti	M, 21y	Healthy	n.a.		
hVS201	VUi027-A	AMS	Lenti	F, 12y	4H	POLR3A	169G>A 2098A>T	
hVS449a	VUi029-A	AMS	Sendai	M, 24y	4H	POLR3A	1771-6C>G 3205C>T	
hVS450a	VUi030-A	AMS	Sendai	F, 2y	4H	POLR3A	1771-7C>G 1048+5G>T	
GLD5.2	Gaslini Biobank FFF0042010	MLN	mRNA	F	GLD, infantile	GALC	c.1657G>A	
KOX19	Life technologies, HDF C0045C	MLN	mRNA	M, neonatal	GLD	GALC	Frameshift exon 1	A
KIH4	Life technologies, HDF C0045C	MLN	mRNA	M, neonatal	GLD	GALC	c.1657G>A	A

AMS = Amsterdam, The Netherlands, Vrije Universiteit, Departement of Complex Trait Genetics, Stem Cell Lab. MLN = Milan, San Raffaele Telethon Institute for Gene Therapy, IRCCS San Raffaele Scientific Institute, 20132 Milan, Italy. Repr. Method = Reprogramming Method. F = Female, M = Male. Life tech. = Life Technologies.

Supplementary Table II: Statistical test results co-cultures

Culture Conditions	Assay	Parameter	Test	Statistic	Pvalue	Post-Hoc (Dunn's Multiple Comparisons)					
						Ctrl vs. 4H		Ctrl vs. GLD		4H vs. GLD	
						Mean rank diff.	Pvalue	Mean rank diff.	P-value	Mean rank diff.	Pvalue
Co-Culture	Outgrowth	Neurite Length	KW	1.889	0.4464	n.a.					
		Axon Length	KW	0.1111	0.9679	n.a.					
	Microtubule dynamics	Comet Density	KW	5.088	0.0571	-3	0.3939	1.833	>0.9999	4.833	0.089
		Comet Velocity	KW	0.25	0.8964	n.a.					
	Mitochondria	Stationary	KW	1.889	0.4464	n.a.					
		Motile	KW	1.889	0.4464	n.a.					
		Anterograde	KW	0.5556	0.8071	n.a.					
		Retrograde	KW	1.111	0.6714	n.a.					
		Both Directions	KW	1.111	0.6714	n.a.					
		Velocity Antero	KW	0.25	0.8964	n.a.					
		Velocity Retro	KW	1.361	0.5643	n.a.					
		Velocity Both	KW	0.25	0.8964	n.a.					
		Length Antero	KW	0.6944	0.7571	n.a.					
		Length Retro	KW	0.02778	>0.9999	n.a.					

Mean rank diff. = Mean rank difference, KW = Kruskal-Wallis test, Ctrl = control, 4H = 4H leukodystrophy, GLD = Globoid Leukodystrophy, N.a. = not applicable.

Supplementary Table III: Statistical test results mono-cultures

Culture Conditions	Assay	Parameter	Test	Statistic	Pvalue	Post-Hoc (Tukey's Multiple Comparisons)						Assumptions			
						Ctrl vs. 4H		Ctrl vs. GLD		4H vs. GLD		Homogeneity of var.?		Residuals Normal?	
						Mean diff.	Pvalue	Mean diff.	Pvalue	Mean diff.	Pvalue	Brown-Forsythe	P-Value	Shapiro-Wilk	P-Value
Mono-Culture	Outgrowth	Neurite Length	ANOVA	5.657	0.0416	31.17	0.3899	-42.4	0.2104	-73.57	0.0355	0.3282	0.7324	0.8939	0.2187
		Axon Length	ANOVA	2.926	0.1297	*n.a.*						0.6353	0.562	0.966	0.8583
	Microtubule dynamics	Comet Density	ANOVA	3.039	0.1226	*n.a.*						0.147	0.8663	0.9215	0.4046
		Comet Velocity	ANOVA	0.389	0.3195	*n.a.*						0.5497	0.6037	0.9068	0.2943
	Mitochondria	Stationary	ANOVA	4.28	0.07	*n.a.*						0.5096	0.6246	0.9555	0.7499
		Motile	ANOVA	4.28	0.07	*n.a.*						0.5096	0.6246	0.9555	0.7499
		Anterograde	ANOVA	0.7895	0.4962	*n.a.*						0.7174	0.5256	0.9219	0.4081
		Retrograde	ANOVA	0.4442	0.6609	*n.a.*						0.7522	0.7522	0.9049	0.282
		BothDirections	ANOVA	0.7439	0.5145	*n.a.*						0.1325	0.8784	0.8725	0.1309
		Velocity Antero	ANOVA	0.1156	0.8927	*n.a.*						0.07362	0.9299	0.9262	0.4463
		Velocity Retro	ANOVA	0.3743	0.7028	*n.a.*						0.2314	0.8002	0.9006	0.2554
		Length Antero	ANOVA	0.2927	0.7563	*n.a.*						0.3445	0.7217	0.9679	0.8764
		Length Retro	ANOVA	0.1023	0.9043	*n.a.*						0.6103	0.5738	0.9529	0.7219

Mean rank diff. = Mean rank difference, KW = Kruskal-Wallis test, Ctrl = control, 4H = 4H leukodystrophy, GLD = Globoid Leukodystrophy, N.a. = not applicable, Homogeneity of var. = Homogeneity of variances.

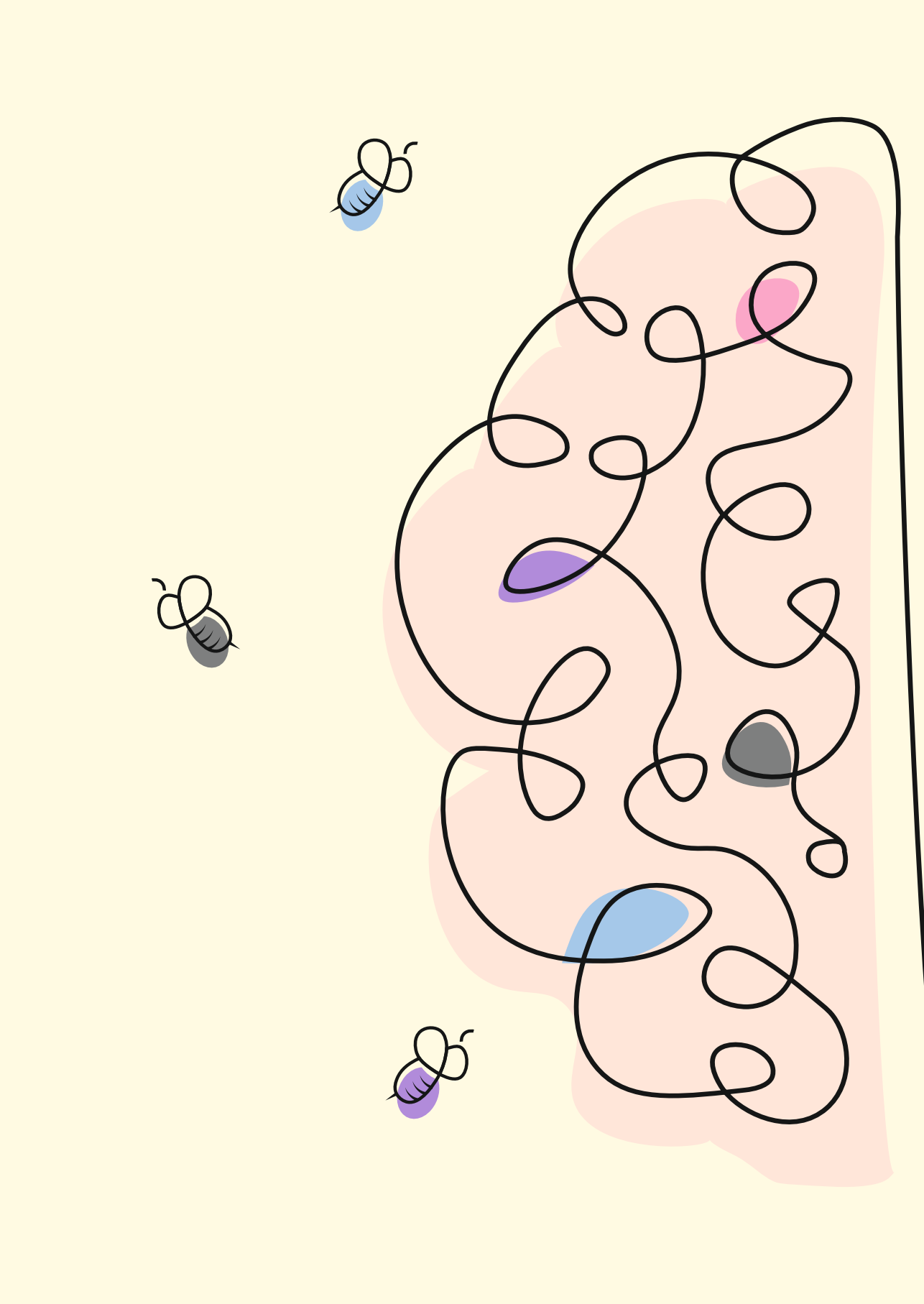

04

Towards a 3D spheroid system for modelling leukodystrophies

Liza M. L. Kok, Elisabeth Mangiameli, Clarissa Rosato, Giovanna Cenini, Polina Oberst, Francesca Cupaioli, Roberta Alfieri, Ivan Merelli, Angela Gritti, Oliver Brüstle, Vivi M. Heine

ABSTRACT

Leukodystrophies (LDs) are a heterogeneous group of rare genetic disorders characterized by progressive white matter (WM) degeneration. Often, the genetic cause is known, but knowledge of underlying disease mechanisms remains poorly understood, limiting therapeutic development. Advances in *in vitro* disease models, particularly brain spheroids, might recapitulate the cellular diversity of brain tissue, enabling the study of complex cell interactions during development. In this study, we aimed to investigate whether 3D spheroids can be used to model and study several leukodystrophies.

We applied a 3D spheroid model derived from human induced pluripotent stem cells (iPSCs) to investigate Globoid Leukodystrophy (GLD), 4H Leukodystrophy, and Canavan Disease (CD). We characterized spheroid growth, cellular composition, and myelination capacity using immunofluorescence and electron microscopy, confirming the presence of a diverse range of brain cell types, including neurons, oligodendrocytes, and astrocytes. Single-cell mRNA sequencing identified 27 cell clusters. Notably, the clusters of cycling radial glia and neural progenitor cells were significantly underrepresented in all LD spheroids. Furthermore, differential gene expression and gene set enrichment analysis identified numerous disease-specific changes. For example, the gene sets “translation” and “oxidative phosphorylation” were significant in many clusters across all leukodystrophies. However, the dynamics are intricate, as they are upregulated in some clusters and timepoints and downregulated in others. Additionally, we showed that including more than one disease model can help prevent overinterpretation based on biases in existing knowledge.

To summarize, this work establishes 3D spheroids as a suitable model for studying leukodystrophies and provides interesting candidate DEGs and gene sets that can guide follow-up studies. Additionally, our dataset offers a resource for future investigations into leukodystrophy mechanisms and treatment strategies.

Keywords: Leukodystrophies, spheroids, single-cell mRNA sequencing, *in vitro* disease modelling.

INTRODUCTION

Leukodystrophies (LDs) are a heterogenous group of rare genetic brain disorders characterized by progressive degradation of white matter (WM), typically diagnosed in early childhood and often reducing life expectancy. Due to their progressive nature, there is an urgent need for curative treatments. However, the development of such therapies is challenged by limited knowledge on cell types and cellular mechanisms primarily affected in disease aetiology.

Although the genetic basis of LDs often lies in genes that are expressed ubiquitously, due to the prominent white matter abnormalities these disorders have traditionally been attributed to glial dysfunction. Recent studies, however, point to significant neuronal involvement in the WM pathology of LDs, suggesting that not just myelin but all white matter constituents are essential for maintaining WM integrity and function. These new insights have significant impact on how we need to approach therapy development for LDs and emphasize the need to expand our knowledge on neurons, glia and their interactions in WM pathology.

Given that LDs arise during critical stages of brain development, it is essential to study WM-pathology in tissue that mimics these stages of brain development. Post-mortem tissue is not suitable as it reflects the end stage of disease and the rarity of LDs makes post-mortem tissue scarce. Studying LDs in animal models would enable the insight in developmental stages, however the translation from findings in animal models to human disease is complicated by species differences. To overcome these challenges, there is a growing need for *in vitro* models that recapitulate later stages of brain development. Advances in human *in vitro* models, particularly spheroids, offer a promising solution. Spheroids, derived from human stem cells, can recapitulate the cellular diversity of brain tissue, enabling the study of complex cell interactions during development. When combined with recent advances in analytical techniques, spheroids can be useful for studying neurodevelopmental disorders, including LDs. However, certain concerns about how brain-like spheroids are and which developmental stages can be reached using spheroids are often not addressed in depth.

This study investigates whether 3D spheroid models can effectively replicate the cellular composition and interactions relevant to white matter (WM) pathology in leukodystrophies. To address this, we characterized the spheroids based on size, immunofluorescence and electron microscopy. We showed that all cells of interest; neurons, oligodendrocytes and

astrocytes, are present in our model. Next, we performed single-cell mRNA sequencing (scRNA-seq) to further elucidate the cellular composition of the spheroids. Cluster annotation showed diverse cellular populations. Some clusters were significantly different over time, emphasizing the dynamic nature of the models. Interestingly, the two clusters cycling radial glia and neural progenitors were severely underrepresented in leukodystrophy organoids. The scRNA-seq data was subsequently used to investigate the validity of comparing all healthy donors (HD) against specific LDs, by comparing the findings of isogenic comparisons and HD x GLD. We showed that the most significant genes are consistently up or downregulated in both isogenic comparison and HD x GLD. Next, the scRNA-seq data was used to investigate which specific cell clusters highly express the genes GALC, POLR3A and ASPA, which are causative in three leukodystrophies respectively, Globoid Leukodystrophy (GLD), 4H Leukodystrophy, and Canavan Disease (CD). As no particular cell cluster seemed to be more relevant in all leukodystrophies, but all leukodystrophies show myelin pathology in the clinic, we decided to investigate the DEG of all three clusters of the oligodendrocyte lineage as well as gene set enrichment analysis (GSEA). Interestingly, we identified many DEGs but only a few could be directly linked to oligodendrocytes, such as down regulation of *MAG* (Myelin Associated Glycoprotein) in 4H. GSEA showed possible relevance of translation and oxidative phosphorylation in LD pathology, as they are often significant, but further research is required to confirm their involvement. DEG analysis on a selection of clusters from the neuron and astrocyte lineage again showed plenty differential genes, but their relevance is yet to be determined. Together, this work shows that 3D spheroid models are a valuable platform for studying the cellular and molecular mechanisms underlying leukodystrophies and guiding therapeutic development.

RESULTS

OL spheroids develop white matter-like cell types capable of myelination

To investigate whether OL spheroids effectively model white matter-like cell development, we generated 3D spheroids from induced pluripotent stem cells (iPSCs) derived from five healthy donor (HD) lines and eight leukodystrophy (LD) lines of which three globoid leukodystrophy (GLD), two 4H leukodystrophy and three Canavan disease lines (CD). Spheroids were cultured for 150 days using a previously published protocol (Marton et al., 2019), at a centralized facility to ensure consistency across experimental conditions (Fig. 1A).

Growth curve analysis of spheroid diameter revealed steady growth during the first 50 days of culture, followed by a plateau phase (Fig. 1B). While overall growth dynamics were comparable between HD and LD spheroids, subtle differences in the growth plateau phase were observed among specific lines. Immunofluorescence (IF) staining confirmed the presence of key white matter cell types, including neurons (neurofilament-positive), astrocytes (GFAP-positive), and oligodendrocytes (MBP-positive) in both HD and LD spheroids (Fig. 1C, 1E, 1I). Interestingly, NF^+ area decreases between day 100 and day 150 (Fig. 1C, $P = 0.0002$). While marker for inhibitory neurons (GABA) increased (Fig. 1D, $P = 0.0488$). We further analysed oligodendrocyte lineage progression by quantifying $Olig2^+$ and MBP^+ area. $Olig2^+$ area was consistent across all lines and differentiation stages, with no significant differences observed between HD and LD lines (Fig. 1F). Myelinating oligodendrocytes, marked by MBP positive area, showed a significant difference by time (Fig. 1G, $P = 0.0085$). Specifically, an increase in positive area from day 50 to day 100 and from day 50 to day 150 in both HD and LD spheroids (Fig. 1G, $P = 0.0160$ and $P = 0.0127$). Electron microscopy further confirmed the presence of compacted myelin structures surrounding neuronal axons (Fig. 1H), demonstrating that OL spheroids are capable of generating functional myelinating cells. Lastly, area of astrocytic marker expression (GFAP) showed significant difference on time ($P < 0.0001$), disease status ($P = 0.0014$) and the interaction of time and disease status ($P = 0.0012$). Post-hoc tests showed significant increase in GFAP positive area for both control ($P = 0.0256$) and LDs ($P < 0.0001$) between day 100 and 150 as well as significant higher GFAP expression in LDs compared to control at day 150 (Fig. 1I, $P < 0.0001$).

Overall, these findings demonstrate that OL spheroids can model key aspects of WM cell development and myelination.

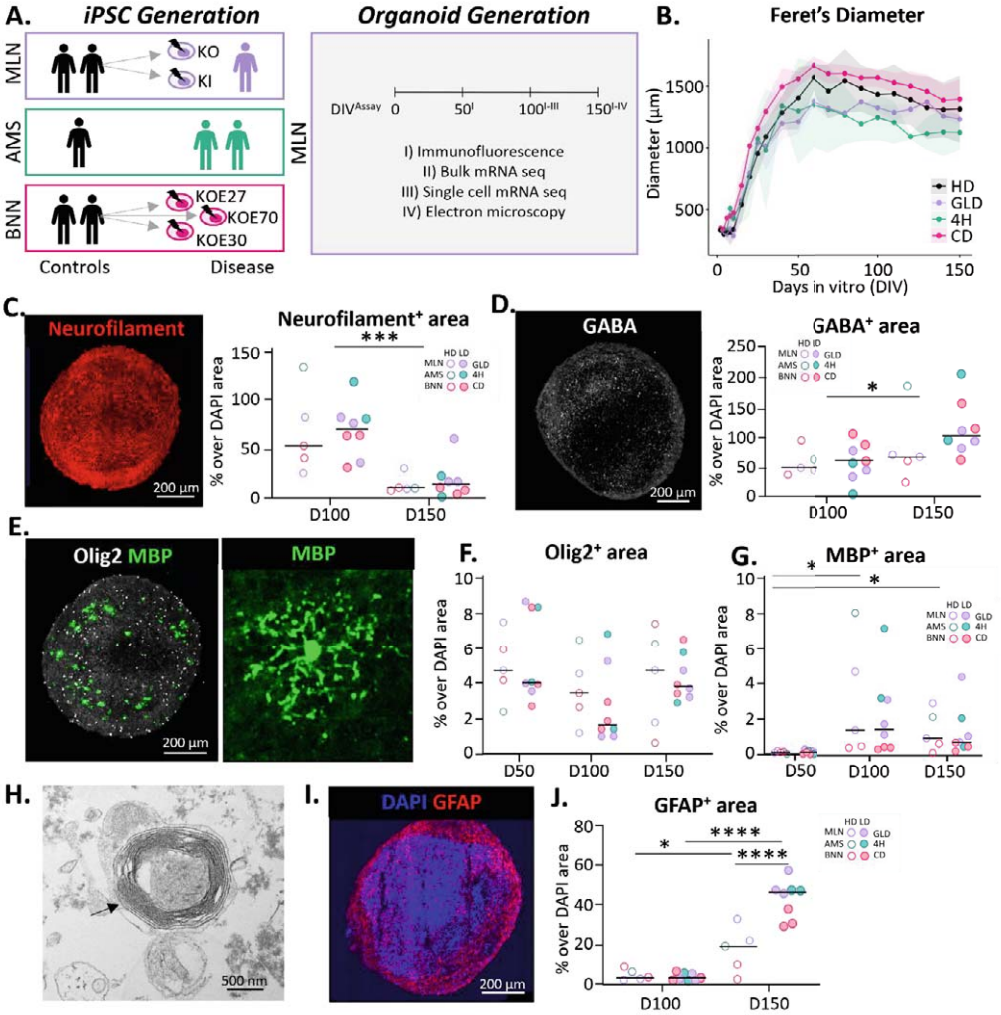

Figure 1: Characterization of OL spheroids and their cell composition. A) Schematic representation of experimental set-up. **B)** Spheroid diameter per cell line, shaded ribbons represent the average standard deviation of the lines. Representative immunofluorescent (IF) image and quantification of the positive area for **C)** neuron marker (Neurofilament, NF in red), **D)** inhibitory neuron marker (GABA in white), **E-G)** oligodendrocyte precursor (Olig2 in white) and myelinating oligodendrocytes (MBP in green). **H)** Electron microscopy image of compacted myelin around an axon. **I)** Representative IF image showing GFAP expression, with quantification of GFAP+ area between HD and LD spheroids over time. *$P < 0.05$,**$P < 0.01$, ***$P < 0.001$, **** $P < 0.0001$.

Single-cell RNA sequencing reveals cellular diversity in OL spheroids in all HD lines

To further elucidate the cellular composition and developmental trajectory of the spheroids, we performed single-cell mRNA sequencing (scRNA-seq) on both HD and LD lines at days 100 and 150 of differentiation. Following quality control and data preprocessing, 27 distinct cell clusters were identified in organoids of HD lines (Fig. 2A). In addition, both clusters were present at both timepoints (Fig. 2B). We showed that there are no residual pluripotent cells and all cells show neuroectoderm identity (Supplementary Fig. 1A-D). The cells show gene expression profiles indicating neuronal cells of medial ganglionic eminence (MGE) and caudal ganglionic eminence (CGE) (Supplementary Fig. 1G-L). Annotation of the clusters, using differentially expressed genes (Fig. 2C, Supplementary Fig. 1E-N) and predefined marker genes, revealed the presence of all three brain cell lineages, namely oligodendrocytes, astrocytes and neurons with both excitatory and inhibitory features (Supplemental Fig. 1E-M). In line with our expectations, microglia-like cells were not present in this model (Supplemental Fig. 1N). We present that HD spheroids provide cellular diversity as in the developing brain.

LD lines map well onto HD data and show signs of disease specific changes

Next, was to determine whether the current experimental set-up allows for the comparison between diseases. To start, we evaluated potential sources of experimental variability, including donor institute and batch effects. Principal component analysis (PCA) revealed that PC1, accounting for 34.1% of the variance, was not associated with these factors, as samples from the same institute and batch appeared distributed across PC1 (Fig. 3A). In contrast, PC2, explaining 16.7% of the variance, clearly separated samples by differentiation timepoint (D100 vs. D150). Notably, line E70 was the only sample positioned incorrectly on the y-axis, just above zero, and it clustered far from its isogenic control (Fig. 3A). Comparison of cell percentages per cluster showed that time significantly influenced cell proportions in 7 out of 27 clusters (Fig. 3B-D, Supplemental Fig. 2). Consistent with later-stage maturation, two of the three oligodendrocyte lineage clusters (OPC and cycling OPC) significantly increased over time (Fig. 3E-F).

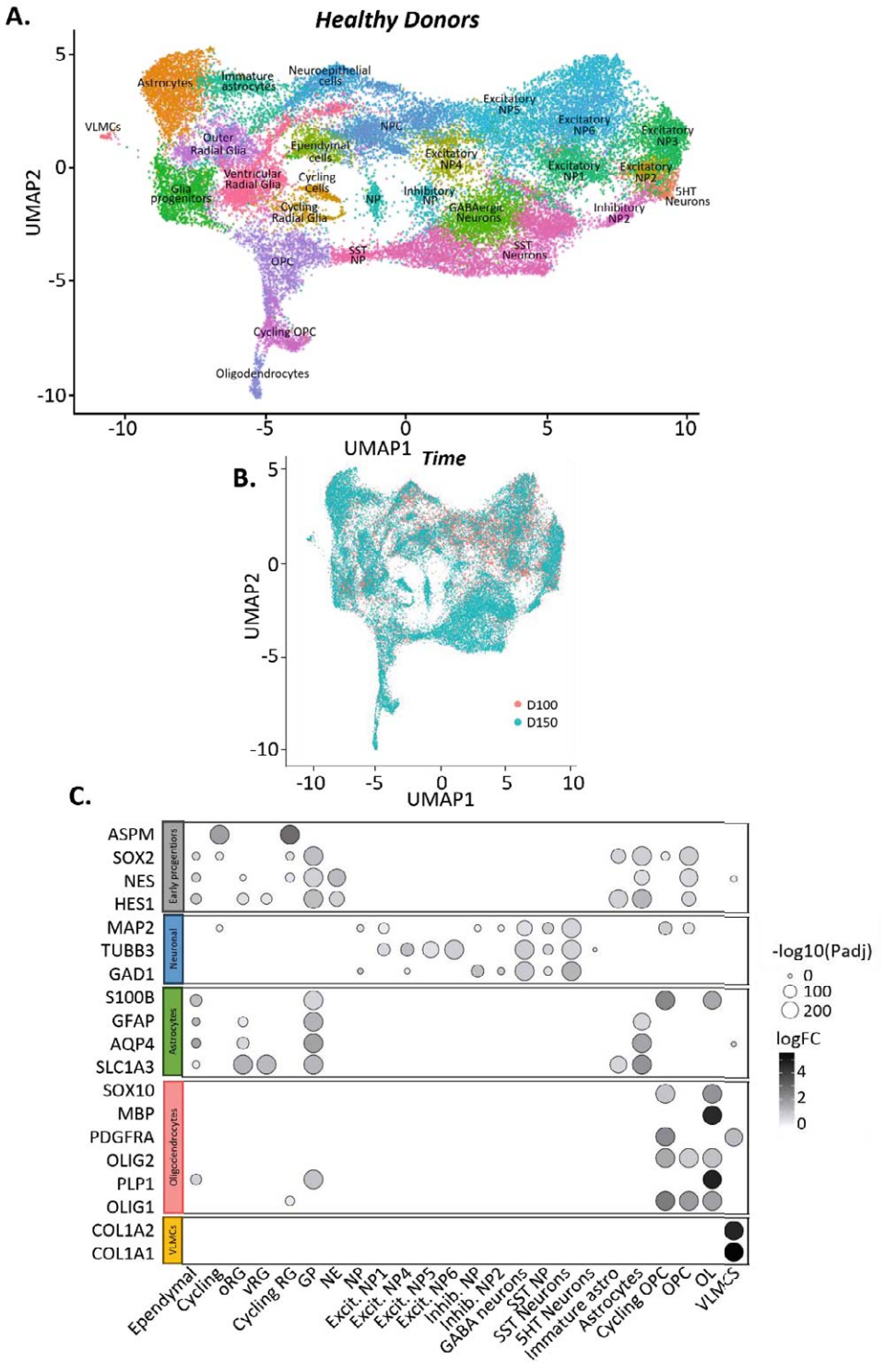
A.
Healthy Donors
Astrocytes
Immature astrocytes
Neuroepithelial cells
VLMCs
Outer Radial Glia
Ependymal cells
NPC
Excitatory NP5
Excitatory NP6
Excitatory NP3
Excitatory NP4
Excitatory NP1
Excitatory NP2
5HT Neurons
Ventricular Radial Glia
Cycling Cells
Glia progenitors
NP
Inhibitory NP1
Inhibitory NP2
GABAergic Neurons
Cycling Radial Glia
SST NP
SST Neurons
OPC
Cycling OPC
Oligodendrocytes
UMAP1
UMAP2
B.
Time
D100
D150
C.
ASPM
SOX2
NES
HES1
Early progenitors
MAP2
TUBB3
GAD1
Neuronal
S100B
GFAP
AQP4
SLC1A3
Astrocytes
SOX10
MBP
PDGFRA
OLIG2
PLP1
OLIG1
Oligodendrocytes
COL1A2
COL1A1
VLMCs
Ependymal
Cycling
oRG
vRG
Cycling RG
GP
NE
NP
Excit. NP1
Excit. NP4
Excit. NP5
Excit. NP6
Inhib. NP
Inhib. NP2
GABA neurons
SST NP
SST Neurons
5HT Neurons
Immature astro
Astrocytes
Cycling OPC
OPC
OL
VLMCs
-log10(Padj)
0
100
200
logFC
4
2
0

To further explore variability, we examined differences in percentage of cells per cluster. Projecting LD spheroids onto the HD UMAP revealed that several cell types were underrepresented or absent in LD samples (Fig. 3G). A mixed-effects model confirmed disease-specific differences in six out of the 27 clusters (Fig. 3H-J, Supplemental Fig. 3). Specifically, cycling radial glia were severely reduced in all LDs (Fig. 3H), while outer radial glia was notably reduced in 4H and GLD (Fig. 3I). Although neural progenitors (NPs) were only significantly affected in GLD, they were also reduced in 4H and CD (Fig. 3J). Inhibitory progenitors showed reductions in GLD (Supplemental Fig. P-Q), while excitatory NP1 cells were more abundant in CD compared to controls (Supplemental Fig. 3J).

Combined, this confirms cellular heterogeneity in LDs and indicates that even at the cellular composition level, disease-specific differences are detectable. The absence of clustering by institute and experimental batch supports the model's plausibility for cross-disease comparisons, as known technical factors were effectively controlled. Nevertheless, findings need to be interpreted with caution, as we did not identify clear disease-specific clustering patterns either.

◀ **Figure 2: Single cell transcriptomics to identify cellular composition in myelinating spheroids. A)** UMAP showing all cellular clusters in healthy donor (HD) spheroids. **B)** UMAP showing all clusters are represented at both timepoints. **C)** Bubble plot indicating a selection of positive gene markers used for cluster annotation. Size of bubble indicates the log10(adjusted significant difference) compared to all other clusters. Shade represents log fold change.

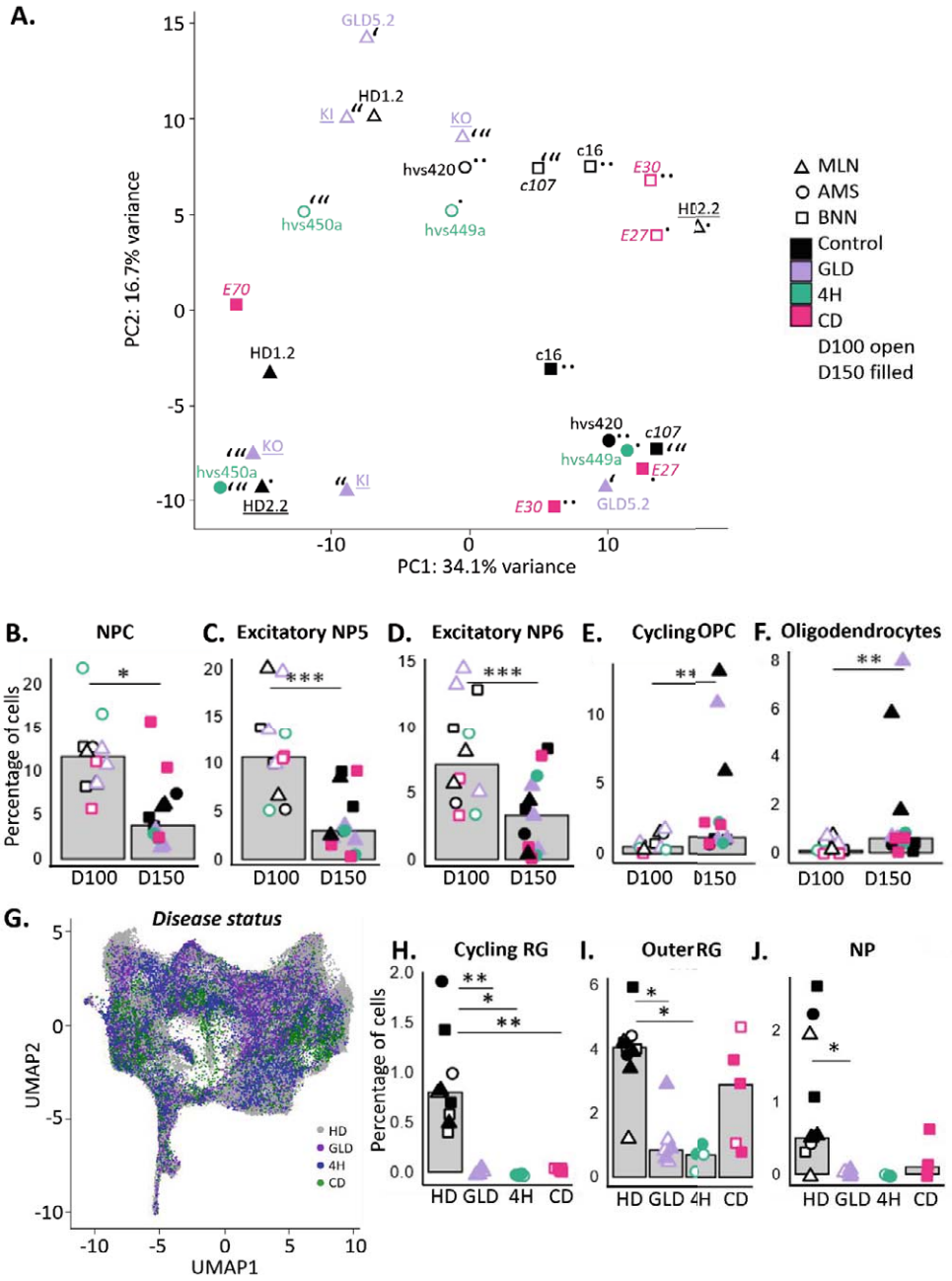

Figure 3: Addressing variance between spheroids using single cell mRNA sequencing data. A) PC plot showing the variance explained by PC1 and PC2. Underlined and italic line names form isogenic lines. Experimental batches are indicated with batch 1: none additions, batch 2: ‘, batch 3: “, batch 4: ‘“, batch 5: .., batch 6:. **B-F)** Cell clusters with significant differences in percentage of cells per cluster between d100 and d150. **G)** UMAP showing differences in cellular composition based on disease status of spheroids. **H-J)** Cell clusters with significant differences in percentage of cells per cluster between healthy donor (HD) and leukodystrophy spheroids (either GLD, 4H, or CD). *$P < 0.05$,**$P < 0.01$, ***$P < 0.001$.

Defining valid contrasts in the data set

Building on our analysis of heterogeneity, we wanted to shed some light on the variation between samples using the isogenic pairs. The inclusion of isogenic pairs allowed us to control for genetic background and focus on disease-associated changes. We first compared the correlation of log2FC of the genes significant at day 150 in both HD2.2xKI and HD2.2xKO contrast. We observed a high correlation (Pearson $r > 0.800$) in three out of five investigated clusters, except for OPC and astrocytes (Fig. 4A-E, Pearson r: 0.669 and 0.547 respectively). When including genes significant in only one of the contrasts (Fig. 4F-J) correlation of the findings between the contrasts decreases in all clusters. Similarly, when investigating all genes (Fig. 4K-O) correlation decreases even further in three out of five clusters. Interestingly, the astrocyte (Pearson $r = 0.831$) and NPC (Pearson $r = 0.559$) clusters still show high and medium correlation. To conclude, there are quite some differences between the findings of the isogenic lines. However, if a gene is significant in both contrasts it is often correlated. The findings of the clusters NPC and astrocytes seem to correlate more strongly. Possibly indicating disease specific changes in these clusters.

Next, we wanted to investigate if significant findings of isogenic comparisons correlate with non-isogenic comparisons with larger sample size (HD x GLD). First, we compared the significant genes for the contrasts HD x GLD and HD2.2 x KI at day 150, we observed a weak correlation in the OPC cluster (Fig. 5a) and a strong correlation (Pearson $r > 0.800$) in the proliferating OPCs and oligodendrocytes (Fig. 5A-C). In the astrocyte cluster there was a negative correlation (Fig. 5D). The NPCs cluster mainly showed replication of the upregulated genes (Fig. 5E, blue). For the comparison of HD x GLD and HD2.2 x KO we see a similar picture, there is some correlation in the oligodendrocyte lineage, although less compared to the KI comparison (Fig. 5F-H). Again, we find no correlation in astrocytes and again mainly overlay of upregulated genes in the NPC cluster (Fig. 5I-J). Noteworthy, most extreme DEGs such as DPP6 and CHCHD2 in OPC and VAMP2 in NPC are replicated in all contrasts.

We conclude that there are, as expected, differences in findings when changing contrasts. Nevertheless, it is reassuring that some of the most significant genes are consistently up or down-regulated independent of the contrast. Hence, we felt confident to use the current data set for the exploration of disease specific findings in the other leukodystrophies as well.

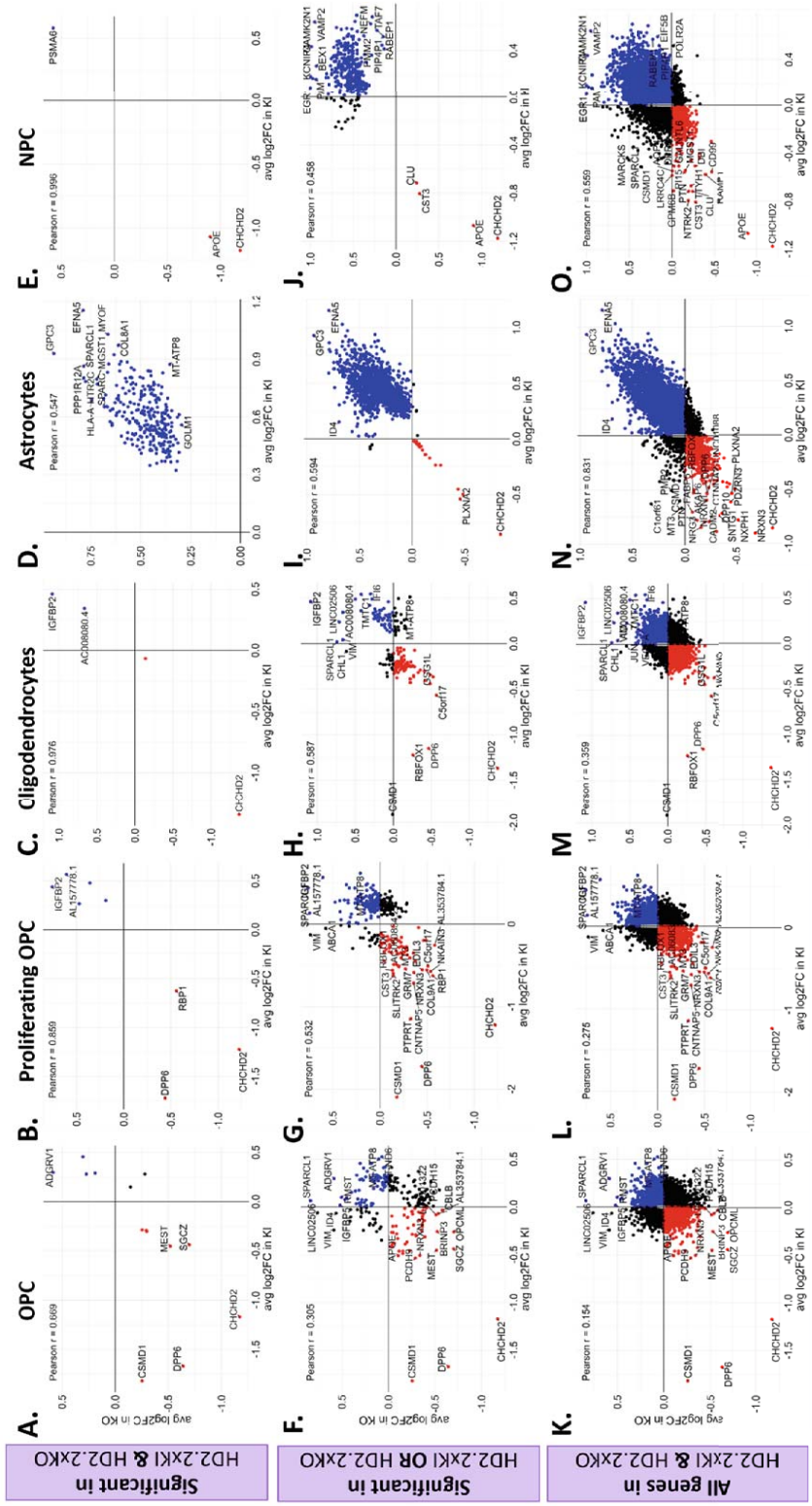

▲ **Figure 4: Comparison of the isogenic pairs HD2.2 x KI and HD2.2 x KO at d150.** Comparison displays the log fold changes of **A-E)** genes significant in both contrasts, **F-J)** one of the contrasts and **K-O)** all genes. Comparison is done at day 150 for the five cell clusters OPC, proliferation OPC, oligodendrocytes, astrocytes and NPC. Blue: genes upregulated in both contrasts. Red: genes downregulated in both contrasts. Black: genes are inconsistently up & down regulated between the contrasts. Pearson correlation coefficient is displayed in the graph.

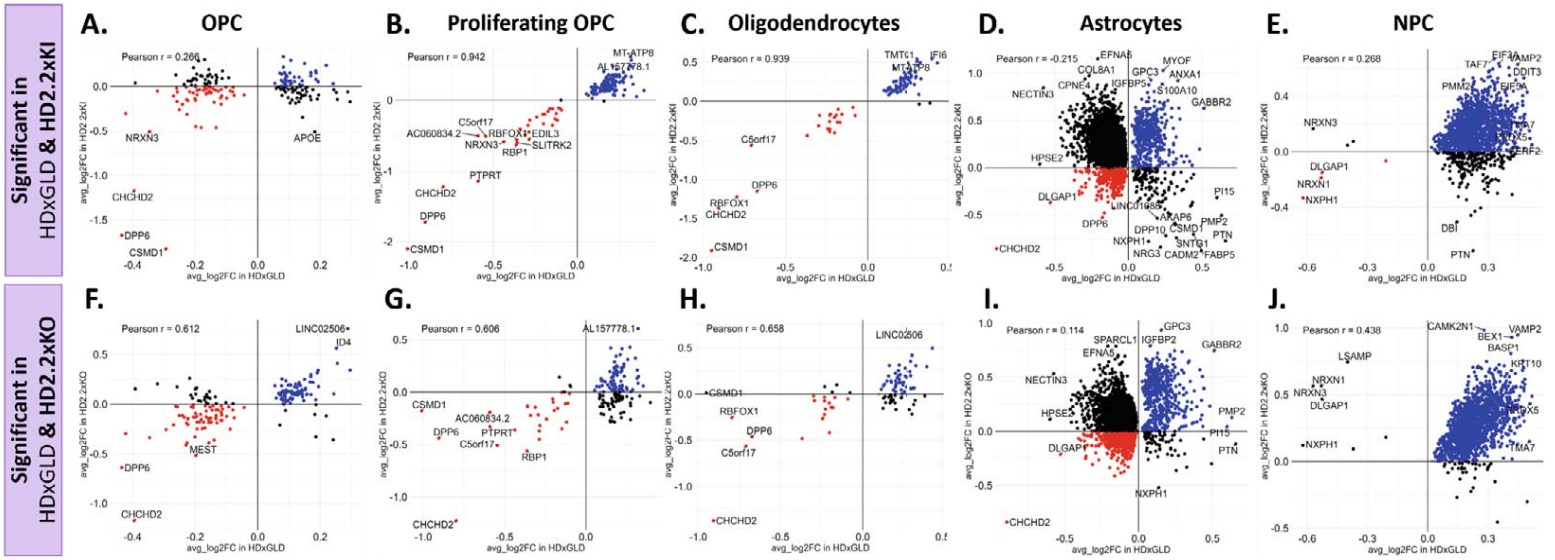

▲ **Figure 5: Comparison of isogenic pairs and healthy donor x globoid leukodystrophy (HD x GLD) at day 150.** Comparison displays the log fold changes of **A-E)** genes significant in both HD x GLD and HD2.2xKI, **F-J)** HD x GLD and HD2.2 x KO. Comparison is done at day 150 for the five cell clusters OPC, proliferating OPC, oligodendrocytes, astrocytes and NPC. Blue: genes upregulated in both contrasts. Red: genes downregulated in both contrasts. Black: genes are inconsistently up & down regulated between the contrasts. Pearson correlation coefficient is displayed in the graph.

Identifying clusters for follow-up analysis by expression of disease associated genes

As we identified 27 clusters, we opted to focus on a subset of disease relevant clusters. Considering that the 3 diseases under investigation are all leukodystrophies, we are particularly interested in investigating the oligodendrocyte lineage. However, to investigating whether there are other cell clusters in OL spheroids that warrant our investigation, we investigated expression of key disease-related genes and downstream products linked to GLD, 4H and CD. Spatial expression analysis using UMAP revealed that *GALC* was primarily localized to the left side of the UMAP, encompassing astrocyte and glial progenitor clusters (Fig. 6A). In contrast, 4H related gene *POLR3A* displayed broad, non-specific expression across multiple cell types without a distinct spatial pattern (Fig. 6B). Attempts to refine *POLR3A* localization by examining co-expression with *POLR3B* yielded no additional specificity (Fig. 6C). *ARX*, a gene previously implicated in 4H, was notably expressed in cycling cells, cycling radial glia, NPCs, excitatory neuronal progenitor 4 (NP4), inhibitory neurons, GABAergic neurons, SST neurons, and SST neuronal progenitors (Fig. 6D). While *ASPA*, the gene linked to CD, was only moderately expressed in astrocytes, its closely related gene *NAT8L* showed high expression in this NPC cluster as well (Fig. 6E-F). Interestingly, we found that *GALC* and *POLR3A*, associated with GLD and 4H respectively, were highly expressed in a subset of cells within the neural progenitor cell (NPC) cluster (Fig. 6A-B).

To summarize, we will have a more detailed look at the oligodendrocyte lineage. Additionally, we decided that astrocyte lineage is particularly interesting to investigate regarding disease-gene expression in GLD and CD, we opted for glia progenitors, immature astrocytes and astrocytes. Additionally, previous research on 4H shows that the neuronal lineage requires attention, hence we focussed on some neuron specific clusters. To get a complete overview we decided to investigate, NPCs, excitatory NP1, 5HT neurons, inhibitory NP1, SST neurons and GABAergic neurons.

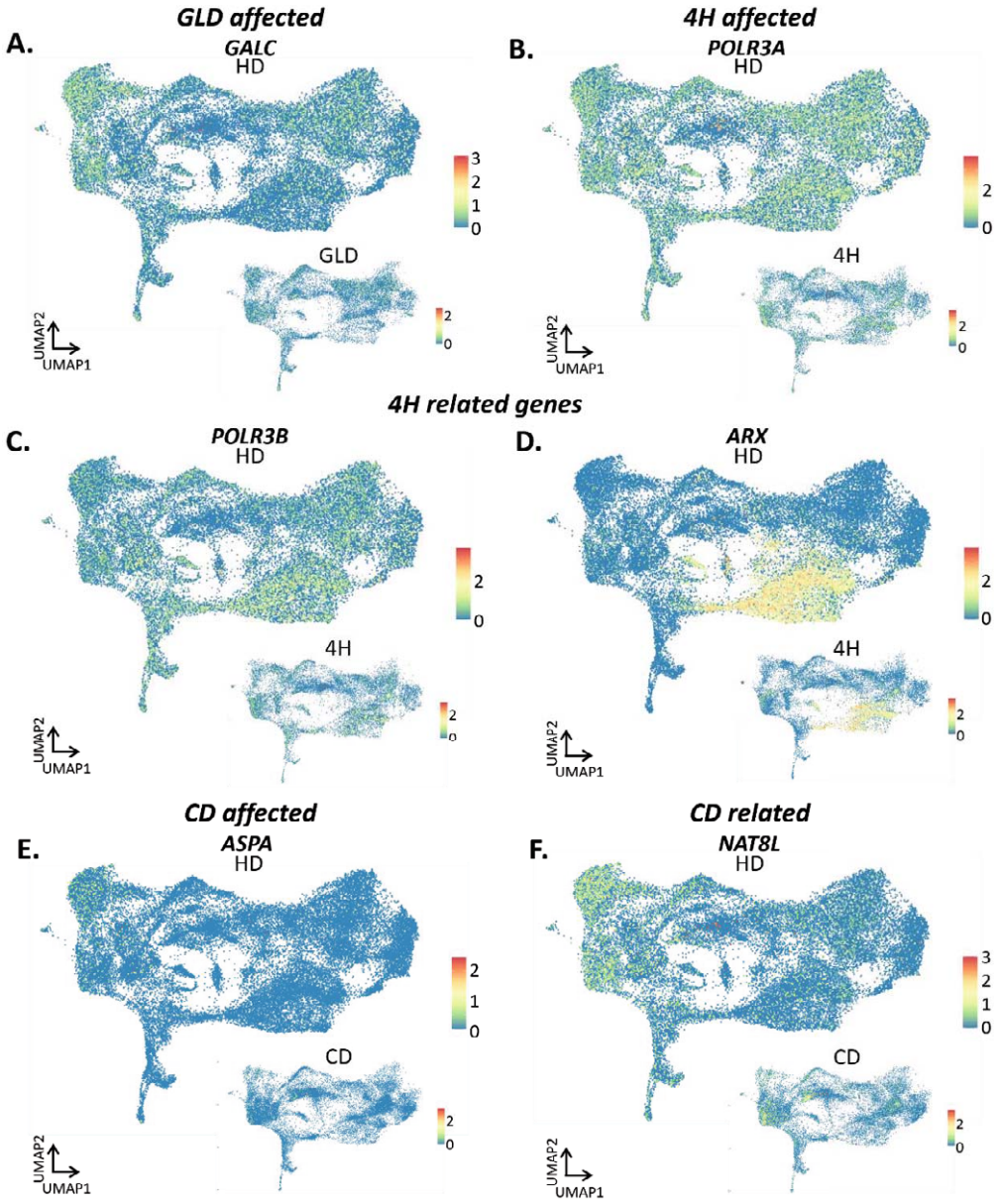

Figure 6: Expression of leukodystrophy disease genes in single cell clusters. UMAPs of healthy donor (HD) and leukodystrophy spheroids (either GLD: globoid leukodystrophy, 4H: 4H leukodystrophy or CD: Canavan disease), coloured by abundance of the disease genes **A)** *GALC*, **B)** *POLR3A*, **C)** *POLR3B*, **D)** *ARX*, **E)** *ASPA* and **F)** *NAT8L*.

Disease specific differential gene expression in oligodendrocyte lineage

For the cell cluster specific investigation, we used the contrasts HD x GLD, HD x 4H and HD x CD. First, the oligodendrocyte lineage was investigated at D150, as oligodendrocyte clusters were more abundant at this timepoint. For all leukodystrophies we identified multiple differentially expressed genes (DEGs). To note, for GLD in all three clusters of the oligodendrocyte lineage the genes *C5orf17*, *CSMD1*, *DPP6* and *CHCHD2* were significantly downregulated (Fig. 7A-C, note: gene labels are not always attributed in the graphs, but raw data was consulted to draw conclusions). *C5orf17* is also down regulated in the oligodendrocyte lineage of 4H cells. Interestingly, *CHCHD2* is upregulated in 4H OPC, and not significantly different in proliferating OPC and oligodendrocytes. For 4H there is upregulation of *MEG3* and *MEG8* in all cells of the oligo lineage (Fig. 7D-F). In addition, there is down regulation of *MAG* (Myelin Associated Glycoprotein) in 4H specifically (Fig. 7F). For CD oligo lineage, it stands out that many mitochondrial related genes are upregulated at the OPC stage (Fig. 7G). *RPS4Y1* is downregulated in all cells of the oligodendrocyte lineage (Fig. 7G-I). *MEG3*, which was also identified for 4H is also up in all clusters of the oligodendrocyte lineage in CD. The gene *AX119673.2* is upregulated in the oligodendrocyte cluster of all leukodystrophies.

Since the investigation of DEG is very limited and often biased, we also applied gene set enrichment analysis (GSEA). Although the current data set, shows ample pathways to be significantly different in LDs, their significance and direction are context dependent. Considering the size of the data set this makes it hard to draw conclusions. To illustrate, GSEA on GLD oligodendrocyte lineages using the pathways database shows *"Disease of signal transduction by growth factor receptors and second messengers"* to be down regulated in OPC and proliferating OPC at D100 while upregulated in D150 (Supplemental Fig. 4A-D). Initially, this could be identified as a disease specific alteration. However, if we look at significant pathways like "*translation*" and "*rRNA processing*", which are consistently upregulated in the oligodendrocyte lineage clusters of GLD (Supplemental Fig. 4A-F), we show that those pathways are also often significant in other leukodystrophies 4H and CD (Supplemental Fig. 5 & 6). This dysregulation of translation could be leukodystrophy specific, however when looking at 4H, the pathways are inconsistent. Sometimes they are upregulated other times downregulated (Supplemental Fig. 5). Similarly, the pathway of oxidative phosphorylation was highly significant when comparing HDs to any of the LDs. Also this pathway, was context dependent (Supplemental Fig. 7).

Although we identified DEGs that were consistently regulated, GSEA for the oligodendrocyte lineage and other cell clusters (data not shown) is very variable by disease but also per cluster and timepoint. At this stage of the analysis, it is too early to make any conclusion based on the pathway analysis. Hence, we do not display it for the other lineages.

Disease specific differential gene expression in astrocyte lineage

Next, we investigated the astrocyte lineage, to be specific the glia progenitors, immature astrocytes and astrocytes. To obtain the most relevant findings, we visualized genes significant at both timepoints following the contrasts HD x GLD, HD x 4H or HD x CD and plotted the logfold2 change against each other. In the glia progenitors *CSMD1*, *DPP6* and *CHCHD2* are again significant and most drastically down regulated (Fig. 8A). In immature astrocytes and astrocytes they also occur but not always significant at both timepoints (Fig. 8B-C). Interestingly, in GLD there is quite a large cluster that is significantly upregulated in D100 and downregulated in D150. For 4H, *SERPIN1*, *HOPX* and *CD9* are amongst the most upregulated genes in all timepoints and all three clusters (Fig. 8D-F). *HSE4*, *NNAT*, *RALYL*, *DLGAP1* are consistently amongst the most down regulated genes in immature and mature astrocytes (Fig. 8E-F). For CD, there is a very large cluster of genes that is significant at both timepoints, but are upregulated in D100 and downregulated at D150. *SPARCL1* is downregulated in both timepoints of glia progenitors and immature astrocytes, and only astrocytes on D150 (Fig. 8G-I).

In conclusion, for GLD and CD the astrocyte lineage shows inconsistent up and down-regulation of significant genes. Pointing towards drastic changes at the different timepoints, which might be interesting for future research. Additionally, for all LDs some significant genes for future research are identified.

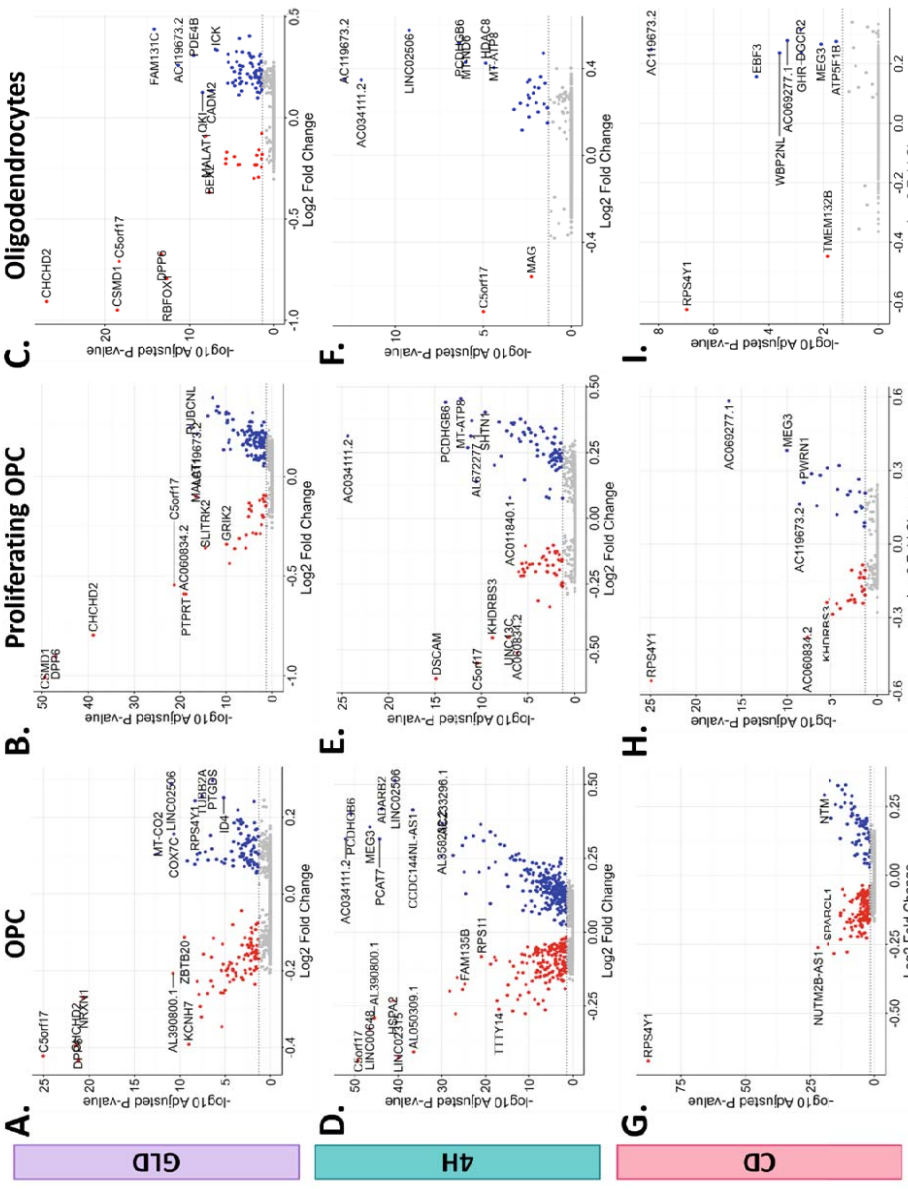

Figure 7: Differentially expressed genes between control and leukodystrophies in the oligodendrocyte lineage clusters at day 150. Vulcano plots of differentially expressed genes in the OPC, proliferation OPC and oligodendrocyte cluster for the contrasts **A-C)** HD x GLD, **D-F)** HD x 4H, **G-I)** HD x CD at day 150. Blue: genes upregulated compared to HD. Red: genes downregulated compared to HD. Gray: genes that do not exceed the significance threshold.

Disease specific differential gene expression in neuron lineage

Lastly, we investigated the DEG in the neuronal lineage (Fig. 9 and 10). For GLD NPCs specifically, significant genes in both timepoints show to be mainly upregulated (Fig. 9A). Some genes that were differentially expressed in the oligo lineage are also downregulated in the neuron lineage, specifically *DPP6* and *CSMD1* (Fig. 9B-C). Similarly to NPC, also the inhibitory NP population shows mainly significant upregulated genes (Fig. 10A). *MEG3* is upregulated in D100 and down regulated in D150 of SST and GABAergic neurons, and was upregulated in 4H oligo's as well (Fig. 10B-C). MEG3 again is upregulated in 4H neuronal clusters as well (Fig. 9D-F). On the contrary, gene *CHCHD2*, observed to be downregulated in GLD oligo's, is significantly upregulated in some 4H neuron clusters. For 4H, it also stands out that *CHL1* is downregulated in all but the serotonergic cluster (Fig. 9D-F and Fig. 10D-F). In the inhibitory cluster it is interesting to note that *SST*, a gene related to subtypes of interneurons, is downregulated in 4H (Fig. 10D-F). Additionally, while 4H has shown quite consistent up and down regulation of significant genes, in the GABAergic cluster there seems to be less consistency (Fig. 10F). For CD, *EBF1*, *EBF3* and *GRIK2* are quite often upregulated (Fig. 9G-I and 10G-I). And while there is high consistency of down and upregulation of significant genes in 5HT neurons, there is quite some inconsistency again in the other neuronal clusters (Fig. 9G-I and 10G-I). Interestingly, in the NPC lineage there seems to be mainly upregulation of gene expression for GLD, while there is mainly down regulation in 4H and an inconsistent pattern in CD. This are potentially interesting clusters for future investigations (Fig. 9A, D, G). To conclude, there are many differential expressed genes. Future investigation should explore their potential involvement in disease processes in the different leukodystrophies diseases.

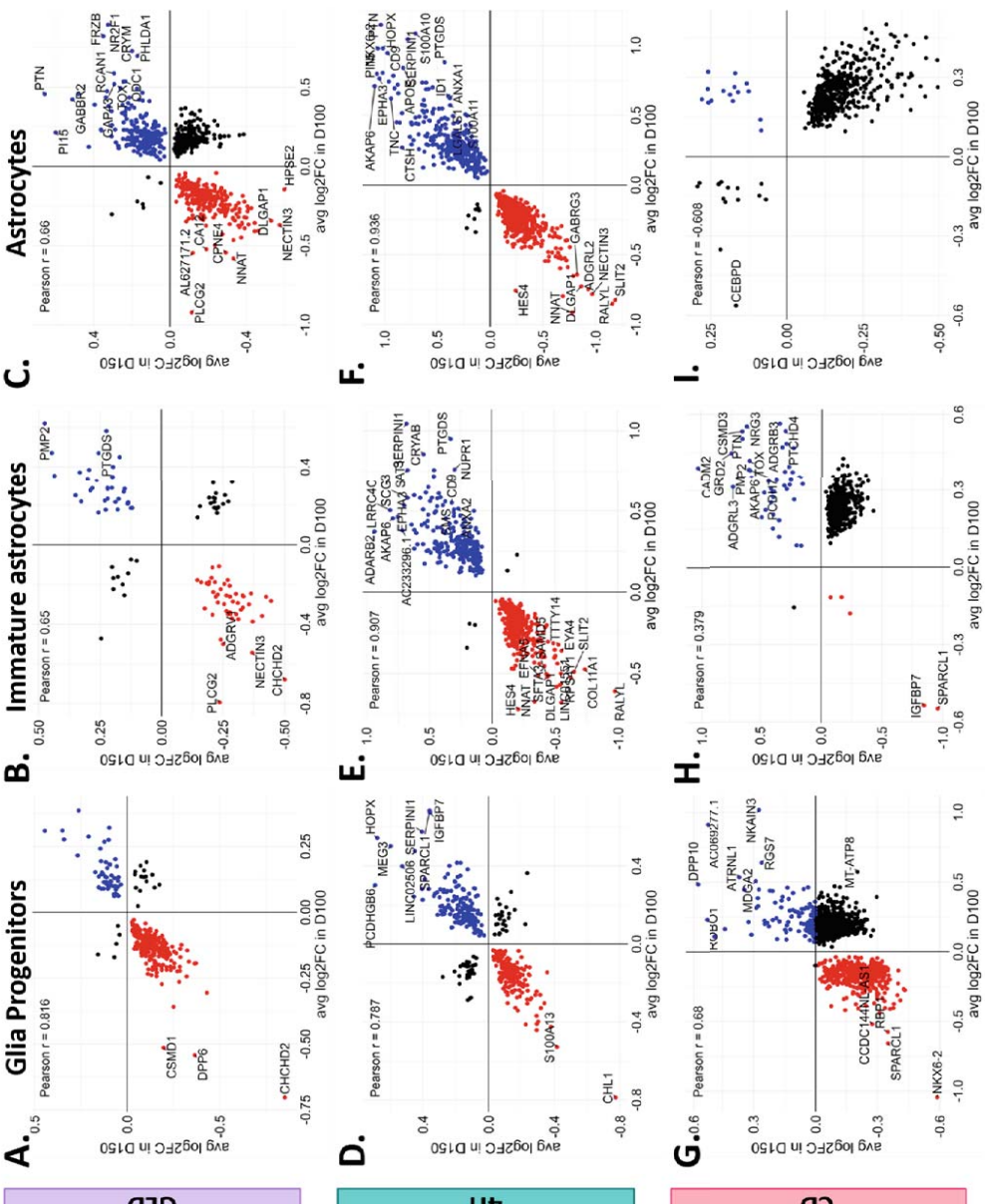

Figure 8: Comparison of significant differentially expressed genes of astrocyte lineage clusters at both day 100 and day 150. Log 2-fold changes at day 100 and day 150 of significant genes in the glia progenitors, immature astrocytes and astrocytes cluster for the contrasts **A-C)** HD x GLD, **D-F)** HD x 4H, **G-I)** HD x CD. Blue: genes upregulated compared to HD. Red: genes downregulated compared to HD. Gray: genes that do not exceed the significance threshold.

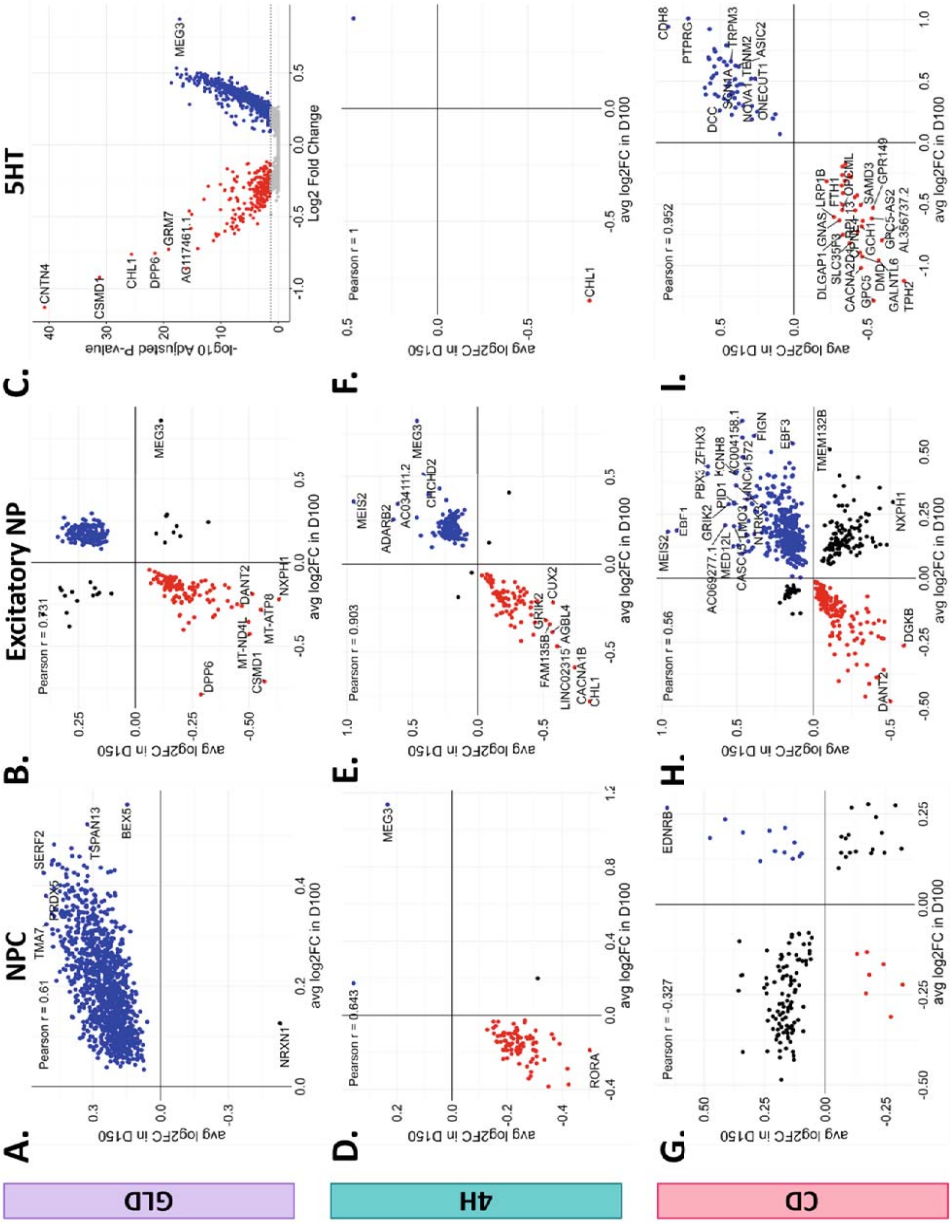

Figure 9: Comparison of significant differentially expressed genes of neuron lineage clusters at both day 100 and day 150.

Log 2-fold changes at day 100 and day 150 of significant genes in the neural progenitor cell (NPC), excitatory neural progenitor (NP) and serotonergic neuron (5HT) clusters for the contrasts **A-B)** HD x GLD, **D-F)** HD x 4H, **G-I)** HD x CD. Blue: genes upregulated compared to HD. Red: genes downregulated compared to HD. Gray: genes that do not exceed the significance threshold. **C)** The serotonergic cluster of GLD is depicted using a volcano plot of day 100 since there were no significant genes at day 150.

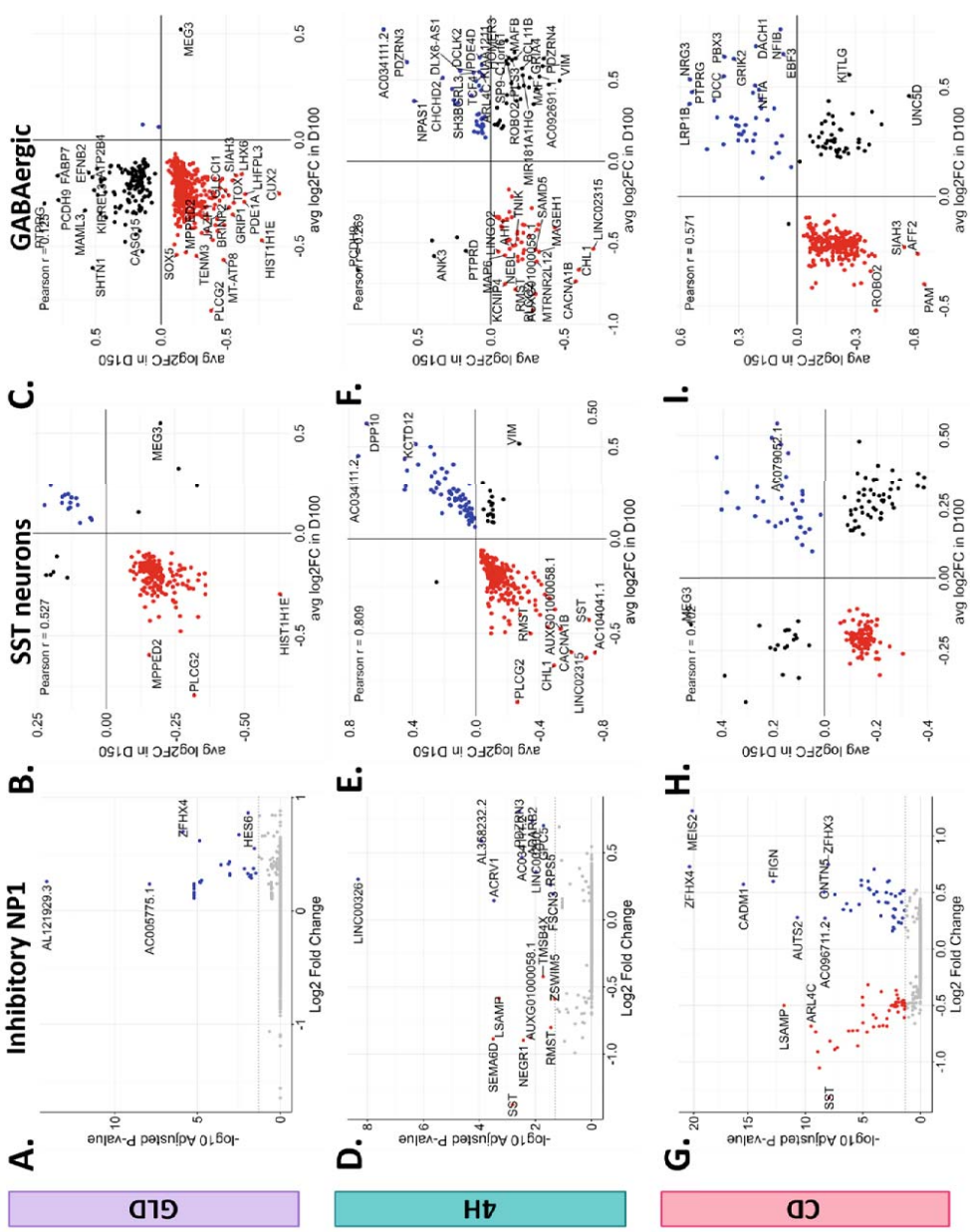

Figure 10: Comparison of significant differentially expressed genes of neuron lineage clusters at both day 100 and day 150.

Log 2-fold changes at day 100 and day 150 of significant genes in the inhibitory neural progenitor 1 (NP1), somatostatin (SST) and GABAergic neuron clusters for the contrasts **A-B)** HD x GLD, **D-F)** HD x 4H, **G-I)** HD x CD. Blue: genes upregulated compared to HD. Red: genes downregulated compared to HD. Gray: genes that do not exceed the significance threshold. **A, D, E)** The inhibitory NP1 cluster is depicted using a volcano plot of day 150 since there were no significant genes at day 150.

DISCUSSION

Our study demonstrates that 3D spheroid models provide valuable access to leukodystrophy-relevant cell types and molecular pathways, enabling the exploration of both known and potentially novel disease mechanisms. With immunofluorescence, we confirmed the presence of key white matter cell types, including oligodendrocytes, astrocytes, and neurons. Using single cell RNA-seq we showed more detailed cellular diversity. The generation of spheroids in a single centralized facility enabled meaningful disease-specific comparisons. This was particularly evident in the replication of differentially expressed genes (DEGs) identified through both cell cluster-based analysis and isogenic line comparisons. These findings underline the model's robustness in detecting disease-driven molecular signatures. Beyond confirming previously implicated pathways, this model serves as a dynamic platform for generating novel hypotheses in leukodystrophy research. The integration of high-throughput sequencing with advanced bioinformatics pipelines supports comprehensive data exploration, allowing for the identification of new molecular targets and potential therapeutic pathways. Although we have shown the potential use of this data set, results as described in this thesis are preliminary, hence, we point out future directions of research that should be explored before publication.

Disease-specific alterations of cellular composition

We identified cellular, molecular and pathway differences in clusters from the oligodendrocyte, astrocyte, and neuronal lineage in spheroids of several leukodystrophies. Particularly interesting is the underrepresentation of some clusters in LDs such as the clusters cycling radial glia and outer radial glia. Radial glial cells develop early in development from neuroepithelial stem cells that line the ventricular zone. Radial glial cells both provide a scaffold for neuronal migration and give rise to intermediate progenitors for neurogenesis and later gliogenesis. Outer radial glia are a type of radial glia specifically present in primate brains, which are involved in cortical expansion and also give rise to specific oligodendrocyte progenitor cell populations (Pollen et al., 2015; Zhou et al., 2024). It would be interesting to study whether radial glial cells show a normal abundance in early spheroids, and whether this would be correlated to a normal neurogenesis but possible disrupted gliogenesis, which only starts in later developmental stages. Possibly, pseudotime analysis of the existing data can be applied to see from which clusters those underrepresented clusters originate and if other clusters are derived from those clusters. Next, is to wonder whether those cells are completely absent in the model, or severely affected by the pathology and hence mislabelled or not sequenced in the single cell

sequencing work-up. For this, it might be useful to use bulk mRNA sequencing and search for differential expression of genes that are indicative for the underrepresented clusters. Interestingly, the underrepresentation of radial glia is a common feature in these LDs. This is an interesting lead for future research as shared pathology among leukodystrophies could mean that future therapeutic strategies developed for one leukodystrophy might be repurposed for others, potentially broadening the clinical applicability of future treatments.

Disease-specific differential gene expression

In addition to common mechanisms, the spheroid models were used to study disease specific mechanisms. A minimal requirement for the spheroids to serve as a disease model for LDs is the expression of disease genes, which was indeed confirmed. Specifically, 4H leukodystrophy patients have mutations in subunits of POLR3. As expected, the POLR3 subunits where broadly expressed in all cell types. Further DEG analysis revealed a number of interesting changes in 4H 3D spheroids. For example, the lncRNA Maternally Expressed Gene 3 (*MEG3*) shows upregulation in the different neuron cellular clusters of 4H cells. Previous studies showed that although *MEG3* is expressed throughout the brain, it shows an especially high expression in the cerebellum and pituitary gland (Zhang et al., 2003). Interestingly, 4H patients often show cerebellar atrophy and hormonal issues associated with pituitary gland dysfunction (Wolf et al., 2014). Previous studies showed that upregulation of *MEG3* improves cognitive impairment, alleviates neuronal damage, and inhibits activation of astrocytes in hippocampus tissues in Alzheimer's disease through inactivating the PI3K/Akt signalling pathway (Yi et al., 2019; Zhang et al., 2020). It is possible that the observed upregulation of *MEG3* is an effect of neuronal stress, which is in line with the observed upregulation of neuroprotective peptide Y (NPY) in certain 4H neuronal clusters (Zhang et al., 2021).

Disease-specific gene set enrichment analysis

We have performed extensive, gene set enrichment analysis (GSEA) which revealed ample pathway dysregulations. Those findings provide a base for validation of existing disease-specific hypothesis or the formation of new hypothesis to determine the direction of future research. However, the pathway findings warrant further investigation before publication as they are sensitive to bias. To exemplify, initially we discovered the pathway “translation” often to be differentially expressed in 4H compared to control. This aligned well with our hypothesis that *POLR3A* variants cause changes in translation, however, “*translation*” was also often significantly different in the other leukodystrophies. Although, “*translation*”

could still be a shared pathological mechanism in leukodystrophies, we do not have other evidence to support those observations. Similarly, oxidative phosphorylation was found to be highly significant in all leukodystrophies, but also this pathways was down and upregulation changed per cluster and per timepoint. Since oxidative stress is linked to impaired OPC differentiation in neurological disorders, it is an interesting topic for future research, but no conclusions can be drawn yet (Spaas et al., 2021). This emphasizes the necessity for this data set to become publicly available for other researchers to use as validation and discovery data set. Simultaneously it shows that when designing spheroid studies it is important to consider the inclusion of more than one disease, as this prevents overinterpretation of the data.

Methodological Considerations

While our data provides robust evidence for cellular and molecular changes, several methodological limitations should be considered. First, the annotation of cell clusters into predefined categories potentially introduces biases, particularly when clusters may not correspond to well-defined *in vivo* populations. Although the annotation is done carefully, more standardized clustering protocols throughout the field could avoid potential bias. Including isogenic controls can improve the precision of disease-specific findings by minimizing background noise, but the largest changes in gene expression in GLD were observed in comparison to both healthy donors and isogenic controls. Conversely, the lack of population-level genetic diversity in isogenic models may also be a limitation, as it does not capture the full range of human genetic variability relevant to disease expression.

CONCLUSION

To conclude, this study provides a comprehensive overview of cell types and gene expression changes involved in leukodystrophies GLD, CD and 4H. The 3D spheroids offer a promising platform for studying leukodystrophies by recapitulating key aspects of white matter development and pathology. By studying 3 different leukodystrophies in one experiment, we were able to identify a number of shared mechanisms. This commonality raises the possibility that therapeutic strategies developed for one leukodystrophy could be repurposed for others, potentially broadening the clinical applicability of future treatments. Additionally, disease-specific findings were observed and provide interesting candidate DEGs and pathways for follow-up studies. The generated dataset will be freely available for further analysis by the broader research community, allowing for more in-depth analysis of specific cell types and/or disorders and novel hypothesis generation.

MATERIALS & METHODS

iPSC culture

iPSCs were generated by each institute according to previously described protocols (Dooves et al., 2023; Holmes & Heine, 2017; Mangiameli et al., 2021) All subjects have given informed consent in accordance with the declaration of Helsinki. Briefly, fibroblasts were reprogrammed into iPSCs using either the CytoTune™-iPS 2.0 Sendai Reprogramming Kit (Invitrogen, A16517), polycistronic construct with *OCT4*, *SOX2*, *KLF4*, and *C-MYC* within a lentiviral vector or StemMACS mRNA Reprogramming Kit (Miltenyi Biotec, Bergisch Gladbach, Germany). Pluripotency was confirmed by immunocytochemistry, alkaline phosphatase assay, PCR, embryoid body formation and/or pluritest. Karyotype analysis was also performed to exclude chromosomal abnormalities.

GALC KO and KI iPSC were produced by CRISPR/Cas9 mediated gene editing of the HD2 iPSC line: in particular GALC KO iPSC were obtained using the Gene Knockout Kit v2 (Synthego), designed to target the first exon of the human GALC gene, according to the manufacturer directions; while the production of GALC KI iPSC was outsourced to Synthego and was obtained by inserting the pathogenic G553R mutations (*GALC*, c.1657G>A) in both alleles.

After generation and characterization, all cell culture procedures were performed centralized in the IRCCs San Raffaele Scientific Institute. iPSCs from IRCCs San Raffaele Scientific Institute and the Institute of Reconstructive Neurobiology, were thawed and maintained in matrigel-coated (Merck Millipore, CLS354230) plates with StemMACS iPS-Brew XF medium (iPS-Brew, Miltenyi Biotech, 130-104-368). iPSCs were refreshed daily and incubated at 37°C in controlled humidified atmosphere (5% CO_2, 5% O_2). When confluent, cells were split in a 1:3 to 1:10 ratio using 0.5 mM EDTA (ThermoFisher, 15575020) diluted in PBS, for further maintenance. iPSCs of the Vrije Universiteit were thawed in the culture condition of the origin institute, TeSR™-E8™ (STEMCELL Technologies, 05990) supplemented with 10 µM ROCK inhibitor Y-27632 (Selleckchem, S1049) on Vitronectin XF™ coating (STEMCELL Technologies, 07180). The following passage, cells were plated on Matrigel-coated plates and were adapted to iPS-Brew medium. An overview of the used stem cell lines can be found in Supplementary Table I.

Spheroid culture

Spheroids from a total of five control, three Globoid Leukodystrophy, three Canavan disease and two 4H leukodystrophy iPSC lines (See Supplementary Table I) were generate according

to an adapted version of the Marton protocol (Marton et al., 2019). Prior to differentiation, EB formation was started from single cells suspension generated by accutase dissociation (Merck Millipore, A6964) for 5-7 minutes. Cells were collected by centrifugation (5 min, 400 rcf) in E8 medium (Thermo Fisher, A1517001). Pellets were resuspended in E8 medium supplemented with ROCK inhibitor Y-27632 (10 µM, SIGMA, Y0503). Uniform spheroids were obtained by dropwise plating of 3 x 10^6 cells in each well of an AggreWell™800 (STEMCELL Technologies, 34815) which was pretreated with Anti-Adherence Rinsing Solution (STEMCELL Technologies 07010). After plating, cells were captured in the bottom by centrifugation at 100 rcf for 3 minutes and placed in an incubator (37°C, 5% CO_2). After 24 hours, spheroids of approximately 300 µm had formed in each of the 300 microwells. Spheroids were collected by pipetting up and down the medium with sterile wide-bore tips (Thermo Fisher, 11374245) and transferred to low attachment 10 cm petridishes. To initiate the differentiation, at day 1 of the protocol, spheroids were plated in E6 medium (Thermo Fisher, A1516401) supplemented with SMAD pathway inhibitors dorsomorphin (2.5 µM, Sigma-Aldrich, P5499) and SB-431542 (10 µM, Sigma-Aldrich, S4317). The medium was refreshed daily on the next two days. On day 4 and 5 also Wnt pathway inhibitor IWP-2 (5 µM, Selleckchem, S7085) was used in the medium. The following six days medium was still refreshed daily but with Differentiation and Maintenance Medium (DMM), which consisted of DMEM/F12 1:1 (Gibco) (Thermo Fisher Scientific, 11-330-057) with 1x B-27 supplement without vitamin A (Thermo Fisher Scientific, 12587010), 1x N2 supplement (Invitrogen, 17502048), 1x MEM NEAA (Invitrogen, 11140035), 1x Glutamax (Invitrogen, 35050038), 25 µg/ml Human Insulin (Sigma-Aldrich, I9278-5ML), 0.1 mM β-mercaptoethanol (Invitrogen, 31350010), 100 U/ml P/S and supplemented with 20 ng/ml EGF (Peprotech, AF10015B) 20 ng/ml FGF-2 (Peprotech, 167100-18B) and 5 µM IWP-2 (Selleckchem, S7085). Between day 12 and 17, also 1 µM of Smoothened agonist (Cayman, 11914) was supplemented to the daily refreshed medium. From day 18 onward, frequency of medium changes was reduced to every other day. On day 25, DMM was supplemented with 60 ng/ml T3 (Sigma-Aldrich, T2877), 100 ng/ml Biotin (Sigma-Aldrich, B4639), 20 ng/ml NT-3 (Peprotech, 450-03), 20 ng/ml BDNF (Peprotech, 450-02), 1 µM cAMP (Sigma-Aldrich, D0627), 5 ng/ml HGF (Peprotech, 315-23), 10 ng/ml IGF-1 (VWR, 100-11), 10 ng/ml PDGF-AA (R&D Systems, 221-AA). On day 37, DMM was supplemented with 60 ng/ml T3, 100 ng/ml Biotin, 1 µM cAMP and 20 µg/ml Ascorbic Acid (SIGMA, A4403). Spheroids were maintained in this medium until the end of the experiment, from day 44 onwards, the medium changes were reduced to twice a week.

Cryopreservation

Organoids were cryopreserved on day 50, 100 and 150 of the differentiation protocol. Cryopreservation was performed by fixation of PBS washed spheroids in 4% PFA for 15 minutes followed by thorough PBS wash. Then, organoids were allowed to dehydrate overnight in 30% sucrose (in PBS) at 4°C. Dehydrated spheroids were transferred to embedding moulds with embedding medium (Bio-Optica, 05-9801V) and snap frozen using dry ice and isopropanol. Frozen samples were stored at -80°C until cryo-sectioning. Cryo-sections of 20 µm were made using a standard cryostat and transferred to Superfrost® Plus adhesive microscope slides (Thermo Scientific). Samples were stored at -80°C until immunofluorescence staining.

Immunofluorescence

To perform immunofluorescence staining, cryosectioned organoids were rehydrated by washing in PBS. After, sections were incubated for 1 hour with blocking solution, PBS containing 0.3% TritonX-100 (Sigma) and 10% Normal Goat Serum (NGS, Sigma-Aldrich, #g9023-10). Primary antibodies made up in blocking solution were incubated overnight at 4°C (See Supplementary Table II). The next day, slides were washed 3 times with PBS prior to 2 hour room temperature incubation with secondary antibodies (Supplementary Table III) made up in PBS with 1% NGS. After incubation, the slides were washed with PBS 3 times. Nuclear visualization was achieved by 10 minutes incubation with Hoechst (1:1000, in PBS). Final wash with PBS was performed before mounting coverslips using FluorSave mounting medium (WR, 345789-20). Images were acquired at the Advanced Light and Electron Microscopy Bioimaging Center (ALEMBIC) at IRCCS San Raffaele Scientific Institute. A Mavig RS-G4 confocal microscope and a 40x oil immersion objective were used. Image analysis and quantification were performed using ImageJ and Imaris software (NIH, Bethesda, MD) to obtain the percentage of positive area of the staining over the DAPI area. For each donor at each timepoint an average was generated by analysing at least 8 up to 29 sections from various organoids. Statistical analysis was then performed using RM two-way ANOVA with Geisser-Greenhouse correction (GraphPad Prism 10.2.0). A full model was fitted. When significant Uncorrected Fisher's LSD or Tukey's multiple comparisons test were performed to determine which groups were different.

Electron microscopy

Organoids were fixed using 2.5% glutaraldehyde in 0.1 M cacodylate buffer (pH 7.4) overnight at 4°C. Samples were post-fixed for 1 hour in a reduced osmium solution (1.5%

potassium ferricyanide and 1% aqueous osmium tetroxide in 0.1 M cacodylate buffer). Following the initial incubation with the heavy metal-based solutions, the pellets were washed with bi-distilled water at room temperature, then immersed in a 0.5% uranyl acetate solution and left overnight at 4 °C. The samples were dehydrated using a graded ethanol series (70%, 80%, 90%, 100%) and acetone for 10 minutes each, before being embedded in Epon resin. After curing at 60 °C for 48 hours, thin sections were cut using a Leica UC7 ultramicrotome (LeicaMicrosystems, Vienna, Austria). The sections were mounted onto 300-mesh copper grids and imaged using a Talos L120C G2transmission electron microscope (Thermo Fisher Scientific Inc., Waltham, MA, USA) at an acceleration voltage of 120 kV. Images were acquired at Advanced Light and Electron Microscopy Bio-Imaging Centre of San Raffaele Scientific Institute (ALEMBIC) at IRCCS San Raffaele Scientific Institute. A Fei Talos L120C G2 transmission electron microscope was used. Image analysis and quantification were performed using ImageJ and Imaris software (NIH, Bethesda, MD).

Bulk mRNA sequencing

Total RNA was extracted from individual spheroids with the RNeasy Mini Kit (Qiagen, 74104) according to manufacturer protocol. Per donor, RNA of three spheroids were pooled to make one bulk mRNA sequencing sample. The RNA concentration and purity were determined using a NanoDrop spectrophotometer (Thermo Fisher Scientific). Purified RNA samples were sent to Genewiz (Azenta Life Sciences) for RNA sequencing (RNA-seq) analysis. Libraries were prepared with NEBnext Ultra II Directional RNA Library Preparation kit (New England Biolabs), and sequencing was performed on an Illumina NovaSeq 6000 platform. A minimum of 40 million read depth per sample was achieved. Quality control (QC) was conducted by the service provider to remove adapter sequences and low-quality reads using Trimmomatic v.0.36. Cleaned reads were aligned to the human reference genome GRCh38 available on ENSEMBL using the STAR aligner v.2.5.2b. BAM files were generated as a result of this step, unique gene hit counts were calculated by using featureCounts from the Subread package v.1.5.2.

Single cell RNA-seq

To obtain single cell transcriptomic data, three spheroids of each line at day 100 and 150 were dissociated. Brain spheroids were harvested from culture dishes and mechanically dissociated by mincing them into smaller pieces using a sterile scalpel blade (Bisturi) for 2–3 minutes, until spheroids were visibly fragmented into fragments smaller than 1 mm in diameter. Care was taken to avoid excessive mechanical force to minimize cell damage.

Following mechanical trituration, enzymatic dissociation was performed using the Papain Dissociation System (Worthington Biochemical Corporation, LK003150) following the manufacturer's instructions, with minor modifications. Briefly, the minced spheroids were incubated with papain and transferred to an orbital shaker at 70 rpm inside a tissue culture incubator for 70 minutes. To stop the reaction, dissociated fragments were pelleted and resuspend with a papain inhibitor. After being resuspended in 0.2 % bovine serum albumin diluted in PBS supplemented with 10uM Y-27632, cells were filtered through a 70 µm cell strainer to remove any undissociated tissue clumps. Cell counting was performed using TC20 automated cell counter (BioRad), and viability was calculated as the percentage of live cells (trypan blue-negative) over the total cell count. Viability for each individual sample was evaluated to ensure it was above 90%. Finally, cells were suspended in sterile PBS 0.04% BSA to a final concentration of 1 × 106 cells/mL (1,000 cells/µl).

For single cell sequencing approximately 6400 cells were loaded onto a single-cell chip for GEM generation using the 10x Genomics Chromium Controller (10× Genomics, Pleasanton, CA), to obtain a target output of 4000 cells per sample. 3′mRNA-seq gene expression libraries were constructed using the Chromium Single Cell 3′ Library & Gel Bead Kit v2 (10x Genomics) according to the manufacturer's guidelines. All reactions were performed in a C1000 Touch Thermal Cycler (Bio-Rad Laboratories, Hercules, CA). Twelve cycles were used for cDNA amplification, while the number of total cycles for the sample index PCR was calculated based on the cDNA concentration. Amplified cDNA and final libraries were evaluated using a Tape Station 4200 (Agilent Technologies, Santa Clara, CA) with a high sensitivity chip. scRNA-seq libraries were sequenced using an Illumina NovaSeq6000 with the standard sequencing protocol of R1 28; I1 10; I2 10; R2 90 nt read length to obtain 50.000 reads per cell. Single cell encapsulation, cDNA amplification, library prep and sequencing were performed at COSR (Center for Omic Sciences).

Bioinformatics

Analysis of the scRNA-seq data was performed by the Bioinformatics core of the San Raffaele Telethon Institute for Gene Therapy according to previously described methods (Naldini et al., 2023).

FUNDING

This work was supported by the European Joint Programme on Rare Diseases (EJPRD19-201, NG4LEUKO).

COMPETING INTERESTS

The authors report no competing interests.

AUTHOR CONTRIBUTIONS

EM, CR generated spheroids and collected samples with assistance of LMLK and GC. FC, RA and IM analysed scRNA-seq data. VMH, AG and OB supervised the project. LMLK visualized the data and wrote the chapter in consultation with other authors.

REFERENCES

Dooves, S., Kok, L. M. L., Holmes, D. B., Breeuwsma, N., Breur, M., Bugiani, M., Wolf, N. I., & Heine, V. M. (2023). Cortical interneuron development is affected in 4H leukodystrophy. *Brain*, *146*(7), 2846-2860. https://doi.org/10.1093/brain/awad017

Holmes, D. B., & Heine, V. M. (2017). Simplified 3D protocol capable of generating early cortical neuroepithelium. *Biol Open*, *6*(3), 402-406. https://doi.org/10.1242/bio.021725

Mangiameli, E., Cecchele, A., Morena, F., Sanvito, F., Matafora, V., Cattaneo, A., Della Volpe, L., Gnani, D., Paulis, M., Susani, L., Martino, S., Di Micco, R., Bachi, A., & Gritti, A. (2021). Human iPSC-based neurodevelopmental models of globoid cell leukodystrophy uncover patient- and cell type-specific disease phenotypes. *Stem Cell Reports*, *16*(6), 1478-1495. https://doi.org/10.1016/j.stemcr.2021.04.011

Marton, R. M., Miura, Y., Sloan, S. A., Li, Q., Revah, O., Levy, R. J., Huguenard, J. R., & Pasca, S. P. (2019). Differentiation and maturation of oligodendrocytes in human three-dimensional neural cultures. *Nat Neurosci*, *22*(3), 484-491. https://doi.org/10.1038/s41593-018-0316-9

Naldini, M. M., Casirati, G., Barcella, M., Rancoita, P. M. V., Cosentino, A., Caserta, C., Pavesi, F., Zonari, E., Desantis, G., Gilioli, D., Carrabba, M. G., Vago, L., Bernardi, M., Di Micco, R., Di Serio, C., Merelli, I., Volpin, M., Montini, E., Ciceri, F., & Gentner, B. (2023). Longitudinal single-cell profiling of chemotherapy response in acute myeloid leukemia. *Nat Commun*, *14*(1), 1285. https://doi.org/10.1038/s41467-023-36969-0

Pollen, A. A., Nowakowski, T. J., Chen, J., Retallack, H., Sandoval-Espinosa, C., Nicholas, C. R., Shuga, J., Liu, S. J., Oldham, M. C., Diaz, A., Lim, D. A., Leyrat, A. A., West, J. A., & Kriegstein, A. R. (2015). Molecular identity of human outer radial glia during cortical development. *Cell*, *163*(1), 55-67. https://doi.org/10.1016/j.cell.2015.09.004

Spaas, J., van Veggel, L., Schepers, M., Tiane, A., van Horssen, J., Wilson, D. M., 3rd, Moya, P. R., Piccart, E., Hellings, N., Eijnde, B. O., Derave, W., Schreiber, R., & Vanmierlo, T. (2021). Oxidative stress and impaired oligodendrocyte precursor cell differentiation in neurological disorders. *Cell Mol Life Sci*, *78*(10), 4615-4637. https://doi.org/10.1007/s00018-021-03802-0

Wolf, N. I., Vanderver, A., van Spaendonk, R. M., Schiffmann, R., Brais, B., Bugiani, M., Sistermans, E., Catsman-Berrevoets, C., Kros, J. M., Pinto, P. S., Pohl, D., Tirupathi, S., Stromme, P., de Grauw, T., Fribourg, S., Demos, M., Pizzino, A., Naidu, S., Guerrero, K., . . . Bernard, G. (2014). Clinical spectrum of 4H leukodystrophy caused by POLR3A and POLR3B mutations. *Neurology*, *83*(21), 1898-1905. https://doi.org/10.1212/WNL.0000000000001002

Yi, J., Chen, B., Yao, X., Lei, Y., Ou, F., & Huang, F. (2019). Upregulation of the lncRNA MEG3 improves cognitive impairment, alleviates neuronal damage, and inhibits activation of astrocytes in hippocampus tissues in Alzheimer's disease through inactivating the PI3K/Akt signaling pathway. *J Cell Biochem*, *120*(10), 18053-18065. https://doi.org/10.1002/jcb.29108

Zhang, H., Tao, J., Zhang, S., & Lv, X. (2020). LncRNA MEG3 Reduces Hippocampal Neuron Apoptosis via the PI3K/AKT/mTOR Pathway in a Rat Model of Temporal Lobe Epilepsy. *Neuropsychiatr Dis Treat*, *16*, 2519-2528. https://doi.org/10.2147/NDT.S270614

Zhang, X., Zhou, Y., Mehta, K. R., Danila, D. C., Scolavino, S., Johnson, S. R., & Klibanski, A. (2003). A pituitary-derived MEG3 isoform functions as a growth suppressor in tumor cells. *J Clin Endocrinol Metab*, *88*(11), 5119-5126. https://doi.org/10.1210/jc.2003-030222

Zhang, Y., Liu, C. Y., Chen, W. C., Shi, Y. C., Wang, C. M., Lin, S., & He, H. F. (2021). Regulation of neuropeptide Y in body microenvironments and its potential application in therapies: a review. *Cell Biosci*, *11*(1), 151. https://doi.org/10.1186/s13578-021-00657-7

Zhou, Y., Song, H., & Ming, G. L. (2024). Genetics of human brain development. *Nat Rev Genet*, *25*(1), 26-45. https://doi.org/10.1038/s41576-023-00626-5

SUPPLEMENTARY FIGURES

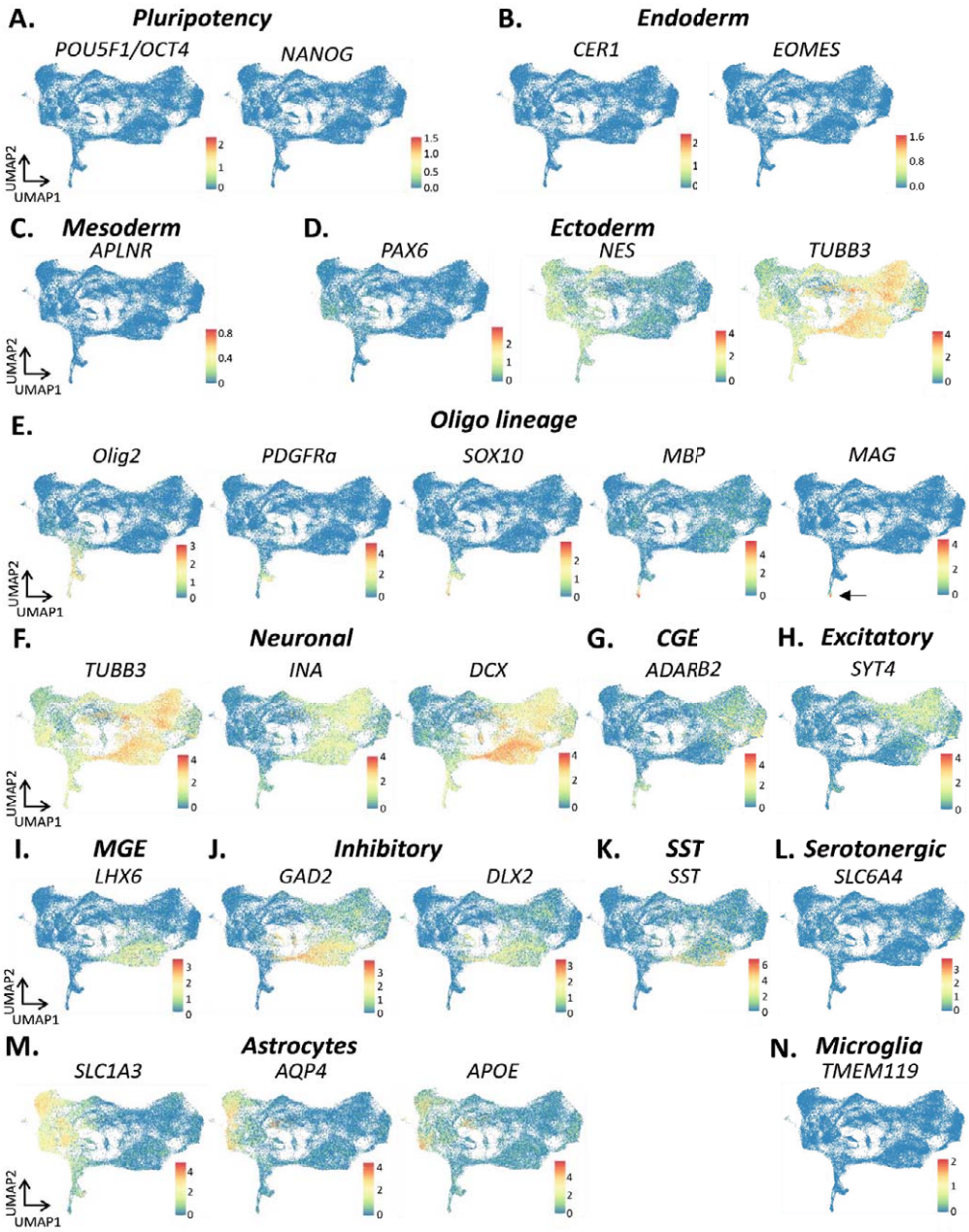

Supplementary Figure 1: Marker gene expression to confirm cluster identity. MGE: medial ganglionic eminence, CGE: caudal ganglionic eminence, SST: somatostatin

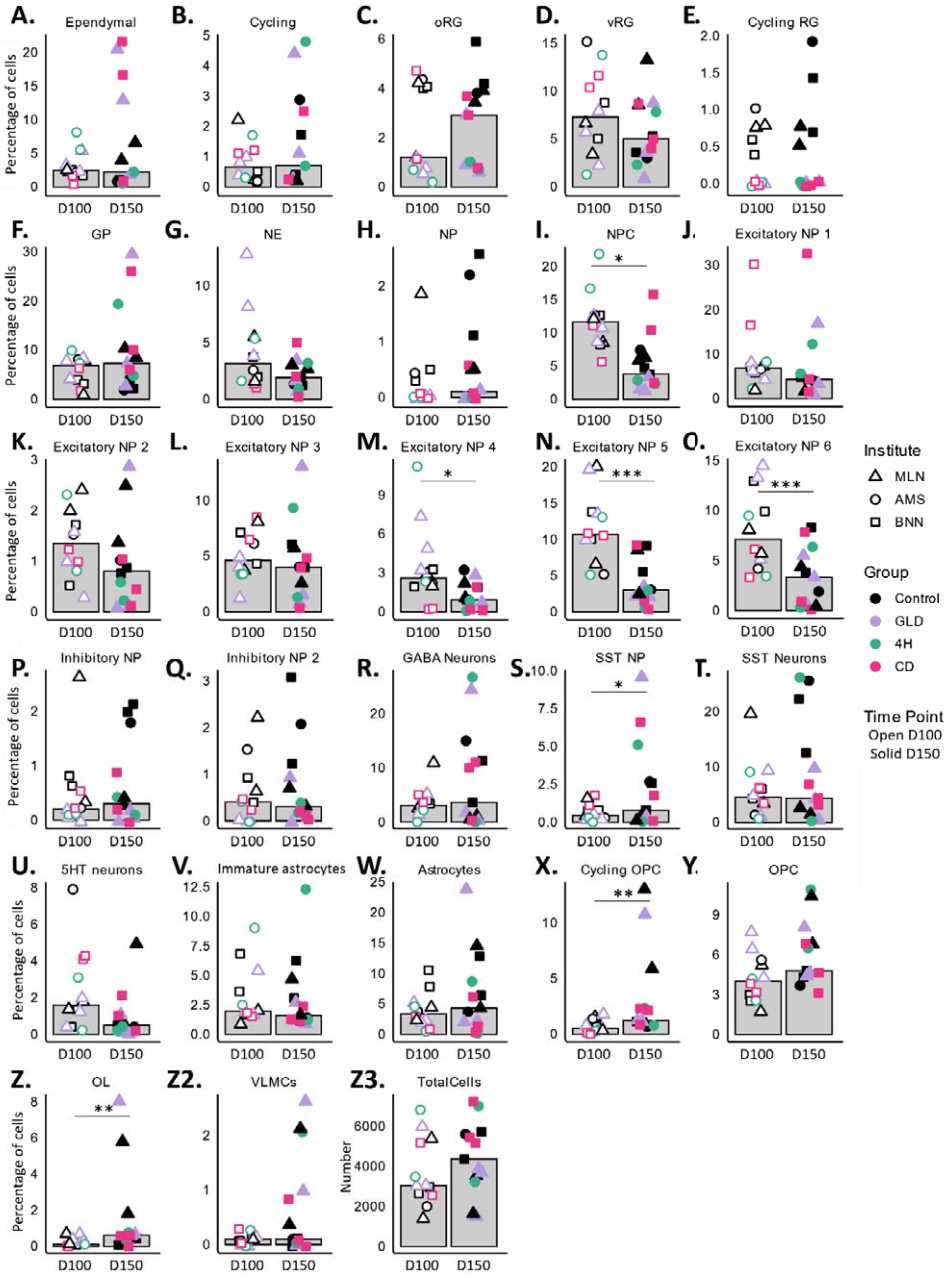

Supplementary Figure 2: Percentage of cells in clusters over time. A) Ependymal, **B)** Cycling, **C)** Outer radial glia, **D)** ventricular radial glia, **E)** cycling radial glia, **F)** glia progenitors, **G)** neuroepithelial, **H)** Neural progenitor, **I)** Neural progenitor cell, **J)** Excitatory neural progenitor 1, **K)** 2, **L)** 3, **M)** 4, **N)** 5, **O)** 6, **P)** Inhibitory neural progenitor, **Q)** Inhibitory neural progenitor 2, **R)** GABA neurons, **S)** somatostatin (SST) neural progenitor, **T)** SST neurons, **U)** Serotonergic (5HT) neurons, **V)** Immature astrocytes, **W)** Astrocytes, **X)** Cycling oligodendrocyte precursors (OPC), **Y)** OPC, **Z)** oligodendrocyte (OL), **Z2)** vascular leptomeningeal cell, **Z3**) total cells sequenced.

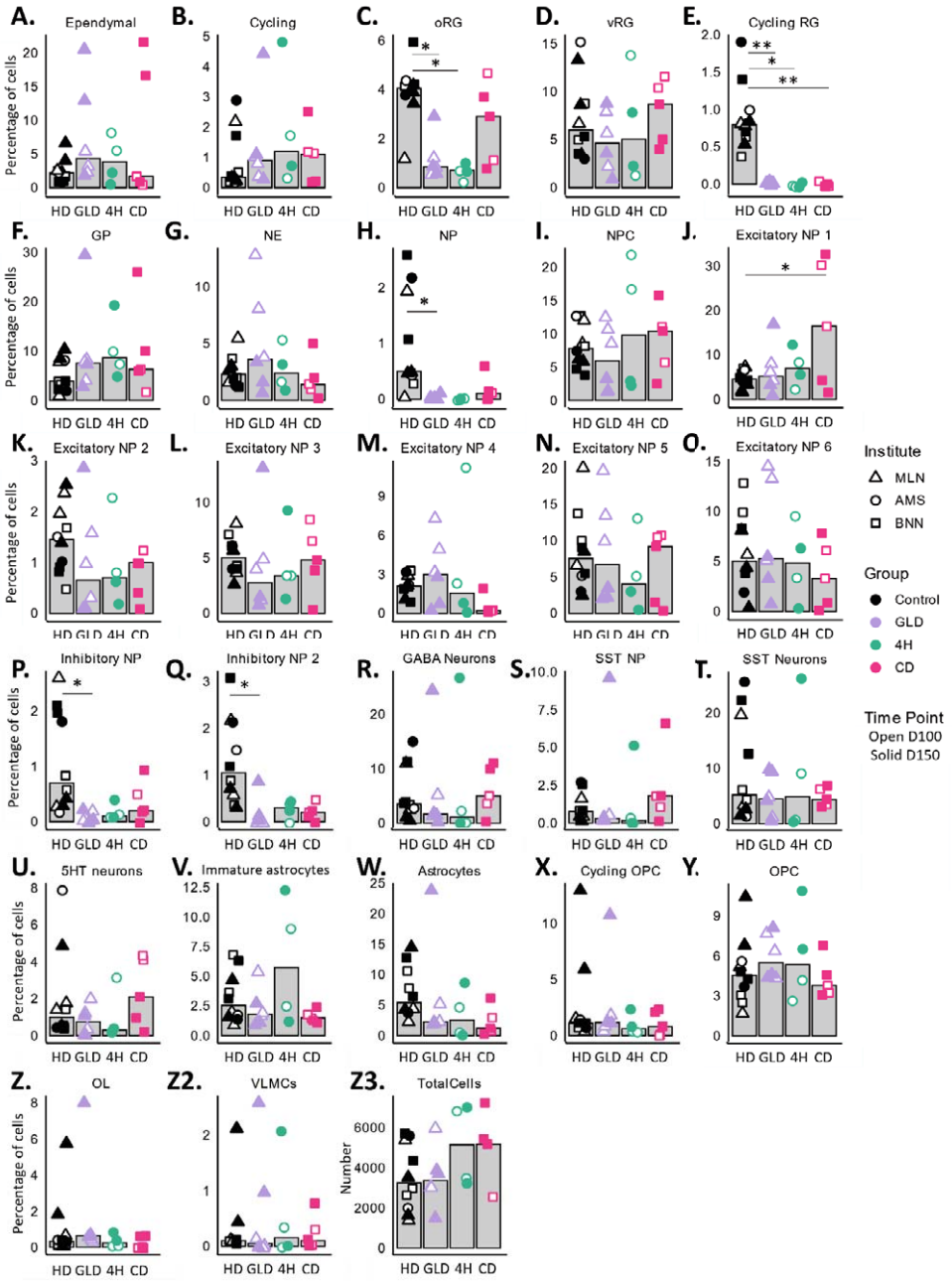

Supplementary Figure 3: Percentage of cells in clusters based on disease status. A) Ependymal, **B)** Cycling, **C)** Outer radial glia, **D)** ventricular radial glia, **E)** cycling radial glia, **F)** glia progenitors, **G)** neuroepithelial, **H)** Neural progenitor, **I)** Neural progenitor cell, **J)** Excitatory neural progenitor 1, **K)** 2, **L)** 3, **M)** 4, **N)** 5, **O)** 6, **P)** Inhibitory neural progenitor, **Q)** Inhibitory neural progenitor 2, **R)** GABA neurons, **S)** somatostatin (SST) neural progenitor, **T)** SST neurons, **U)** Serotonergic (5HT) neurons, **V)** Immature astrocytes, **W)** Astrocytes, **X)** Cycling oligodendrocyte precursors (OPC), **Y)** OPC, **Z)** oligodendrocyte (OL), **Z2)** vascular leptomeningeal cell, **Z3**) total cells sequenced. HD: healthy donor

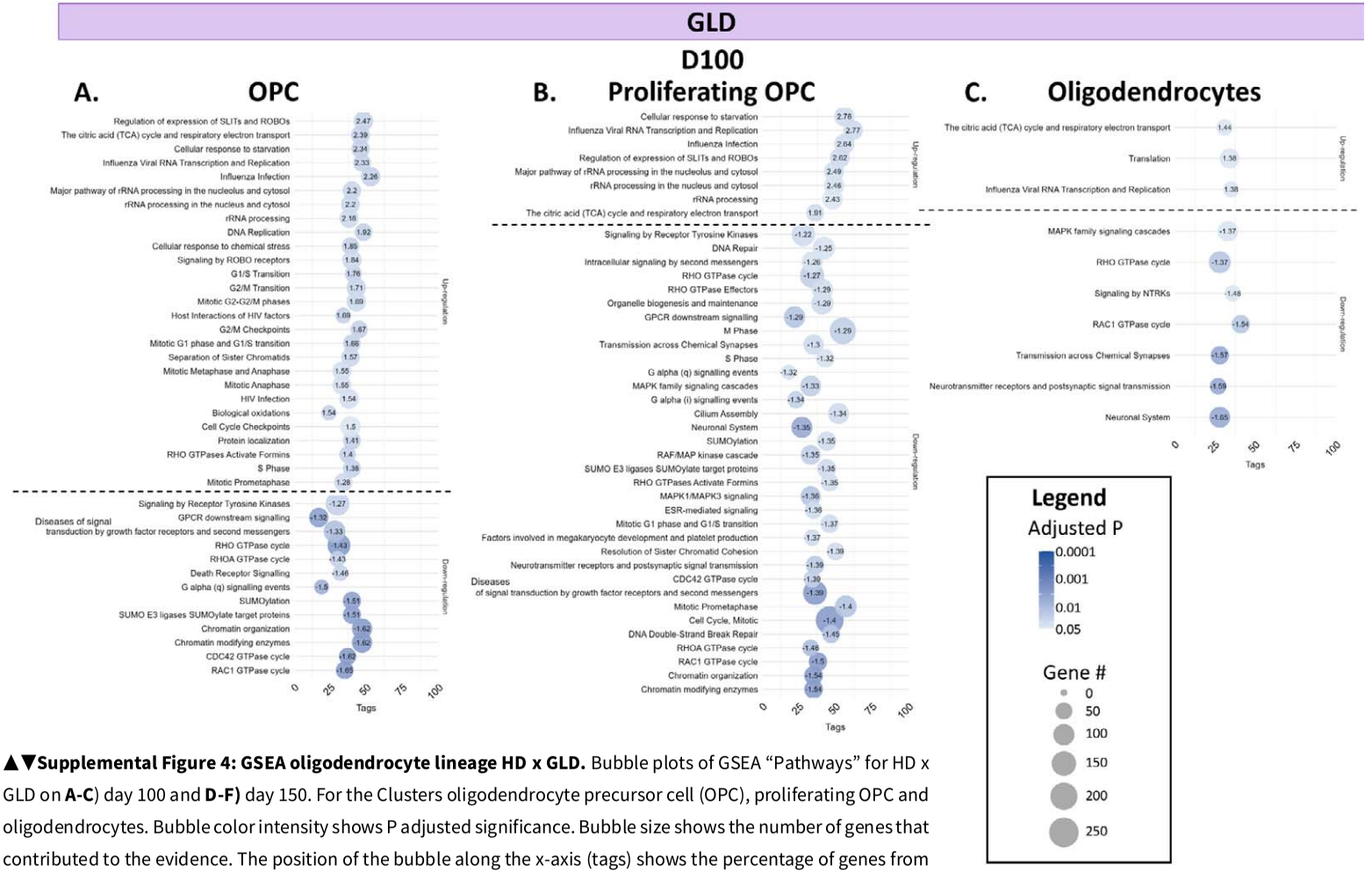

▲▼Supplemental Figure 4: GSEA oligodendrocyte lineage HD x GLD. Bubble plots of GSEA "Pathways" for HD x GLD on **A-C**) day 100 and **D-F)** day 150. For the Clusters oligodendrocyte precursor cell (OPC), proliferating OPC and oligodendrocytes. Bubble color intensity shows P adjusted significance. Bubble size shows the number of genes that contributed to the evidence. The position of the bubble along the x-axis (tags) shows the percentage of genes from the entire gene set that contributed to the evidence. Dashed line separates up and down regulated pathways.

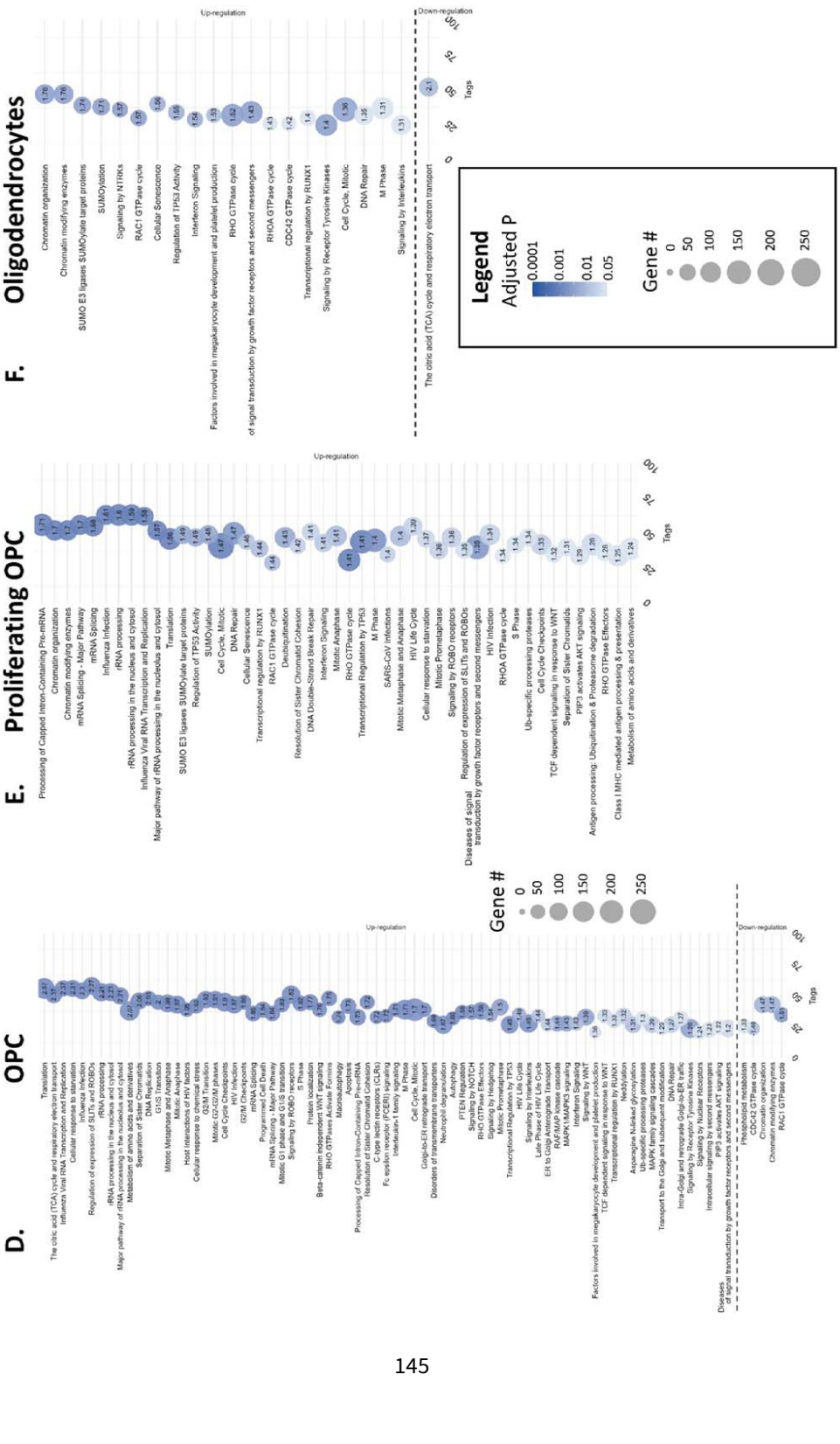
D150
D. OPC
E. Proliferating OPC
F. Oligodendrocytes
Up-regulation
Down-regulation
Tags
Gene #
0
50
100
150
200
250
Legend
Adjusted P
0.0001
0.001
0.01
0.05

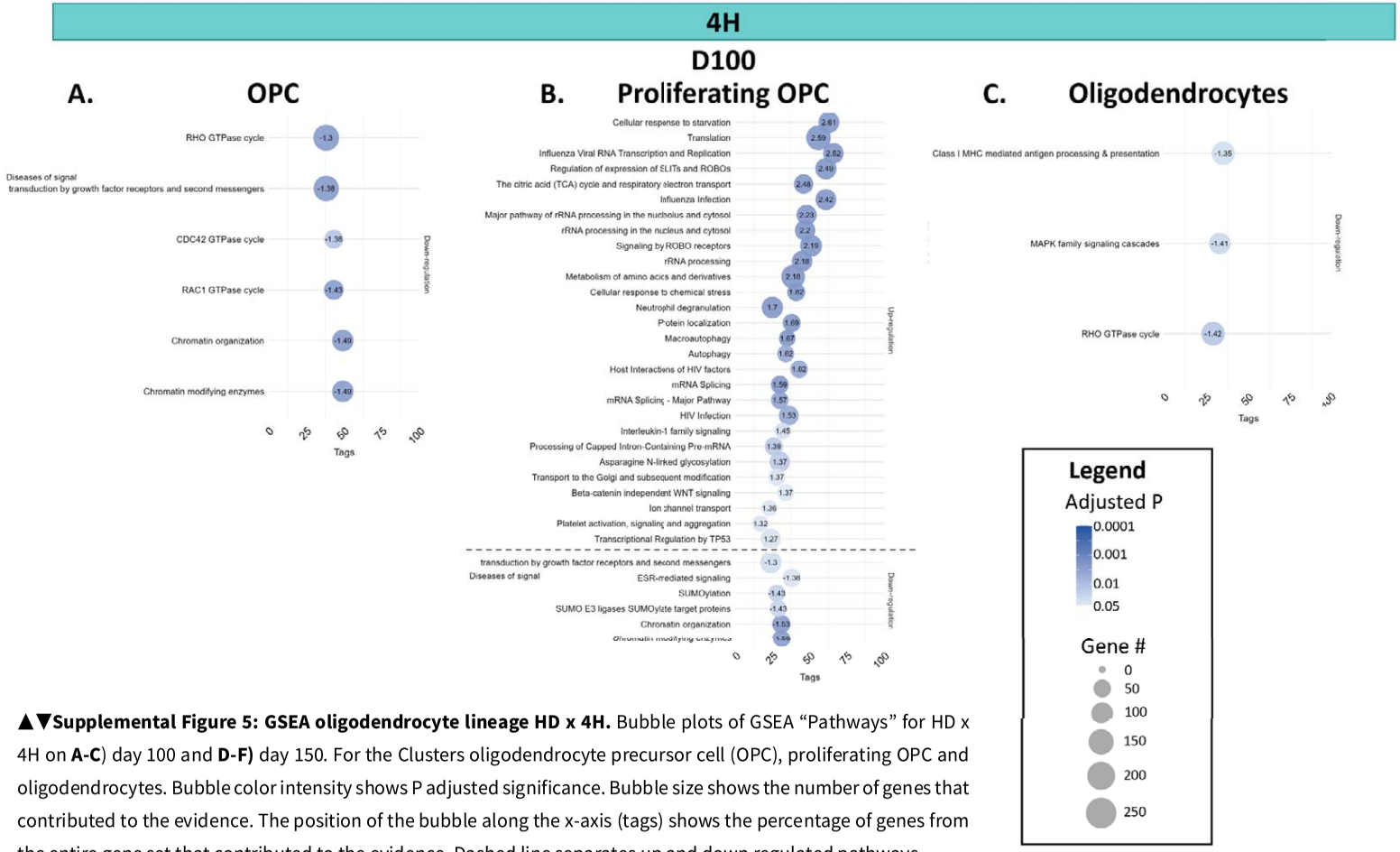

▲▼Supplemental Figure 5: GSEA oligodendrocyte lineage HD x 4H. Bubble plots of GSEA "Pathways" for HD x 4H on **A-C**) day 100 and **D-F)** day 150. For the Clusters oligodendrocyte precursor cell (OPC), proliferating OPC and oligodendrocytes. Bubble color intensity shows P adjusted significance. Bubble size shows the number of genes that contributed to the evidence. The position of the bubble along the x-axis (tags) shows the percentage of genes from the entire gene set that contributed to the evidence. Dashed line separates up and down regulated pathways.

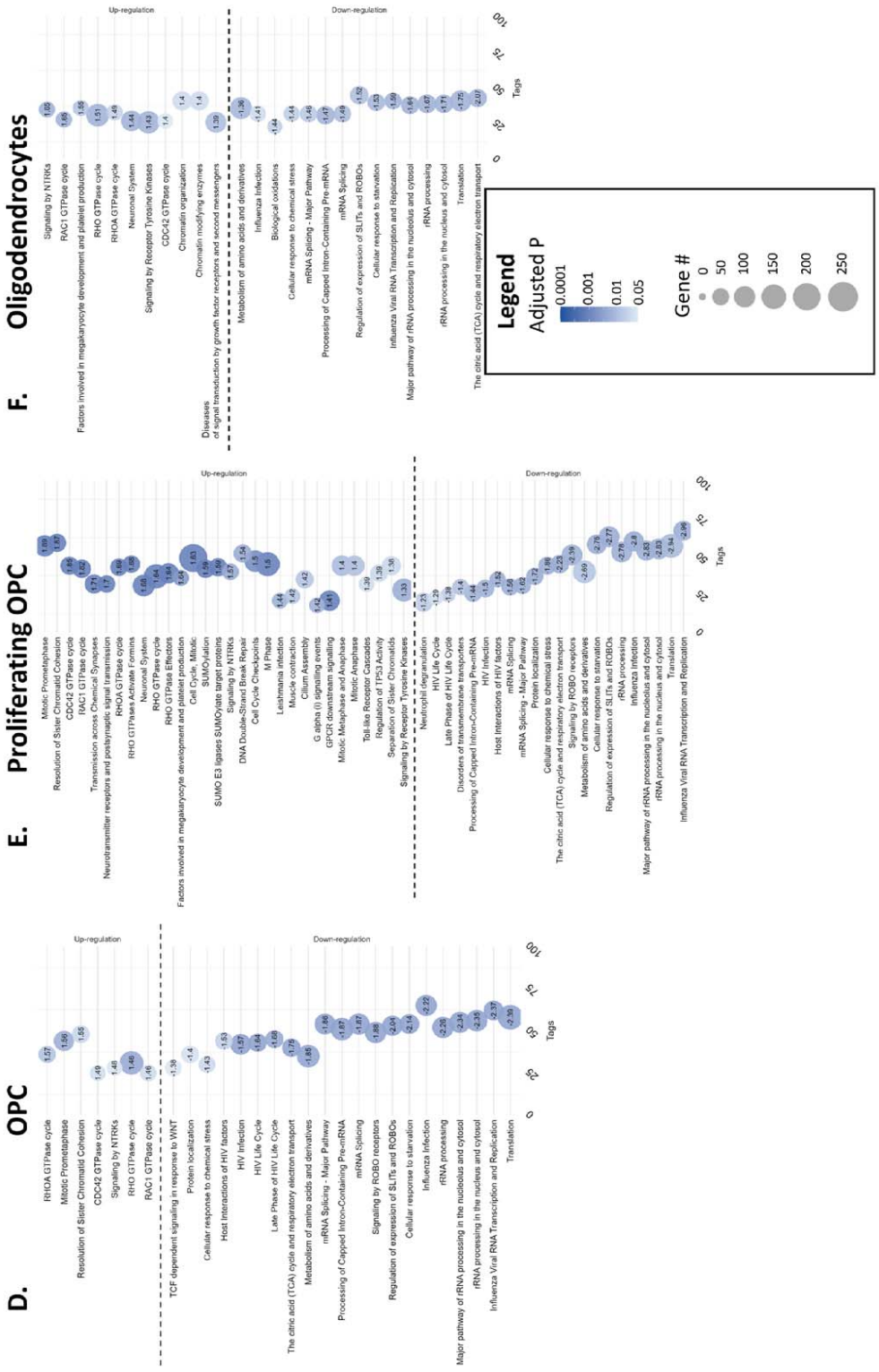
D150
D. OPC
E. Proliferating OPC
F. Oligodendrocytes
Up-regulation
Down-regulation
Tags
Legend
Adjusted P
0.0001
0.001
0.01
0.05
Gene #
0
50
100
150
200
250

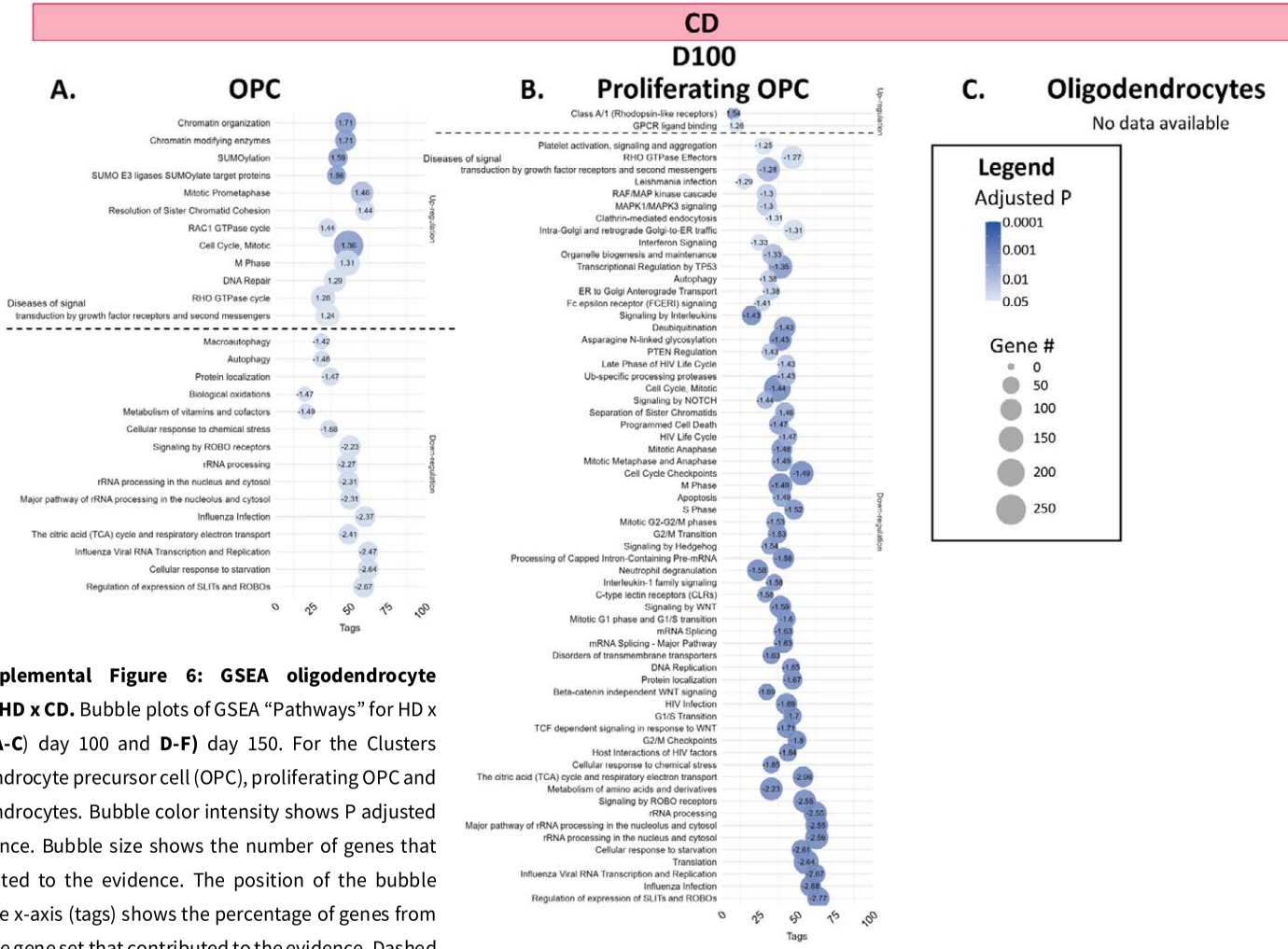

▲▼Supplemental Figure 6: GSEA oligodendrocyte lineage HD x CD. Bubble plots of GSEA "Pathways" for HD x CD on **A-C**) day 100 and **D-F)** day 150. For the Clusters oligodendrocyte precursor cell (OPC), proliferating OPC and oligodendrocytes. Bubble color intensity shows P adjusted significance. Bubble size shows the number of genes that contributed to the evidence. The position of the bubble along the x-axis (tags) shows the percentage of genes from the entire gene set that contributed to the evidence. Dashed line separates up and down regulated pathways.

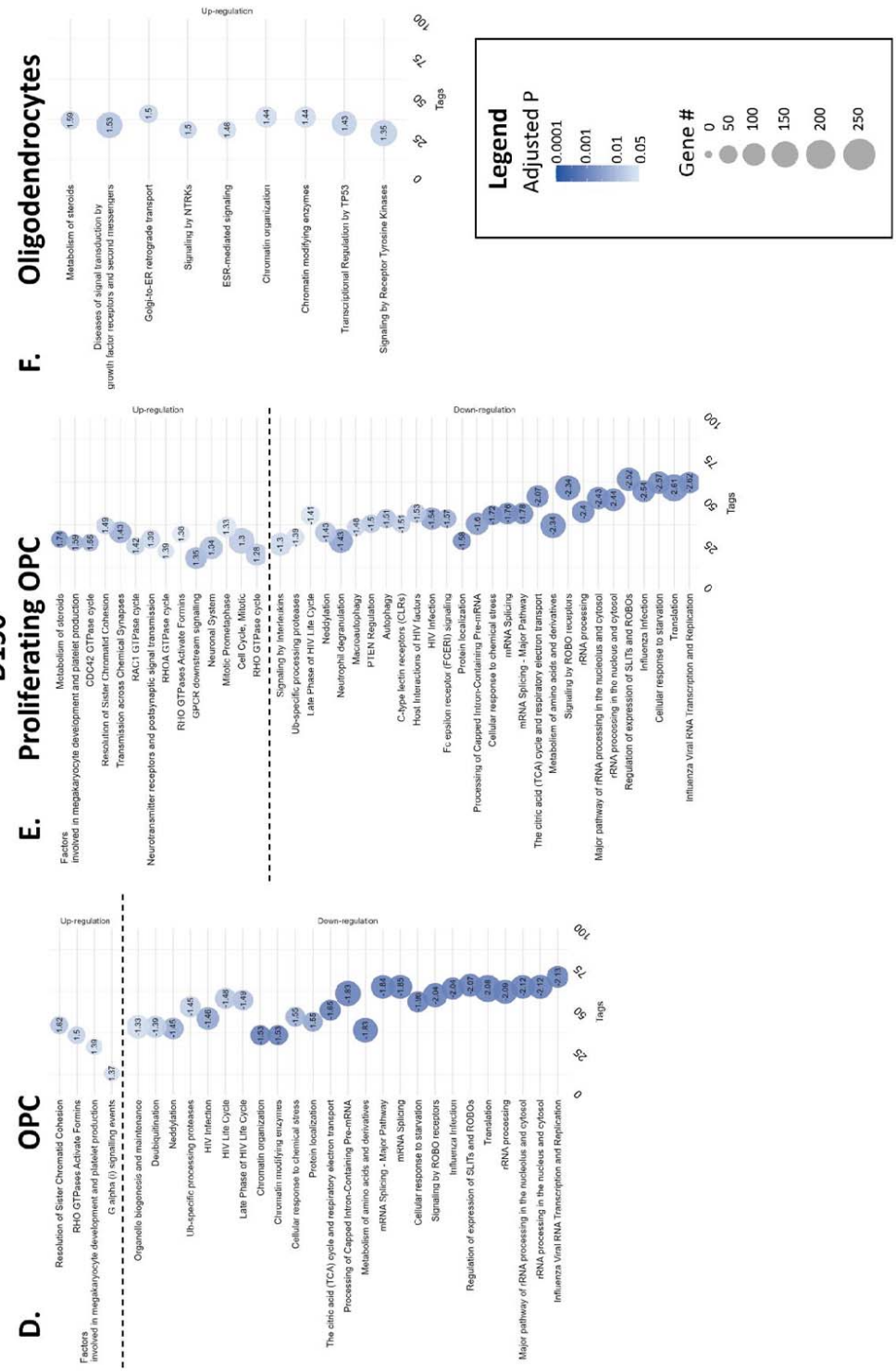
D150
D. OPC
Up-regulation
Resolution of Sister Chromatid Cohesion
Factors involved in megakaryocyte development and platelet production
RHO GTPases Activate Formins
G alpha (i) signalling events
Down-regulation
Organelle biogenesis and maintenance
Deubiquitination
Neddylation
Ub-specific processing proteases
HIV Infection
HIV Life Cycle
Late Phase of HIV Life Cycle
Chromatin organization
Chromatin modifying enzymes
Cellular response to chemical stress
Protein localization
The citric acid (TCA) cycle and respiratory electron transport
Processing of Capped Intron-Containing Pre-mRNA
Metabolism of amino acids and derivatives
mRNA Splicing - Major Pathway
mRNA Splicing
Cellular response to starvation
Signalling by ROBO receptors
Influenza Infection
Regulation of expression of SLITs and ROBOs
Translation
rRNA processing
Major pathway of rRNA processing in the nucleolus and cytosol
rRNA processing in the nucleus and cytosol
Influenza Viral RNA Transcription and Replication
Tags
E. Proliferating OPC
Up-regulation
Metabolism of steroids
Factors involved in megakaryocyte development and platelet production
CDC42 GTPase cycle
Resolution of Sister Chromatid Cohesion
Transmission across Chemical Synapses
RAC1 GTPase cycle
Neurotransmitter receptors and postsynaptic signal transmission
RHOA GTPase cycle
RHO GTPases Activate Formins
GPCR downstream signaling
Neuronal System
Mitotic Prometaphase
Cell Cycle, Mitotic
RHO GTPase cycle
Down-regulation
Signaling by Interleukins
Ub-specific processing proteases
Late Phase of HIV Life Cycle
Neddylation
Neutrophil degranulation
Macroautophagy
PTEN Regulation
Autophagy
C-type lectin receptors (CLRs)
Host Interactions of HIV factors
HIV Infection
Fc epsilon receptor (FCERI) signaling
Protein localization
Processing of Capped Intron-Containing Pre-mRNA
Cellular response to chemical stress
mRNA Splicing
mRNA Splicing - Major Pathway
The citric acid (TCA) cycle and respiratory electron transport
Metabolism of amino acids and derivatives
Signaling by ROBO receptors
rRNA processing
Major pathway of rRNA processing in the nucleolus and cytosol
rRNA processing in the nucleus and cytosol
Regulation of expression of SLITs and ROBOs
Influenza Infection
Cellular response to starvation
Translation
Influenza Viral RNA Transcription and Replication
Tags
F. Oligodendrocytes
Up-regulation
Metabolism of steroids
Diseases of signal transduction by growth factor receptors and second messengers
Golgi-to-ER retrograde transport
Signaling by NTRKs
ESR-mediated signaling
Chromatin organization
Chromatin modifying enzymes
Transcriptional Regulation by TP53
Signaling by Receptor Tyrosine Kinases
Tags
Legend
Adjusted P
0.0001
0.001
0.01
0.05
Gene #
0
50
100
150
200
250

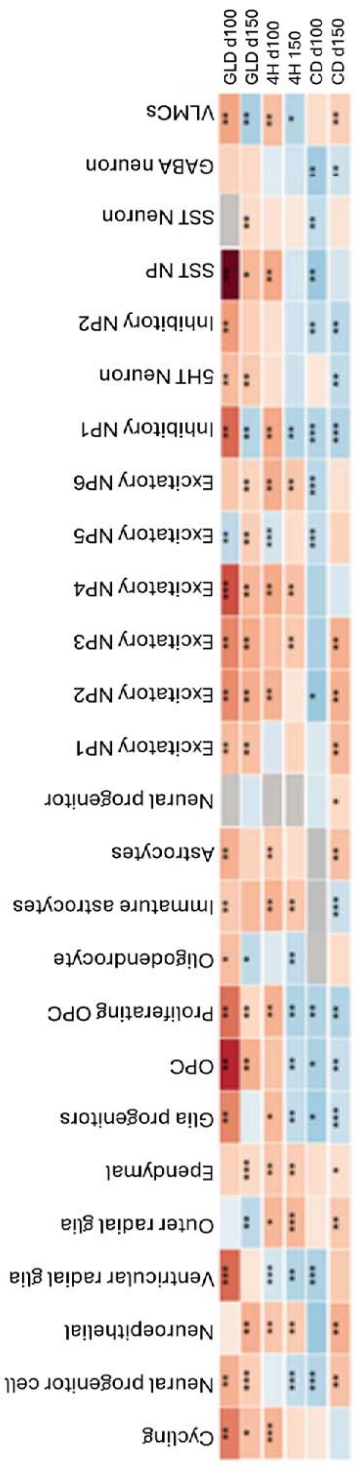

Supplemental Figure 7: Comparison of GSEA "Oxidative phosphorylation" across all timepoints, diseases and clusters.
Blue: decreased. Red: increased. Significant findings indicated with asterisk (P adjusted significant). Gray: no data available.

SUPPLEMENTARY TABLES

Supplementary table I: iPSC lines.

	Line ID	Donor Sex, Age	Cell Origin	hPSCreg ID	Disease status	Genotype	Isogenic Pair	Repr. method	Origin Institute (City, Country)
C1	HD1.2	F, adult	Fibroblasts, Life tech., HDF C0135C	TIGETi001-A	Healthy	-		mRNA	IRCCs San Raffaele Scientific Institute (MLN, IT)
C2	HD2.2	M, neonatal	Fibroblasts, Life tech., HDF C0045C		Healthy	-	A	mRNA	IRCCs San Raffaele Scientific Institute (MLN, IT)
C3	hvs420	M, 21y	Fibroblasts, Amsterdam UMC	VUi036-A	Healthy	-		Lentiviral	Vrije Universiteit (AMS, NL)
C4	C107	M, 34y			Healthy	-			Institute of Reconstructive Neurobiology (BNN, DE)
C5	C16	M, 79y			Healthy	-			Institute of Reconstructive Neurobiology (BNN, DE)
P1	KI H4	M, neonatal	iPSC HD2.2		GLD	*GALC*, c.1657G>A / c.1657G>A	A	mRNA	IRCCs San Raffaele Scientific Institute (MLN, IT)
P2	KO X19	M, neonatal	iPSC HD2.2		GLD	*GALC* KO	A	mRNA	IRCCs San Raffaele Scientific Institute (MLN, IT)
P3	GLD5.2	F, 1y	Fibroblasts, Gaslini Biobank FFF0042010		GLD	*GALC*, c.1657G>A / c.1657G>A		mRNA	IRCCs San Raffaele Scientific Institute (MLN, IT)
P4	hvs449a	M, 24y	Patient-derived fibroblasts, Amsterdam UMC	VUi029-A	4H	POLR3A c.1771-6C>G & c.3205C>T (p.Arg1069Trp)		Sendai	Vrije Universiteit (AMS, NL)
P5	hvs450a	F, 2y	Patient-derived fibroblasts, Amsterdam UMC	VUi030-A	4H	POLR3A c.1771-7C>G & c.1048+5G>T		Sendai	Vrije Universiteit (AMS, NL)
P6	KO E27	M, 34y			CD	*ASPA*			Institute of Reconstructive Neurobiology (BNN, DE)
P7	KO E30	M, 34y			CD	*ASPA*			Institute of Reconstructive Neurobiology (BNN, DE)
P8	KO E70	M, 34y			CD	*ASPA*			Institute of Reconstructive Neurobiology (BNN, DE)

4H: 4H Leukodystrophy, GLD: Globoid Leukodystrophy, CD: Canavan Disease. MLN: Milan, IT: Italy, AMS: Amsterdam, NL: The Netherlands, BNN: Bonn, DE: Germany. Life tech.: Life Technologies. Underlined isogenic pairs are the origin lines.

Supplementary Table II: Primary Antibodies

Target	Host	Dilution	Company	Number
GABA	Rabbit	1:300	Sigma	A2052
GFAP	Mouse	1:1000	Millipore	MAB3402
MBP	Rat	1:300	Chemicon	MAB386
NF	Mouse	1:300	Sigma	N0142
Olig2	Rabbit	1:200	Abcam	ab136253
TUBB3	Mouse	1:1000	Biolegend	801202

Supplementary Table III: Secondary Antibodies

Target	Host	Dilution
Alexa 488	Goat anti-mouse IgG (Mol.Probes, A11001)	1:1000
	Goat anti-rabbit IgG (Mol.Probes, A11008)	1:1000
	Goat anti-rat IgG (Mol.Probes, A11006)	1:1000
Alexa 546	Goat anti-mouse IgG (Mol.Probes, A11003)	1:2000
	Goat anti-rabbit IgG (Mol.Probes, A11010)	1:2000
Alexa 647	Goat anti-rabbit IgG (Mol.Probes, A21246)	1:500

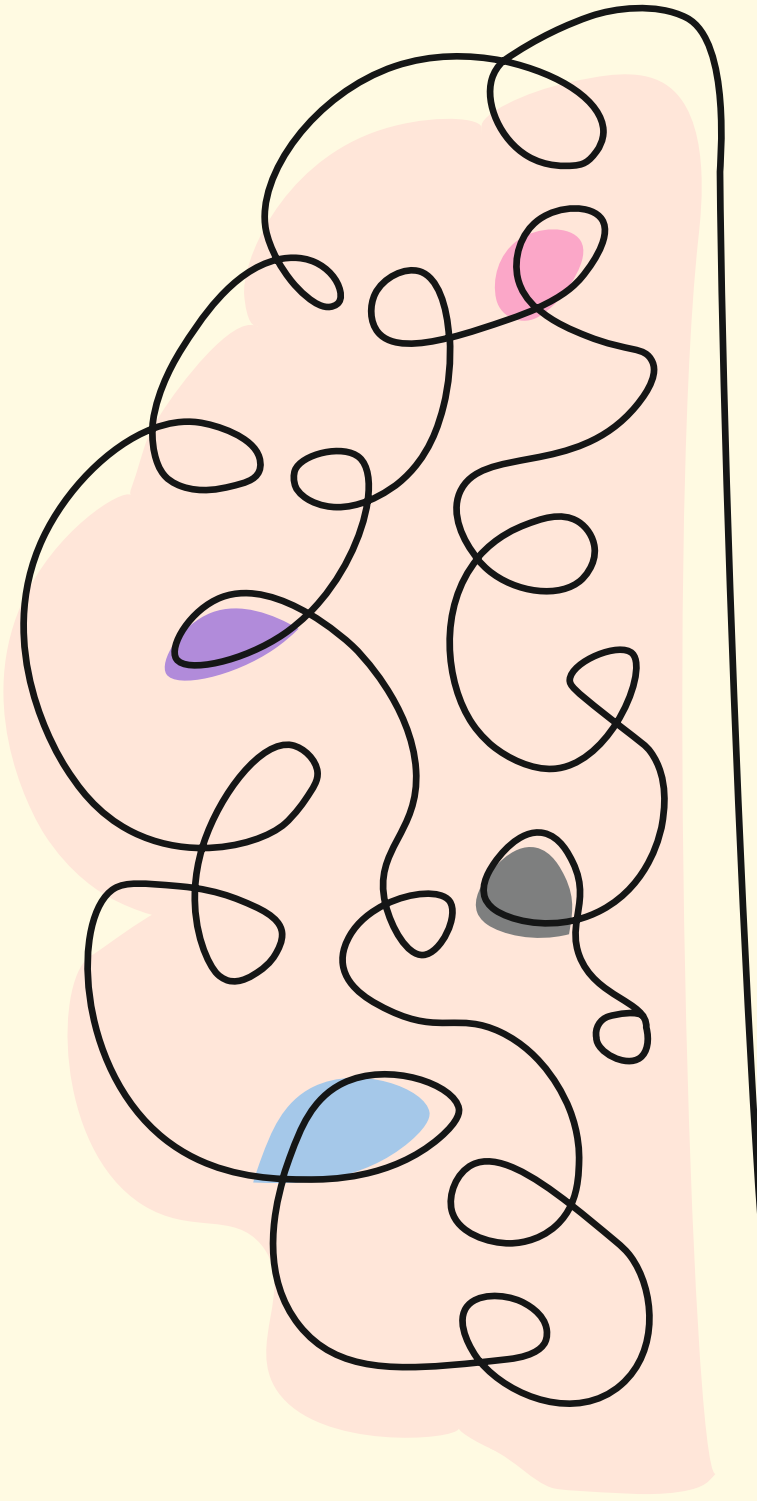

05

Human pluripotent stem cell-derived microglia shape neuronal morphology and enhance network activity in vitro

Liza M. L. Kok, Koen Helwegen, Nicki Coveña, Marc Engelen, Stephan Kemp, Vivi M. Heine

Adapted from: Journal of Neuroscience Methods, 2025, Volume 415, 110354

ABSTRACT

Microglia, the resident immune cells of the central nervous system, play a critical role in maintaining neuronal health, but are often overlooked in traditional neuron-focused *in vitro* models. In this study, we developed a novel co-culture system of human pluripotent stem cell (hPSC)-derived microglia and neurons to investigate how hPSC-derived microglia influence neuronal morphology and network activity. Using high-content morphological analysis and multi-electrode arrays (MEA), we demonstrate that these microglia successfully incorporate into neuronal networks and modulate key aspects of neuronal function. hPSC-derived microglia significantly reduced cellular debris and altered neuronal morphology by decreasing axonal and dendritic segments and reducing synapse density. Interestingly, despite the decrease in synapse density, neuronal network activity increased. In addition, we applied the model to investigate if hPSC-derived microglia from 4H and adrenoleukodystrophy modulate the neuronal networks differentially. We identified differences in axons between co-cultures with healthy and ALD microglia. Our findings underscore the importance of including hPSC-derived microglia in *in vitro* models to better simulate *in vivo* neuroglial interactions and provide a platform for investigating neuron-glia dynamics in health and disease.

Keywords

human *in vitro* modelling, microglia-neuron co-culture, multi-electrode arrays, hPSC

INTRODUCTION

Human pluripotent stem cell (hPSC) technologies have revolutionized neuroscience by enabling generation of human- and patient-specific neuronal cultures. This has facilitated the development of advanced disease models for neurodegenerative and neurodevelopmental disorders, including Alzheimer's disease (AD), Parkinson's disease (PD), and autism spectrum disorders. Initially, research primarily focused on neuron-only cultures, but more recent efforts have incorporated glial cell populations, such as astrocytes, oligodendrocytes and microglia in both 2D or 3D culture systems (Gordon & Geschwind, 2020; Kim et al., 2015; Slanzi et al., 2020). These glial cells are critical to brain development, homeostasis, and the maintenance of neuronal networks. Moreover, there is growing recognition of their roles in the pathology of neurodegeneration and neurodevelopmental diseases (Colonna & Butovsky, 2017; Molofsky et al., 2012).

Microglia, in particular, have garnered increasing attention due to their roles as key regulators of synaptic pruning, neuroinflammation, and debris clearance (Paolicelli & Ferretti, 2017). Dysregulation of microglial function has been implicated in the progression of several neurodegenerative conditions, including AD and PD (Leng & Edison, 2021; Poppell et al., 2023), but also in leukodystrophies. Particularly for adrenoleukodystrophy (ALD), there is a specific suspicion for microglia involvement since ALD is caused by mutations in ABCD1, a gene that is highly expressed in microglia. Additionally, the positive results of early hematopoietic stem cell transplantation (HSCT) point towards a role for microglia (Aubourg et al., 1990). Although leukodystrophies share common pathology, microglia involvement is not described in all leukodystrophies. For 4H leukodystrophy, which is caused by mutations in genes coding for subunits of RNA polymerase III, no association with impaired microglia is made yet. However, RNA polymerase III is utilized in all cell types, hence microglia might still play a role in disease pathology. The progressive nature of leukodystrophies and the lack of curative treatment options stress the need to elucidate the role of microglia in these diseases, hence the quest to include microglia in *in vitro* models of leukodystrophies (Bonkowsky et al., 2010; Bonkowsky et al., 2018; Vanderver et al., 2012).

Recent advancements in hPSC technology now allow derivation of microglia-like cells from hPSCs. However, co-culture systems that integrate microglia-like cells with human neurons to study their interactions and their impact on neuronal network development remain limited. The absence of such models restricts our understanding of how microglia influence neural circuit dynamics and contribute to both normal brain function and disease pathology.

In this study, we describe the development of a novel in vitro co-culture system that combines hPSC-derived microglia-like cells with cortical neurons. Utilizing high-content morphological analysis and multi-electrode arrays (MEAs), we assess the influence of microglia-like cells on neuronal morphology and network activity. Our results demonstrate that the presence of microglia-like cells in neuronal cultures reduces cellular debris, reduces synaptic density, and enhances neuronal network activity, suggesting that these hPSC-derived microglia-like cells actively shape the neuronal circuits *in vitro*. Additionally, we show that the morphology of microglia-like cells is influenced by the neuronal background, underscoring the bidirectional interactions between these cell types. We continued to use this model for the investigation of microglia-like cells from two leukodystrophies and identified that both ALD and 4H microglia-like cells in co-culture had no sign of intrinsic defects, as measured by numbers and roundness. However, co-cultures with ALD microglia-like cells did display changes in axon morphology. This co-culture model represents an important advancement towards the creation of more physiologically relevant *in vitro* systems to study both normal brain function and the role of microglia in neurodegenerative and neurodevelopmental diseases.

RESULTS

Microglia-like cells dynamically interact with cortical neurons *in vitro*

To develop a human-based *in vitro* assay suitable to study the modulating effects of microglia on neuronal network development, we created microglia-neuron co-cultures based on earlier established hPSC-derived microglia (Haenseler et al., 2017) and human cortical neuron (Dooves et al., 2023; Nadadhur et al., 2017) derivation protocols. Microglia-like cells were generated from a human GFP-expressing embryonic stem cell line (H09 GFP+) and added to 4 different hPSC-derived mixtures of glutamatergic and GABAergic cortical neuron cultures at week 6 of neuron maturation. To the control group microglia-like cells were not added, but this group did get the same media regime. The cultures were maintained for an additional 6 weeks, during which we assessed integration, survival, and interaction of microglia-like cells with neurons using immunofluorescence and multi-electrode assays (MEA) (Fig. 1A). We confirmed that microglia-like cells survived for the entire duration of the co-culture on both cellomics (Fig. 1B-E) and MEA plates (Supplementary Fig. 1A-H) across all neuronal backgrounds. In an independent experiment, we confirmed that the hPSC-derived microglia-like cells express Iba1 (Supplementary Fig. 2A-D). Additionally, using microglia-like cell mono-cultures we displayed that all of the plated cells went on to express TMEM119 as indicated by immunocytochemistry, displaying

that a pure pool of microglia-like cell precursors was plated in the co-cultures (Supplementary Fig. 2E). Also on RNA level, these cells show microglia-like expression of canonical microglia markers such as Iba1, P2RY12 and TMEM119 (Supplementary Fig. 2F)(Pettas et al., 2022). While all neuron cultures received the same microglia differentiation batch, the neuronal background had a significant influence on microglia quantities (Supplementary Table III, Fig. 1F). As *in vivo* microglia are highly dynamic and plastic cells that undergo morphology changes, particularly increased cell roundness is an important indicator of altered microglia function, we analyzed morphology (Paolicelli et al., 2022). Our analysis revealed that microglia-like cells in co-culture do not present roundness that is associated with microglia reactivity (mean roundness = 0.49, Fig. 1B-E). Though, neuronal background significantly influenced various aspects of their morphology, including roundness, size, length and width to length ratio (see Supplementary Table III, Fig. 1G-K), underscoring the dynamic interaction between the neurons and microglia-like cells. Additionally, microglia morphology significantly differed between timepoints (see Supplementary Table III, Fig 1G-K). Together, we showed the successful incorporation of hPSC-derived microglia-like cells and their interaction with human cortical neurons *in vitro*.

Microglia support neuronal maturation *in vitro*

In vivo microglia have important functions in brain development and maintaining brain homeostasis by functions such as clearing debris, pruning synapses and shaping neuronal circuits by phagocytosis of, amongst others, neural progenitors, neurons, axons and dendrites (Paolicelli & Ferretti, 2017; Riccomagno & Kolodkin, 2015). Therefore, we hypothesized that co-cultures with microglia-like cells have different morphological features compared to cultures without microglia. Specifically, we hypothesized that microglia co-cultures have decreased nuclear debris and alterations on neuron morphology that we aimed to address by investigating the number of mature neurons (NeuN+) and the number of dendrite and axonal protrusions. High content analysis was used to validate this hypothesis. Results were first tested separately and subsequently aggregated using Fisher's method to avoid multiple testing and improve power. We confirmed that the addition of microglia-like cells had a statistical significant effect on the combination of these parameters ($p < 0.0001$, Fisher's method, Supplementary Fig. 3A-D). Post hoc testing showed reduced nuclear debris (Fig. 2A-C, $p < 0.0001$), unchanged levels of mature neurons (Fig. 2D, $p = 0.609$) and reduced numbers of axonal and dendritic segments in the microglia co-cultures (Fig. 2E, $p = 0.044$ and Fig. 2F, $p = 0.0001$).

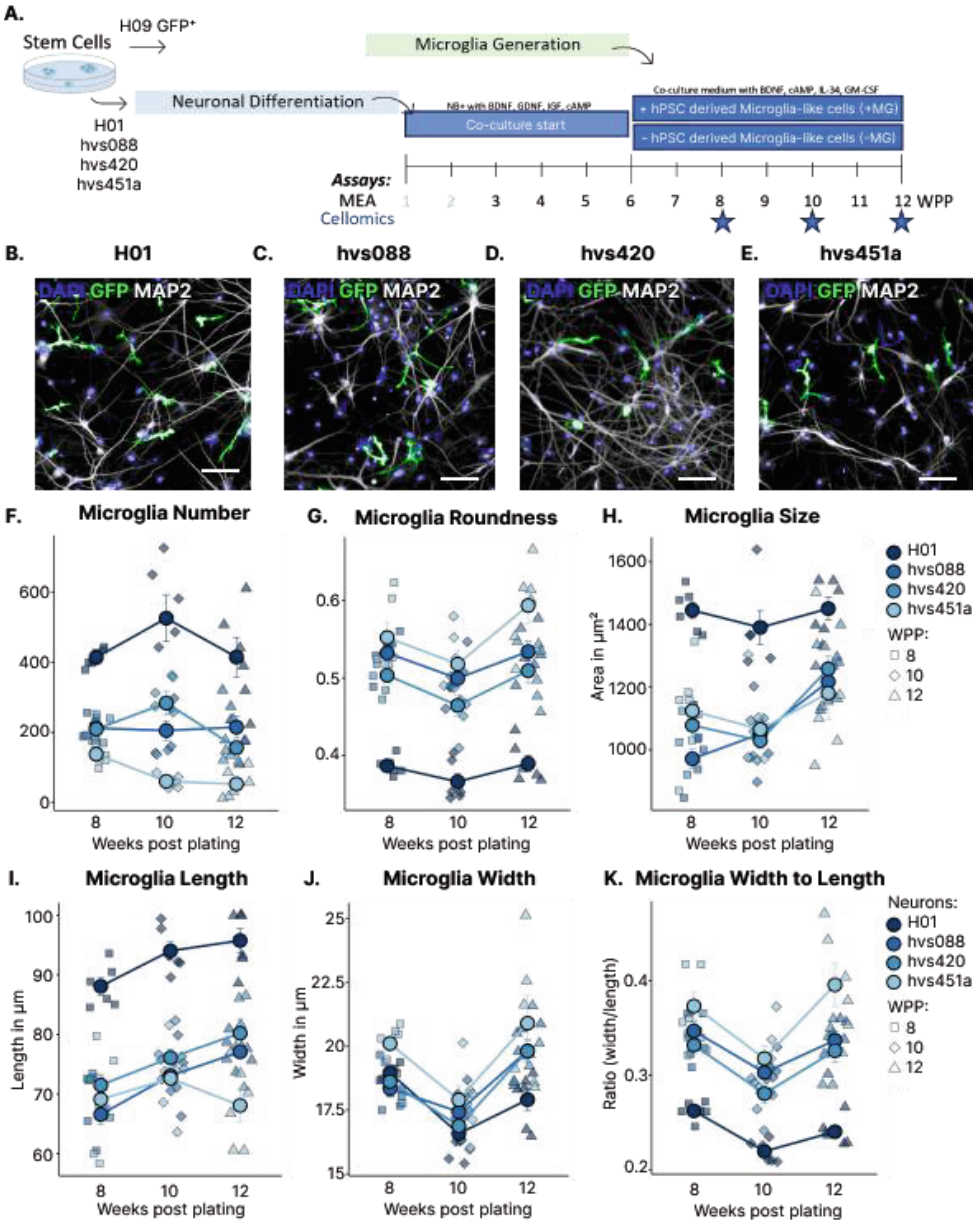

Figure 1: Long survival of human PSC-derived microglia-neuron co-cultures. A) Schematic representation of the experimental set-up. Stars indicating timepoints of cellomics immunofluorescent investigation. Representative immunofluorescent images of nuclei (DAPI, blue) neurons (MAP2, white) and microglia (GFP, green) at 12 weeks after plating of neurons H01 (B), hvs088 (C), hvs420 (D) and hvs451a (E). Quantification of microglia number (F), roundness (G), size (H), length (I), width (J) and ratio of width to length (K). Circles representing means for each neuron type for the three timepoints together. The observations for each timepoint are also represented by rectangle for timepoint 1, diamond for timepoint 2 and triangle for timepoint 3. For each timepoint N = 24 observations on 4 different neuronal backgrounds. WPP = weeks post plating (of neurons). Error bars represent the standard error of the mean. Scale bars 100 µm.

Since the reduced total axonal and dendritic segment numbers point towards altered neuronal morphology, we did additional post-hoc testing to determine if there are specific morphological changes. On the axonal level we showed that in cultures with microglia-like cells each neuron had on average less segments, that were longer, with less extremities and reduced nodes (Fig. 2G). Interestingly for dendrites we only observe the average length of the dendritic segments per neuron to be increased in the presence of microglia-like cells (Fig. 2H, $p = 0.027$, Bonferroni corrected $n = 8$), while per neuron the number of segments, extremities and nodes were not significantly altered. To study synaptic pruning, we measured and observed that both the absolute number of synapses (Mean -MG: 8140, Mean +MG: 6365, $p = 0.0002$) as well as the synapse density were significantly reduced ($p = 0.018$, Fig. 2I) in the presence of microglia-like cells. In conclusion, addition of hPSC-derived microglia-like cells significantly reduced nuclear debris and affects neuronal morphology.

Addition of microglia alters neuronal network activity

To investigate whether the addition of microglia-like cells affects different features of neuronal network activity as well, we analyzed in parallel to the morphological analysis, the same neuron and microglia batches on multi-electrode arrays (MEA) (Fig. 3A). During 6 weeks of microglia-neuron co-culturing, neuronal networks with microglia-like cells showed an increase in activity which was reflected by a significant increase in active electrodes (Figure 3B-C, $p = 0.007$). Additional post-hoc testing showed that changes in activity are caused by increased spike rate (Fig. 3D, $p = 0.0298$, Bonferroni corrected $n = 13$, Supplementary Table IV). The significant effects are observed independent of neuronal background (Supplementary Fig. 4A-H). Other parameters such as burst and network burst counts show a similar trend of increased activity in the presence of microglia-like cells, however, these do not hold after Bonferroni correction (Fig. 3E-F, Supplementary Table IV). We also observed a trend of increased spiking within bursts (Supplementary Fig. 5A) and network bursts (Supplementary Fig. 5B) when neurons were in co-culture with microglia-like cells. Additionally, the shape of bursts and network bursts as defined by duration (Supplementary Fig. 5C-D) and spike count (Supplementary Fig. 5E-F) might show a trend of increased duration and increased spike count. For frequency there only is a trend towards higher spike frequency in network bursts (Supplementary Fig. 5G-H, Supplementary Table IV). Together, we show a significant increase in activity as well as trends in other activity parameters that also point towards increased activity and higher synchronicity in cortical neuron networks when co-cultured with hPSC-derived microglia-like cells.

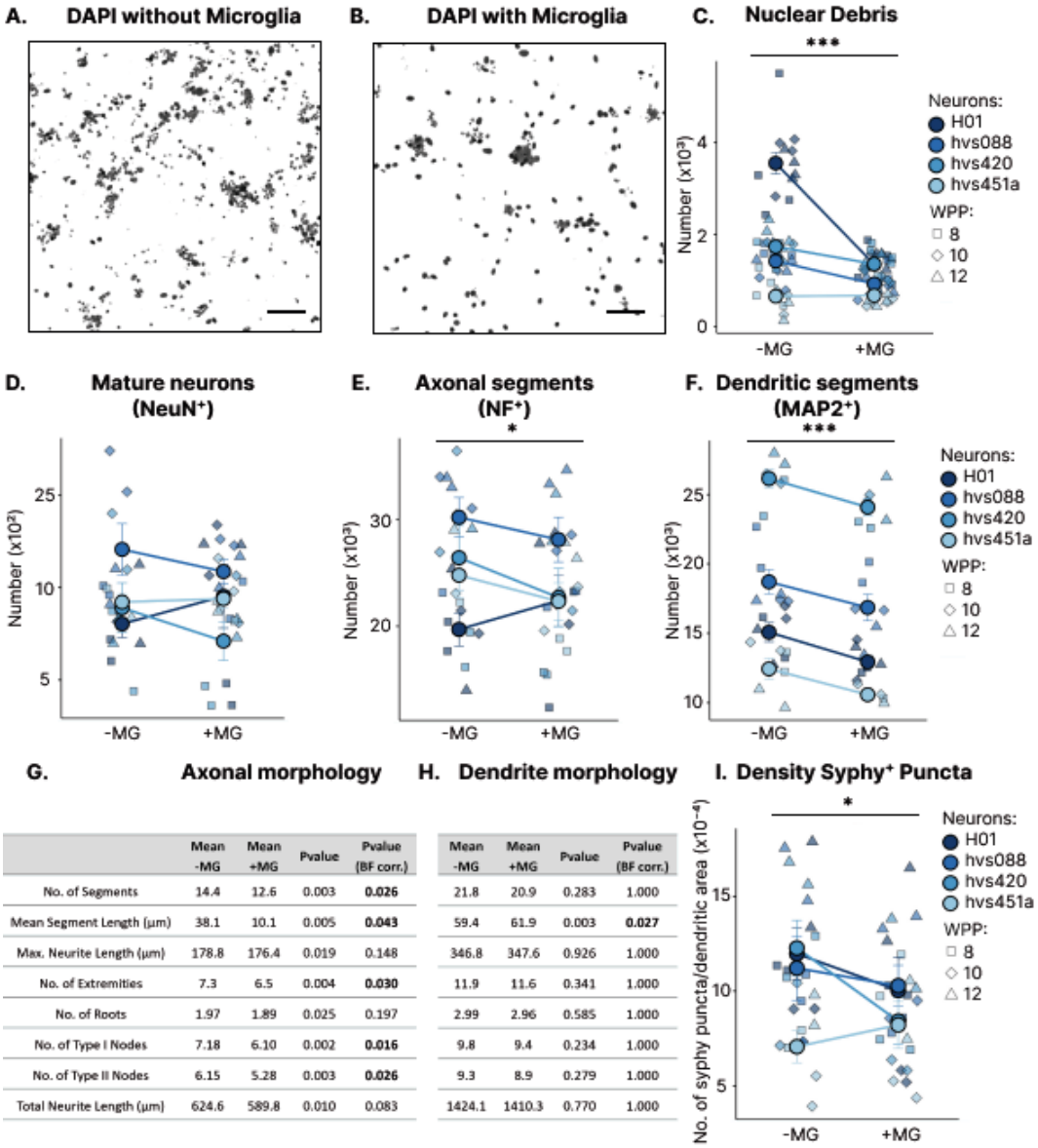

	Mean -MG	Mean +MG	Pvalue	Pvalue (BF corr.)	Mean -MG	Mean +MG	Pvalue	Pvalue (BF corr.)
No. of Segments	14.4	12.6	0.003	**0.026**	21.8	20.9	0.283	1.000
Mean Segment Length (µm)	38.1	10.1	0.005	**0.043**	59.4	61.9	0.003	**0.027**
Max. Neurite Length (µm)	178.8	176.4	0.019	0.148	346.8	347.6	0.926	1.000
No. of Extremities	7.3	6.5	0.004	**0.030**	11.9	11.6	0.341	1.000
No. of Roots	1.97	1.89	0.025	0.197	2.99	2.96	0.585	1.000
No. of Type I Nodes	7.18	6.10	0.002	**0.016**	9.8	9.4	0.234	1.000
No. of Type II Nodes	6.15	5.28	0.003	**0.026**	9.3	8.9	0.279	1.000
Total Neurite Length (µm)	624.6	589.8	0.010	0.083	1424.1	1410.3	0.770	1.000

Fig. 2. Microglia significantly affect morphological features of human cortical neurons in vitro. Illustrative image of nuclear debris as stained by DAPI (black) in co-cultures A) without or B) with microglia. Morphological features nuclear debris (C), mature NeuN positive neurons (D), Neurofilament+ axonal (E) and MAP2+ dendritic segments (F) were significantly affected ($p < 0.0001$, Fisher's method). A table containing further post-hoc testing results shows several axonal (G) and dendritic (H) morphology parameters, that were normalized to the amount of neurons, to be significantly different between cultures with and without microglia. I) Graph displaying reduced density of synaptophysin positive puncta. For each timepoint N = at least 8 observations on 4 neuronal backgrounds. For each measurement WPP = weeks post plating (of neurons). Error bars represent the standard error of the mean. Scale bar 100 µm. *P < 0.05,**P < 0.01, ***P < 0.001.

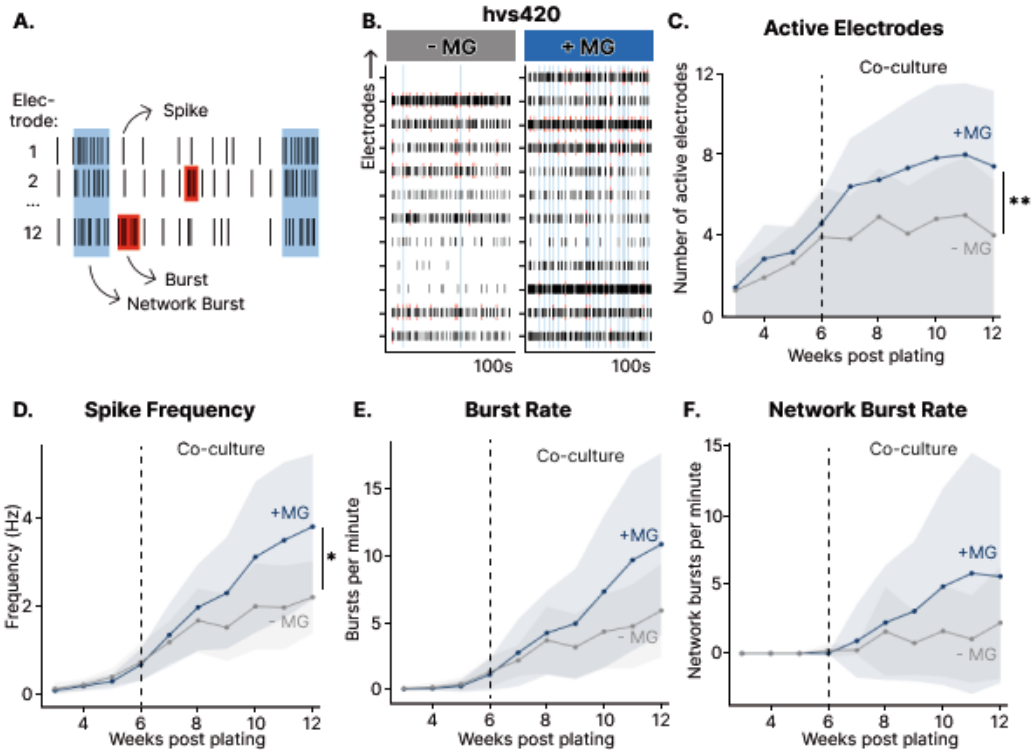

Figure 3: Microglia have significant effect on activity of neuronal co-cultures. A) Schematic representation of spike, burst and network burst events. B) Representative example of 100 s of baseline activity at 12 weeks post-plating of co-cultures without (-MG) and with (+MG). C) Quantification of the activity shows increased number of active channels (P = 0.010) and D) increased spike frequency (P = 0.030) in cultures with microglia. E) Burst Rate and F) Network Burst Rate show a similar but non-significant trend of increased activity. N = 12 MEA well observations on 4 neuronal backgrounds. WPP = weeks post plating (of neurons). Shaded error bars represent the standard deviation. *P < 0.05.

ALD microglia-like cells suitable for co-culture

Now that we established an *in vitro* model for hPSC-derived microglia co-culture, we wanted to explore whether this model can be applied in a disease relevant context. As mentioned before, in ALD a primary involvement of microglia in the cerebral demyelination phenotype is suspected. Hence, we generated microglia-like cells of 8 ALD cell lines, and 4 controls. We applied the same co-culture procedure as in the previous experiments (Fig. 1A) but instead of plating the neurons in separate wells, a mixture of all batches was equally divided over all wells.

Since microglia health is suspected to be influenced by the ALD mutations, we first confirmed the sustained presence of microglia-like cells of ALD throughout the experiment using immunofluorescence (Fig. 4A). After establishing the presence, we determined if there are indications for increased intrinsic stress in ALD microglia. We defined increased stress by decreased numbers and changes in morphology, specifically increased roundness. We did not find evidence for changed numbers or roundness in ALD microglia-like cells compared to control microglia-like cells (Supplementary Fig. 6A-B, $p = 0.909$, Fisher's method). Also, other morphological parameters were similar between ALD and control microglia-like cells (Supplementary Fig. 6C-F, Supplementary Table VI). Additional investigation about the reactive state of the cells using CD68+, showed no difference in reactivity between ALD and control microglia-like cells (Fig. 4A-B, T-test, $p = 0.616$). Together, we show that hPSC-derived microglia of ALD remain in co-culture and there is no evidence for increased death or reactivity caused by ALD.

Axons are differentially affected by ALD microglia-like cells

Now that we established that ALD microglia-like cells can be used in the co-culture model. We wanted to investigate the effect of the ALD-microglia like cells on the neurons. We hypothesized that ALD microglia-like cells might be hampered in their function compared to control microglia-like cells. To address this, we again investigated nuclear debris, neuron count and dendrite and axonal protrusions. The combination of these four parameters was indeed significantly different between co-cultures with control and ALD microglia-like cells (Fisher's method $p = 0.032$). Additional post-hoc testing shows that this alteration is caused by increased axonal segments ($p = 0.012$). To elaborate on the change in axonal segments, we did additional post-hoc analysis we only find a trend of reduced axon segment length in cultures with ALD microglia (Fig. 4G, uncorrected $p = 0.053$). Since previous experiments showed a large effect of microglia-like cells on dendrites and synapses, we investigated if ALD microglia-like cells affect synapse density differential to control cells, we did not find evidence for this (Fig. 4H and 4I). Lastly, we previously showed that microglia-like cells increase neuronal activity. Here, we determined that ALD microglia-like cells can alter neuronal activity in the same way as control microglia-like cells (Fig. 4J, $p = 0.897$). Combined, ALD microglia-like cells are largely affecting the neurons similar to control microglia-like cells. However, neuron axonal morphology measures are changed in presence of ALD microglia-like cells, suggesting a possible impairment in ALD microglia which requires further research.

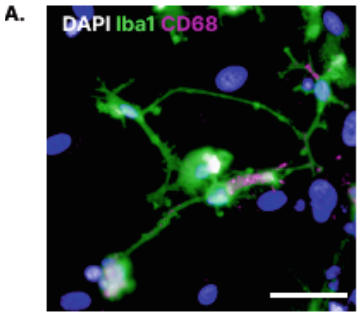

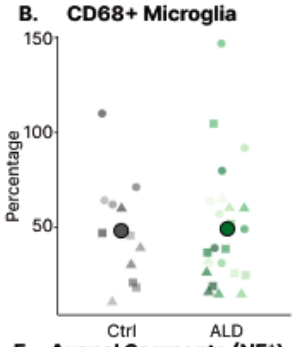

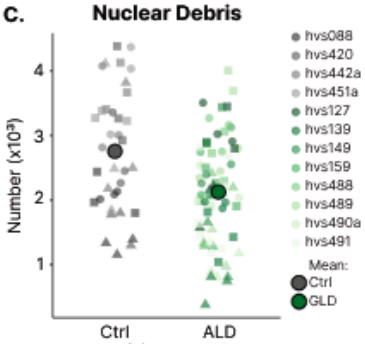

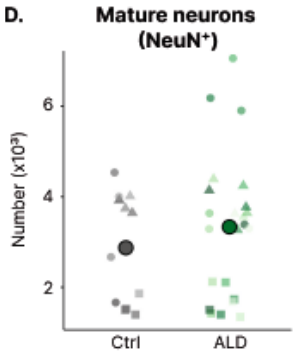

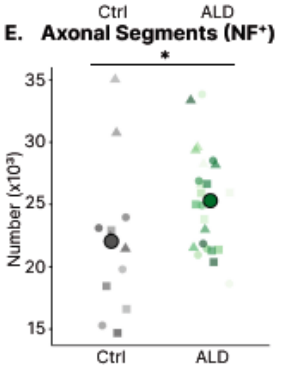

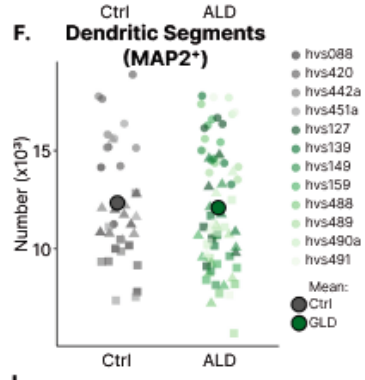

G. **Axonal morphology**

	Mean Ctrl	Mean ALD	Pvalue	Pvalue (BF corr.)
No. of Segments	9.92	10.36	0.830	1.000
Mean Segment Length	46.97	43.77	0.053	0.420
Max. Neurite Length	176.1	169.6	0.803	1.000
No. of Extremities	5.44	5.62	0.860	1.000
No. of Roots	1.87	1.87	0.990	1.000
No. of Type I Nodes	4.49	4.74	0.802	1.000
No. of Type II Nodes	3.98	4.19	0.442	1.000
Total Neurite Length	534.7	537.2	0.981	1.000

H. **Dendrite morphology**

Mean Ctrl	Mean ALD	Pvalue	Pvalue (BF corr.)
16.32	16.42	0.860	1.000
66.07	66.58	0.708	1.000
324.4	328.8	0.546	1.000
9.25	9.33	0.797	1.000
2.72	2.75	0.479	1.000
7.06	7.08	0.926	1.000
6.72	6.76	0.902	1.000
1192	1206	0.697	1.000

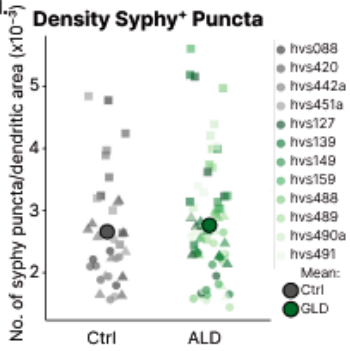

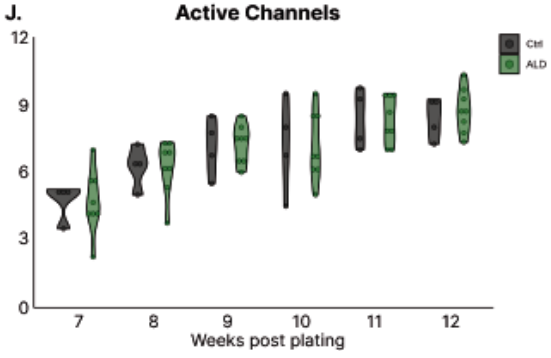

◀ Figure 4: Axonal segment number increased in presence of ALD microglia-like compared to control microglia-like cell co-cultures

(A) Immunofluorescent image of neuronal co-cultures showing nuclei (DAPI, blue), microglia (Iba1, green), and reactive microglia marker CD68 (magenta). (B) Quantification of CD68+ reactive microglia-like cells in ALD and control co-cultures. High-content analysis of nuclear debris (C), mature NeuN+ neurons (D), axonal (NF+) segments (E), and dendritic (MAP2+) segments (F) revealed significant differences in axonal segments between ALD and control co-cultures ($p = 0.032$, Fisher's method). (G, H) Detailed post-hoc analysis of axonal and dendritic morphology parameters. (I) Synaptic density (Synaptophysin+ puncta per dendritic area) comparison between ALD and control microglia-like cell co-cultures. Larger circles denote control (gray) and ALD (green) group means and smaller symbols indicating line observations per line on different time points (circles: 8 weeks post plating of neurons (WPP), triangles: 10 WPP, squares: 12 WPP). Statistical analysis was performed on line means across time points. (J) Comparison of mean active channels over time (7–12 WPP) in ALD (green) and control (gray) microglia-like cell co-cultures. Scale bar = 50 µm. *$P < 0.05$

4H microglia-like cells suitable for co-culture

In addition, we generated hPSC-derived microglia from five 4H patient lines (three with POLR3A and two with POLR3B mutations) and three control lines and co-cultured them on one neuron background that consisted of a mixture of 4 control lines in equal parts. Visualization of Iba1 positive cells shows that 4H microglia also remain present during the entire length of the co-culture. Similarly, to ALD microglia-like cells, there are no indications for increased intrinsic stress in 4H microglia-like cells as determined by their numbers and roundness (Fisher's method, $p = 0.570$, Supplementary Fig. 7A-7B), even though one of the 4H lines had few microglia-like cells in the co-cultures, their morphology was similar to the other lines (Supplementary Fig. 7A-F, Supplementary Table VII). We conclude that hPSC-derived microglia of 4H are suitable for co-culture and do not show signs of intrinsic impairment due to 4H.

4H microglia-like cells shape the neuronal circuit in a similar way as control microglia

Next, we wanted to investigate if the modulations made by 4H microglia-like cells are similar to the changes made by control cells. Again, we investigated nuclear debris, neuron numbers and the axonal and dendritic protrusions. We did not identify differences in cultures with control and 4H microglia-like cells (Fisher's method, $p = 0.836$). Since there were no changes found in co-culture morphology parameters we did not do any further post-hoc testing. Also the neuronal activity, measured by the amount of active channels, did not show any difference between co-cultures with control and 4H microglia-like cells (Fig. 5E, T-test, $p = 0.532$).

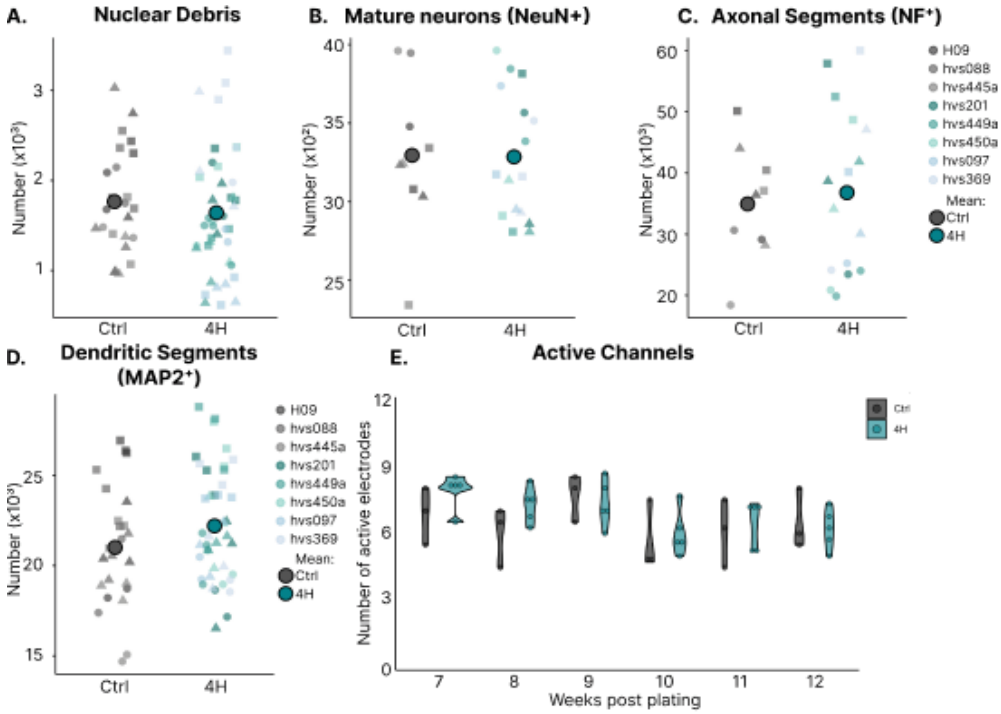

Figure 5: Co-cultures with 4H microglia-like cells do not show detectable differences compared to control microglia-like cell co-cultures A) Quantification of nuclear debris (A), mature NeuN positive neurons (B), axonal (C) and dendritic segments (D) was not significantly different between co-cultures with 4H and control microglia-like cells (p=0.836, Fisher's method). Larger circles denote control (gray) and 4H (blue) group means and smaller symbols indicating observations per line on different time points (circles: 8 weeks post plating of neurons (WPP), triangles: 10 WPP, squares: 12 WPP). E) Comparison of mean active channels over time (7–12 WPP) in 4H (blue) and control microglia-like cell (gray) co-cultures.

CONCLUSION / DISCUSSION:

In this study, we developed an *in vitro* co-culture model integrating hPSC-derived microglia-like cells and neurons, providing a more physiologically relevant system to investigate neuron-glia interactions. Our results show that the hPSC-derived microglia-like cells actively incorporate into the neuronal networks, influencing both neuronal morphology and network activity, which mirrors several known *in vivo* functions of microglia. Additionally, we did not observe differences in intrinsic microglia pathology as displayed by similar numbers and roundness between microglia-like cells of control and leukodystrophy iPSC-lines. However, we did identify show that ALD microglia-like cells had a different effect on axonal morphology compared to control microglia-like cells. This model offers a valuable tool for future studies to explore neuron-glia interactions in the context of neurodevelopmental and neurodegenerative disorders.

We demonstrated that hPSC-derived microglia-like cells reduce cellular debris and decreased density of synaptophysin positive puncta. These results align well with the established roles of microglia in brain development and homeostasis, including their key functions in debris clearance and synaptic pruning (Paolicelli & Ferretti, 2017). While these changes are consistent with microglial phagocytic behavior, further investigation is needed to determine whether they are driven by direct microglial engulfment or mediated by microglia secreted factors.

We demonstrated that neuronal morphology is altered in the presence of microglia-like cells. Given the well-documented interactions between microglia and neuronal structures (Nimmerjahn et al., 2005) and the secretion of neurotrophic and anti-inflammatory factors by microglia (Elkabes et al., 1996; Hanisch & Kettenmann, 2007) the identification of morphological changes aligned well with our expectations. Specifically, we observed a decrease in axonal and dendritic segments. Considering the secretion of neurotrophic factors by microglia, a decrease in axonal and dendritic segments seems contradicting. We hypothesize that the effects of microglial-secreted factors may have been masked, since both microglia-containing and microglia-free cultures were maintained in media supplemented with neurotrophic factors such as BDNF. Subsequently, the decrease in segments might be caused by phagocytosis or neurotoxins secreted by microglia-like cells that cleared nuclear debris (Bonkowsky et al., 2010; Giulian et al., 1994). More research is required to determine whether neurotrophic factor supplementation is necessary in these co-cultures and whether the microglia-like cells directly engulf axonal and dendritic structures or secrete neurotoxins.

The functional impact of microglia on neuronal networks was evident from the MEA experiments, which revealed significantly increased neuronal activity in the presence of microglia-like cells. Enhanced spike rates, alongside trends toward increased burst activity and network synchronicity, suggest that microglia influence not only individual neuronal behavior but also broader network dynamics. Interestingly, this increase in activity co-occurred with morphological changes, including a reduction in synaptophysin-positive puncta density—a proxy for synapse density. As synapses are the physical sites of action potential transmission between neurons, these findings may seem counterintuitive. However, less active synapses are more likely to be pruned (Schafer et al., 2012), suggesting that microglia may retain active synapses, thereby enhancing overall network activity.

Further research is required to confirm this hypothesis and to explore the mechanisms underlying these changes.

In the context of ALD, microglia-like cells appear to impair neuronal morphology, as indicated by changes in axonal segments. While ALD microglia-like cells themselves do not seem to exhibit increased stress, the alterations in axonal morphology raise intriguing questions about disease-specific microglial dysfunction. Interestingly, axonal abnormalities are a characteristic feature in ALD (Bergner et al., 2021). This study suggests that ALD microglia may contribute to the neuronal phenotype in ALD. However, further research is necessary as the observation of shorter axonal segments observed in ALD co-cultures could also reflect change in neuronal subtypes or subtype-specific vulnerabilities. Additionally, the engulfing of debris from healthy cells, potentially affects the disease presentation of microglia. It would be very interesting to make co-cultures with ALD neurons and/or ALD astrocytes. Nevertheless, we do show that this *in vitro* model can be used to identify microglia induced alterations to neuronal networks.

In conclusion, we have established an in vitro co-culture model that successfully incorporates hPSC-derived microglia with neuronal networks, offering a more physiologically relevant system for studying neuron-glia interactions. This model presents a promising platform for future research into the complex roles of microglia and their connections to both normal brain function and disease. By leveraging this system, researchers may deepen their understanding of the cellular mechanisms underlying neurodegenerative and neurodevelopmental diseases, potentially paving the way for novel therapeutic approaches.

MATERIALS & METHODS

hPSC culture

iPSC were generated from fibroblasts of healthy donors according to the previously described procedure (Holmes & Heine, 2017) or via CytoTune™-iPS 2.0 Sendai Reprogramming Kit according to manufacturer protocol. Pluripotency was confirmed by immunocytochemistry, alkaline phosphatase assay, PCR, embryoid body formation, pluritest and/or karyotyping. The human embryonic stem cell lines H01 and H09 GFP were obtained from WiCell. Pluripotent stem cells were maintained in TeSR™-E8™ (STEMCELL Technologies, 05990) on Vitronectin XF™ coated plates (STEMCELL Technologies, 07180). Media was replaced daily, or using double feedings over the weekend. Confluent wells were

split with a ratio of 1:10 - 1:50 into a new well for further maintenance. All subjects have given informed consent in accordance with the declaration of Helsinki. An overview of the used stem cell lines can be found in Supplementary Table I.

Neural differentiation

Human cortical neurons were generated using the previously published protocol (Nadadhur et al., 2017). In short, high-density human PSCs on Geltrex™ coated plates (±150 µg/ml, Gibco, A1413302) were induced into neurons by dual inhibition of the BMP and Activin/Nodal/TGF-β signaling pathways using 1 µM Dorsomorphin (Selleckchem, S7306) and 10 µM SB431542 (Selleckchem, S1067) in Neural Maintenance Medium (NMM) which consisted of 50% DMEM/F-12 with GlutaMAX™ (Gibco, 31331028), 50% Neurobasal™ medium (*Gibco, 21103-049)*, 0.5x N2 supplement (Gibco, 17502001), 0.5x B27 supplement (*Gibco, 17504-044)*, 2.5 µg/ml Insulin (Merck/Sigma-Aldrich, I9278), 1 mM L-Glutamine (Gibco, 25030081), 50 µM Minimum Essential Medium (MEM) Non-Essential Amino Acids (Gibco, 11140050), 50 µM Beta-Mercaptoethanol (Gibco, 21985023) and 1x P/S (Penicillin/Streptomycin, *Sigma, P0781*). Neural rosettes formed between 8 and 12 days after neural induction and were manually picked for transfer to PLO (20 µg/ml, Sigma-Aldrich, P3655)/ mouse laminin (20 µg/ml, Sigma-Aldrich, L2020) coated wells containing NMM supplemented with 20 ng/ml FGF2 (PeproTech, 100-18B) and 20 ng/ml EGF (PeproTech, AF-100-15). When confluent, neural rosettes were split 1:2 to 1:3 using TrypLE™ (Gibco, 12563-011) and defined trypsin inhibitor (DTI, Gibco, R007100) or frozen in KnockOut™ Serum Replacement (KSR, Gibco, 10828028) with 10% dimethyl sulfoxide (DMSO, Sigma-Aldrich, D2650).

Passage 1 – 3 of NES were used for differentiation into neurons using N2 medium, which consisted of DMEM/F-12 (without L-Glutamine, Gibco, 21331020), 1x N2 supplement, 0.1 mM MEM-NEAA, 2 mM L-Glutamine, 2 µg/ml Heparin (Sigma-Aldrich, H3393) and 1x P/S, supplemented with 400 ng/ml Human Sonic Hedgehog (Shh, PeproTech, 100-45) for 4 days. This was followed by 3 days of 10 µM Valproic acid (VPA, Sigma-Aldrich, P4543) in NB+ medium which consisted of Neurobasal™ medium (*Gibco, 21103-049)* with 1x B27 (*Gibco, 17504-044)*, 18 mM HEPES (*Gibco, 15630-056)*, 0.25x GlutaMAX™ (*Gibco, 35050-038)* and 1x P/S. On day 8, cells are passaged 1:2 – 1:4 (depending on density) using accutase and maintained in NB+ medium supplemented with 20 ng/ml BDNF (PeproTech, 450-02), 10 ng/ml GDNF (PeproTech, 450-10), 10 ng/ml IGF (PeproTech, 100-11) and 1 µM cyclic-AMP (Sigma-Aldrich, D0260) until day 18. At day 18 the cells were frozen in KSR with 10% DMSO.

Microglia differentiation

Human microglia-like cells were generated using an adapted version of a previously published protocol (Haenseler et al., 2017). First, hPSCs were detached in small fragments using 0.5 mM EDTA. EDTA was inactivated by dilution in PBS. hPSC fragments were resuspended in TeSR1 medium containing 1x P/S supplemented with 50 ng/ml Bone Morphogenetic Protein-4 (BMP4, PeproTech, 120-05ET), 50 ng/ml Vascular Endothelial Growth Factor (VEGF, PeproTech, 100-20), 20 ng/ml Stem cell factor (SCF, R&D systems, 255-SC), and 10 µM ROCK inhibitor Y-27632 (Selleckchem, S1049) and transferred to low attachment 6 well plates for the formation of embryoid bodies (EBs). The following three days, the medium was replaced daily using the same formulation but without supplementation of ROCK inhibitor. After, differentiation was started by plating 15-20 EBs onto 6 well plates in X-vivo 15 medium (Lonza, 02-060F) containing 1x P/S and supplemented with 100 ng/ml M-CSF + 25 ng/ml hIL3 + 1x GlutaMAX™ + 55 µM Beta-Mercaptoethanol, this is considered day 0 of differentiation. From this point on, the medium was replaced entirely weekly. Microglia-like cells were collected between day 55-70 by collecting the medium and passing it through a 40 µm cell strainer.

Microglia mono-culture

To address conversion into microglia-like cells they were plated on poly-l-ornithine and fibronectin-coated plates with Advanced DMEM/F-12 + N2 supplement, Glutamax, penicillin, streptomycin, and β-mercaptoethanol supplemented with IL-34 (100 ng/ml), GM-CSF (10 ng/ml), M-CSF (25 ng/ml) and TGFB-1 (50 ng/ml) and Rock-Inhibitor Y-27632. Media refreshments were performed every 6 days using the same media but excluding Rock-Inhibitor. For immunocytochemistry, cells were plated on glass coverslips at a density of 25k cells/cm^2 and PFA fixed after 14 days, immunostainings were performed according to the protocol described below. For RNA isolation microglia were plated at a density of 50k cells/cm^2 and collected in Trizol Reagent (Thermo Fisher Scientific) after 14 days. Total RNA was extracted according to manufacturer's protocol. cDNA synthesis was performed using SuperScript™ IV First-Strand Synthesis System (Invitrogen, 18091050) with 1 µg of RNA and random hexamer primers, according to the manufacturer's protocol. 1x Phire Reaction Buffer (Thermo Scientific, F524L) with dNTPs (0.2 mM) and Phire Hot Start II DNA polymerase (Thermo Scientific, F122L) and primers (0.5 µM, TMEM119 FW: ACTCT CTCTT CCAGC CCAGG, RV: CCAGG ACCAG TTCCT TGGCG TA, IBA1, FW: CCCTC CAAAC TGGAA GGCTT C, RV: CTTTA GCTCT AGGTG AGTCT TGG, P2RY12 FW: TCCAG GGTCA GATTA CAAGA GCAC, RV: ACTGT TGATT CTGGA GGGTT TGA) were combined and PCR reaction was started with 1

minute 98°C, followed by 30 cycles of 98°C for 5 seconds, 60°C for 15 seconds, 72°C for 15 seconds. After the cycles the PCR was and finalized with 30 seconds of 72°C. Products were loaded onto 1.5% agarose gel and ran for 40 minutes at 125V.

Neuron-microglia co-culture

Co-cultures were started by thawing and plating day 18 neurons and primary derived rat astrocytes onto PLO / mLam coated plates in NB+ medium supplemented with BDNF, GDNF, IGF, cAMP and 10 µM Y-27632. Rat astrocytes were obtained by papaïn dissociation of cortex of postnatal day 1 pups. To minimize contamination of other cells rat astrocytes were vigorously tapped before each medium change. Astrocytes of passage 3 were used for experiments. For multi-electrode array (MEA) cultures 120k neurons were plated together with 20k rat astrocytes on 24 well MEA plates (Multi Channel Systems, 24W300/30G-288). For cellomics purposes 12k neurons were plated together with 2k rat astrocytes on the CELLSTAR® 96 wp µClear®. For the ALD and 4H microglia-like cell co-cultures, a mixture of neurons from line hvs088, hvs420, hvs451a and H01 in equal parts was made. Half of the medium was replaced biweekly, with supplements for the entire volume, Rock-Inhibitor Y-27632 was only supplemented at plating.

Co-cultures were started at day 53 neurons, at the beginning of the 6th week. From this point the culture were divided in two groups; with and without microglia-like cells. The without microglia group received the same media changes as the with microglia-like cells group, but microglia-like cells were not plated. The microglia containing group got 3k microglia-like cells in each well of the 96wp and 30k in the 24w MEA plates. The plating medium was co-culture medium consisting of 50% Neurobasal™ and 50% DMEM/F-12 (Gibco, 21331020) with 1x N1 (Sigma-Aldrich, N6530), 1x B27 (without Vitamin A, Gibco, 12587001), 60 ng/ml T3 (Sigma-Aldrich, T6397), 100 ng/ml Biotin (Sigma-Aldrich, B4639), 1x GlutaMAX™ and 1x P/S supplemented with 20 ng/ml BDNF, 1 µM cyclic-AMP, 100 ng/ml IL-34 (PeproTech, 200-34) and 10 ng/ml GM-CSF (Gibco, PHC2015). At plating also 10 µM of Rock-Inhibitor Y-27632 was added to the medium. Half of the medium was replaced biweekly, with supplements for the entire volume.

MEA

Baseline activity of neuronal networks was measured according to a previously described procedure (Dooves et al., 2023). Briefly, activity was recorded for 10 minutes at a sampling rate of 10 kHz and at 37°C in controlled atmosphere (humidified air with 5% CO_2) using the

Multiwell-Screen Software (Multi Channel Systems). Raw data was filtered using high-pass 2nd order Butterworth filter with 100 Hz cut-off and low-pass 4th order Butterworth with 3500 Hz cut-off. Dysfunctional electrodes were excluded after visual inspection. Multiwell-Analyzer Setup Software (Multi Channel Systems) was used to derive activity measures such as active channels, spike rate, burst count and network burst count. Spike detection threshold was set at -5.0 standard deviations from baseline. Active electrodes were defined as 10 spikes per minute with a minimum amplitude of 20 µV. Bursts started when at least 4 consecutive spikes were each less than 50 milliseconds (ms) apart and bursts ended when a spike was more than 50 ms after the previous. New burst detection started 100 ms after the last burst. Network bursts were detected if 25% or more of the electrodes in one well had simultaneous bursts and if 50% or more of the electrodes were active during this time window.

Immunostaining

Cultures were fixed, after 2, 4 and 6 weeks of microglia-like cell addition, using 2% PFA in culture medium for 20 minutes followed by 4% PFA in PBS for 20 minutes. Fixed cells were washed with PBS followed by blocking with blocking buffer (PBS + 5% NGS + 0.3% Triton X-100 + 0.1% BSA) for 1 hour at room temperature. Primary antibodies, made up in blocking buffer, were incubated at 4°C overnight. After washing off excess of primary antibodies (See Supplementary Table II), secondary antibodies (Goat-anti-chicken/mouse/guinea pig/rabbit Alexa Fluor 568/647) were incubated for 2 hour at room temperature. Cells were washed again and nuclei were visualized using DAPI. High content screening was performed using the Cell Insight CX7 HCS platform (Thermo Fisher) in widefield mode with either a 10x or 20x objective with 25 images per well, an overview of number of analyzed images is displayed in Supplementary Table V.

Cellomics

Images were analyzed with Columbus analysis software (v2.5.2; PerkinElmer) by in-house developed scripts. From each well 25 images were acquired and quantified. Briefly, microglia numbers were determined by quantifying the GFP+ signal using the Find Image Region module. Identified regions that were excessively large (>5000 µm, probably caused by overlapping microglia), small (<400 µm), or on the border of the image were omitted. All remaining regions were considered microglia-like cells and their morphology properties were calculated using the Calculate Morphology Properties module, an average per well was obtained from the software. Nuclear debris were quantified by detecting all DAPI positive

areas bigger than 10 µm^2 using the Find Nuclei module. Any areas between 10 and 50 µm^2 with a roundness lower than <0.8 were considered to be nuclear debris. Mature neuron number was determined by determining how many nuclei (DAPI area > 50 µm^2) had a high intensity of NeuN. First, we excluded nuclei over 240 µm^2 in size, as neurons are known to have small nuclei. Next, the Select population module was used and for each timepoint intensity cut-offs for NeuN positivity were manually set by inspection of the settings on at least 5 pictures from different wells. Before proceeding, Select Population module on HuNu intensity was used to determine if neurons had indeed human origin. After this quality control, Find Neurites module with the build in CSIRO neurite analysis 2 was used to identify NF+ neurites. This analysis provides an overview of axonal morphological properties corrected for the amount of neurons present. Similarly, MAP2 positive nuclei were identified and the dendrite morphology obtained. Next, using the Select Region module the dendrites were investigated on containing synaptophysin positive puncta using the Find Spots module. Again, intensity parameters for detection of spots were manually set for each time point based on at least 5 pictures from different wells. The amount of synaptophysin positive puncta is corrected per unit of dendritic length.

Statistical analysis with vs without microglia-like cells

To determine whether microglia numbers and morphology were affected by neuronal background or changed over time, a two-way ANOVA using the cell line and timepoints as independent variables was performed. P-values were corrected for multiple testing using Bonferroni correction (n = 18).

Four proxy metrics were used to determine if the co-culture morphology is changed upon microglia addition: nuclear debris, mature neuron count (NeuN+) and number of axonal and dendritic segments. The conditions with and without microglia-like cells are compared per proxy metric. No directional hypothesis was specified and all comparisons were performed through two-sided tests. Tests were performed using a linear model including neuronal background and timepoint as covariates. A Shapiro-Wilk test for normality was performed on the residuals, and when normality was rejected ($p < 0.05$), a Mann-Whitney U test was performed instead. To assess whether there was an overall impact on neuronal cultures, while minimizing the number of multiple comparisons, p-values for each of the four proxy metrics were aggregated using Fisher's method. If Fisher's method was significant, post-hoc analysis was performed using the outcomes of the tests on the proxy metrics. Dendrite and axon morphology post-hoc analysis were performed using either Ordinary Least Square

regression or, when normality of the residuals was violated according to Shapiro-Wilk tests, Mann-Whitney U. P-values were corrected by applying Bonferroni correction for multiple comparisons (n = 8), both the p-value and adjusted p-values are reported. Similarly the effect of microglia addition on the functionality MEA measurements was determined, for this we compared parameters from with and without microglia at 12 weeks post plating. If the two-sided t-test on the amount of active electrodes showed a significant increase in activity, other parameters for activity were addressed with post-hoc analysis. These involved either Ordinary Least Square regression or, when normality of the residuals was violated according to Shapiro-Wilk tests, Mann-Whitney U. P-values were corrected by applying Bonferroni correction for multiple comparisons (n = 13), both the p-value and adjusted p-values are reported (Supplementary Table IV).

Statistical analysis control vs leukodystrophy microglia-like cells

Data sets comparing control vs. leukodystrophy microglia-like cell conditions, were all normally distributed, as determined by Shapiro-Wilk test. Sample size was either 4 cultures containing microglia-like cells from control lines against 8 from ALD lines, or 3 control lines against 5 of 4H leukodystrophy. Intrinsic microglia stress in ALD and 4H was determined by comparing numbers and roundness of microglia-like cells to controls. Two-sided T-Test were performed, and Fisher's method was used to aggregate the intrinsic stress proxy metrics. Remaining microglia morphology measures and CD68+ percentage (for ALD) were compared by comparing the line averages, across all timepoints, of the controls to the leukodystrophy lines with T-Test using GraphPad Prism (v.10.2.0). To determine if the co-culture morphology is changed upon microglia addition the four proxy measures: nuclear debris, mature neuron count (NeuN+) and number of axonal and dendritic segments were again used. Per line, one average from all timepoints, was created and two-sided T-Tests were used to compare control vs. leukodystrophy. Fisher's method was again used to aggregate the proxy measures. If Fisher's method was significant, post-hoc analysis was performed using the outcomes of the tests on the proxy metrics. Dendrite and axon morphology post-hoc analysis were performed using T-Test. P-values were corrected by applying Bonferroni correction for multiple comparisons (n = 8), both the p-value and adjusted p-values are reported. Active channels for control vs leukodystrophy microglia-like cell conditions were compared using the average of active channels across 7 to 12 weeks post plating, difference between Ctrl and ALD or Ctrl and 4H were addressed with T-Test, after checking for normality using Shapiro-Wilk test. No differences were found hence, no post-hoc testing was performed. In general, any significant parameters can be found in the

main figures, accompanied by the means of the compared groups. For non-significant parameters, supplementary Tables provide information on the P-values.

Data availability

Code used for statistical analysis is available on Github. Data is available upon request.
https://github.com/koenhelwegen/hpsc-microglia-neuron-co-culture

FUNDING

This work was supported by the European Joint Programme on Rare Diseases (EJPRD19-201, NG4LEUKO)

COMPETING INTERESTS

The authors declare no competing or financial interests

AUTHOR CONTRIBUTIONS

V.H. and L.K. designed the study. V.H. acquired the funding. L.K. performed the experiments, L.K. and N.C. developed the methodology. LK wrote the original draft in consultation with V.H., N.C. and K.H. Formal analysis was performed by K.H.

DECLARATION OF GENERATIVE AI AND AI-ASSISTED TECHNOLOGIES IN THE WRITING PROCESS.

During the preparation of this work the author(s) used ChatGPT in order to improve readability and language. After using this tool/service, the author(s) reviewed and edited the content as needed and take(s) full responsibility for the content of the published article.

REFERENCES

Aubourg, P., Blanche, S., Jambaque, I., Rocchiccioli, F., Kalifa, G., Naud-Saudreau, C., Rolland, M. O., Debre, M., Chaussain, J. L., Griscelli, C., & et al. (1990). Reversal of early neurologic and neuroradiologic manifestations of X-linked adrenoleukodystrophy by bone marrow transplantation. *N Engl J Med*, *322*(26), 1860-1866. https://doi.org/10.1056/NEJM199006283222607

Bergner, C. G., Genc, N., Hametner, S., Franz, J., van der Meer, F., Mitkovski, M., Weber, M. S., Stoltenburg-Didinger, G., Kuhl, J. S., Kohler, W., Bruck, W., Gartner, J., & Stadelmann, C. (2021). Concurrent axon and myelin destruction differentiates X-linked adrenoleukodystrophy from multiple sclerosis. *Glia*, *69*(10), 2362-2377. https://doi.org/10.1002/glia.24042

Bonkowsky, J. L., Nelson, C., Kingston, J. L., Filloux, F. M., Mundorff, M. B., & Srivastava, R. (2010). The burden of inherited leukodystrophies in children. *Neurology*, *75*(8), 718-725. https://doi.org/10.1212/WNL.0b013e3181eee46b

Bonkowsky, J. L., Wilkes, J., Bardsley, T., Urbik, V. M., & Stoddard, G. (2018). Association of Diagnosis of Leukodystrophy With Race and Ethnicity Among Pediatric and Adolescent Patients. *JAMA Netw Open*, *1*(7), e185031. https://doi.org/10.1001/jamanetworkopen.2018.5031

Colonna, M., & Butovsky, O. (2017). Microglia Function in the Central Nervous System During Health and Neurodegeneration. *Annu Rev Immunol*, *35*, 441-468. https://doi.org/10.1146/annurev-immunol-051116-052358

Dooves, S., Kok, L. M. L., Holmes, D. B., Breeuwsma, N., Breur, M., Bugiani, M., Wolf, N. I., & Heine, V. M. (2023). Cortical interneuron development is affected in 4H leukodystrophy. *Brain*, *146*(7), 2846-2860. https://doi.org/10.1093/brain/awad017

Elkabes, S., DiCicco-Bloom, E. M., & Black, I. B. (1996). Brain microglia/macrophages express neurotrophins that selectively regulate microglial proliferation and function. *J Neurosci*, *16*(8), 2508-2521. https://doi.org/10.1523/JNEUROSCI.16-08-02508.1996

Giulian, D., Li, J., Leara, B., & Keenen, C. (1994). Phagocytic microglia release cytokines and cytotoxins that regulate the survival of astrocytes and neurons in culture. *Neurochem Int*, *25*(3), 227-233. https://doi.org/10.1016/0197-0186(94)90066-3

Gordon, A., & Geschwind, D. H. (2020). Human in vitro models for understanding mechanisms of autism spectrum disorder. *Mol Autism*, *11*(1), 26. https://doi.org/10.1186/s13229-020-00332-7

Haenseler, W., Sansom, S. N., Buchrieser, J., Newey, S. E., Moore, C. S., Nicholls, F. J., Chintawar, S., Schnell, C., Antel, J. P., Allen, N. D., Cader, M. Z., Wade-Martins, R., James, W. S., & Cowley, S. A. (2017). A Highly Efficient Human Pluripotent Stem Cell Microglia Model Displays a Neuronal-Co-culture-Specific Expression Profile and Inflammatory Response. *Stem Cell Reports*, *8*(6), 1727-1742. https://doi.org/10.1016/j.stemcr.2017.05.017

Hanisch, U. K., & Kettenmann, H. (2007). Microglia: active sensor and versatile effector cells in the normal and pathologic brain. *Nat Neurosci*, *10*(11), 1387-1394. https://doi.org/10.1038/nn1997

Holmes, D. B., & Heine, V. M. (2017). Simplified 3D protocol capable of generating early cortical neuroepithelium. *Biol Open*, *6*(3), 402-406. https://doi.org/10.1242/bio.021725

Kim, Y. H., Choi, S. H., D'Avanzo, C., Hebisch, M., Sliwinski, C., Bylykbashi, E., Washicosky, K. J., Klee, J. B., Brustle, O., Tanzi, R. E., & Kim, D. Y. (2015). A 3D human neural cell culture system for modeling Alzheimer's disease. *Nat Protoc*, *10*(7), 985-1006. https://doi.org/10.1038/nprot.2015.065

Leng, F., & Edison, P. (2021). Neuroinflammation and microglial activation in Alzheimer disease: where do we go from here? *Nat Rev Neurol*, *17*(3), 157-172. https://doi.org/10.1038/s41582-020-00435-y

Molofsky, A. V., Krencik, R., Ullian, E. M., Tsai, H. H., Deneen, B., Richardson, W. D., Barres, B. A., & Rowitch, D. H. (2012). Astrocytes and disease: a neurodevelopmental perspective. *Genes Dev*, *26*(9), 891-907. https://doi.org/10.1101/gad.188326.112

Nadadhur, A. G., Emperador Melero, J., Meijer, M., Schut, D., Jacobs, G., Li, K. W., Hjorth, J. J. J., Meredith, R. M., Toonen, R. F., Van Kesteren, R. E., Smit, A. B., Verhage, M., & Heine, V. M. (2017). Multi-level characterization of balanced inhibitory-excitatory cortical neuron network derived from human pluripotent stem cells. *PLoS One*, *12*(6), e0178533. https://doi.org/10.1371/journal.pone.0178533

Nimmerjahn, A., Kirchhoff, F., & Helmchen, F. (2005). Resting microglial cells are highly dynamic surveillants of brain parenchyma in vivo. *Science*, *308*(5726), 1314-1318. https://doi.org/10.1126/science.1110647

Paolicelli, R. C., & Ferretti, M. T. (2017). Function and Dysfunction of Microglia during Brain Development: Consequences for Synapses and Neural Circuits. *Front Synaptic Neurosci*, *9*, 9. https://doi.org/10.3389/fnsyn.2017.00009

Paolicelli, R. C., Sierra, A., Stevens, B., Tremblay, M. E., Aguzzi, A., Ajami, B., Amit, I., Audinat, E., Bechmann, I., Bennett, M., Bennett, F., Bessis, A., Biber, K., Bilbo, S., Blurton-Jones, M., Boddeke, E., Brites, D., Brone, B., Brown, G. C., . . . Wyss-Coray, T. (2022). Microglia states and nomenclature: A field at its crossroads. *Neuron*, *110*(21), 3458-3483. https://doi.org/10.1016/j.neuron.2022.10.020

Pettas, S., Karagianni, K., Kanata, E., Chatziefstathiou, A., Christoudia, N., Xanthopoulos, K., Sklaviadis, T., & Dafou, D. (2022). Profiling Microglia through Single-Cell RNA Sequencing over the Course of Development, Aging, and Disease. *Cells*, *11*(15). https://doi.org/10.3390/cells11152383

Poppell, M., Hammel, G., & Ren, Y. (2023). Immune Regulatory Functions of Macrophages and Microglia in Central Nervous System Diseases. *Int J Mol Sci*, *24*(6). https://doi.org/10.3390/ijms24065925

Riccomagno, M. M., & Kolodkin, A. L. (2015). Sculpting neural circuits by axon and dendrite pruning. *Annu Rev Cell Dev Biol*, *31*, 779-805. https://doi.org/10.1146/annurev-cellbio-100913-013038

Schafer, D. P., Lehrman, E. K., Kautzman, A. G., Koyama, R., Mardinly, A. R., Yamasaki, R., Ransohoff, R. M., Greenberg, M. E., Barres, B. A., & Stevens, B. (2012). Microglia sculpt postnatal neural circuits in an activity and complement-dependent manner. *Neuron*, *74*(4), 691-705. https://doi.org/10.1016/j.neuron.2012.03.026

Slanzi, A., Iannoto, G., Rossi, B., Zenaro, E., & Constantin, G. (2020). In vitro Models of Neurodegenerative Diseases. *Front Cell Dev Biol*, *8*, 328. https://doi.org/10.3389/fcell.2020.00328

Vanderver, A., Hussey, H., Schmidt, J. L., Pastor, W., & Hoffman, H. J. (2012). Relative incidence of inherited white matter disorders in childhood to acquired pediatric demyelinating disorders. *Semin Pediatr Neurol*, *19*(4), 219-223. https://doi.org/10.1016/j.spen.2012.10.001

SUPPLEMENTAL FIGURES

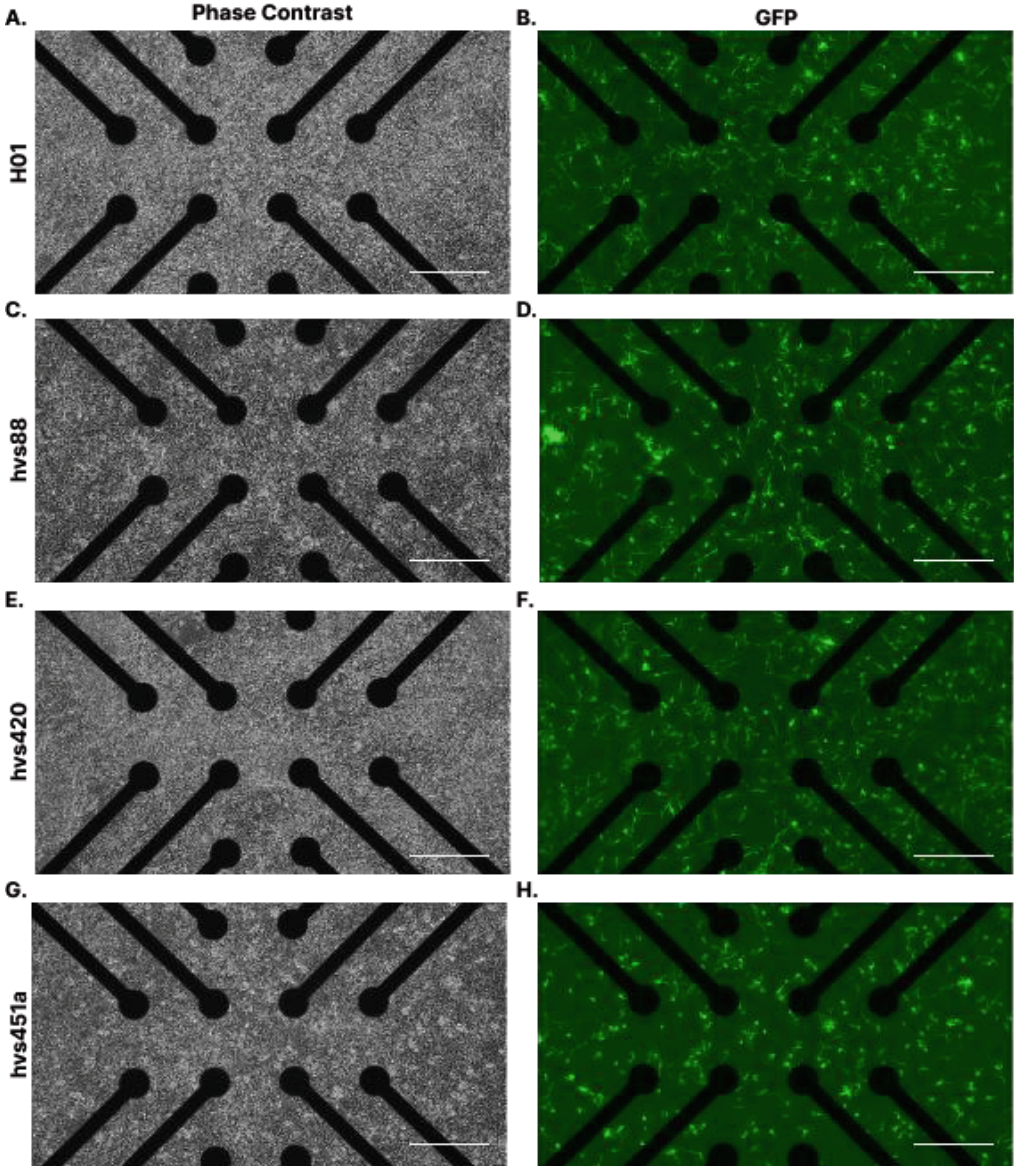

Supplementary Figure 1: Microglia present at week 12 on MEA across all neuronal backgrounds

Representative phase contrast and GFP microscopy images at week 12 of the experiment shows confluent co-culture (A, C, E, G) with GFP+ hPSC-derived microglia (B, D, F, H). Scale bars 300 µm.

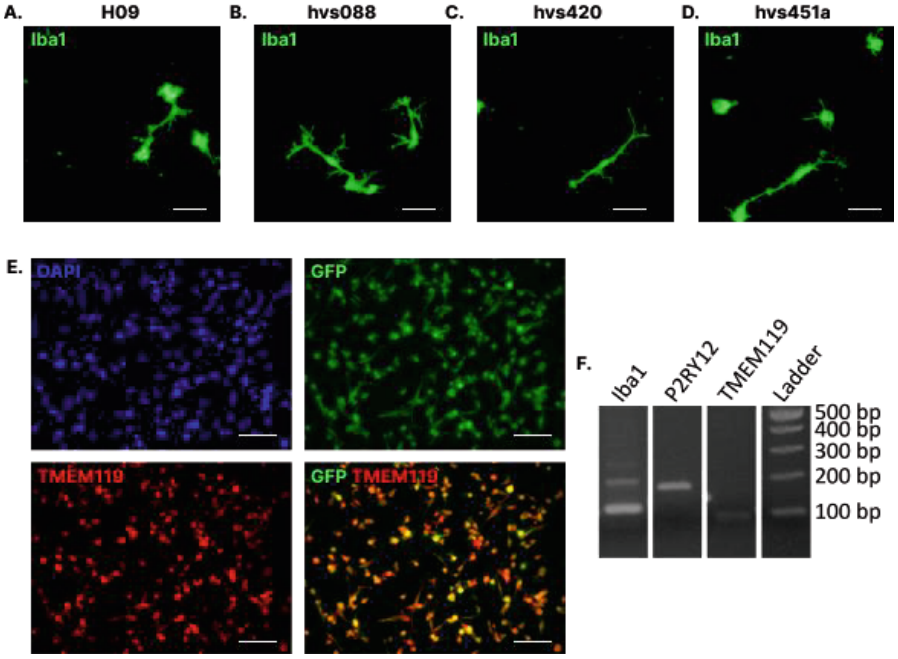

Supplementary Figure 2: Independent experiments show that hPSC-derived cells are microglia-like

A-D) Microglia-like cells from different hPSC lines are all Iba1+ at week 10 of experiment. Scale bars 50 µm. E) In mono-culture all microglia-like cells from line GFP+ H09 (green) went on to express TMEM119 (red). Nuclei are stained using DAPI (blue). Scale bars 100 µm. F) Microglia-like cells in mono-culture also went on to express microglia markers Iba1, P2RY12, and TMEM119 on RNA level.

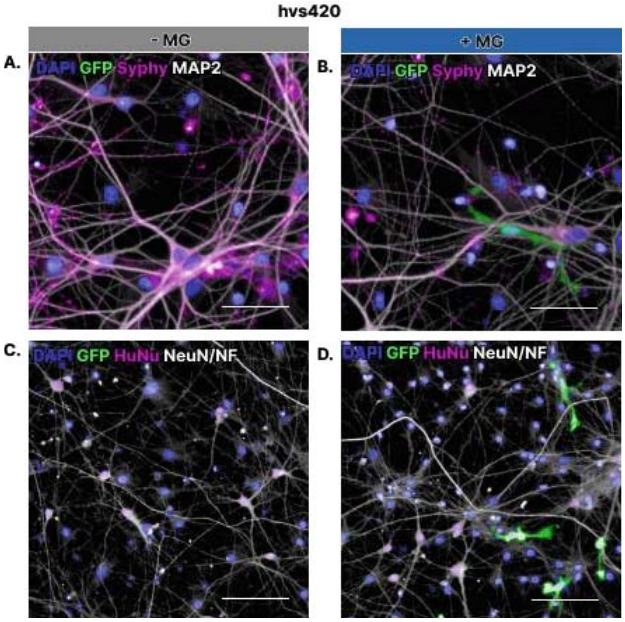

Supplementary Figure 3: Representative images used for high-content analysis

Scale bars A&B 50 µm, C&D 100 µm.

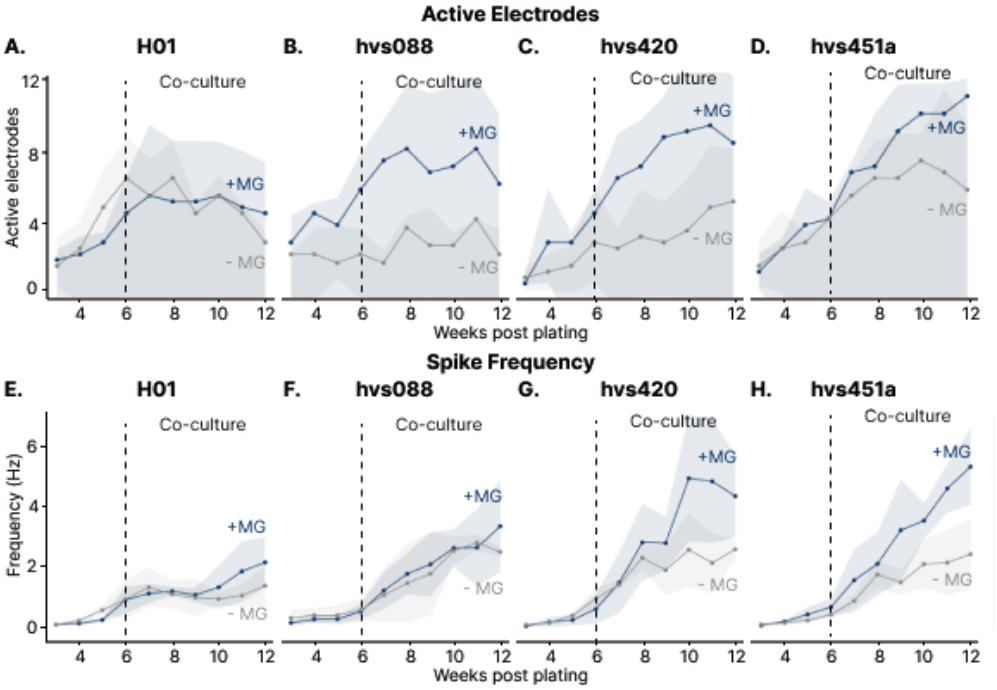

Supplementary Figure 4: Significant MEA parameters displayed for each neuronal background

A-D) Active electrode and E-H) Spike Frequency parameter are increased upon microglia addition in all neuronal backgrounds with some line specific changes in the size of the effect. Shaded error bars represent the standard deviation.

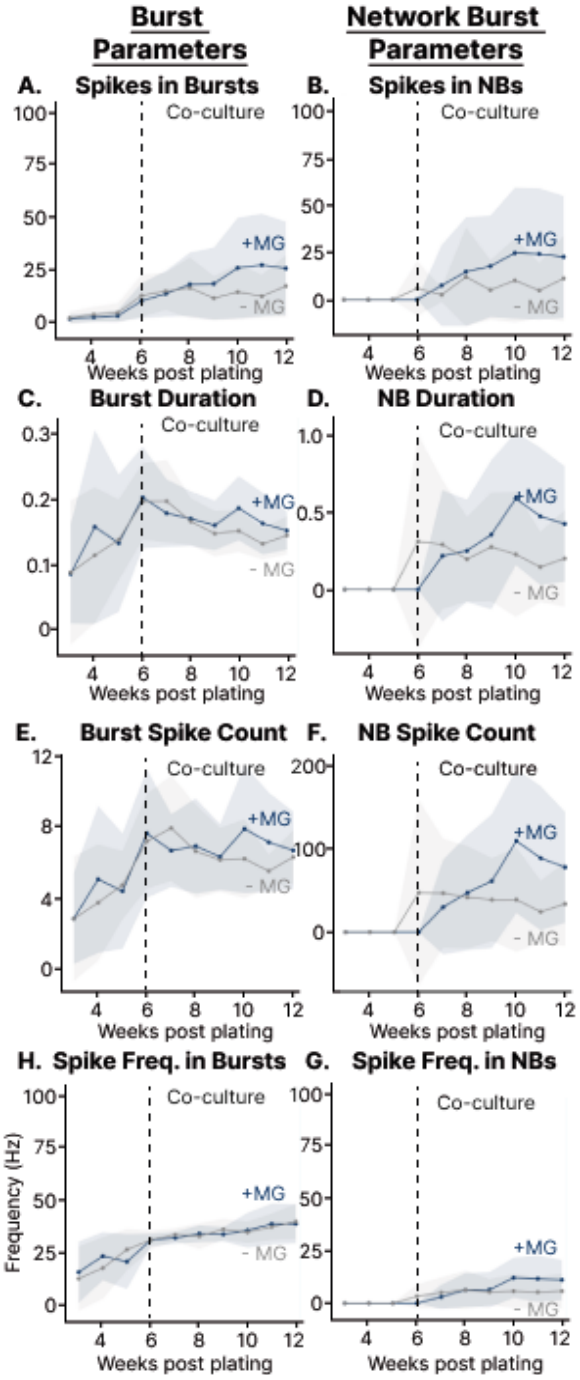

Supplementary Figure 5: Other investigated MEA parameters show similar trend in increased activity upon microglia addition.

Freq. = frequence. NB = network burst. MG = microglia.

Shaded error bars represent the standard deviation.

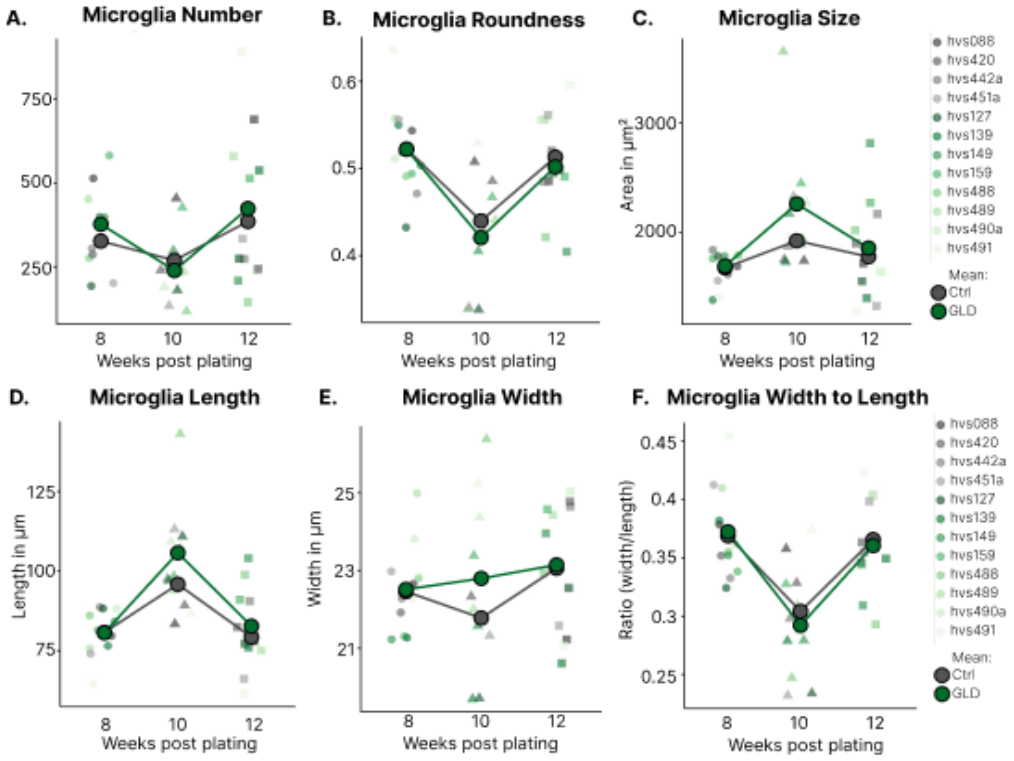

Supplemental Figure 6: Morphology of microglia-like cells in ALD co-culture Experiments

Quantification of microglia-like cell number (A), roundness (B), size (C), length (D), width (E) and ratio of width to length (F) in the ALD co-culture experiments. Larger circles denote control (gray) and GLD (green) group means and smaller symbols indicating observations per line on different time points (circles: 8 weeks post plating of neurons (WPP), triangles: 10 WPP, squares: 12 WPP).

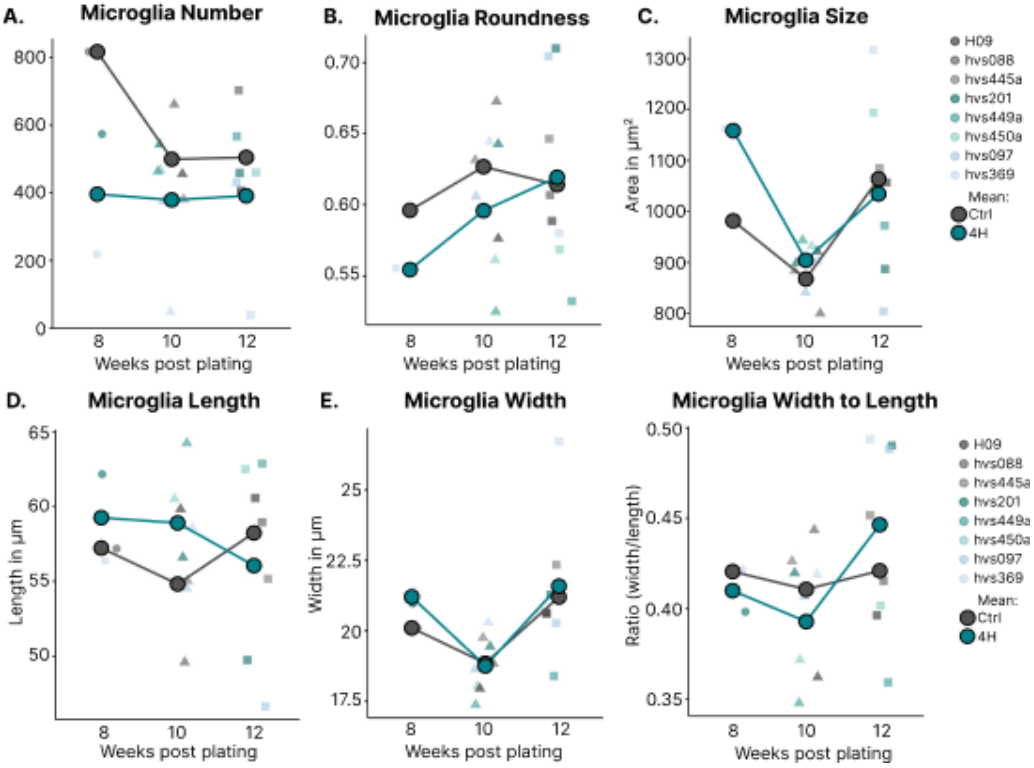

Supplemental Figure 7: Morphology of microglia-like cells in 4H co-culture experiments

Quantification of microglia-like cell number (A), roundness (B), size (C), length (D), width (E) and ratio of width to length (F) in the 4H co-culture experiments. Larger circles denote control (gray) and 4H (blue) group means and smaller symbols indicating observations per line on different time points (circles: 8 weeks post plating of neurons (WPP), triangles: 10 WPP, squares: 12 WPP).

SUPPLEMENTAL TABLES

Supplementary Table I: Overview of stem cell lines

Line ID	hPSCreg ID	Repr. method	Biobank donor	Disease status	Genotype	Protein	Donor sex, age
hVS88	VUi031-A	Lenti	n.a	Control	n.a.	n.a.	M, 0y
hVS420	VUi036A	Lenti	GM23964	Control	n.a.	n.a.	M, 21y
hVS442a		Sendai	GM23970	Control	n.a.	n.a.	M, 50y
hVS444a	VUi038-A	Sendai	GM01651	Control	n.a.	n.a.	F, 13y
hVS445a	VUi033-A	Sendai	GM02036	Control	n.a.	n.a.	F, 11y
hVS451a	VUi032-A	Sendai	GM23973	Control	n.a.	n.a.	M, 19y
H01	WAe001-A	n.a.	n.a	Control	n.a.	n.a.	M, Embryo
H09	WAe009-A	n.a.	n.a	Control	n.a.	n.a.	F, Embryo
H09 GFP						n.a.	
hVS93	VUi025-A	Lenti	n.a	4H	POLR3B c.2180T>C & c.1788C>A	p.Leu727Ser p.Tyr596*	F, 10y
hVS97	VUi026-A	Lenti	n.a	4H	POLR3B c.1568T>A & c.2084-6A>G	p.Val523Glu ?	M, 2y
hVS201	VUi027-A	Lenti	n.a	4H	POLR3A, c.169G>A & c.2098A>T	p.Asp57Asn p.Ile700Phe	F, 12y
hVS369	VUi028-A	Lenti	n.a	4H	POLR3B, c.303+1G>A & c.1568T>A	? p.Val523Glu	F, 4/5y
hVS449a	VUi029-A	Sendai	n.a	4H	POLR3A, c.1771-6C>G & c.3205C>T	? p.Arg1069Trp	M, 24y
hVS450a	VUi030-A	Sendai	n.a	4H	POLR3A, c.1771-7C>G & c.1048+5G>T	? ?	F, 2y
hVS149		Lenti	n.a	ALD, AMN	ABCD1, c.446G>A	p.Ser149Asn	M, 4y
hVS489		Sendai	n.a	ALD, AMN	ABCD1, c.1A>G	p.Met1Val	M, 56y
hVS490		Sendai	n.a	ALD, AMN	ABCD1, c.1A>G	p.Met1Val	M, 61y
hVS491		Sendai	n.a	ALD, AMN	ABCD1, c.1166G>A	p.Arg389His	M, 23y
hVS127		Lenti	n.a	ALD, cALD	ABCD1, c.1390C>T	p.Arg464Ter	M, 17y
hVS139		Lenti	n.a	ALD, cALD	ABCD1, c.1866-10G>A	p.Pro623fs*?	M, 2y
hVS159		Lenti	n.a	ALD, cALD	ABCD1, c.346G>A	p.Gly116Arg	M, 9y
hVS488		Sendai	n.a	ALD, cALD	ABCD1, c.901-5C>A	p.Val301fs*?	M, 60y

F: Female, M: Male, y:year, n.a. not applicable, Repr. Method: Reprogramming method,
ALD: adrenoleukodystrophy with cALD: cerebral ALD or AMN: Adrenomyeloneuropathy phenotype,
4H: 4H leukodystrophy

Supplementary Table II: Antibodies

Target	Host	Dilution	Company	Number
MAP2	Chicken	1:5000	Millipore	ABB5442
Synaptophysin	Guinea Pig	1:500	SySy	101 004
NeuN	Chicken	1:500	SySy	266 006
NF200	Rabbit	1:500	Sigma	N4142
HuNu	Mouse	1:500	Sigma	MAB1281
TMEM119	Rabbit	1:1000	Atlas Antibodies	HPA051870
Iba1	Rabbit	1:1000	Abcam	AB178847
CD68	Mouse	1:1000	DAKO	M0814

Supplementary Table III: Effect of neuronal background on microglia

	WPP	Mean H01	Mean hvs088	Mean hvs420	Mean hvs451a		Pvalue	Pvalue (BF corr.)
Microglia Number	8	412.8	211.3	208.5	137.3	**Neurons**	**<0.0001**	**<0.0001**
	10	524.8	204.5	283.0	59.7	**Timepoint**	**0.035**	0.624
	12	414.2	214.2	155.5	52.0	**Interaction**	**0.041**	0.738
Microglia Roundness	8	0.39	0.53	0.50	0.55	**Neurons**	**<0.0001**	**<0.0001**
	10	0.37	0.50	0.46	0.52	**Timepoint**	**<0.0001**	**0.002**
	12	0.39	0.53	0.51	0.59	**Interaction**	0.581	1.000
Microglia Size (µm)	8	1445.3	970.9	1077.8	1123.7	**Neurons**	**<0.0001**	**<0.0001**
	10	1390.3	1050.0	1028.6	1064.7	**Timepoint**	**<0.0001**	**0.002**
	12	1450.6	1217.1	1258.6	1180.4	**Interaction**	0.141	1.000
Microglia Length (µm)	8	88.1	66.6	71.5	69.1	**Neurons**	**<0.0001**	**<0.0001**
	10	94.0	73.1	76.1	72.6	**Timepoint**	**<0.0001**	**0.002**
	12	95.8	77.1	80.2	68.1	**Interaction**	0.123	1.000
Microglia Width (µm)	8	19.0	18.4	18.6	20.1	**Neurons**	**0.0002**	**0.004**
	10	16.6	17.4	16.9	17.9	**Timepoint**	**<0.0001**	**<0.0001**
	12	17.9	19.8	19.8	20.9	**Interaction**	0.139	1.000
Microglia Width to Length Ratio	8	0.26	0.35	0.33	0.37	**Neurons**		
	10	0.22	0.30	0.28	0.32	**Timepoint**		
	12	0.24	0.34	0.33	0.40	**Interaction**		

WPP: weeks post plating. BF corr. : corrected for Bonferonni multiple testing (n=18)

Supplementary Table IV: Difference in neuronal activity between with and without microglia

Spikes	Pvalue	Pvalue (BF corr.)
Spike Frequency (Hz)	**0.0023**	**0.030**

Bursts	Pvalue	Pvalue (BF corr.)
Burst Frequency (/min)	**0.0170**	**0.221**
Spikes in Bursts (%)	**0.0352**	0.457
Burst Duration (s)	0.3729	1.000
Burst Spike Count	0.3821	1.000
Spike Frequency in Burst (Hz)	0.7785	1.000
Inter Burst Interval (s)	0.8530	1.000

NBs	Pvalue	Pvalue (BF corr.)
NB Frequency (/min)	**0.0154**	0.2000
Spikes in NBs (%)	0.0585	0,761
NB Duration (s)	0.2019	1.000
NB Spike Count	0.1681	1.000
Spike Frequency in NBs (Hz)	0.1535	1.000
Inter NB Interval (s)	0.3419	1.000

NBs: Network Bursts

Supplementary Table V: Replicates used for cellomics with and without microglia

Analysis	Objective	Timepoints (WPP)	Replicate Wells per Condition	Pictures
Microglia number & morphology	10x	8, 10, 12	6	25
Nuclear Debris	20x	8, 10, 12	4	25
Mature NeuN+ Neurons & NF+ axons	10x	8, 10, 12	2	25
MAP2+ dendrites & Syphy+ puncta	20x	8, 10, 12	2	25

WPP: weeks post plating

Supplementary Table VI: Statistical testing of ctrl vs ALD microglia-like cell cultures

Culture Conditions	Assay	Parameter	Test	Pvalue	Pvalue corrected	Assumption Normality
Ctrl vs. ALD	Intrinsic stress?	Microglia numbers	T-test	0.818	*n.a.*	True
		Microglia Roundness	T-test	0.740	*n.a.*	True
		COMBINATION	Fisher	0.909	*n.a.*	*n.a.*
	Microglia morphology	Size	T-test	0.444	*n.a.*	True
		Length	T-test	0.596	*n.a.*	True
		Width	T-test	0.491	*n.a.*	True
		Width to Length Ratio	T-test	0.829	*n.a.*	True
	Different effect?	Debris	T-test	0.102	*n.a.*	True
		Neuron number	T-test	0.266	*n.a.*	True
		Axon segment number	T-test	**0.012**	*n.a.*	True
		Dendrite segment number	T-test	0.657	*n.a.*	True
		COMBINATION	Fisher	**0.032**	*n.a.*	n.a.
	CD68	CD68+ percentage	T-Test	0.616	*n.a.*	True
	Axon	No. of Segments	T-test	0.830	1.000	True
		Mean Segment Length	T-test	0.053	0.420	True
		Max. Neurite Length	T-test	0.803	1.000	True
		No. of Extremities	T-test	0.860	1.000	True
		No. of Roots	T-test	0.990	1.000	True
		No. of Type I Nodes	T-test	0.802	1.000	True
		No. of Type II Nodes	T-test	0.442	1.000	True
		Total Neurite Length	T-test	0.981	1.000	True
	Dendrite	No. of Segments	T-test	0.860	1.000	True
		Mean Segment Length	T-test	0.708	1.000	True
		Max. Neurite Length	T-test	0.546	1.000	True
		No. of Extremities	T-test	0.797	1.000	True
		No. of Roots	T-test	0.479	1.000	True
		No. of Type I Nodes	T-test	0.926	1.000	True
		No. of Type II Nodes	T-test	0.902	1.000	True
		Total Neurite Length	T-test	0.697	1.000	True
	Syphy	Syphy puncta density per dendritic area	T-test	0.150	*n.a.*	True
	Activity	Active channels (WPP>7)	T-test	0.897	*n.a.*	True

Supplementary Table VII: Statistical testing of ctrl vs 4H microglia-like cell cultures

Culture Conditions	Assay	Parameter	Test	Pvalue	Pvalue corrected	Assumption Normality
Ctrl vs. 4H	Intrinsic stress?	Microglia numbers	T-test	0.407	*n.a.*	True
		Microglia Roundness	T-test	0.568	*n.a.*	True
		COMBINATION	Fisher	0.570	*n.a.*	*n.a.*
	Microglia morphology	Size	T-test	0.803	*n.a.*	True
		Length	T-test	0.996	*n.a.*	True
		Width	T-test	0.752	*n.a.*	True
		Width to Length Ratio	T-test	0.966	*n.a.*	True
	Different effect?	Debris	T-test	0.809	*n.a.*	True
		Neuron number	T-test	0.962	*n.a.*	True
		Axon segment number	T-test	0.624	*n.a.*	True
		Dendrite segment number	T-test	0.248	*n.a.*	True
		COMBINATION	Fisher	0.836	*n.a.*	n.a.
	Activity	Active channels (WPP>7)	T-test	0.532	*n.a.*	True

n.a.: not applicable. WPP: weeks post plating (of neurons)

Pvalue corrected: corrected for Bonferonni multiple testing (n=8)

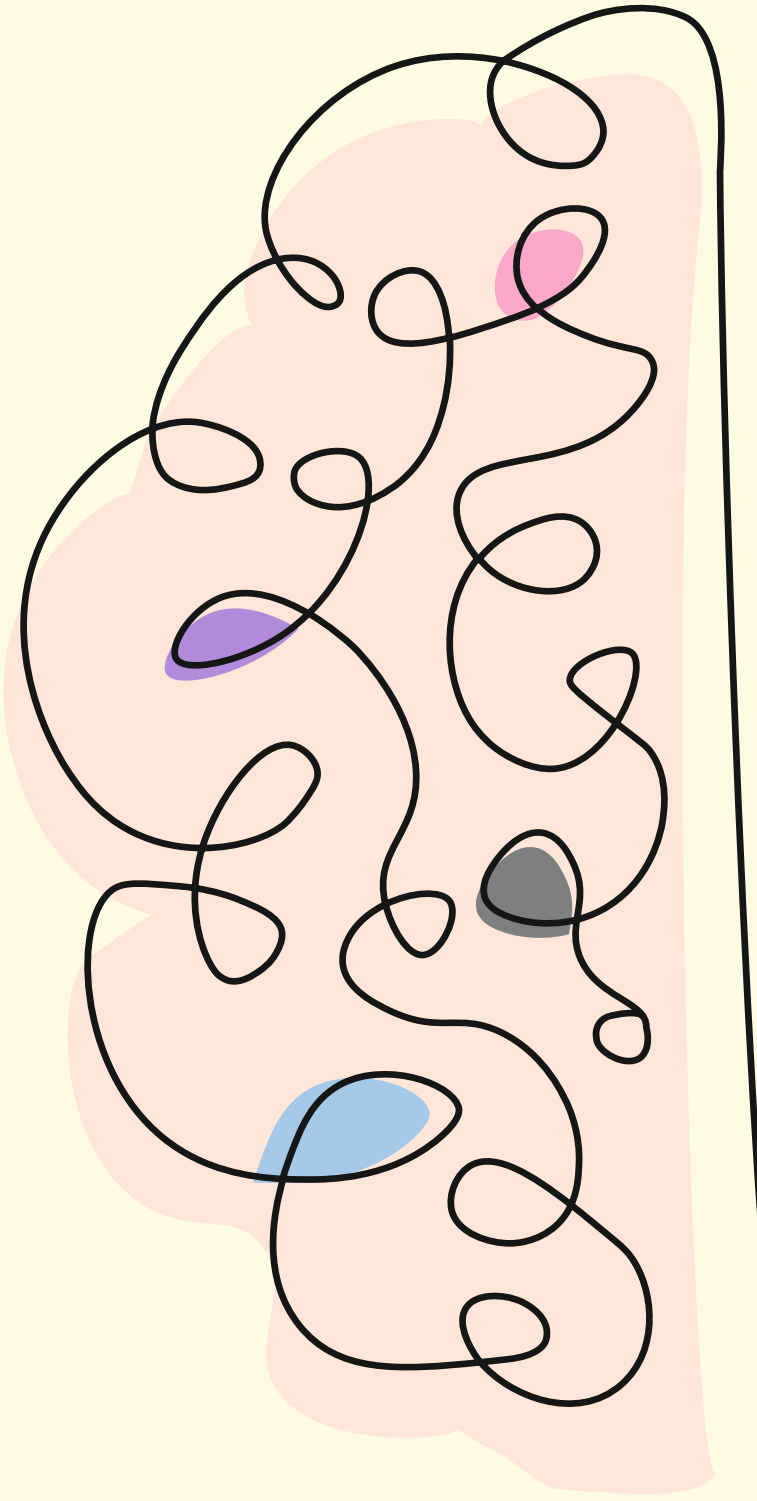

06

POLR3 gene and protein expression dynamics in 4H leukodystrophy using iPSC-derived neuronal lineages

Liza M. L. Kok, Heiletjé van Zyl, Felice Götte, Evanne Lichtendahl, Nicole Breeuwsma, Nicole I. Wolf, Vivi M. Heine

Under revision; Stem Cell Research, 2025

ABSTRACT

Induced pluripotent stem cell (iPSC) technology offered new tools for studying disease mechanisms by modeling patient-specific genetics in disease-relevant cell types. Here, we focus on 4H leukodystrophy, a genetic brain white matter disorder linked to *POLR3* variants with distinct clinical characteristics, which manifests with considerable clinical variability. Although 4H leukodystrophy primarily features white matter abnormalities, emerging research highlights the involvement of neuronal pathology. To address this, we analyzed *POLR3* gene and protein expression throughout neuronal lineage differentiation, from the iPSC state to neuroepithelial stem cells (NES) and mature neurons. We identified elevated *POLR3* gene expression in NES. However, Pol III protein levels were notably reduced in 4H patient cells. Despite these protein-level alterations, overall Pol III-transcribed transcript levels, including tRNAs and *BC200* RNA were unchanged in 4H cells. Notably, patient-specific genetic backgrounds were found to have a significant impact on *POLR3A* expression. These results underscore the necessity of considering individual genetic backgrounds and specific developmental cell states when investigating the pathology of 4H leukodystrophy. Furthermore, our work demonstrates the utility of iPSC-based models in unraveling patient-specific disease mechanisms, thereby facilitating the development of more tailored therapeutic strategies.

Highlights:

- cell type dependent POLR3 gene expression, increased in neuronal lineage cells
- 4H patient-specific reductions in Pol III protein
- iPSC models reveal (possible) patient-specific molecular changes in 4H

Keywords

iPSC, 4H Leukodystrophy, RNA polymerase III**,** neuronal cell lineages, gene expression

INTRODUCTION

Induced pluripotent stem cell (iPSC) technology has revolutionized the study of patient-specific genetics, enabling researchers to investigate how genetic variations influence cellular phenotypes. This is especially important for disorders with complex and variable clinical presentations, where treatment targets remain ambiguous (Nicholson et al., 2022; Shi et al., 2017). By modeling patient-derived cells, iPSCs offer a unique platform to explore the genetic and molecular underpinnings of such diseases and identify how these differences manifest in relevant cell types. However, despite advances in identifying disease-causing genes, translating these findings into effective therapies has been challenging. This is largely due to the context-dependent nature of gene expression and protein function, which vary across cell types and developmental stages. Therefore, it is critical to determine the specific cell populations and developmental contexts that are most affected by disease variants to design targeted therapeutic strategies.

In this study, we focus on the genetic brain white matter disorder known as 4H leukodystrophy, or *POLR3*-related leukodystrophy. This disorder, caused by biallelic variants in either *POLR3A*, *POLR3B*, *POLR3K*, *POLR3D* or *POLR1C* genes, is characterized by a clinical triad: hypomyelination, hypogonadotropic hypogonadism, and hypodontia (Bernard et al., 2011; Dorboz et al., 2018; Macintosh et al., 2023; Tetreault et al., 2011; Thiffault et al., 2015). Despite these hallmark features, 4H leukodystrophy exhibits considerable clinical variability. Some patients present with significant neurological involvement despite minimal hypomyelination (Harting et al., 2020; La Piana et al., 2016), while others may experience isolated endocrine abnormalities such as hypogonadotropic hypogonadism (Richards et al., 2017). The causative genes encode subunits of RNA Polymerase III, which synthesizes various essential small non-coding RNAs, including transfer (t), ribosomal (r), small nuclear (sn), small nucleolar (sno), and micro (mi) RNAs. Given the progressive and debilitating nature of 4H leukodystrophy, there is an urgent need for therapeutic development. Current treatments are limited to symptomatic management (Adang et al., 2017). Identifying the specific cell types vulnerable to *POLR3* variants is crucial for developing effective, targeted therapies.

Previous studies have suggested a neuronal component to 4H pathology, at least in some patient subsets (Dooves et al., 2023; Harting et al., 2020; La Piana et al., 2016). Yet, it remains unclear which molecular mechanisms underlie these neuronal phenotypes and whether these alterations are exclusive to neurons or present earlier in neural precursor cells, such

as neuroepithelial stem cells (NES). To address this, we investigated how patient-specific *POLR3* variants influence gene expression, protein levels, and subcellular localization in different neuronal lineage cell types, including iPSCs, NES, and neurons. Additionally, we examined the impact of individual genetic variability on these molecular characteristics.

Our findings demonstrate that *POLR3* gene expression is different in cell subtype- and between individuals. In contrast, Pol III protein levels were affected by disease status but showed no significant variation across different individuals. Interestingly, the localization of Pol IIIA was determined to be an influential outlier, warranting further investigation to determine if this is disease related. Importantly, we did not find significant differences in Pol III transcript products related to disease status and cell type. These insights provide a deeper understanding of the molecular alterations contributing to neuronal dysfunction in 4H leukodystrophy. Furthermore, our study highlights the potential of iPSC-based models to uncover patient-specific genetic effects, offering a foundation for future therapeutic development.

RESULTS

POLR3 gene expression varies by cell type

To investigate how *POLR3* gene expression contributes to neuronal vulnerability in 4H leukodystrophy, we analyzed *POLR3A* and *POLR3B* gene expression in iPSCs, NES, and neurons derived from a 4H patient cohort with *POLR3A* and *POLR3B* variants, along with controls (Supplementary Table I and Supplementary Fig. 1A-C). A linear mixed-effects model (LMEM) indicated some evidence of a global significant effect of cell type on POLR3A expression ($\chi 2$ (2) = 6.180, p = 0.046). However, when focusing on specific level contrasts for cell type (via post-hoc pairwise comparisons) such statistical significance was not revealed. From visual inspection of Fig. 1A, some trends of increased expression were observed between iPSCs and neurons (p = 0.0723) and between iPSCs and NES (p = 0.0723). (Fig. $1A_1$). There was no difference between controls and 4H patients (Fig. $1A_2$; $\chi^2(1) = 2.541$, p = 0.111). *POLR3B* expression also varied significantly across cell types ($\chi^2(2) = 21.340$, p <0.001), with significant differences identified between iPSCs and NES (p = 0.0024) and between NES and neurons (p = 0.0021) (Fig. 1 B_1). There was no significant effect of disease status on *POLR3B* expression (Fig. $1B_2$; $\chi^2(1) = 0.077$, p=0.782). In conclusion, both *POLR3A* and *POLR3B* gene expressions are influenced by cell type, with higher expression levels observed in NES compared to iPSCs, suggesting a cell-type-specific regulation of *POLR3* genes.

Individual differences in POLR3 gene expression

To assess the contribution of individual differences to *POLR3* gene expression, intraclass correlation coefficients (ICCs) were calculated. *POLR3A* expression showed substantial inter-individual variability (ICC = 0.676; i.e., after accounting for disease status and cell type, 67.6% of the variability in *POLR3A* expression is due to differences between individuals), whereas *POLR3B* expression demonstrated that more between-individual (i.e., residual) variance contributes to its variability (ICC = 0.270). These results indicate that individual genetic background contributes considerably to *POLR3A* expression variability, but this is less so for *POLR3B*.

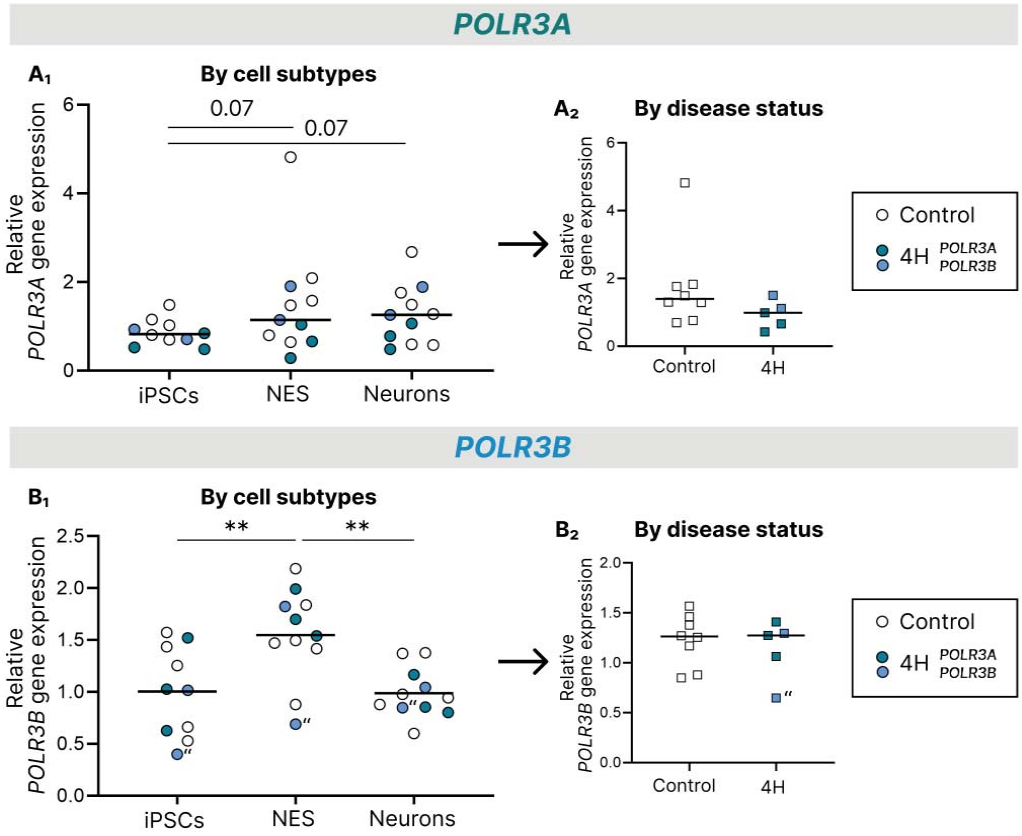

Figure 1: *POLR3A* and *POLR3B* gene expression varies between cell types. Relative gene expression of *POLR3A* (A) and *POLR3B* (B) as determined by quantitative PCR comparing cell types (iPSC, NES, neurons) and control against 4H. Open circles represent controls, solid circles represent individuals with 4H caused by *POLR3A* (dark) or *POLR3B* (light) variants. Disease status graphs (A_2, B_2) represent the average relative gene expression across all three cell types, indicated with squares. Horizontal lines across the circles/squares reflect the median. Data was analyzed using a linear mixed-effects model after removal of influential outliers (indicated with "). * Significance was assessed at $p < 0.05$, ** $p < 0.01$ or *** $p < 0.001$.

Pol III protein expression is disease status dependent

Western blot analysis showed a significant difference in Pol IIIA protein expression between cell types ($\chi^2(2) = 11.252$, $p = 0.004$). Post-hoc pairwise comparisons revealed decreased Pol IIIA protein expression in neurons compared to iPSCs ($p = 0.0152$) and in neurons compared to NES ($p = 0.035$, Fig. $2A_1$). Additionally, we identified a significant decrease in 4H cells compared to control cells (Fig. $2A_2$; $\chi^2(1) = 4.857$, $p = 0.028$). Similarly, analysis of Pol IIIB protein expression was performed, for this subunit there was no significant difference based on cell subtypes ($\chi^2(2) = 4.812$, $p = 0.090$; Fig. $2B_1$). Though, expression of Pol IIIB subunit was again significantly lower in 4H patient cells compared to controls ($\chi^2(1) = 6.204$, $p = 0.013$; Fig. $2B_2$) In conclusion, 4H status affects Pol III protein levels, suggesting that 4H may alter Pol III subunit expression (independent of cell type).

Minimal impact of individual differences on Pol III protein levels

To understand the contribution of individual differences to protein expression of Pol IIIA and Pol IIIB, we again calculated the ICC. We identified minimal influence of individual differences on Pol III protein expression, with only 6.1% of residual variance for Pol IIIA and 0% for Pol IIIB being explained by inter-individual variability. So unlike gene expression, Pol III protein levels are not substantially affected by individual genetic differences.

► **Figure 2: Pol III protein subunit A and B expression in different cell types.** Relative protein expression of Pol III subunit A (A) and Pol III subunit B (B) as determined by western blot, comparing cell type (iPSC, NES and neurons) and control against 4H. Open circles represent controls, solid circles represent individuals with 4H caused by *POLR3A* (dark) or *POLR3B* (light) variants. Disease status graphs (A_2, B_2) represent the average relative protein expression across all three cell types, indicated with squares. Horizontal lines across circles/squares reflect the median. Data was analyzed using a linear mixed-effects model after removal of influential outliers (indicated with “). * Significance was assessed at $p < 0.05$, ** $p < 0.01$ or *** $p < 0.001$.

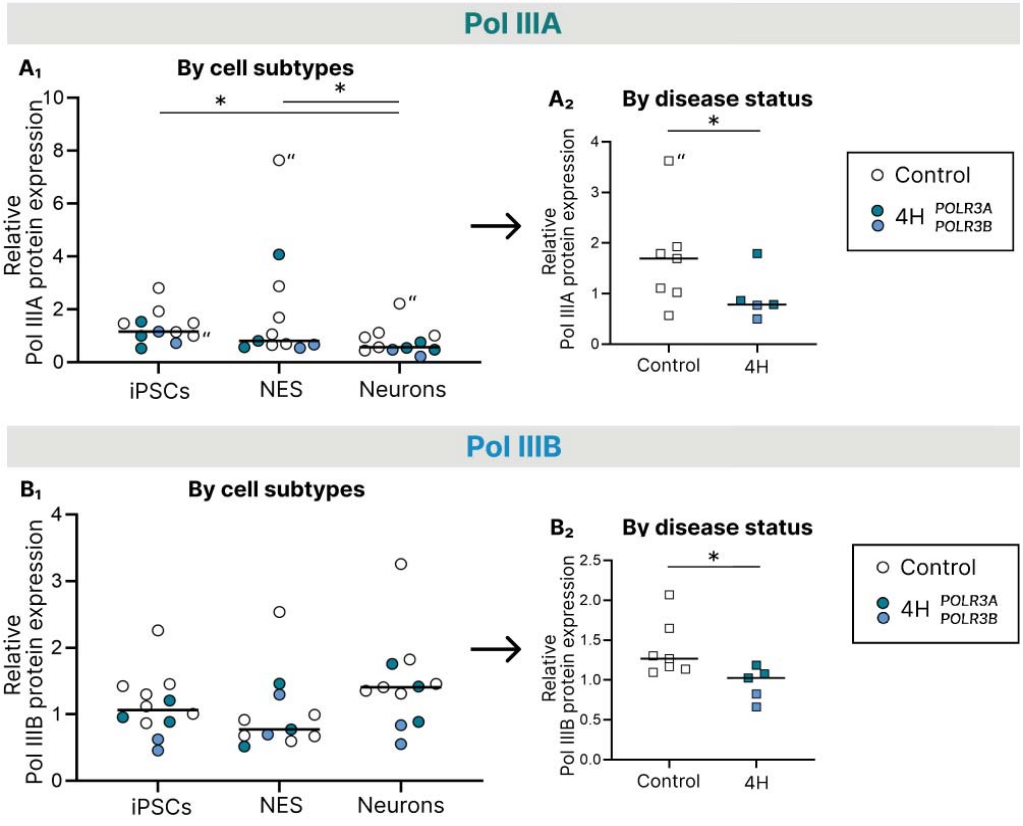

Subcellular localization of Pol III subunits

To explore the functional implications of altered POLR3 gene expression in NES, we analyzed the subcellular localization of Pol IIIA and IIIB using immunocytochemistry (Supplementary Fig. 2). After removing one influential outlier, a 4H line with *POLR3A* variants, we did not observe a difference in subcellular localization of Pol IIIA subunit between control and 4H cells ($\chi^2(1) = 2.161$, $p = 0.142$; Fig. 3A). Similarly, no significant differences were found in Pol IIIB localization between controls and 4H cells ($\chi^2(1) = 0.300$, $p = 0.584$; Fig. 3B). ICC analysis revealed modest contributions of individual differences to Pol IIIA (ICC = 0.096) and Pol IIIB (ICC = 0.1166) localization. These results do not show evidence for impaired localization caused by 4H variants and individual variability does not appear to be a major factor.

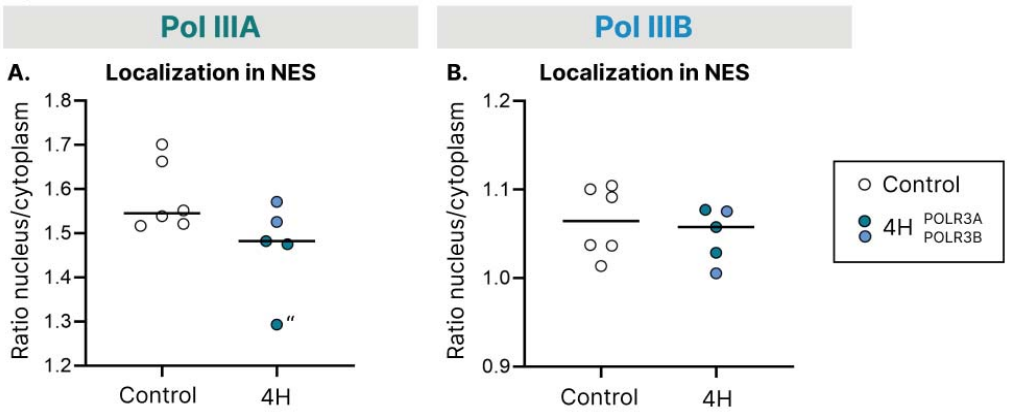

▲ **Figure 3: Localization of Pol III subunits in NES cells.** Comparing ratio of nucleus/cytoplasm localization of Pol III subunit A (A) or subunit B (B) in NES of control vs. 4H. Horizontal bars across circles/squares reflect the median. Open circles represent controls, solid circles represent individuals with 4H caused by POLR3A (dark) or POLR3B (light) variants. Data was analyzed using a linear mixed-effects model after removal of influential outliers (indicated with "). * Significance was assessed at $p < 0.05$, ** $P<0.01$ or *** $P <0.001$.

Pol III-driven transcript expression unaffected by 4H status

To assess potential functional consequences of *POLR3* variants we measured abundance of Pol III transcribed products. Specifically, the expression of two tRNA transcripts. Neither $tRNA^{Ala}$ and $tRNA^{Leu}$ had a significant difference of expression in cell subtypes (Respectively, $\chi^2(2) = 0.570$, $p = 0.752$; Fig. $4A_1$, and $\chi^2(2) = 3.516$, $p = 0.172$; Fig. $4B_1$) nor a difference in expression between control and 4H cells (Respectively, $\chi^2(1) = 0.309$, $p = 0.578$; Fig. $4A_2$, and $\chi^2(1) = 0.086$, $p = 0.769$; Fig. $4B_2$). Additionally, we investigated expression of Pol III transcript BC200 which was also not significantly different between both cell subtypes and between control and 4H cells (Respectively, $\chi^2(2) = 4.036$, $p = 0.133$; Fig. $4C_1$; and $\chi^2(1) = 0.174$, $p = 0.676$; Fig. $4C_2$) ICC values for $tRNA^{Ala}$ (16.5%), $tRNA^{Leu}$ (0%), and *BC200* (32.3%) suggest variable contributions of individual differences to Pol III transcript expression. This indicates that the level of Pol III transcribed transcripts are largely unchanged in 4H cells and minimal inter-individual variability in transcript expression is observed.

DISCUSSION

In this study, we aimed to identify molecular alterations associated with the neuronal phenotype in 4H leukodystrophy that could point toward primary cell type vulnerabilities. We investigated *POLR3* gene expression, Pol III protein levels, and subcellular localization across different cell types. We identified several key alterations, including cell-type-dependent *POLR3* gene expression and 4H specific reductions in Pol III A and B protein.

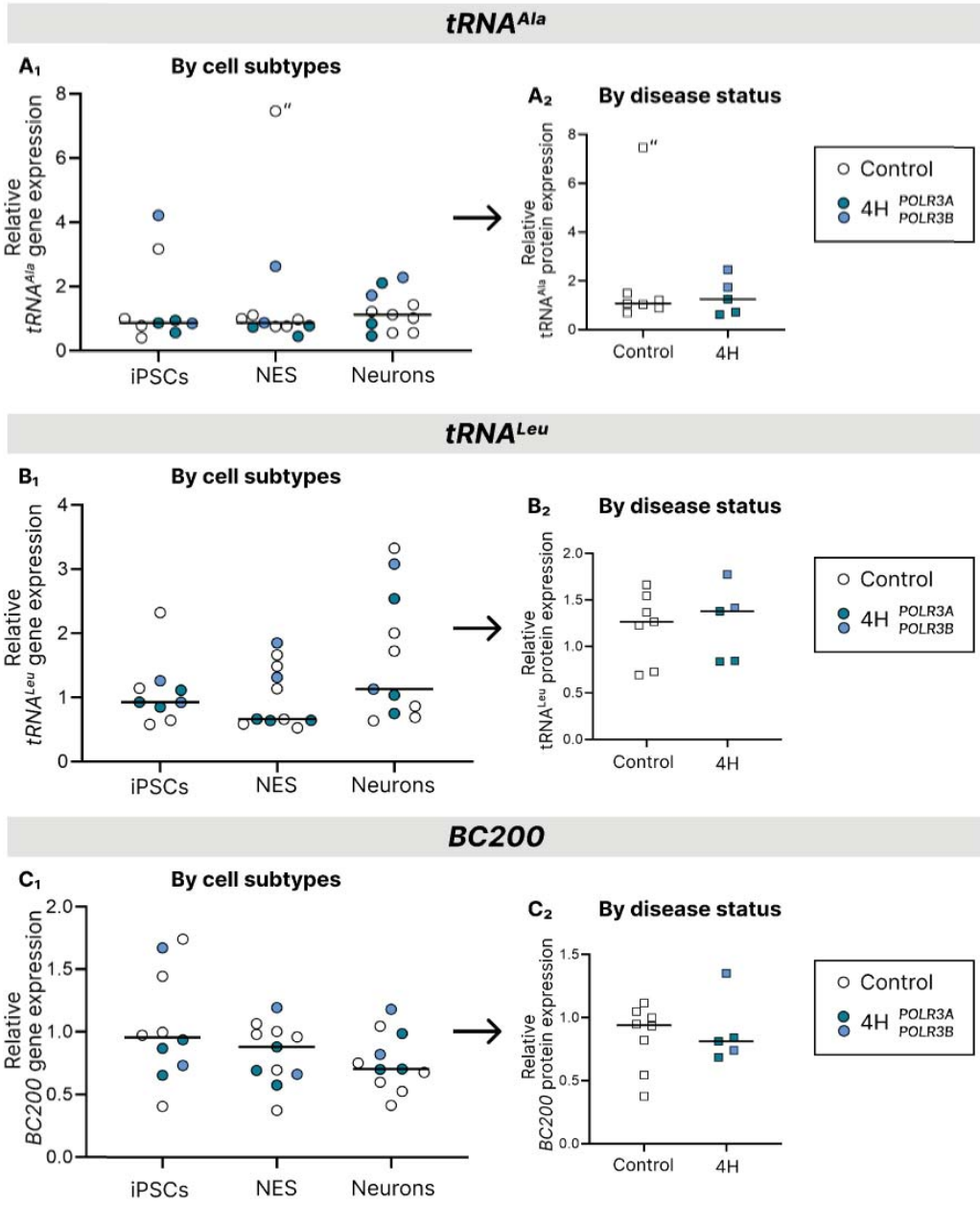

Figure 4: Products of Pol IIIA, tRNAs and *BC200* remain unaffected by disease status. Relative gene expression of $tRNA^{Ala}$ (A), $tRNA^{Leu}$ (B), and *BC200* (C) in control and 4H subjects, comparing cell type (iPSC, NES and neurons) and control against 4H. Open circles represent controls, solid circles represent individuals with 4H caused by *POLR3A* (dark) or *POLR3B* (light) variants. Disease status graphs (A_2, B_2, C_2) represent the average relative gene expression across all three cell types, indicated with squares. Horizontal lines reflect the median. Data was analyzed using a linear mixed-effects model after removal of influential outliers (indicated with ").

Further research is however required to elucidate the specific contribution of these findings to 4H phenotypes. Our study underscores the importance of context-specific and patient-specific research and how iPSC technology could contribute to personalized research approaches.

Cell-specific POLR3 gene expression and implications

One of the clearest findings is the upregulation of *POLR3B* gene expression in NES compared to iPSCs, and a similar trend in *POLR3A*. Possibly, there is an increased transcriptional demand during the early stages of neuronal differentiation. This upregulation could be part of the explanation why the neuronal lineage is affected by *POLR3*-variants found in 4H. However, further research is needed to validate this hypothesis and establish a direct link between *POLR3* expression and neuronal vulnerability. Although we did not find an effect of 4H status on *POLR3* gene expression levels, interestingly, one 4H patient with *POLR3B* variants was identified as influential outlier in the *POLR3B* gene expression analysis. This could possibly be 4H related, future studies with larger sample size are required to determine if gene expression levels are or are not affected.

Disease-specific changes in Pol III protein

We identified reduced Pol III protein levels in 4H cells. This is in line with previous case reports that describe reduced Pol III protein levels in 4H patients and in mutant cell lines (Choquet, Forget, et al., 2019; Perrier et al., 2020). Interestingly, the patients with *POLR3B* variants have the lowest levels of Pol IIIB expression. Additionally, we did observe one 4H patient with *POLR3A* variants to be an influential outlier in the nuclear localization of Pol IIIA. Again, due to small sample sizes we cannot rule out whether this is actually disease related. Since Pol III has its function in the nucleus, but assembles in the cytoplasm, reduced nuclear localization possibly has negative impact and contributes to the disease phenotype (Tian et al., 2023). In literature, impaired nuclear import is described for a 4H patient with biallelic variants in *POLR1C* (Thiffault et al., 2015). Additionally a number of other variants causing *POLR3* related leukodystrophy are reported to impair proper assembly of Pol III (Choquet, Pinard, et al., 2019), often causing a retention of the unassembled subunits in the cytoplasm (Thiffault et al., 2015). Possibly, protein level and localization are early indicators of neuron cellular dysfunction, but this requires further exploration.

Absence of *POLR3* Transcript Product Alterations

Despite reduced protein expression in 4H cells, there is no significant alteration in level of Pol III transcribed transcript, raising questions about the downstream functional effects of *POLR3* variants. No effect of disease status was found on expression levels of tRNAs, which is contradicting literature that describes altered tRNA profiles in a mouse model of 4H (Moir et al., 2024). Additionally, we did not identify a cell type effect on tRNA expression, while it is known that human tRNA expression vary widely in human tissue (Dittmar et al., 2006). Together, this made us believe that we did not have either sensitive enough assays or large enough sample sizes to detect the altered tRNA levels. The structural complexity of tRNAs poses additional challenges for accurate quantification via qPCR, as their secondary and tertiary structures can interfere with detection. Additionally, we also found no effect of disease status on *BC200* expression, despite reports of *BC200* downregulation in *POLR3A* mutants (Choquet, Forget, et al., 2019). Given that we analyzed *POLR3A* and *POLR3B* patients together, it is conceivable that *BC200* downregulation may be specific to certain subgroups. Further studies are needed to clarify these inconsistencies and determine the functional relevance of Pol III transcript expression.

Impact of individual variability on POLR3 expression

Our study highlighted considerable inter-individual variability in *POLR3* gene expression, independent of disease status and cell type. However, this variability was not mirrored at the protein level, suggesting that post-transcriptional regulatory mechanisms may buffer these differences. The substantial individual differences underscore the complexity of *POLR3* gene regulation and could have implications for personalized treatment approaches in 4H leukodystrophy. The need for tailored therapies becomes particularly apparent when considering the genetic and phenotypic heterogeneity observed among patients.

Conclusions

Overall, our findings support the idea that genetic and molecular alterations in 4H are highly context-dependent, reinforcing the importance of identifying the specific cell populations and developmental stages most affected by these variants. The inter-individual variability we observed in *POLR3* gene expression across individuals also points to a need for personalized approaches in both research and therapy. By using patient-derived iPSCs, we can better capture this complexity and work towards refining targeted interventions. Future studies should delve deeper into splicing variations and protein assembly disruptions, as these may hold the key to understanding and potentially mitigating the cellular dysfunction observed in 4H leukodystrophy.

MATERIAL & METHODS

iPSC generation and maintenance

The Institutional Research Board of the VU University Medical Center approved the study, and written consent was obtained from all participants in accordance with the declaration of Helsinki. iPSCs were generated from fibroblasts of healthy donors and 4H patients according to the previously described procedure (Holmes & Heine, 2017) or via CytoTune™-iPS 2.0 Sendai Reprogramming Kit according to manufacturer protocol. Pluripotency was confirmed by immunocytochemistry, alkaline phosphatase assay, PCR, embryoid body formation and/or pluritest. Additionally karyotyping and/or confirmation of disease variants was carried out. The human embryonic stem cell lines H01 and H09 were obtained from WiCell. Pluripotent stem cells were maintained in TeSR™-E8™ (STEMCELL Technologies, 05990) on Vitronectin XF™ coated plates (STEMCELL Technologies, 07180). Media was replaced daily or using double feedings over the weekend. Confluent wells were split with a ratio of 1:10 to 1:50 into a new well for further maintenance. An overview of the used stem cell lines can be found in Supplementary Table I.

Differentiation into neuronal lineage

Cortical neurons were generated using the previously published protocol (Nadadhur et al., 2017). In short, high-density iPSCs on Geltrex™ coated plates (±150 µg/ml, Gibco, A1413302) were induced into neurons by dual inhibition of the BMP and Activin/Nodal/TGF-β signaling pathways using 1 µM Dorsomorphin (Selleckchem, S7306) and 10 µM SB431542 (Selleckchem, S1067) in Neural Maintenance Medium (NMM) which consisted of 50% DMEM/F-12 with GlutaMAX™ (Gibco, 31331028), 50% Neurobasal™ medium (Gibco, 21103-049), 0.5x N2 supplement (Gibco, 17502001), 0.5x B27 supplement (Gibco, 17504-044), 2.5 µg/ml Insulin (Merck/Sigma-Aldrich, I9278), 1 mM L-Glutamine (Gibco, 25030081), 50 µM Minimum Essential Medium (MEM) Non-Essential Amino Acids (Gibco, 11140050), 50 µM Beta-Mercaptoethanol (Gibco, 21985023) and 1x P/S (Penicillin/Streptomycin, Sigma, P0781). Neural rosettes formed between 8 and 12 days after neural induction and were manually picked for transfer to PLO (20 µg/ml, Sigma-Aldrich, P3655)/ mouse laminin (20 µg/ml, Sigma-Aldrich, L2020) coated wells containing NMM supplemented with 20 ng/ml FGF2 (PeproTech, 100-18B) and 20 ng/ml EGF (PeproTech, AF-100-15). When confluent, neural rosettes were split 1:2 to 1:3 using TrypLE™ (Gibco, 12563-011) and defined trypsin inhibitor (DTI, Gibco, R007100) or frozen in KnockOut™ Serum Replacement (KSR, Gibco, 10828028) with 10% dimethyl sulfoxide (DMSO, Sigma-Aldrich, D2650).

Passage 1 – 3 of NES were used for differentiation into neurons using N2 medium, which consisted of DMEM/F-12 (without L-Glutamine, Gibco, 21331020), 1x N2 supplement, 0.1 mM MEM-NEAA, 2 mM L-Glutamine, 2 µg/ml Heparin (Sigma-Aldrich, H3393) and 1x P/S, supplemented with 400 ng/ml Human Sonic Hedgehog (Shh, PeproTech, 100-45) for 4 days. This was followed by 3 days of 10 µM Valproic acid (VPA, Sigma-Aldrich, P4543) in NB+ medium which consisted of Neurobasal™ medium (Gibco, 21103-049) with 1x B27 (Gibco, 17504-044), 18 mM HEPES (Gibco, 15630-056), 0.25x GlutaMAX™ (Gibco, 35050-038) and 1x P/S. On day 8, cells are passaged 1:2 – 1:4 (depending on density) using accutase and maintained in NB+ medium supplemented with 20 ng/ml BDNF (PeproTech, 450-02), 10 ng/ml GDNF (PeproTech, 450-10), 10 ng/ml IGF (PeproTech, 100-11) and 1 µM cyclic-AMP (Sigma-Aldrich, D0260) until day 18. At day 18 the cells were frozen in KSR with 10% DMSO.

Protein isolation

iPSCs, NES or neurons were quickly thawed in a 37˚C water bath. The cells were re-suspended in pre-warmed DMEM/F12 (#21331-020, Technologies) and centrifuged at 300x g for 5 minutes. The cell pellet was washed with 1x Phosphate-buffered saline (PBS, # 14200-083, Gibco™) and spun down again. The supernatant was removed and the pellet was re-suspended in RIPA lysis buffer consisting of NaCl 150mM (S9888, VWR™), Triton-X100 1% (T8787, Merck), DOC 0,5%, SDS 0,1% (#74255, Merck) and Tris pH 8 50mM (T6066, Sigma-Aldrich®) freshly supplemented with dithiothreitol 1mM (R0861, Thermo Scientific™), 1x Protease inhibitor (#11836145001, Thermo Scientific™) and 1x phosphatase inhibitor cocktail (#5870s, Cell signaling Technologies™). The cell mixture was put on ice for 30 minutes and centrifuged at 300x g for 20 minutes. The cell lysate was collected in a new tube. The concentration was measured using Bradford reagent (B6916, Sigma-Aldrich®) according to manufacturers protocol.

Western blot

Invitrogen™ NuPAGE™ LDS Sample Buffer 1X (#NP0007, Thermo Scientific™) was added to protein lysates. The samples were heated for 5 minutes at 100˚C and 20 µg was loaded into a 4–15% Criterion™ TGX Stain-Free™ Protein Gel (#5678084, BioRad) together with the Precision Plus Protein™ All Blue Prestained Protein Standard (#1610373, BioRad). Electrophoresis was performed at 200V for 15 minutes in running buffer (24.8 mmol/L Tris-base, 250 mmol/L glycine, 0.1% SDS). Next, the gel was imaged using the GelDoc EZ Gel Imaging System (BioRad). Following imaging the gel was transferred to an methanol activated (5 minutes) Immun-Blot® PVDF Membrane (#1620177, BioRad) by blotting

overnight at 40V and 4˚C in transfer buffer (15 mmol/L Tris Base, 120 mmol/L Glycine, 20% Methanol). After transfer the blot was rinsed using washing buffer (1x TBS and 0.05% Tween P1379, Sigma-Aldrich®) and imaged with the GelDoc EZ Gel Imaging System.

Next, the blot was blocked using 5% non-fat milk (A0830, PanReac AppliChem) in washing buffer for one hour at RT. After blocking the primary antibodies Pol IIIA (AA: 607-698, PA5-58170, Invitrogen™) or Pol IIIB from Bioscience (AA:1083-1133, A301-855A) were incubated in a 1:1000 dilution in 3% Milk in washing buffer for 3 hours at RT. Next, the blots were washed with washing buffer 3 times every 10 minutes. The secondary antibody HRP (# 7074S, Cell Signaling Technology®) was then added in a dilution of 1:2000 in washing buffer and incubated for 2 hours at RT. Following the secondary antibody, the blots were washed 3 times every 10 minutes with washing buffer. The stained blots were then prepared for detection using Pierce™ ECL Western Blotting Substrate (#34095, Thermo Scientific™) following manufacturers protocol and visualized with the Odyssey® XF Imaging System (LI-COR). Western blots were quantified by measuring the intensity of each band using the ImageJ software. The intensity of each band was first corrected for background intensity to remove any non-specific signal. Additionally, the band intensity was normalized to the total protein level to ensure accurate comparison between samples. A standard sample was included on every blot, serving as a control to correct for variations between different blots, ensuring consistency in quantification across all experiments.

Immunocytochemistry

For the localization of the target proteins subunit A and subunit B, immunocytochemistry was performed. NES cells were plated in densities of 10k cells/cm^2. The cells were fixated with 2% paraformaldehyde (PFA, #15710-S, Electron Microscopy Sciences) in PBS for 20 minutes at RT. Followed by a 4% PFA fixation for another 20 minutes at RT. After fixation the cells were washed with PBS 3 times every 10 minutes. Blocking buffer consisting of 5% Normal goat serum (16210064, Gibco) 0.3% TritonX100 (T8787, Sigma-Aldrich) and 0.1% BSA (bovine serum albumin, A9418, Sigma-Aldrich) was then added to the cells and incubated for 1 hour at RT. The primary antibody Pol III A (Amino acid: 607-698, PA5-58170, Invitrogen™) or Pol III B (Amino acid: 1083-1133, A301-855A, Bioscience) was then added in a dilution of 1:500 in blocking buffer and incubated for 2 hours at RT. After incubation the cells were washed with PBS 3 times every 10 minutes. The secondary antibody was added in a dilution of 1:1000 in blocking buffer and incubated for 2 hours at RT. Following the secondary antibody, the cells were washed with PBS 3 times every 10 minutes. Lastly, DAPI

(D9542, Sigma-Aldrich®) was added in a dilution of 1:1000 in washing buffer and incubated for 5 min at RT. The cells were then washed a final time with PBS for 10 minutes. After washing, the cells were imaged with the CellInsight™CX7 LED Pro High-Content Screening Platform (Thermo Scientific™). Example images are displayed in Supplementary Figure 2. After imaging cell segmentation was performed with ImageJ (plugin: Trackmate). Using the region of interest (ROIs) data, quantification was performed. The measured integrated intensity was divided by the measured area (25-40 µm) and multiplied by the mean of 5 background measurements.

qPCR

Total RNA was extracted from iPSCs, NES and neurons using Trizol Reagent (Thermo Fisher Scientific) according to manufacturer's protocol. cDNA synthesis was performed using SuperScript™ IV First-Strand Synthesis System (Invitrogen, 18091050) with 1 µg of RNA and random hexamer primers, according to the manufacturer's protocol. qPCR was carried out on a QuantStudio Real-Time PCR System (Thermo Fisher Scientific) and Sensi Fast Sybr Hi-ROX-kit (Bioline, BIO-92005). Each reaction consisted of 2 µl 1:12 diluted cDNA, 10 µM of forward and reverse primers, and 5 µL of the Sensi mix mix, with a final reaction volume of 10 µL. The following cycling conditions were used: initial denaturation at 95 °C for 10 minutes, followed by 40 cycles of denaturation at 95 °C for 20 seconds, annealing and extension at 60 °C for 30 seconds. A melt curve analysis was performed at the end of the amplification cycles to confirm the specificity of the PCR products. Gene expression levels were normalized to SDHA reference gene, and relative expression levels were calculated using the 2^−ΔΔCt method. All samples were run in technical duplicates, and data from seven controls and five 4H individuals were used for analysis. Primer sequences for the target genes and reference genes are provided in Supplementary Table II.

Statistics

Linear mixed-effect models All statistical analyses were performed using R (version 4.4.1). The Shapiro-Wilk test (S-W test) for normality was performed to determine whether the underlying distribution of *POLR3* gene expression, Pol III protein expression and localization as well as the expression of Pol III transcripts, are Gaussian (Normal). If this test failed on the response scale of these expressions/transcripts/subunits, a log-transformation to the data was applied, and the S-W test was carried out again to confirm normality. A linear mixed-effect model (LMEM) was applied to the log-transformed *POLR3* gene expression, Pol III protein expression, and Poll III transcripts. For each LMEM, the fixed effects of cell type (iPSC,

NES and neurons) as well as disease status (control or 4H) on gene and protein expression as well as transcripts was evaluated. A random effect was also included in the LMEM to account for inter-individual variability, where repeated measures (across the different cell types) for each donor line was predominately prevalent. For instances where the three repeated measures for a specific donor line were not all present, the chosen LMEM appropriately handled such missingness by utilizing all available data through restricted maximum likelihood (REML) estimation (under the assumption of missing at random or MAR). Similarly, a LMEM was fitted for the Pol III subunits on the original response scale and included a fixed effect (disease status only) and a random effect which accounted for twelve (or slightly less) repeated measures given by the number of technical replicates. Again, any missing data was dealt with through REML estimation under the MAR assumption. All LMEMs results are summarized in a Type-II ANOVA table, which tests for each main, fixed effect (e.g., cell type) after the other main, fixed effect (e.g., disease status). It is noted that all reported findings are on the original data scale (i.e., log-scaled results were back-transformed via exponentiation). Diagnostic checks to validate the fit of all LMEMs (and associated output) was done via residual analysis, by inspecting the Quantile-Quantile (Q-Q) as well as the residuals-versus-fitted-values plots and performing the S-W test to check for residual normality. More details on the exact formulation of the aforementioned models are detailed in the Supplementary Material.

Influential outliers The data exploration stage identified the potential presence of influential outliers. This implicated data (of a specific disease status and cell type) tend to deviate significantly from the general data pattern observed and has a disproportionate effect on the output of the LMEMs. More specifically, the parameter estimates are distorted, the model fit is altered, and the interpretation is impacted (resulting in misleading conclusions). Cook's Distance was used to formally quantify the influence of a data point by assessing the change in fitted values when the said data point was entirely removed from the analysis. This diagnostic measure combines the leverage of a data point (i.e., how far the independent variable values are from mean) and the residual (how far the observed value is from the fitted value) to provide a single measure of influence. The reader is referred to Nieuwenhuis et al. (2012) for Cook's Distance in context of LMEMs (Nieuwenhuis et al., 2012). After the removal of these influential outliers, the same above-described analyses for all expressions/transcripts/subunits were re-run, thereby serving as a sort of sensitivity analysis to ensure the overall reliability and validity of the fitted models as well as the implicated inference.

Intra-cluster correlation The random effects extracted from the fitted LMEMs were used to estimate the proportion of variance explained by inter-individual variability (i.e., the between donor-line specific differences) compared to within-individual variability (i.e., the residual variance or error term). Here, a higher-valued ICC indicates that a large proportion of the total variability prevalent in the gene/protein expressions, transcripts, or subunits is due to differences between donors. Consequently, a lower-valued ICC represents that most of the variability is within individuals or attributable to other unknown sources (like measurement error). The ICC formula is outlined in the Supplementary Excel file.

False discovery rate The (Benjamini-Hochberg) False Discovery Rate (FDR) was utilized as a post-hoc adjustment method to address multiple hypothesis testing (i.e., to control the probability of incurring a Type 1 error) when comparing across all combinations of the different cell types. Given there are possible three tests (iPSC-NES, iPSC-neurons, and NES-neurons), the adjusted significance thresholds for each rank (one, two, three) are as follows: 0.01667, 0.0333, and 0.0500. The three p-values associated with the cell-type pairwise comparisons are first sorted (in ascending order) and then compared to three adjusted thresholds (0.0167, 0.0333, and 0.0500) such that significance can be determined.

FUNDING

This work was supported by the European Joint Programme on Rare Diseases (EJPRD19-201, NG4LEUKO) and by Netherlands Organization for Scientific Research (NWO; Gravitation: BRAINSCAPES: A Roadmap from Neurogenetics to Neurobiology; grant 024.004.012)

COMPETING INTERESTS

The authors declare no competing or financial interests

AUTHOR CONTRIBUTIONS

LK and VH designed the study. VH acquired the funding. LK performed the experiments assisted by FG, EL and NB. LK visualized the data and wrote the original draft in consultation with HvZ, VH and NW. Formal analysis was performed by HvZ

DECLARATION OF GENERATIVE AI AND AI-ASSISTED TECHNOLOGIES IN THE WRITING PROCESS.

During the preparation of this work the author(s) used ChatGPT in order to improve readability and language. After using this tool/service, the author(s) reviewed and edited the content as needed and take(s) full responsibility for the content of the published article.

REFERENCES

Adang, L. A., Sherbini, O., Ball, L., Bloom, M., Darbari, A., Amartino, H., DiVito, D., Eichler, F., Escolar, M., Evans, S. H., Fatemi, A., Fraser, J., Hollowell, L., Jaffe, N., Joseph, C., Karpinski, M., Keller, S., Maddock, R., Mancilla, E., . . . Global Leukodystrophy Initiative, C. (2017). Revised consensus statement on the preventive and symptomatic care of patients with leukodystrophies. *Mol Genet Metab*, *122*(1-2), 18-32. https://doi.org/10.1016/j.ymgme.2017.08.006

Bernard, G., Chouery, E., Putorti, M. L., Tetreault, M., Takanohashi, A., Carosso, G., Clement, I., Boespflug-Tanguy, O., Rodriguez, D., Delague, V., Abou Ghoch, J., Jalkh, N., Dorboz, I., Fribourg, S., Teichmann, M., Megarbane, A., Schiffmann, R., Vanderver, A., & Brais, B. (2011). Mutations of POLR3A encoding a catalytic subunit of RNA polymerase Pol III cause a recessive hypomyelinating leukodystrophy. *Am J Hum Genet*, *89*(3), 415-423. https://doi.org/10.1016/j.ajhg.2011.07.014

Choquet, K., Forget, D., Meloche, E., Dicaire, M. J., Bernard, G., Vanderver, A., Schiffmann, R., Fabian, M. R., Teichmann, M., Coulombe, B., Brais, B., & Kleinman, C. L. (2019). Leukodystrophy-associated POLR3A mutations down-regulate the RNA polymerase III transcript and important regulatory RNA BC200. *J Biol Chem*, *294*(18), 7445-7459. https://doi.org/10.1074/jbc.RA118.006271

Choquet, K., Pinard, M., Yang, S., Moir, R. D., Poitras, C., Dicaire, M. J., Sgarioto, N., Lariviere, R., Kleinman, C. L., Willis, I. M., Gauthier, M. S., Coulombe, B., & Brais, B. (2019). The leukodystrophy mutation Polr3b R103H causes homozygote mouse embryonic lethality and impairs RNA polymerase III biogenesis. *Mol Brain*, *12*(1), 59. https://doi.org/10.1186/s13041-019-0479-7

Dittmar, K. A., Goodenbour, J. M., & Pan, T. (2006). Tissue-specific differences in human transfer RNA expression. *PLoS Genet*, *2*(12), e221. https://doi.org/10.1371/journal.pgen.0020221

Dooves, S., Kok, L. M. L., Holmes, D. B., Breeuwsma, N., Breur, M., Bugiani, M., Wolf, N. I., & Heine, V. M. (2023). Cortical interneuron development is affected in 4H leukodystrophy. *Brain*, *146*(7), 2846-2860. https://doi.org/10.1093/brain/awad017

Dorboz, I., Dumay-Odelot, H., Boussaid, K., Bouyacoub, Y., Barreau, P., Samaan, S., Jmel, H., Eymard-Pierre, E., Cances, C., Bar, C., Poulat, A. L., Rousselle, C., Renaldo, F., Elmaleh-Berges, M., Teichmann, M., & Boespflug-Tanguy, O. (2018). Mutation in POLR3K causes hypomyelinating leukodystrophy and abnormal ribosomal RNA regulation. *Neurol Genet*, *4*(6), e289. https://doi.org/10.1212/NXG.0000000000000289

Harting, I., Al-Saady, M., Krageloh-Mann, I., Bley, A., Hempel, M., Bierhals, T., Karch, S., Moog, U., Bernard, G., Huntsman, R., van Spaendonk, R. M. L., Vreeburg, M., Rodriguez-Palmero, A., Pujol, A., van der Knaap, M. S., Pouwels, P. J. W., & Wolf, N. I. (2020). POLR3A variants with striatal involvement and extrapyramidal movement disorder. *Neurogenetics*, *21*(2), 121-133. https://doi.org/10.1007/s10048-019-00602-4

Holmes, D. B., & Heine, V. M. (2017). Simplified 3D protocol capable of generating early cortical neuroepithelium. *Biol Open*, *6*(3), 402-406. https://doi.org/10.1242/bio.021725

La Piana, R., Cayami, F. K., Tran, L. T., Guerrero, K., van Spaendonk, R., Õunap, K., Pajusalu, S., Haack, T., Wassmer, E., Timmann, D., Mierzewska, H., Poll-Thé, B. T., Patel, C., Cox, H., Atik, T., Onay, H., Ozkınay, F., Vanderver, A., van der Knaap, M. S., . . . Bernard, G. (2016). Diffuse hypomyelination is not obligate for POLR3-related disorders. *Neurology*, *86*(17), 1622-1626.

Macintosh, J., Perrier, S., Pinard, M., Tran, L. T., Guerrero, K., Prasad, C., Prasad, A. N., Pastinen, T., Thiffault, I., Coulombe, B., & Bernard, G. (2023). Biallelic pathogenic variants in POLR3D alter tRNA transcription and cause a hypomyelinating leukodystrophy: A case report. *Front Neurol*, *14*, 1254140. https://doi.org/10.3389/fneur.2023.1254140

Moir, R. D., Merheb, E., Chitu, V., Stanley, E. R., & Willis, I. M. (2024). Molecular basis of neurodegeneration in a mouse model of Polr3-related disease. *bioRxiv*. https://doi.org/10.1101/2023.12.12.571310

Nadadhur, A. G., Emperador Melero, J., Meijer, M., Schut, D., Jacobs, G., Li, K. W., Hjorth, J. J. J., Meredith, R. M., Toonen, R. F., Van Kesteren, R. E., Smit, A. B., Verhage, M., & Heine, V. M. (2017). Multi-level characterization of balanced inhibitory-excitatory cortical neuron network derived from human pluripotent stem cells. *PLoS One*, *12*(6), e0178533. https://doi.org/10.1371/journal.pone.0178533

Nicholson, M. W., Ting, C. Y., Chan, D. Z. H., Cheng, Y. C., Lee, Y. C., Hsu, C. C., Huang, C. Y., & Hsieh, P. C. H. (2022). Utility of iPSC-Derived Cells for Disease Modeling, Drug Development, and Cell Therapy. *Cells*, *11*(11). https://doi.org/10.3390/cells11111853

Nieuwenhuis, R., te Grotenhuis, M., & Pelzer, B. (2012). influence.ME: tools for detecting influential data in mixed effects models. *The R Journal*, *4(2)*, 38-47.

Perrier, S., Gauquelin, L., Fallet-Bianco, C., Dishop, M. K., Michell-Robinson, M. A., Tran, L. T., Guerrero, K., Darbelli, L., Srour, M., Petrecca, K., Renaud, D. L., Saito, M., Cohen, S., Leiz, S., Alhaddad, B., Haack, T. B., Tejera-Martin, I., Monton, F. I., Rodriguez-Espinosa, N., . . . Bernard, G. (2020). Expanding the phenotypic and molecular spectrum of RNA polymerase III-related leukodystrophy. *Neurol Genet*, *6*(3), e425. https://doi.org/10.1212/NXG.0000000000000425

Richards, M. R., Plummer, L., Chan, Y. M., Lippincott, M. F., Quinton, R., Kumanov, P., & Seminara, S. B. (2017). Phenotypic spectrum of POLR3B mutations: isolated hypogonadotropic hypogonadism without neurological or dental anomalies. *J Med Genet*, *54*(1), 19-25. https://doi.org/10.1136/jmedgenet-2016-104064

Shi, Y., Inoue, H., Wu, J. C., & Yamanaka, S. (2017). Induced pluripotent stem cell technology: a decade of progress. *Nat Rev Drug Discov*, *16*(2), 115-130. https://doi.org/10.1038/nrd.2016.245

Tetreault, M., Choquet, K., Orcesi, S., Tonduti, D., Balottin, U., Teichmann, M., Fribourg, S., Schiffmann, R., Brais, B., Vanderver, A., & Bernard, G. (2011). Recessive mutations in POLR3B, encoding the second largest subunit of Pol III, cause a rare hypomyelinating leukodystrophy. *Am J Hum Genet*, *89*(5), 652-655. https://doi.org/10.1016/j.ajhg.2011.10.006

Thiffault, I., Wolf, N. I., Forget, D., Guerrero, K., Tran, L. T., Choquet, K., Lavallee-Adam, M., Poitras, C., Brais, B., Yoon, G., Sztriha, L., Webster, R. I., Timmann, D., van de Warrenburg, B. P., Seeger, J., Zimmermann, A., Mate, A., Goizet, C., Fung, E., . . . Bernard, G. (2015). Recessive mutations in POLR1C cause a leukodystrophy by impairing biogenesis of RNA polymerase III. *Nat Commun*, *6*, 7623. https://doi.org/10.1038/ncomms8623

Tian, K., Wang, R., Huang, J., Wang, H., & Ji, X. (2023). Subcellular localization shapes the fate of RNA polymerase III. *Cell Rep*, *42*(8), 112941. https://doi.org/10.1016/j.celrep.2023.112941

SUPPLEMENTARY FIGURES

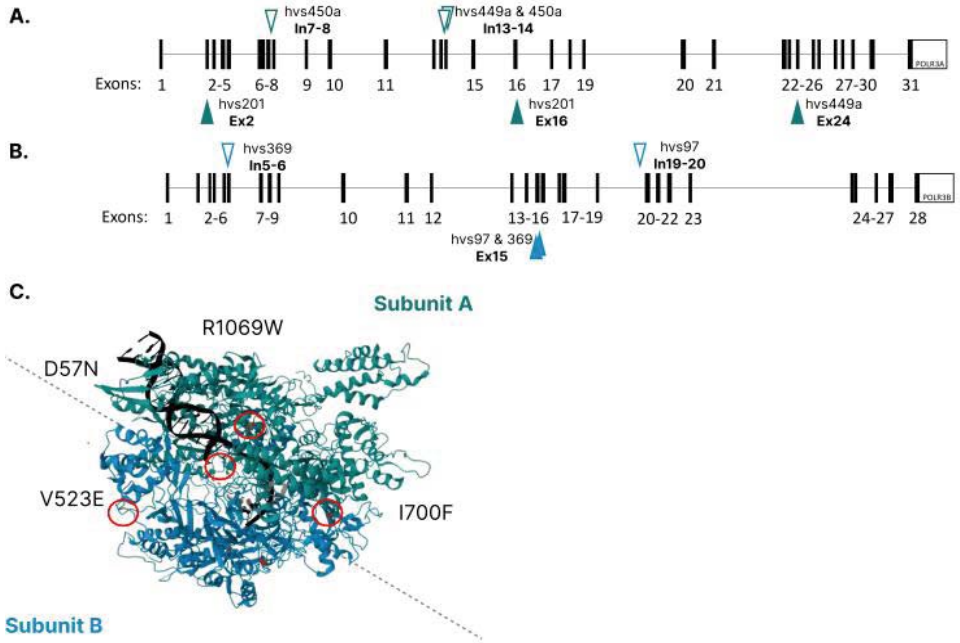

▲ **Supplementary Figure 1: Overview of variants identified in 4H patients within this study.** Schematic presentation of location of POLR3A (A) and POLR3B (B) variants on the respective genes, or on the protein subunits (C)

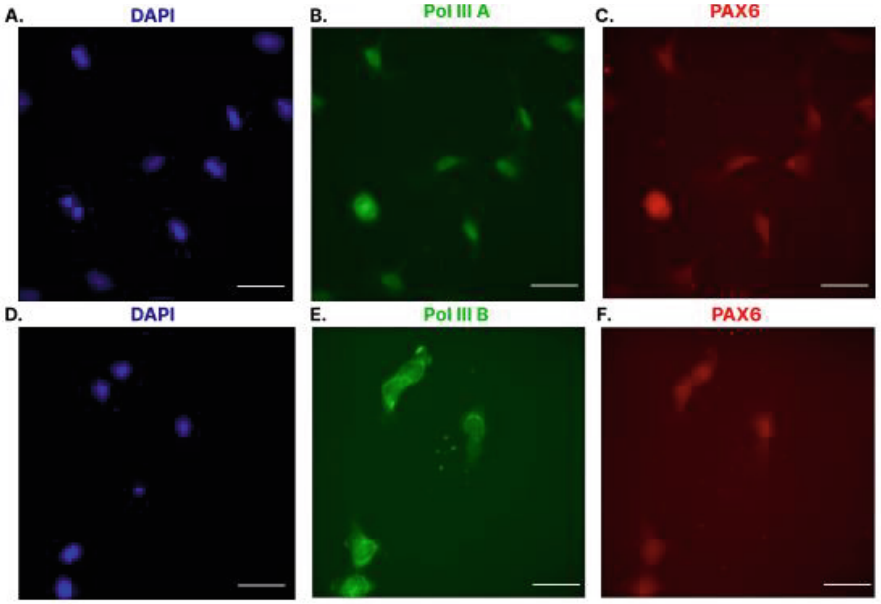

▲ **Supplementary Figure 2: Example immunocytochemistry images** Example of immunofluorescence pictures used for the quantification of localization of subunit B) Pol III A and E) Pol III B, with DAPI (blue, A&D) which outlines the nucleus and PAX6 (red, C&F) which marks the cytoplasm. Scale bars are 50 µm.

SUPPLEMENTARY TABLES

Supplementary Table I: Overview Cell Lines

Line ID	hPSCreg ID	Repr. method	Donor sex, age	Disease status	Disease Gene	Genotype	Protein
hVS201	VUi027-A	Lenti	F, 12y	4H leukodystrophy	POLR3A	159G>A 2098A>T	D57N I700F
hVS449a	VUi029-A	Sendai	M, 24y	4H leukodystrophy	POLR3A	1771-6C>G 3205C>T	? R1069T
hVS450a	VUi030-A	Sendai	F, 2y	4H leukodystrophy	POLR3A	1771-7C>G 1048+5G>T	? ?
hVS97	VUi026-A	Lenti	M, 2y	4H leukodystrophy	POLR3B	1568T>A 2084-6A>G	V523E ?
hVS369	VUi028-A	Lenti	F, 4-5y	4H leukodystrophy	POLR3B	1568T>A 303+1G>A	V523E ?
hVS88	VUi031-A	Lenti	M, 0y	Control	n.a.	n.a.	n.a.
hVS420	VUi036-A	Lenti	M, 21y	Control	n.a.	n.a.	n.a.
hVS442a	n.a.	Sendai	M, 50y	Control	n.a.	n.a.	n.a.
hVS444a	VUi038-A	Sendai	F, 13y	Control	n.a.	n.a.	n.a.
hVS445a	VUi033-A	Sendai	F, 11y	Control	n.a.	n.a.	n.a.
hVS451a	VUi032-A	Sendai	M, 19y	Control	n.a.	n.a.	n.a.
H01	WAe001-A	n.a. (Embryonic)	M, 0y	Control	n.a.	n.a.	n.a.
H09	WAe009-A	n.a. (Embryonic)	F, 0y	Control	n.a.	n.a.	n.a.

Repr. Method: reprogramming method, F: female, M: male, Y: age in years, n.a.: not applicable, ?: unknown protein consequences

Supplementary Table II: qPCR Primers

Target		Sequence
POLR3A	Forward	GTGGCCAAGAAAATAAGCCACA
	Reverse	ATGTTGGTTGTCCTGGCTGT
POLR3B	Forward	TGGACGTGCTAGCGGAG
	Reverse	TCACAAGGCCTTTCACCTTT
tRNA_Ala	Forward	GAACCCGGGACCTCATACAT
	Reverse	GGGGGTGTAGCTCAGTGGTA
tRNA_Leu	Forward	CTCAAGCTTGGCTTCCTCGT
	Reverse	GAACCCACGCCTCCATTG
BC200	Forward	GGTGGCTCACGCCTGTAATC
	Reverse	GAACTCCTGGGCTCAAGCTATC
Housekeeping	Forward	CCAGGGAAGACTACAAGGTGCGGA
SDHA	Reverse	AGGGTGTGCTTCCTCCAGTGCT

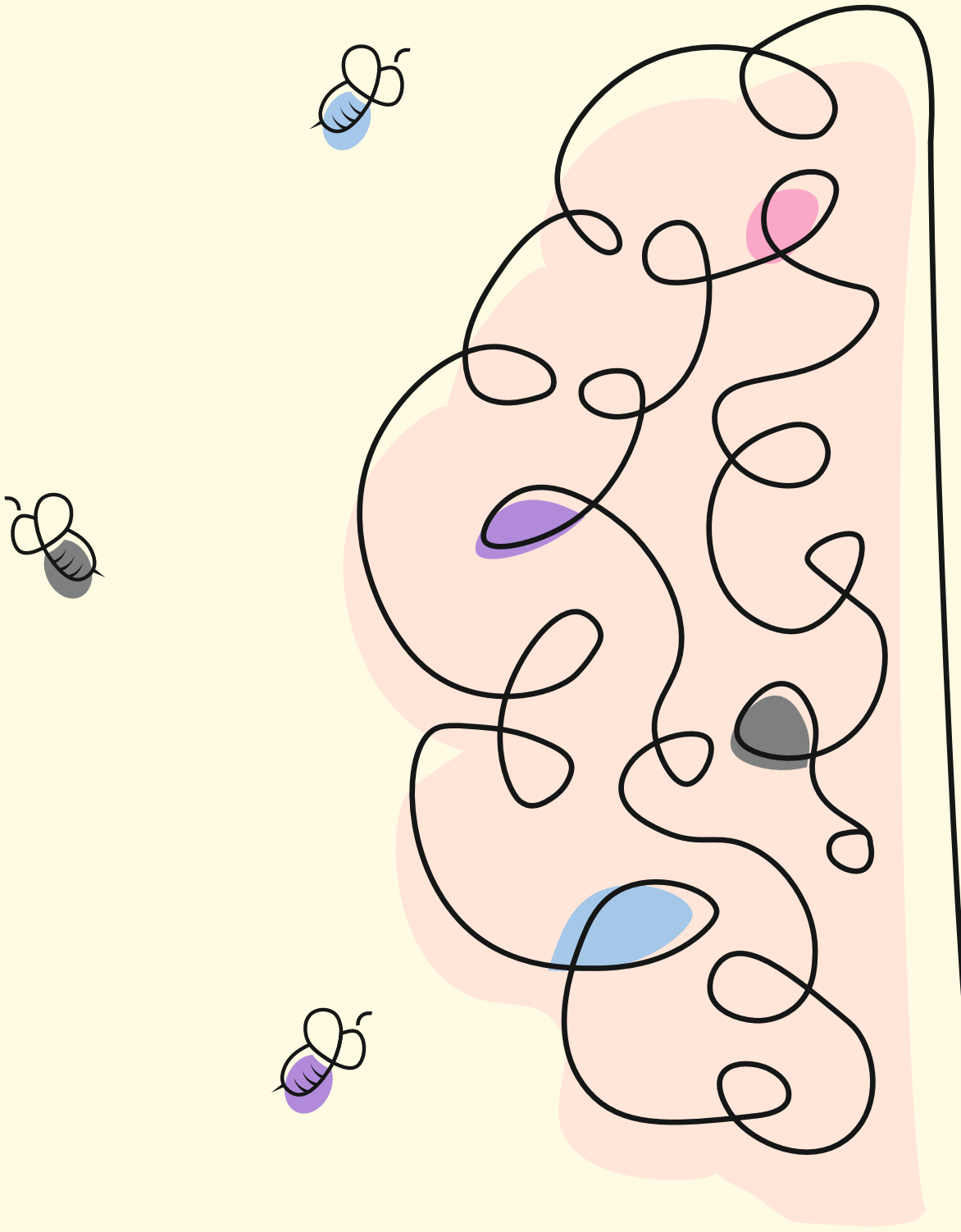

07

Discussion

Liza M. L. Kok

DISCUSSION

The aim of this thesis was to advance the understanding of 4H leukodystrophy by identifying the key cell types and molecular mechanisms implicated in the disease. Results presented in this thesis highlight that intrinsic neuronal deficits are a defining feature of 4H leukodystrophy, independent of the surrounding glial environment. The use of diverse model systems — ranging from 2D cultures to advanced 3D spheroid and co-culture models — generated an extensive dataset that provides unique insights into cell-specific vulnerabilities, molecular alterations, and addressed the interplay of neuronal, glial, and microglial elements in 4H pathology, creating a foundation for future investigations and therapeutic strategies.

1. Neuron intrinsic defects in 4H

Our investigations revealed that *ARX* expression was downregulated in cerebellar differentiation products derived from 4H patient samples. *ARX* has a known involvement in interneuron generation, development and migration (Lee et al., 2017). Additionally loss of *ARX* expression alters interneuron excitability and causes epilepsy in mice (Joseph et al., 2021; Marsh et al., 2016). Therefore, *ARX* dysregulation implicated potential interneuron involvement in 4H. In cortical neuron cultures containing both glutamatergic neurons and interneurons, we indeed identified abnormalities in GABAergic synapse formation and neuronal activity. Further investigations explored intrinsic neuronal dysfunction in 4H through assessments of neurite outgrowth, axonal transport, and microtubule dynamics in various *in vitro* models. While these parameters showed no significant differences between 4H and control samples, reduced neurite outgrowth in 4H mono-cultures compared to another leukodystrophy, Globoid Cell Leukodystrophy, was evident. Transcriptomic analyses provided additional insights, identifying downregulation of synapse formation and cortical development pathways, which collectively underscore that neuronal deficits in 4H are intrinsic and not secondary to external factors (Chapter 3). While these results point to neuronal involvement in 4H pathomechanisms, we still do not understand how. Here I will discuss if specific interneuron subclasses are more affected and how this could be studied further: How could Shh pathway dysfunctions lead to brain abnormalities in 4H? What other molecular pathways interact with Shh signalling that could contribute to 4H pathogenesis?

1.1 Interneuron vulnerability

We investigated if we could pinpoint interneuron subtype vulnerability. Analysis of genes associated with interneuron subtypes revealed increased *ERBB4* expression in 4H cortical neurons both with qPCR (Chapter 2) and bulk mRNA sequencing of mono-culture setups (Chapter 3). *ERBB4* expression is related to parvalbumin (PV) interneuron development. Conversely, no changes were detected in *RELN* (NDNF interneurons) or *CNTNAP2* (VIP interneurons) using qPCR, though bulk sequencing on mono-cultures suggested modest alterations (*RELN*; *CNTNAP2*). Also in the spheroid models, single-cell RNA sequencing revealed changes in interneuron related genes, specifically downregulation of *SST* expression in the cell cluster SST-expressing GABAergic neurons on both day 100 and 150 (Chapter 4). This consistent dysregulation supports the hypothesis that specific interneuron subclasses, particularly PV- and SST-interneurons, may be more vulnerable in 4H pathology. However, it remains unclear whether interneurons represent primarily affected cell types or if their dysfunction is a secondary consequence of broader neuronal deficits. Interneurons are known to play critical roles in coordinating cortical circuits, and their impairment may exacerbate functional deficits observed in 4H. Future research should evaluate whether interneurons can be selectively targeted for therapeutic interventions and whether these strategies may ameliorate cellular phenotypes *in vitro*.

1.2 Sonic hedgehog pathway dysregulation

As mentioned our investigations identified *ARX* downregulation in cerebellar differentiation products, corroborated by qPCR findings in cortical co-cultures. Since *ARX* is an important regulator of sonic hedgehog (Shh) gradients during development (Cho et al., 2014), we hypothesized that interneuron development is possibly affected through the Shh pathway. But *ARX* downregulation was not replicated in neuron mono-cultures, possibly as this difference is cell stage-dependent. And, therapeutic targeting of the Shh pathway using SAG failed to restore neuronal function (Chapter 2), Interestingly, *ARX* is not the only dysregulated gene in 4H that can be linked to the Shh pathway. *ITGA11* was significantly upregulated in cerebellar differentiation products of 4H. It was shown in human hepatic stellate cells that *ITGA11* can be regulated by the hedgehog signalling pathway, and inhibition of the hedgehog pathway can reduce *ITGA11* (Bansal et al., 2017). Also, *CHL1*, which exhibited significant yet modest downregulation in 4H cortical mono-cultures (Chapter 3), can be linked to Shh. Specifically, since *CHL1* is known to interact with Ptch1 during neuronal apoptosis and cerebellar development (Huang et al., 2011). Ptch1 is a receptor of hedgehog and regulates proliferation, neurogenesis and axon guidance

(Iulianella & Stanton-Turcotte, 2019). Other evidence of the involvement of Shh in 4H leukodystrophy, is found in the gene set enrichment analysis (GSEA) of spheroid single cell mRNA sequencing. Here, the gene set “Shh signalling” is downregulated in several neuron cell clusters (Chapter 4), including glutamatergic neurons and *SST*-expressing GABAergic neurons. While dysregulation of *ARX* was not consistent across all experiments, Shh signalling appears to be relevant as shown by independent experiments. Until now, we did not successfully interfere with the pathway to ameliorate 4H disease phenotypes. Hence, future research should investigate the therapeutic potential of targeting these pathways and assess their interactions.

1.3 Other molecular pathways

Since reduced *ARX* expression pointed us to the possible involvement of the Shh pathway, it is tempting to try to relate every new finding to this hypothesis. However, other assays revealed significant genes, that could also be linked to other pathways. For example, while *CHL1* contributes to Shh-related processes, it can also trigger PTCH1-, SMO-, RhoA- and ROCK-dependent signal transduction pathways in cerebellar development and promote neuronal survival (Katic et al., 2017). Besides hedgehog signalling, GSEA analysis of cortical neurons showed possible relevance of mTORC1 signalling (Chapter 2). Interestingly, this pathway is also often significant in cell clusters in the single cell data (Chapter 4). In this dataset, it is also intriguing that oxidative phosphorylation is highly significant in many clusters in all leukodystrophies (Chapter 4). The diversity of these findings do not point towards one disease mechanism involved in 4H. This highlights the need for integrative pathway analyses to identify converging nodes of dysfunction and potential points of therapeutic intervention. Expanding the focus to these broader molecular networks could help uncover novel targets beyond Shh signalling, addressing unresolved aspects of neuronal pathology in 4H.

In summary, our research on different *in vitro* models of 4H provides a foundation for understanding the intrinsic neuronal defects in 4H leukodystrophy, highlighting specific vulnerabilities in interneurons, potential dysregulation of the Shh pathway, and the involvement of broader molecular networks. Future research should prioritize integrative approaches that investigate whether these pathways are causal in 4H pathology or a consequence. Identifying key drivers of 4H pathology will be critical for guiding the development of effective targeted therapies.

2. Human iPSC based disease modelling

We successfully applied several *in vitro* systems to investigate 4H leukodystrophy relevant cell types and tissue. These models provided us, in absence of scarce 4H relevant human tissue, to identify pathological changes such as altered inhibitory neuron populations (Chapter 2) and transcriptomic differences (Chapter 3 and Chapter 4). We also demonstrated that the selection of model systems greatly influences the research outcomes (Chapter 3). To exemplify, we showed that both iPSC-derived neuron rat astrocyte co-cultures and neuron mono-cultures in maturation medium lacked typical psychosine build-up in GLD lines. This accumulation however was shown in our early neuron mono-cultures and spheroids (data not shown), highlighting that certain model systems may obscure key pathological features. As familiarizing yourself with *in vitro* techniques is a long, labour intensive and expensive process, it is crucial to select appropriate models. But, how to select the most promising model? Here I will discuss some of my takes on iPSC model selection and reflect on the models we used. In hindsight were they the appropriate models? Subsequently I will pay some attention to how I would continue by discussing the selection of samples and read outs.

2.1 iPSC model selection

We have used various iPSC models such as hiPSC-derived neuron mono-cultures, co-cultures of those neurons with rat astrocytes and hPSC-derived microglia as well as spheroids. These models were all based on classical differentiation using patterning factors, a method we choose because it resembles more closely the *in vivo* developmental stages (Nadadhur et al., 2018), during which leukodystrophies often appear. While other iPSC-derived models and other disease modelling approaches exist, we will discuss here what we have learned about selecting iPSC-based strategies to model leukodystrophies.

Mono-cultures (Chapter 3) i.e., no astrocytes present, revealed transcriptional changes in 4H neurons but lacked clear hallmark phenotypes in GLD. This model was applied because of previous shown neuronal deficits in 4H and GLD, and because co-cultures were void of psychosine build up, a GLD hallmark. The benefit of these cultures is that the limited complexity of these models allow for the investigation of one cell type in great detail, with usually less lengthy and less difficult protocols. Additionally, these cultures have been optimized for years, providing detailed knowledge on the cells created. However, mono-cultures also have notable limitations. Neurons and astrocytes benefit from the presence of each other, they become more mature (Supakul et al., 2024). Although results are not

shown, neurons in NB+ medium did not develop axonal transport, indicating reduced maturation, without the presence of astrocytes. Hence, the use of more costly commercial media, STEMdiff Forebrain Neuron Maturation Medium, was required. These factors highlight the need to carefully consider mono-culture limitations in the context of specific research objectives.

Co-cultures, which in this thesis involved iPSC-derived neurons on rat astrocytes with or without hPSC-derived microglia (Chapter 2, 3 and 5), improved functionality, intercellular crosstalk, and a more accurately represented *in vivo* situation. The presence of multiple cell types influenced the observed responses, underscoring the potential advantages of more complex models when evaluating compounds or studying pathological mechanisms. For example, co-cultures have been shown to alter cellular reactions in ways that mono-cultures cannot (De Simone et al., 2017), suggesting they may be more suitable for assessing therapies or exploring disease interactions.

Spheroid systems represent another layer of complexity, incorporating multiple cell types to mimic *in vivo* interactions more closely. These models allow for unbiased exploration of affected cell types, potential therapeutic targets, and their response to therapies. Though we have only used one spheroid system, the models are rapidly evolving including bioreactor culture, organ-on-a-chip and/or biomaterials (Gong et al., 2021). Their structural similarity to the brain is argued to make them better for testing interventions at both the cellular and system levels. While those complex models are promising, in our research we have shown unexpected results. For example, we hypothesized that when using a spheroid system with myelination we capture the hypomyelinating phenotype. Nevertheless, there were no differences in OPC and oligodendrocyte abundance and compacted myelin was identified in all spheroids (Chapter 4). This raises critical questions: does hypomyelination occur only within a specific time window, or are factors like growth medium supplementation masking the phenotype? Such advanced models are also costly, labor-intensive, and prone to batch effects, highlighting the need for careful protocol optimization.

Another important factor in *in vitro* modelling is the use of all-human component vs xeno-assisted systems. In general, the field of *in vitro* modelling is moving towards all-human, xeno-free systems, which aligns with eliminating animal-derived components to better replicate human biology and safety when used for cell replacement therapy. In our

laboratory, we have moved towards xeno-free hPSC cultures years ago, reflecting this paradigm shift. Though, some of our differentiation protocols continue to rely on products such as Matrigel, a mouse sarcoma extracellular matrix (ECM) product (Nadadhur et al., 2017). Similarly, bovine serum, a product not normally found in the brain, is used to generate astrocytes (Nadadhur et al., 2018) but this pushes them in a reactive state (Du et al., 2010). In our research, we not only used cultures with animal-derived products, we co-cultured with rat astrocytes. Formerly, rat astrocytes were the gold standard for co-cultures. However, reliable, more physiological all human systems protocols now exist (Batenburg et al., 2023; Dooves et al., 2021; Lendemeijer et al., 2024; White et al., 2024). Nevertheless, we identified 4H neuronal deficits in the presence of rat astrocytes, but also show that their presence obscured GLD phenotypes. We hypothesize that this happened as they did not have GLD associated mutations. Since additional experiments (Chapter 3) showed that 4H neurons co-cultured with rat astrocytes, also exhibit pathological changes, co-cultures with rat astrocytes could still be a plausible option for modelling 4H leukodystrophy, but moving towards all human systems would be a next step to model 4H more physiological.

The current thesis emphasizes that iPSC model selection depends on the disease and research question under investigation. To continue 4H research, a logic next step is to formulate new hypotheses based on the leukodystrophy spheroid dataset, which will become publicly available. These hypotheses can be tested in simpler mono- or co-culture settings before advancing to spheroid or brain-on-chip systems for preclinical validation. Additionally, we have been intrigued by the absence of psychosine build-up in GLD mono-cultures in maturation medium. Investigation of the spent medium could reveal whether certain factors in this medium mask the phenotype, or in the best case, could relief the phenotype. Lastly, the future of iPSC models likely lies in adopting all-human systems for increased relevance, though xeno (assisted) cultures will retain value where more rapid maturation or scalability is needed.

2.2 Sample selection

The main focus has been to investigate 4H syndrome utilizing patient-derived iPSC lines. Additionally, we used KO and KI lines with isogenic controls to investigate GLD and CD. Isogenic controls are typically used to gain higher power than when using case-control designs only. However the ability to generalize findings from isogenic models can be limited (Brunner et al., 2023). This section evaluates sample selection decisions made during this work and proposes strategies for future research.

Case-control vs. isogenic designs

The 4H-iPSC cohort used throughout this thesis existed of 5 patients, with either *POLR3A* or *POLR3B* mutations. However, for monogenic diseases like leukodystrophies, gene editing to introduce disease variants into standard control lines or repair the disease mutation in patient-derived iPSCs is a very plausible option. In fact, the neuron and spheroid experiments (Chapter 3 and 4) included isogenic pairs for GLD and CD. However, looking at the PCA plots generated from both sequencing data sets, isogenic pairs were not more similar than non-isogenic lines. This raises the question: were isogenic lines valuable, and should we create such pairs for 4H in the future?

As mentioned, isogenic controls in experiment design comes with certain advances such as increased power (Brunner et al., 2023). With a general failure of power in neuroscience this is very welcome (Button et al., 2013; Nord et al., 2017). However, their utility depends on the research question and the following considerations. Isogenic lines can elucidate subtle phenotypes that might be missed in heterogeneous case-control studies. For 4H, where neuronal and spheroid mono-cultures showed no striking phenotypes, isogenic lines might uncover additional pathologies. Introducing common mutations into standard control lines is advantageous for studying specific mechanisms. However, this approach lacks the link to the clinical context (patient-specificity), and information on the wide clinical heterogeneity seen in 4H patients, possibly caused by other (non)-genetic factors as well (Wolf et al., 2014). Therefore, patient-derived iPSC lines with diverse backgrounds remain crucial for translational research. Introducing mutations across multiple clones with varying genetic backgrounds could enhance understanding but would remain resource intensive.

Considering all of the above, while 4H research could benefit from isogenic lines to discover more clear phenotypes addressing the variability and heterogeneity inherent to this disorder, future work should consider a balanced approach, integrating the strengths of both patient-derived and isogenic lines. As processes are time consuming, it is important to register and biobank those iPSC-lines so they can be shared with other 4H-leukodystrophy researchers.

Collaboration to increase sample size

One of the most elegant experimental designs used in this thesis has been the sample cohorts as presented in the spheroids chapter (Chapter 4). The collaboration between several institutes increased the available resources, respectively expertise, personnel and

of course money. Because of this, we could include 5 control lines and 8 leukodystrophy lines, while maintaining feasible practical burden. Of course, there was variation and unfortunately, sample sizes were not large enough to address the cause of this variation. However, the experimental set-up, allowed for the comparison of findings between leukodystrophies. Interestingly, we identified two cell clusters, cycling radial glia and neural progenitors, being largely absent in all leukodystrophies. Additionally, cluster specific findings were identified, however, the comparison of these findings between leukodystrophies revealed that results need to be interpreted with caution. To illustrate, GSEA analysis revealed "ribosomal subunit" to be upregulated in 4H neuron mono-cultures compared to controls, although not p-adjusted significant. We utilized the scRNA sequencing data set to determine whether this was a true finding. Indeed, Ribosomal subunit related GO_CC terms were frequently significant in 4H, though they were not consistently up or down regulated. For example, certain clusters showed upregulation at D100 (proliferating OPC), but downregulation at D150 (maturing cells). Initially, we hypothesized this might reflect a 4H-specific translation dysfunction, which would be in line with 4H-related mutations in RNA Polymerase III. However, ribosomal-related GO_CC terms were also significant in datasets from GLD and CD, suggesting a possible leukodystrophy-specific phenomenon. This overlap between pathways suggests shared mechanisms or potential limitations in dataset resolution, complicating distinctions among these leukodystrophies. Upon closer inspection of genes within these pathways, we found an overexpression of ribosomal genes (e.g. *RPL* and *RPS*), raising the possibility of technical biases in the dataset that might also lead to their frequent significance. We need to continue our research on this, possibly, including pseudotime analysis using the D100 and D150 subsets we can shed light on which findings are relevant.

Although findings such as rRNA processing gene sets being significant in 4H proliferating OPC, initially were linked to the POLR3 mutations in 4H, we showed that these pathways were also different in CD and GLD. The findings highlight the value of studying broader leukodystrophy cohorts to identify universal and subtype-specific mechanisms. Despite this progress, variability within small sample sizes prevented definitive conclusions about the causes of certain phenotypes. Future research should focus on further increasing sample sizes and standardizing experimental designs across collaborative studies.

Time points for sample collection

Considering that the transcriptomic differences in 4H cortical neurons was observed after only one week of culture, we hypothesize that 4H neuronal defects occur over time, hence future *in vitro* work with similar methods should be done on 4H neurons at later time points. Mature neurons in the models for 4H are critical, considering that we aim to investigate interneurons, a neuronal subtype that arises later in development and takes time to mature (Fitzgerald et al., 2020). Likewise, our myelination models for 4H, using both spheroids (Chapter 4) and 2D co-cultures (Chapter 2), did not reveal significant impairments in myelination. These results suggest that these models may need further optimization to capture the relevant time window or environmental conditions for hypomyelination. Careful selection of sampling timelines is crucial for resolving such questions.

So in conclusion, while decisions made during this work were justified, there is room for improvement: 1) Isogenic lines: We have seen in the neuron-mono cultures (Chapter 3) that changes can be subtle in 4H, for this isogenic experimental set-up that generally have increased power can be useful. We could make either stable genetically modified lines, or use techniques such as RNA interference to create *POLR3A* or B knock-downs; 2) Patient-derived diversity: For generalizing findings to the entire patient population, and later patient-specific treatments, it is still important to use patient-derived lines with larger genetic background variations. In this thesis we have worked with a small patient cohort. Future aims should focus on including more patients to validate whether the findings are representative of the entire patient population. In chapter 5, we have shown that it is possible that there are patient-specific differences. Addressing these issues will be essential for advancing 4H research and improving the reliability of experimental findings; 3) Optimize time points: As subtle changes may emerge over time, longitudinal studies of neurons and spheroids at different maturation stages are essential for capturing the dynamic progression of 4H pathology.

2.3 Read out selection

Selecting the appropriate read-outs is a fundamental aspect of any study. In this thesis, we have used a broad scale of read-outs such as high-throughput morphological analysis using cellomics, electrophysiology analysis using MEAs, classical approaches such as qPCR and western blot, and transcriptomics. Each research question justifies the use of specific techniques; however, I would like to elaborate on the growing prominence of transcriptomics in research.

With rapid experimental advancements, high-throughput tools such as transcriptomics are now more affordable and hence accessible to many researchers. As a result, generating new data is no longer the primary bottleneck in research—it is the analysis and interpretation of these vast datasets. While the availability of such tools can drive new discoveries, it is worth questioning whether they are always the most appropriate approach. With the ease of generating large datasets—often yielding publishable findings—one might wonder if such methods are sometimes chosen out of convenience. In light of this, we should wonder: do small advances in sequencing technology, increased sample size or slightly different *in vitro* approach, really justify the generation of yet another new big data set? What happens to datasets that are already available - are we utilizing them to their full potential? And to what extent do choices in data analysis and research direction shape the outcomes of our studies?

In this thesis, we have generated multiple transcriptome datasets, though our approaches and subsequent decisions varied. For example, in chapter 2, we used a reductionist approach, focussing on a differentially expressed gene (DEG) list to identify a single extreme gene (*ARX*), with known functions. This finding directed further research, leading to the identification of interneuron involvement in 4H. However, this reductionist approach is inherently sensitive to bias, as it relies heavily on pre-existing knowledge (Abedi et al., 2019). While we validated differences in *ARX* expression across other *in vitro* differentiation products, many other significant genes remained unexplored. An alternative, less biased approach involves gene set enrichment analysis (GSEA). In this thesis, we demonstrate that GSEA can yield numerous significant gene sets. However, determining which of these are truly relevant and warrant further investigation remains a challenge. Often, existing knowledge again guides researchers to prioritize gene sets that align with current hypotheses. Yet, as shown in the section on sample selection, including other disease samples revealed that some gene sets that aligned well for one specific disease, were often significant in other disease as well.

To conclude, transcriptome studies have become more accessible, and have led to new discoveries. In my opinion, ensuring that data is Findable, Accessible, Interoperable, and Reusable (FAIR) can maximize the potential of the single cell data set generated in this thesis, instead of generating new ones. Of course, with the reuse of data it is important to address concerns about the reuse of shared data by researchers who were not involved in its collection and hence might not understand all the study parameters (Longo & Drazen, 2016).

3. Translation of findings towards therapy

Considering the absence of curative treatments for 4H, there is still a pressing need for therapy development. In this thesis, we demonstrated a potential role for neuronal deficits in 4H leukodystrophy, possibly mediated through the SHH pathway. Our exploration of SAG, an agonist of Shh, to improve the 4H neuronal phenotype, revealed no significant effects, underscoring the need to investigate alternative targets within this pathway or entirely new pathways. The models and data presented in this thesis establish a critical foundation for these future investigations. However, important validation steps remain necessary to optimize our models and readouts for reliable therapy testing.

For development of future therapies, several steps need to be taken. Those include the identification of a therapeutic target and / or measurable phenotypes. Did we identify those? Possibly. With optimization and standardization, the *in vitro* models displaying interneuron pathology (Chapter 2), could serve as a platform to screen for other drugs modulating the Shh pathway. Additionally, after optimization, FDA-approved drug libraries or CRISPR screens could be used to screen for possible other drugs. These strategies, known as drug repurposing, have the potential to significantly accelerate clinical translation, as Phase II clinical trials may follow logically (Turner et al., 2016), with reduced risk of failure (Rudrapal et al., 2020).

How can we analyse drug screens? There is both merit in simple and complex approaches, depending on available expertise and resources. The most established method is high-content screening of morphology phenotypes (cellomics), as demonstrated in Chapter 2 and 5. With the quick developments in the MEA field, it may soon be feasible to conduct high-throughput screens using MEA platforms, which we have shown to exhibit a strong phenotype already (Chapter 2).

When does therapeutic intervention need to take place? Therapeutic timing is critical, especially for neurodevelopmental disorders with prenatal origins. Early interventions may be necessary to prevent or mitigate phenotypes, but strategies targeting later developmental stages could also hold promise for reversing or ameliorating phenotypes postnatally. Determining the optimal therapeutic window for 4H leukodystrophy will require further exploration, likely guided by developmental studies using *in vitro* and *in vivo* models.

Towards precision medicine. Future therapeutic strategies should focus on tailoring interventions to patient-specific gene and protein expression profiles. Precision medicine approaches, incorporating molecular diagnostics and personalized drug screening, hold significant promise for addressing the heterogeneity of 4H leukodystrophy and investigating potential treatments.

The work presented in this thesis represents an important step towards understanding 4H leukodystrophy and developing targeted therapies. By refining our models, exploring novel targets, and leveraging emerging technologies and precision medicine strategies, we can advance closer to achieving meaningful clinical interventions for patients.

REFERENCES

Abedi, M., Fatehi, R., Moradzadeh, K., & Gheisari, Y. (2019). Big data to knowledge: common pitfalls in transcriptomics data analysis and representation. *RNA Biol*, *16*(11), 1531-1533. https://doi.org/10.1080/15476286.2019.1652525

Bansal, R., Nakagawa, S., Yazdani, S., van Baarlen, J., Venkatesh, A., Koh, A. P., Song, W. M., Goossens, N., Watanabe, H., Beasley, M. B., Powell, C. A., Storm, G., Kaminski, N., van Goor, H., Friedman, S. L., Hoshida, Y., & Prakash, J. (2017). Integrin alpha 11 in the regulation of the myofibroblast phenotype: implications for fibrotic diseases. *Exp Mol Med*, *49*(11), e396. https://doi.org/10.1038/emm.2017.213

Batenburg, K. L., Rohde, S. K., Cornelissen-Steijger, P., Breeuwsma, N., Heine, V. M., & Scheper, W. (2023). A Human Neuron/Astrocyte Co-culture to Model Seeded and Spontaneous Intraneuronal Tau Aggregation. *Curr Protoc*, *3*(10), e900. https://doi.org/10.1002/cpz1.900

Brunner, J. W., Lammertse, H. C. A., van Berkel, A. A., Koopmans, F., Li, K. W., Smit, A. B., Toonen, R. F., Verhage, M., & van der Sluis, S. (2023). Power and optimal study design in iPSC-based brain disease modelling. *Mol Psychiatry*, *28*(4), 1545-1556. https://doi.org/10.1038/s41380-022-01866-3

Button, K. S., Ioannidis, J. P., Mokrysz, C., Nosek, B. A., Flint, J., Robinson, E. S., & Munafo, M. R. (2013). Power failure: why small sample size undermines the reliability of neuroscience. *Nat Rev Neurosci*, *14*(5), 365-376. https://doi.org/10.1038/nrn3475

Cho, G., Lim, Y., Cho, I. T., Simonet, J. C., & Golden, J. A. (2014). Arx together with FoxA2, regulates Shh floor plate expression. *Dev Biol*, *393*(1), 137-148. https://doi.org/10.1016/j.ydbio.2014.06.012

De Simone, U., Caloni, F., Gribaldo, L., & Coccini, T. (2017). Human Co-culture Model of Neurons and Astrocytes to Test Acute Cytotoxicity of Neurotoxic Compounds. *Int J Toxicol*, *36*(6), 463-477. https://doi.org/10.1177/1091581817739428

Dooves, S., van Velthoven, A. J. H., Suciati, L. G., & Heine, V. M. (2021). Neuron-Glia Interactions in Tuberous Sclerosis Complex Affect the Synaptic Balance in 2D and Organoid Cultures. *Cells*, *10*(1). https://doi.org/10.3390/cells10010134

Du, F., Qian, Z. M., Zhu, L., Wu, X. M., Qian, C., Chan, R., & Ke, Y. (2010). Purity, cell viability, expression of GFAP and bystin in astrocytes cultured by different procedures. *J Cell Biochem*, *109*(1), 30-37. https://doi.org/10.1002/jcb.22375

Fitzgerald, M., Sotuyo, N., Tischfield, D. J., & Anderson, S. A. (2020). Generation of cerebral cortical GABAergic interneurons from pluripotent stem cells. *Stem Cells*, *38*(11), 1375-1386. https://doi.org/10.1002/stem.3252

Gong, J., Meng, T., Yang, J., Hu, N., Zhao, H., & Tian, T. (2021). Three-dimensional in vitro tissue culture models of brain organoids. *Exp Neurol*, *339*, 113619. https://doi.org/10.1016/j.expneurol.2021.113619

Huang, X., Zhu, L. L., Zhao, T., Wu, L. Y., Wu, K. W., Schachner, M., Xiao, Z. C., & Fan, M. (2011). CHL1 negatively regulates the proliferation and neuronal differentiation of neural progenitor cells through activation of the ERK1/2 MAPK pathway. *Mol Cell Neurosci*, *46*(1), 296-307. https://doi.org/10.1016/j.mcn.2010.09.013

Iulianella, A., & Stanton-Turcotte, D. (2019). The Hedgehog receptor Patched1 regulates proliferation, neurogenesis, and axon guidance in the embryonic spinal cord. *Mech Dev*, *160*, 103577. https://doi.org/10.1016/j.mod.2019.103577

Joseph, D. J., Von Deimling, M., Hasegawa, Y., Cristancho, A. G., Ahrens-Nicklas, R. C., Rogers, S. L., Risbud, R., McCoy, A. J., & Marsh, E. D. (2021). Postnatal Arx transcriptional activity regulates functional properties of PV interneurons. *iScience*, *24*(1), 101999. https://doi.org/10.1016/j.isci.2020.101999

Katic, J., Loers, G., Tosic, J., Schachner, M., & Kleene, R. (2017). The cell adhesion molecule CHL1 interacts with patched-1 to regulate apoptosis during postnatal cerebellar development. *J Cell Sci*, *130*(15), 2606-2619. https://doi.org/10.1242/jcs.194563

Lee, K., Ireland, K., Bleeze, M., & Shoubridge, C. (2017). ARX polyalanine expansion mutations lead to migration impediment in the rostral cortex coupled with a developmental deficit of calbindin-positive cortical GABAergic interneurons. *Neuroscience*, *357*, 220-231. https://doi.org/10.1016/j.neuroscience.2017.06.010

Lendemeijer, B., Unkel, M., Smeenk, H., Mossink, B., Hijazi, S., Gordillo-Sampedro, S., Shpak, G., Slump, D. E., van den Hout, M., van, I. W. F. J., Bindels, E. M. J., Hoogendijk, W. J. G., Nadif Kasri, N., de Vrij, F. M. S., & Kushner, S. A. (2024). Human Pluripotent Stem Cell-Derived Astrocyte Functionality Compares Favorably with Primary Rat Astrocytes. *eNeuro*, *11*(9). https://doi.org/10.1523/ENEURO.0148-24.2024

Longo, D. L., & Drazen, J. M. (2016). Data Sharing. *N Engl J Med*, *374*(3), 276-277. https://doi.org/10.1056/NEJMe1516564

Marsh, E. D., Nasrallah, M. P., Walsh, C., Murray, K. A., Nicole Sunnen, C., McCoy, A., & Golden, J. A. (2016). Developmental interneuron subtype deficits after targeted loss of Arx. *BMC Neurosci*, *17*(1), 35. https://doi.org/10.1186/s12868-016-0265-8

Nadadhur, A. G., Emperador Melero, J., Meijer, M., Schut, D., Jacobs, G., Li, K. W., Hjorth, J. J. J., Meredith, R. M., Toonen, R. F., Van Kesteren, R. E., Smit, A. B., Verhage, M., & Heine, V. M. (2017). Multi-level characterization of balanced inhibitory-excitatory cortical neuron network derived from human pluripotent stem cells. *PLoS One*, *12*(6), e0178533. https://doi.org/10.1371/journal.pone.0178533

Nadadhur, A. G., Leferink, P. S., Holmes, D., Hinz, L., Cornelissen-Steijger, P., Gasparotto, L., & Heine, V. M. (2018). Patterning factors during neural progenitor induction determine regional identity and differentiation potential in vitro. *Stem Cell Res*, *32*, 25-34. https://doi.org/10.1016/j.scr.2018.08.017

Nord, C. L., Valton, V., Wood, J., & Roiser, J. P. (2017). Power-up: A Reanalysis of 'Power Failure' in Neuroscience Using Mixture Modeling. *J Neurosci*, *37*(34), 8051-8061. https://doi.org/10.1523/JNEUROSCI.3592-16.2017

Rudrapal, M., J. Khairnar, S., & G. Jadhav, A. (2020). Drug Repurposing (DR): An Emerging Approach in Drug Discovery, 2020. In *Drug Repurposing - Hypothesis, Molecular Aspects and Therapeutic Applications*. https://doi.org/10.5772/intechopen.93193

Supakul, S., Murakami, R., Oyama, C., Shindo, T., Hatakeyama, Y., Itsuno, M., Bannai, H., Shibata, S., Maeda, S., & Okano, H. (2024). Mutual interaction of neurons and astrocytes derived from iPSCs with APP V717L mutation developed the astrocytic phenotypes of Alzheimer's disease. *Inflamm Regen*, *44*(1), 8. https://doi.org/10.1186/s41232-023-00310-5

Turner, N., Zeng, X. Y., Osborne, B., Rogers, S., & Ye, J. M. (2016). Repurposing Drugs to Target the Diabetes Epidemic. *Trends Pharmacol Sci*, *37*(5), 379-389. https://doi.org/10.1016/j.tips.2016.01.007

White, K. E., Bailey, H. L., Shaw, B. S., Geiszler, P. C., Mesquita-Ribeiro, R., Scott, D., Layfield, R., & Serres, S. (2024). A convenient model of serum-induced reactivity of human astrocytes to investigate astrocyte-derived extracellular vesicles. *Front Cell Neurosci*, *18*, 1414142. https://doi.org/10.3389/fncel.2024.1414142

Wolf, N. I., Vanderver, A., van Spaendonk, R. M., Schiffmann, R., Brais, B., Bugiani, M., Sistermans, E., Catsman-Berrevoets, C., Kros, J. M., Pinto, P. S., Pohl, D., Tirupathi, S., Stromme, P., de Grauw, T., Fribourg, S., Demos, M., Pizzino, A., Naidu, S., Guerrero, K., . . . Bernard, G. (2014). Clinical spectrum of 4H leukodystrophy caused by POLR3A and POLR3B mutations. *Neurology*, *83*(21), 1898-1905. https://doi.org/10.1212/WNL.0000000000001002

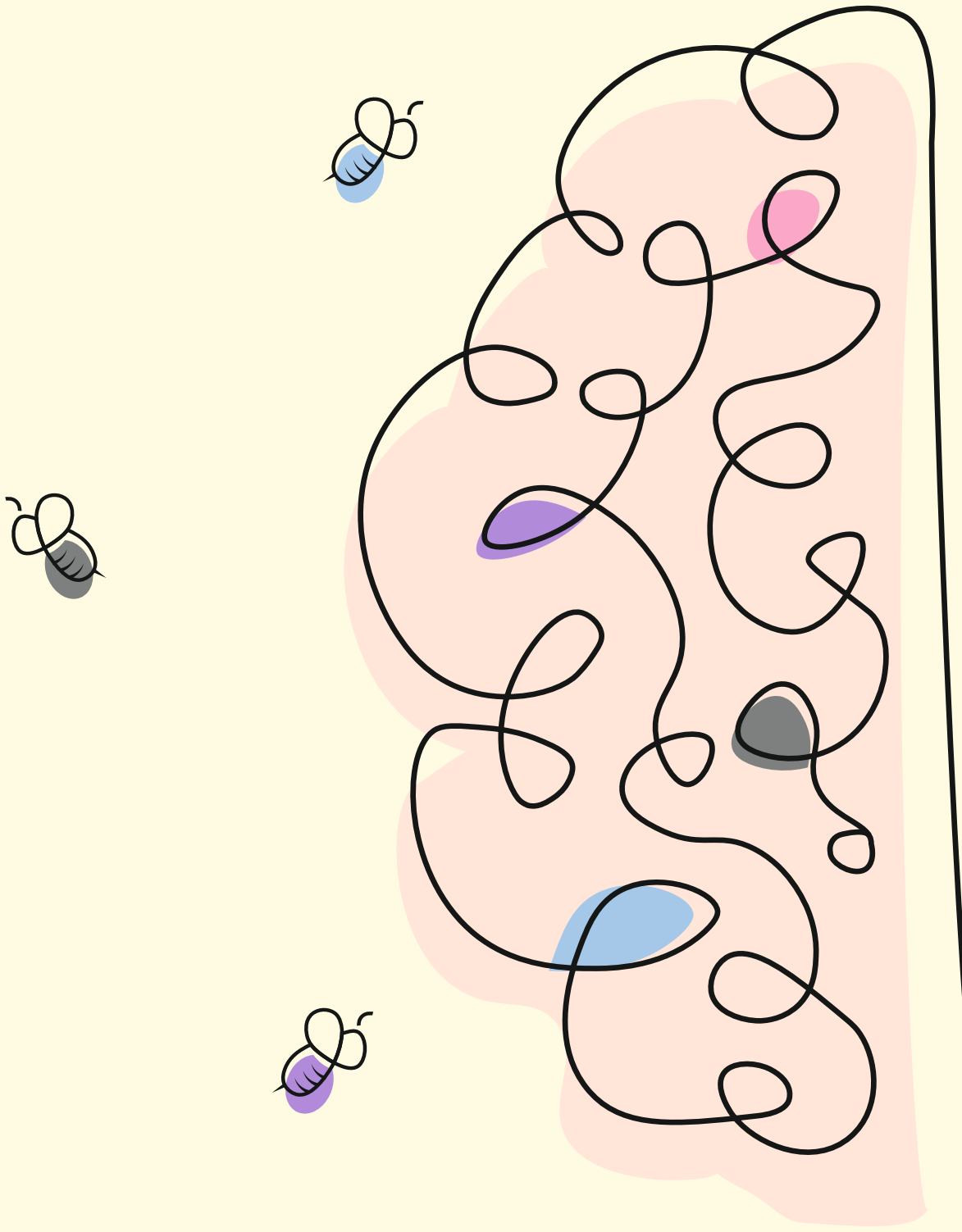

Appendix

Liza M. L. Kok

Summary

4H leukodystrophy is a rare genetic disorder characterized by hypomyelination, hypodontia, and hypogonadotropic hypogonadism. Following the discovery that mutations in the genes encoding for RNA polymerase III (Pol III) subunits, such as *POLR3A* and *POLR3B*, cause the disorder, clinical diagnosis improved. But, today treatments are still solely symptomatic rather than curative. In this thesis we aimed to gain insight into how molecular and cellular mechanisms contribute to the pathology of 4H leukodystrophy using patient-specific iPSC-based models with the goal to facilitate development of new therapeutic strategies.

The first chapter, the **introduction**, outlines the current state of knowledge on 4H syndrome from clinical presentation to the function of RNA pol III and pathogenic mutations in genes encoding for RNA pol III. We point out that the current treatment options only include symptom relief. Furthermore it presents the rationale for using human iPSC-based models to investigate 4H hypomyelination and evaluate which *in vitro* models are potentially suitable.

In **Chapter 2: Cortical interneuron development is affected in 4H leukodystrophy** we explored differential expression of genes in 4H cerebellar cells using patient iPSC technology in combination with RNAseq analysis. This revealed downregulation of *ARX*, a transcription factor required for interneuron development. This was followed by a focused investigation of cortical neuron co-cultures, that showed a reduction in GABAergic synapses and elevated network activity in 4H neurons. Pharmacological manipulation of GABAergic signalling confirmed an inhibitory deficit. Interestingly, myelination appeared normal, and treatment with the Sonic Hedgehog (Shh) agonist SAG did not rescue the phenotype. Expression of the parvalbumin-related gene ERBB4 was increased, suggesting disrupted development of specific interneuron subtypes. Taken together, we concluded that cortical interneuron development is affected in 4H leukodystrophy.

In **Chapter 3: Investigating neuron intrinsic defects in 4H and Globoid Leukodystrophy** we further explored neuronal phenotypes in 4H leukodystrophy. Additionally, we aimed to explore whether neuronal changes are 4H-specific or also occur in other leukodystrophies. Hence control, 4H and GLD neurons were compared. Surprisingly, the *in vitro* cultures with GLD neurons did not show accumulation of psychosine, a hallmark of the disease. This highlights the heterogeneity of leukodystrophies and the necessity of refining disease

models. Nevertheless, the models showed transcriptomic changes in 4H neurons, specifically downregulation of genes related to synaptic and cortical development and upregulation of genes related to morphogenesis and ribosomal genes. This reconfirmed a role for neuronal dysfunction in 4H and can be used to determine focus for future research.

To further explore differences between leukodystrophies and mechanisms underlying 4H specific hypomyelination **Chapter 4: Towards a 3D spheroid system for modelling leukodystrophies** introduces a 3D brain spheroid platform derived from iPSCs to model 4H, GLD, and Canavan Disease (CD). Spheroids exhibited robust cellular diversity, including neurons, astrocytes, and oligodendrocytes, and formed compact myelin as shown by immunofluorescence and electron microscopy. Single-cell RNA sequencing identified 27 cell clusters. Interestingly, with a consistent underrepresentation of cycling radial glia and neural progenitors across leukodystrophies. We report differential expressed genes and significantly different gene sets that can guide future research directions.

Although the spheroids encompass diverse cell types that mimic the *in vivo* brain, the model did not include microglia, while those cells are increasingly recognized as key players in brain development and disease. Therefore, **Chapter 5: Human pluripotent stem cell-derived microglia shape neuronal morphology and enhance network activity *in vitro*** describes a co-culture system using hPSC-derived microglia and neurons. We showed that the microglia incorporate into the cultures where they reduced nuclear debris and altered neuronal morphology by decreasing axonal and dendritic segments and reducing synapse density. Despite the decrease in synapse density, neuronal network activity increased. Interestingly, addition of microglia from adrenoleukodystrophy (ALD) patients caused different axonal changes compared to the addition of 4H and control microglia. These findings demonstrate the importance of including microglia to more accurately model neuron–glia interactions in disease.

To explore how patient-specific genetic variants affect *POLR3* gene and protein expression during neuronal lineage differentiation in 4H leukodystrophy, we examined *POLR3* expression levels, protein localization, and developmental dynamics across iPSCs, neural epithelial cells (NES) and neurons in **Chapter 6: *POLR3* gene and protein expression dynamics in 4H leukodystrophy using iPSC-derived neuronal lineages.** We identified elevated *POLR3* gene expression in NES. However, Pol III protein levels were notably reduced in 4H patient cells. Despite these protein-level alterations, overall Pol III-

transcribed transcript levels, were unchanged in 4H cells. Notably, patient-specific genetic backgrounds were found to have a significant impact on *POLR3A* expression. These results underscore the necessity of considering individual genetic backgrounds and specific developmental cell states when investigating the pathology of 4H leukodystrophy.

The last chapter, the **discussion**, integrates findings across model systems to show that 4H leukodystrophy involves neuron-intrinsic dysfunction, particularly interneurons. While the Shh pathway may contribute to pathology, other molecular processes—including mTORC1 signalling and oxidative phosphorylation—also emerge as candidates for 4H but also GLD and CD. The thesis underscores the strengths and limitations of mono-culture, co-culture, and spheroid systems, emphasizing the need for strategic model selection and study design. Finally, the work advocates for precision medicine approaches that combine patient-derived iPSCs, transcriptomics, and functional assays to identify new therapeutic targets and screening platforms.

In conclusion this thesis advances the understanding of 4H leukodystrophy by demonstrating alterations in neurons - particularly interneurons – in 4H. It introduces and validates a range of iPSC-derived *in vitro* models, including spheroids and microglia co-cultures, as powerful tools for dissecting leukodystrophy mechanisms, while emphasizing on careful selection of suitable *in vitro* models. By revealing candidate pathological pathways this work lays a foundation for future therapeutic development in 4H and related disorders.

DANKWOORD / ACKNOWLEDGEMENTS

Er zijn heel veel dingen beschreven in dit boekje en ondanks dat mijn naam op de voorkant staat, heb ik dit natuurlijk niet alleen gedaan. Ik wil dan ook graag iedereen bedanken die in de afgelopen jaren in welke vorm dan ook heeft bijgedragen aan de voltooiing van dit project. Er zijn een aantal mensen die ik in het bijzonder wil noemen. / There are many things described in this book, and although my name is on the cover, I definitely did not do all of this by myself. I would like to thank everyone that contributed in any way to the completion of this project. There are some people I would like to thank individually.

Te beginnen bij Vivi: bedankt voor het bieden van de kans om van technician naar PhD te gaan. Je expertise met *in vitro* werk en de fijne groep die onder jouw begeleiding is ontstaan waren factoren waardoor ik die stap aandurfde. Ik heb lang getwijfeld of die stap ook de juiste keuze was, maar gelukkig was jij altijd positief en motiverend. Die instelling typeerde onze overleggen, waar ik vaak sceptisch was (of realistisch zoals ik het zelf liever noem), zag jij het altijd van de zonnige kant en gelukkig kwamen we altijd ergens in het midden uit. Het laatste jaar was, waar ik al bang voor was, toch nog pittiger dan verwacht, maar daar had ik niet aan willen staan met een andere PI! Zonder jou was ik misschien nooit aan een PhD begonnen, maar had ik ook niet tot dit punt kunnen komen! Onwijs bedankt! Ik wil ook graag Nicole Wolf bedanken, ik heb de updates altijd als een prettig moment ervaren om zelf alle voortgang weer op een rijtje te krijgen, maar ook het bieden van het klinische perspectief was erg interessant en leerzaam. Bedankt!

Een van de belangrijkste personen tijdens deze hele periode was jij Nicole Breeuwsma. We hebben echt lief en leed gedeeld als collega's maar ook als vriendinnen. Van samen MEAs uitplaten en neuronen invriezen tot brainstormen over (of bemoeien met?) technician dingen, het was allemaal gewoon leuker met jou! Ik ben er nog steeds van overtuigd dat wij een technician dreamteam zouden zijn en vraag mij nog vaak genoeg af waarom ik dan toch die PhD wilde doen? Een vraag waar ik sowieso vaak mee bezig was, en ook in die lastigere periodes was jij er als steun en toeverlaat. Het is jammer dat we geen collega's meer zijn, maar gelukkig heb ik er wel een geweldige vriendin aan over gehouden. Bedankt voor alles! Misschien moeten we maar weer snel samen op vakantie? Naar onze favoriete oud collega? Lisa Gasparotto, it is obviously you that I am talking about! What can I say, you have been my teacher from the master course to the technician position and the first period of the PhD. I was convinced that we as a lab and me as a PhD would collapse without you. It is not a secret that I have had my collapses (all PhD's do right?), but surprisingly the lab did not burn

down, and I am writing a big THANK YOU in my thesis?! So… I guess I made it! Thanks for all the advise along the way, on cell culture but of course also on personal stuff and all things Italy. It was special to have you around! And I will try to squeeze in holidays to Italy whenever I can!

Natuurlijk was er ook steun van andere technicians, zoals Leoni, Paulien, Amber, Julia en Yvonne. Het lab draait niet zonder technicians, het was fijn om jullie support te hebben! Naast technicians valt of staat een lab natuurlijk met een hoop gezellige collega's. Sommige met veel ervaring zoals jij Stephanie. Het leek wel of jij alles al eens had meegemaakt en je altijd de rust kon bewaren. Heel fijn om met je samen te werken en mijn eerste co-auteurschap mee te hebben! Roberto, you started the PhD around the same time as I did, this was definitely helpful in times that we had to push through, but of course we also had our celebrations. I still remember your first Christmas party! And hopefully soon we both have another celebration: our defenses! En natuurlijk ook met jou Karen, startte ik min of meer tegelijk. Super fijn, want daarom móésten we beiden ONWAR studiepunten halen met tripjes naar Griekenland en Berlijn. Dat was afzien hè? De tijd dat we kantoorgenoten waren in het W&N was ook super fijn. Ik heb warme herinneringen aan alle gesprekken zowel over wetenschap als privé aangelegenheden! Of course there are also the PhDs that started later than me and still have some time to go. Lucía, I will remember you as the one with the most amazing ppt design skills and of course for your kindness! Juliette, sorry for mentioning it, I will remember you for not being my intern. But no worries, I forgave you long time ago, it was a pleasure to see you come to the lab anyways and be fellow PhDs! Sophie Lee, thank you for being the best honey customer I have ever had. If it ever seems I don't sell out, I will start shipping to you. And to all of you I want to say one last time: don't stress too much, there is so much more in life than the PhD! But I wonder if it is still convincing, now that I almost have the title... And of course there were many more colleagues with who I shared the lab for longer or shorter periods. Anne, Kevin, Stephanie H., Claudia, Juliët, Lidiia, Lauria, Laura and everyone else thanks for being great colleagues!

Nicki Coveña jij was waarschijnlijk je naam aan het zoeken tussen de mede-PhDs, geen zorgen ik ben je niet vergeten, maar ik vond je ook passen tussen de stagiaires! Het was leuk om je begeleider te zijn, volgens mij hebben we beiden veel geleerd en is dat later over gegaan in een hele leuke samenwerking met de MEA microglia experimenten. Bedankt voor de fijne samenwerking en voor het voortzetten van de MEA legacy natuurlijk! Els Vos, als mijn eerste student heb je natuurlijk ook je steentje bijgedragen aan de MEA experimenten,

bedankt! En dan was daar nog het droom duo: Evanne en Felice. Jullie hebben samen zoveel werk voor mij verzet, jullie waren zulke fijne dames om mee te werken, en het was leuk om te zien hoe veel jullie aan elkaar hadden. Ik ben echt trots op hoe jullie je ontwikkelden tijdens de stage, jullie zijn toppers! En zoals beloofd natuurlijk ook een shout out naar hun supervisor Nick Dekker. Niet alleen bedankt voor de supervisie van Evanne en Felice maar ook voor het zijn van een betrokken HBO docent van ons alle drie. Bij deze is mijn belofte nagekomen, tot ziens tijdens mijn verdediging Nick!

Voor de samenwerkingen buiten het stamcel lab wil ik in het speciaal Koen Helwegen bedanken. Ik vond het erg prettig om met je aan het MEA paper te werken. Ik heb er ook veel van geleerd, vooral dat statistiek altijd lastiger is dan het lijkt haha. Bedankt dat je het voor mij hebt uitgevogeld! And with another imperfect study design, Heiletjé van Zyl came to the rescue! Thanks for figuring out that one! I hope that by now the paper is finally re-submitted. And I promise I will (try to) never have an imperfect study design again! Also thanks to Nathan for working on the MEA script, your contribution is highly appreciated! Kevin Marinus, bedankt voor je input bij de MEAs, het was erg prettig om met je samen te werken, je enthousiasme werkt aanstekelijk! Fallon Ratner, Tanya Phung thank you for exploring the NG4Leuko spheroid data set!

Het is ook op zijn plaats om de geweldige support van Gerda Berkhout en Eline van Zon te noemen, de afdeling liep op rolletjes, daar dragen/droegen jullie zeker aan bij. Danielle Posthuma bedankt dat ik onderdeel mocht zijn van CTG, ondanks dat de onderwerpen ver van elkaar af lagen waren de SPECs leerzaam en was het heel fijn om van een grotere groep deel uit te maken. Over grotere groepen gesproken. A big part of this project was the NG4Leuko collaboration. I would like to thank all people from Bonn (Oliver Brüstle, Michael Peitz, Giovanna Cenini, Polina Oberst) and Paris (Dorien Maas, Maria-Cecilia Angulo). Of course I would also like to thank everyone in Porto (Monica Sousa, Sandra Braz, Joana Rodrigues, Eduardo Veríssimo). It was great to spend some days in your lab and share knowledge. Of course also thanks to the representatives of ELA (Elise Saunier-Vivar, Hélène rochereuil). A special thanks to everyone in Milan (Angela Gritti, Elisabeth Mangiameli, Clarissa Rosato), it was a pleasure to work together in your lab for some weeks. And also many thanks for the big effort on the spheroid experiments! This was really invaluable and I am glad to see that the results from those experiments are taking more and more shape. Of course also the bioinformaticians (Ivan Merelli, Francesca Cupaioli, Roberta Alfieri) play a big role in that, thanks for all the work!

De laatste bedankjes gaan uit naar mijn sociale netwerk, zonder jullie was ik nooit zo ver gekomen. Ten eerste aan al mijn vriendinnen en in het speciaal Isabella, Famke, Marcha en Romy: Bedankt dat jullie altijd klaar stonden om mij te helpen ontspannen. In fijn gezelschap lijkt alles een stuk rooskleuriger! Merel met jou heb ik tijdens de PhD zo veel gedeeld, niet alleen omdat de Italiaanse Zeedijk bijna mijn tweede huis was maar ook omdat we elkaar zo vaak zagen in de trein. Ik had het niet gedacht maar nu mis ik die trein reizen toch! Suzanne, mijn kermis maatje, bedankt dat je vaak de lange afstand hebt afgelegd voor wéér een kermis. Zulke feestjes hielden mij op de been tijdens de PhD, dus je bent altijd welkom als jij ook even je hoofd leeg moet maken! Over PhDs gesproken, Bo, ik snap niet hoe jij het allemaal doet, jij gaat zo hard ik weet zeker dat jouw PhD helemaal goed komt! Het was fijn om na werk soms nog even een hapje te eten en dan was de avond nooit lang genoeg om over alles bij te kletsen! En natuurlijk ook Daphne, zo bijzonder dat ik jouw getuige was en jij nu mijn paranimf! Onze levens zijn zo verweven, je bent meer als een zus, heel fijn om je er deze dag bij te hebben.

Mam en pap, dit is het dan, we zijn aangekomen bij de meest gelezen pagina's van het hele boekje. Jullie hebben de anderen ook wel gelezen toch? Gelukkig betekent dit ook het einde van de PhD, nu echt! Een einde volgens het boekje, namelijk met een boekje. Alleen jullie weten hoe vaak eerder stoppen de betere optie leek. Het stelde me gerust dat die optie altijd bespreekbaar was, en dat jullie niet minder trots zouden zijn. Jullie hadden gelijk, er is meer in het leven dan de PhD. Ik ben blij dat het eindelijk klaar is! Stan, bedankt dat je het tolereerde als ik weer eens onverwachts kwam mee eten, hopelijk ben je niets te kort gekomen. Of was het opa of oma's portie die werd opgegeten? Oma, met jou heb ik zulke goede herinneringen aan de eerste periode van de PhD. Ja dat was de lente van 2020, die van corona, maar daardoor kon ik vaak bij jou langs. Lekker achter het huis in het zonnetje lunchen of een ijsje eten. Helaas ging ik daarna verhuizen, maar gelukkig zijn we nu weer buren! Leg je de ijsjes koud? Mandy en Marco, het was fijn om jullie er ook bij te hebben, maar natuurlijk vooral als de kleine Joah mee was voor knuffels. Ook dan was des te duidelijker, er is meer dan de PhD.

De laatste woorden van deze thesis zijn natuurlijk voor jou Mark. Bedankt voor je geduld, bedankt dat je me soms maar gewoon laat uit razen, bedankt dat je een stapje extra doet als het mij even te veel wordt of dat nu met de PhD is of de verbouwing van ons droomhuis. Je bent mijn rots! Ik hou van je! Zonder jou had ik de laatste periode van de PhD niet door kunnen komen, wat was het een strijd… En nu, is het EINDELIJK klaar! YES!

Nobody said it was easy,
no one ever said it would be so hard.
…
I was just guessing at numbers and figures,
pulling the puzzles apart.
Questions of science, science and progress,
do not speak as loud as my heart.
…
I'm going back to the start

The scientist - Coldplay

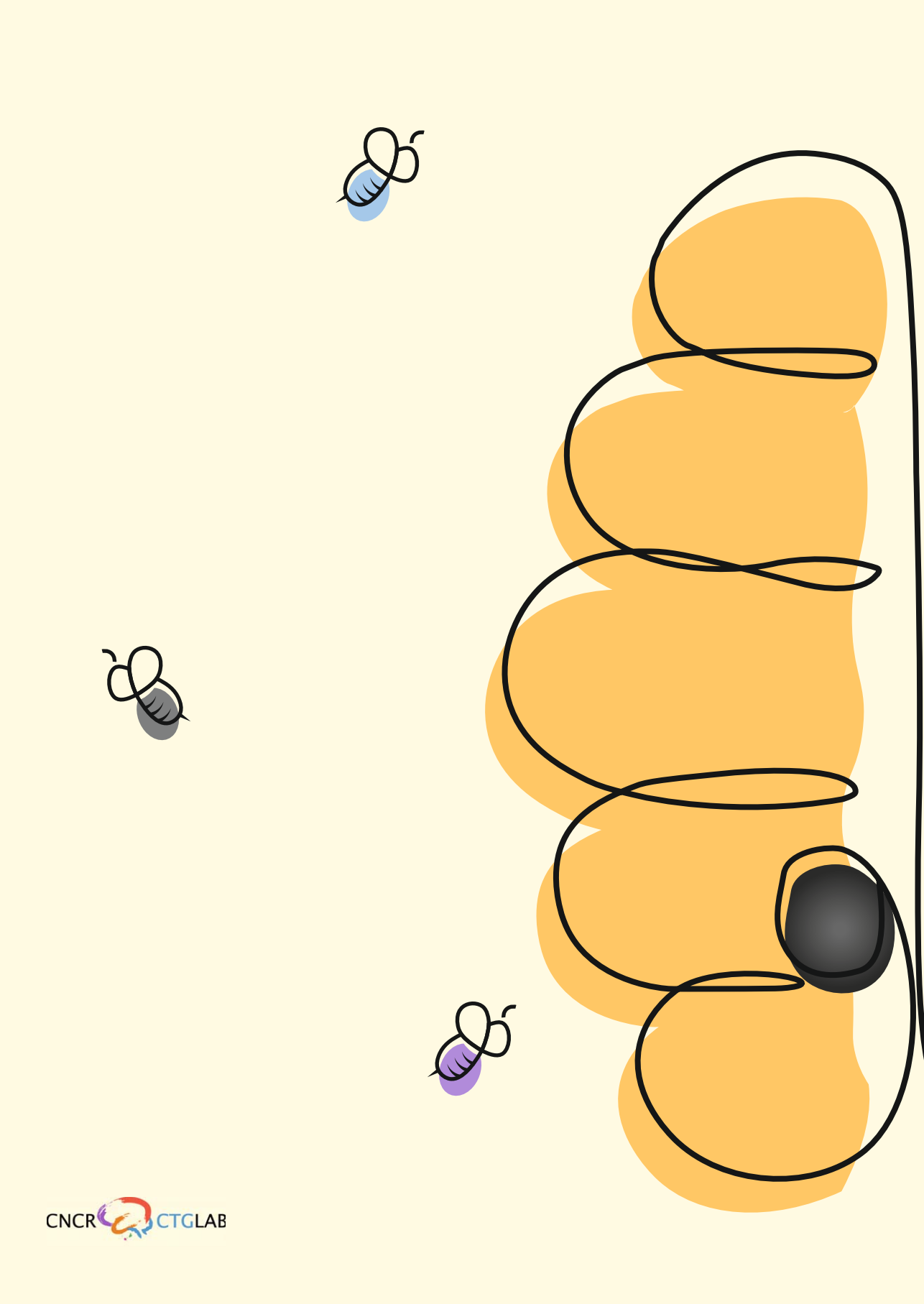

CNCR CTGLAB